Enhanced Concurrent Mapping and Localisation Using Forward-looking Sonar

Ioseba Joaquín Tena Ruiz

Thesis submitted
for the
Degree of Doctor of Philosophy

Heriot-Watt University
Department of Computing and Electrical Engineering

September 2001

Abstract

This thesis examines the use of the stochastic map for the purposes of *Concurrent Mapping and Localisation (CML)* to position an *Autonomous Underwater Vehicle (AUV)*. The stochastic map is a well proven approach which builds a landmark map of the environment and concurrently localises a vehicle within that map. The approach relies on perfect data association. Work on data association techniques has been generally limited to matching range and bearing observations.

This thesis thus enhances the stochastic map tool by meeting the following research objectives:

1. To develop a landmark state vector which, in addition to the landmark's coordinates, includes landmark descriptors. The landmarks in this new state vector will be extracted from the returns of a forward looking sonar.

2. To use the new landmark state vector to improve the data association process.

3. To demonstrate the enhanced CML capabilities using data obtained from a sonar mounted on a real AUV.

Dedication

A Joaquín y Lola.

Acknowledgements

I would like to first thank David Lane for his support and supervision. I must also thank Yvan Petillot for all the useful discussions and his friendship.

Special thanks to Jeff who made it much easier to write up and who dealt very well with all my second hand smoke.

I would also like to thank everybody in the Ocean Systems Laboratory who made it, and make it, a great place to work.

In Boston, I would like to thank John Leonard for giving me the chance to visit that part of the world and Rick for showing me around the M.I.T. maze. I have to thank especially Sarah and Mike for their kindness and friendship while I was there.

I must not forget Mike Chantler, Neil Williams and Dong-Yong Dai who made working in the CLASS project an enjoyable experience.

I also have to thank Claire, Elizabeth, Sarah and Susan for dealing with my too many enquires.

Thank you also to all my friends who have had the patience to remain my friends; Filipo, Rodrigo, Diego, Jose and Stephen suffered it more directly than the others.

Most of all, I would like to thank Joy and my family.

Contents

List of Figures

List of Tables

List of Symbols

$'$:	Matrix transpose
$\mathbf{x}$:	stochastic map state vector
$\mathbf{x_v}$:	vehicle state vector
$\mathbf{x_i}$:	landmark i state vector
$\hat{\mathbf{x}}$:	estimate of the stochastic map state vector
$\hat{\mathbf{x}}_\mathbf{v}$:	estimate of the vehicle state vector
$\hat{\mathbf{x}}_\mathbf{i}$:	estimate of landmark i state vector
$\tilde{\mathbf{x}}$:	error in the stochastic map state vector estimate
$\tilde{\mathbf{x}}_\mathbf{v}$:	error in the vehicle state vector estimate
$\tilde{\mathbf{x}}_\mathbf{i}$:	error in landmark i state vector estimate
$\mathbf{z}$:	observation vector
$\mathbf{z_i}$:	observation vector for landmark i
$\hat{\mathbf{z}}_\mathbf{i}$:	observation prediction vector for landmark i
$\mathbf{P}$:	covariance matrix of the stochastic map state estimate
$\mathbf{P_{vv}}$:	covariance matrix of the vehicle state estimate
$\mathbf{P_{ii}}$:	covariance matrix of landmark i state estimate
$\mathbf{P_{vi}}$:	covariance matrix of the vehicle to landmark i state estimate
$\mathbf{P_{ij}}$:	covariance matrix of landmark i to landmark j state estimate
$\mathbf{S}$:	innovation covariance
$\mathbf{K}$:	Kalman gain matrix
$\mathbf{Q}$:	covariance matrix of the process noise
$\mathbf{R}$:	covariance matrix of the observation noise
$\mathbf{f_x}$:	stochastic map process model
$\mathbf{f_v}$:	vehicle process model
$\mathbf{F_{x_v}}$:	Jacobian of the vehicle process model w.r.t. the vehicle state
$\mathbf{F_{x_v}}$:	Jacobian of the vehicle process model w.r.t. the process noise
$\mathbf{h_i}$:	observation model for landmark i
$\mathbf{H}$:	Jacobian of the observation model w.r.t. the stochastic map state

$\mathbf{H}_{\hat{\mathbf{x}}_\mathbf{v}}$:	Jacobian of the observation model w.r.t. the vehicle state estimate
$\mathbf{H}_{\mathbf{z_{new}}}$:	Jacobian of the observation model w.r.t. the new obervation
S:	size descriptor
P:	perimeter descriptor
C:	compactness descriptor
MD:	maximum dimension descriptor
X:	x-axis centroid descriptor
Y:	y-axis centroid descriptor
M_f:	first invariant moment descriptor
M_s:	second invariant moment descriptor
H_0:	null hypothesis
H_1:	alternative hypothesis
N_{ω_i}:	number of samples of class ω_i
$\bar{\omega}_i$:	mean of class ω_i
$\bar{\omega}_0$:	mean over all classes
ω_{i_j}:	sample j of class ω_i
$P(\omega_i)$:	probability of class ω_i
D:	divergence criterion
B:	Brattacharyya critetion
$\mathbf{S}_w$:	within-class scatter matrix
$\mathbf{S}_b$:	between-class scatter matrix
$\mathbf{S}_m$:	mixture scatter matrix
J_1, J_2, J_3:	scatter matrices separability criterions
d^2:	Mahalanobis distance

Chapter 1

Introduction

Remotely Operated Vehicles (ROVs) have been used extensively as tools to survey the sea bed. These vehicles have allowed sensors to penetrate the deepest oceans. They have also played a fundamental role in making the seas safer. Divers are no longer required to expose themselves to the harsh ocean as most of their activities can also be performed by these vehicles. The spectrum of applications that ROVs are involved in is considerable.

The oil industry has shown a great interest in the sustainable exploitation of the sea. Oil pockets below the earth's sea bed have been exploited and constitute a significant part of the world's oil supply. Access to these pockets is a feat of engineering and human endeavour. ROVs have been an integral part of this achievement. These vehicles have been primarily used for:

- surveying the sea bed for suitable oil rig deployment sites,
- surveying the sea bed for suitable pipeline deployment sites and
- post-lay inspection and maintenance of both oil rig and pipelines.

The scientific community has also benefited from the use of ROVs. These vehicles are extensively used not just to chart the world's depths, but also to improve our understanding of the planet. Geologists and biologists regularly sample the world's oceans and recent discoveries have heightened interest. Archaeologists and treasure hunters have also found ROVs invaluable tools. These were used most famously in the inspection of the Titanic.

The military have used ROVs extensively to perform mine-hunting operations. These systems allow ships to stay well away from the mines and thus contribute to the safety of the crew. ROVs also have the potential to be used in salvage operations, ship inspection, clandestine missions ...

Driven by these numerous interest groups, the ROV industry has flourished and its technologies matured. Different applications have resulted in the development of a range of different designs. All of these share common deployment constraints. These will be examined below.

1.1 ROV Deployment

ROVs are normally linked to the surface via a cable, referred to as the *tether*. This tether supplies the ROV with power and is also used to transfer information to and from the ROV. This configuration implies that most ROV missions require (as well as the ROV itself):

- a ship and crew,
- qualified ROV pilots,
- enough tether for the ROV to reach the required depths,
- a crane mechanism to deploy/recover the ROV and
- a lot of patience (needed during the time spent travelling to and from the bottom).

All of these factors make ROV operations very expensive. This has not limited their appeal, but it has spurred the research community into investigating other types of *Unmanned Underwater Vehicles (UUVs)*. This research has culminated in the development of *Autonomous Underwater Vehicles (AUVs)*.

1.2 The AUV Solution

The AUV solution proposes severing the link between the UUV and the surface, see figure 1.1. In doing this the UUV would no longer be supplied with power and/or telemetry. In other words AUVs have been limited by the lack of *autonomy*. Autonomy can be defined as the ability to provide for oneself without the help of others. Thus, an AUV should be able to:

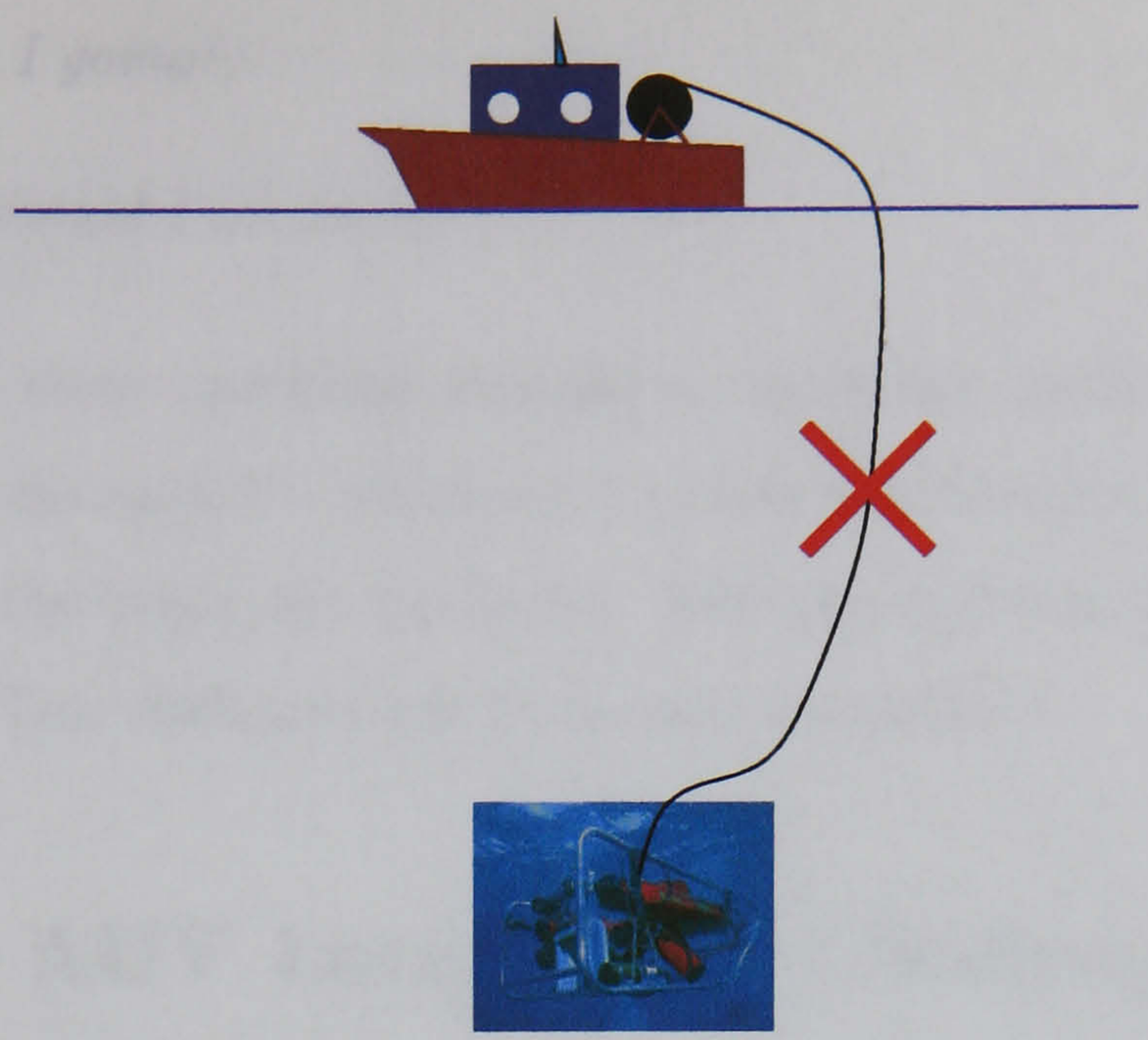

Figure 1.1: The ROV is connected to the ship via a tether to be supplied with power and transmit telemetry. Thus any ROV mission requires the costly deployment of a ship. AUVs will sever the link between the UUV and the surface

- provide its own power,
- provide enough data storage capabilities and,
- take decisions based on inputs from sensors mounted on the AUV.

The current commercially available battery technology seriously limits the range of missions an AUV can tackle. The idea of a vehicle performing 72 hours missions running on batteries has been disregarded by the ROV community. However, new technologies, namely Lithium-Ion and Lithium-Polymer, currently in development have given the AUV community the confidence to develop their products. These technologies will expand the range of AUV tasks as they become available. In [110] the interested reader will find a good review of all these technologies.

Data storage technology has also improved and will continue to improve. Currently, off-the-shelf hardisks can store upto 80 GB at a more than reasonable budget (prize/size/power).

In parallel to these developments the robotics community have also been making good progress in helping machines make decisions. An important part of this process will be the ability to navigate. To successfully navigate, three key questions must be addressed [64]:

- *"Where am I?;*

- *where am I going?;*
- *and how should I get there?"*

The first of these questions remains a significant challenge. An AUV which cannot answer this question will never be truly autonomous. Further it will not be able to answer the other two questions. This one question is the main motivation for this thesis. This challenge will be termed *localisation.*

1.3 The AUV Localisation Challenge

Dead-reckoning sensors have been extensively used to provide position estimates in a wide range of applications. Standard dead-reckoning sensors provide AUVs with speed, acceleration, attitude and rotation.

Gyroscopes are at the core of dead-reckoning systems. The *Electrically Suspended Gyro* (ESG) provides good unaided performance, but with a mean-times-between-failure (MTBF) of less than 500 hours, it is extremely unreliable. Floated rate integrating gyros and dry tuned gyros posses, like the ESG, low reliability, typically less than 2000 hours MTBF. *Ring laser gyros* appear to provide the best solution with a MTBF in excess of 10,000 hours. The latest figures for ring laser gyros demonstrate update rates of 1 to 1600 Hz, with a precision of 0.0018° [113]. The output for these systems must be integrated and if used unaided they will drift. Ring laser gyros for example drift by $0.44°/hour$ [113].

Velocity logs are used for finding out the velocity of the vehicle with respect to the water mass, as is the case for the *Electromagnetic (EM) Log*, or with respect to the sea bed bottom, *Doppler Sonar* and *Correlation Velocity Log* (CVL). The EM Log readings can be corrupted by distortions of the water flow. Doppler Sonar is typically limited to operation at 600 metres depth; in deeper waters it reverts to finding the velocity with respect to the water mass, making it susceptible to currents. CVL provides good accuracy with an error of less than 0.4 percent of distance travelled. Refer to [56] and [113] for a more detailed discussion.

All these systems together with an appropriate dynamic model form the basis of an *Inertial Navigation System (INS).* An INS system can be used to estimate the

position of an AUV. However, errors in the vehicle or sensor models can degrade the performance of such a system and over time the AUVs will drift from their estimated positions. In such cases, the AUVs can benefit from aiding. Aiding systems provide the AUV with an external, known, reference that allows for the vehicle to correct its position.

Many commercial systems exist for finding the absolute position of a submersible vehicle. All of these systems can be used as the aiding source. Some of these include *acoustic positioning* systems: *acoustic super short*, *short* and *long baseline navigation*. The two former methods are only suitable for local area positioning, over a relatively short distance, less than one nautical mile. Long baseline provides positioning and covers an area of up to seven nautical miles. The need for the submersible to be within an envelope covered by these systems limits the exploration capabilities of AUVs.

Radio navigation aids or position fixes systems include *Loran-C* (being phased out), *Omega* and *differential Omega* (accurate within 0.3 nautical miles) and the *Global Positioning System (GPS)*. The removal of Selected Availability has meant that GPS can provide an accuracy of about 30 metres and *differential GPS (DGPS)* can be accurate to within centimetres. AUVs must surface in order to obtain fixes from any of these sensors, thus limiting the vehicle's autonomy. A thorough review of all the aforementioned systems can be found in [56]. Notice however that the GPS systems have evolved considerably since that paper was written.

An up to date commercial absolute positioning system which does fix its position by means of a link with a surface reference unit is the Position and Orientation System for Submersible Vehicles (POS/SV). This system incorporates an IMU aided by an acoustic positioning System and either GPS or DGPS. It offers in excess of 25,000 hours MTBF, a heading accuracy of less than 0.4° to 80° of latitude, roll and pitch accuracy of less than 0.05° and a velocities accurate to approximately 0.2 % of the UUV speed [117]. These figures will be hard to match by an unaided vehicle, but the benefits in breaking the link between the surface and the vehicle cannot be dismissed.

This thesis proposes a different kind of absolute sensor. This absolute sensor is a forward-looking sonar, which maps the environment that surrounds the AUV. This

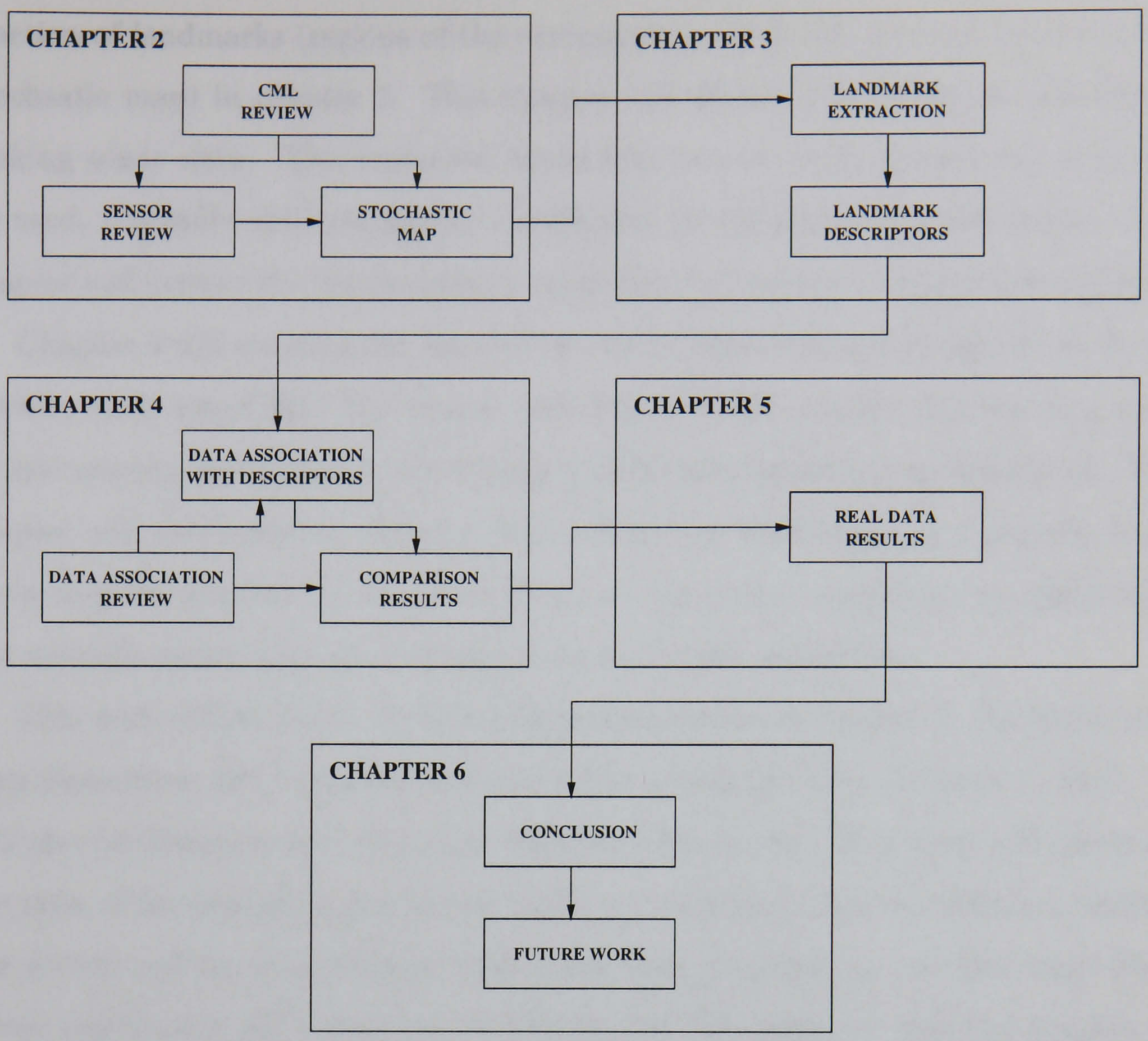

Figure 1.2: Thesis Flow Structure

map is then used by the AUV to localise itself. The thesis presents a system that performs *Concurrent Mapping and Localisation (CML)*. The system requires no a priori map or aid from any other external sensor (baseline or GPS).

1.4 Thesis Structure

Figure 1.2 illustrates a flow diagram of those aspects of work which will be closely examined by this thesis. Each chapter is clearly identified in this diagram.

The thesis has chosen the stochastic map [99] as the preferred mapping and localisation tool. The environment will be explored using a forward-looking sonar. The reasons behind these choices are examined in Chapter 2. This chapter will also clearly identify the aims and objectives of the thesis.

This thesis will then explore the interpretation of the sonar data and the ex-

traction of landmarks (regions of the environment which will serve as inputs to the stochastic map) in chapter 3. This chapter will illustrate the richness of forward-looking sonar data. The extracted landmarks can be given descriptors that will be used, alongside their estimated coordinates, to distinguish the landmarks. The chapter will explore the discriminatory capabilities of common landmark descriptors.

Chapter 4 will examine the state of the art in data association algorithms developed to work with CML. The chapter will illustrate the benefits that can be gained by introducing the landmark descriptors within the stochastic map framework. The chapter will also compare different data association algorithms. It will prove that, given suitable descriptors, the performance of the nearest neighbour standard filter can actually match that of more elaborate and recent algorithms.

This work will be put to the test with real sonar data in chapter 5. The stochastic map framework will be shown to work in the Ocean Systems Laboratory tank. It will also be demonstrated with data obtained from a pier. This data will illustrate the risks of the landmark descriptors when the landmarks look too similar. Finally, the system will be demonstrated with a sequence obtained, for the first time, from a real exploratory AUV mission. It will be with this data set that the benefits of using the landmark descriptors will be fully appreciated.

The final chapter will summarise the contributions of this thesis and outline some possible future work. These future research efforts should include the actual real-time implementation of a CML system for an AUV.

Chapter 2

Solving the Localisation Problem

Research on robot *proprio*-localisation has been significant in the last decade. The most significant efforts aim to achieve this goal by means of *Concurrent Mapping and Localisation (CML)*. These strategies have received a great deal of attention, mainly by the indoor robot community. In section 2.1, the most significant efforts will be detailed. The chosen CML method of this thesis is the *stochastic map*. The reason for this will also be made clear. All CML strategies must explore the environment in order to build a suitable map to localise a robot. In an underwater environment the sensor used to explore the environment will have great relevance in the performance of a CML system. The choice of sensor will always be open for discussion and Section 2.2 will provide an insight into which sensors are most suitable in an underwater environment to achieve the thesis objectives. Along with the most important features of the sensors, the benefits and limitations will also be detailed. The thesis has opted to use forward-looking sonar. Section 2.3 will thus illustrate the design of a stochastic map using a forward-looking sonar. Some additional theoretical properties that make the stochastic map desirable will be examined in section 2.4. The chapter will close by clearly identifying the aims and objectives of the thesis, highlighting the contributions which will be achieved in this field by meeting the specified requirements. The last section will outline the structure of the thesis.

2.1 Concurrent Mapping and Localisation

Much work has been published on mapping for localisation. Most of the work has been preoccupied with indoor robotics. A comprehensive review can be found in [12]. A good understanding of the work carried out in such an environment is

essential as the tasks share similar problems. The CML task has been interpreted in different ways by this community. These interpretations have been dictated by both the sensor used to construct the map and the degree of accuracy required for the localisation and/or mapping task. Initially two types of maps were defined: *grid maps* and *landmark maps*. A grid map normally divides a Cartesian space into equally spaced cells, where each cell represents a certain space in the world. A cell will be empty if its corresponding space in the world is empty and full if there is an object. Landmark maps identify and localise features of the environment which are then used as beacons by the robot.

Two further distinctions can be made in terms of the robot's perception of the world and how it can localise itself in it. A robot can envisage the problem of localisation as a place recognition problem, *topological maps*, or as a metric problem where the need for accurate tracking of the robot's Cartesian coordinates is required, *geometric maps*. These distinctions are perhaps more relevant for the ensuing discussion. In the following section 2.1.1 the reader will be introduced to the theory and reasoning behind the conventional topological map. Section 2.1.2 will outline the most significant work related to geometric maps. Recent years have also seen the development of *hybrid maps*. These will be explored in section 2.1.3. The research efforts realised to localise UUVs will be outlined in section 2.1.4. This thesis has opted for a geometric map of landmarks. The reasons for this choice will be made clear in section 2.1.5.

2.1.1 Topological Maps

These maps have been extensively developed for indoor localisation applications. Early work [70] used competing low-level navigating behaviours to map the environment. These behaviours would be initiated to react to environmental changes. Navigation using these behaviours resulted in wall tracing. The algorithm then sensed the environment and learned large-space structures, in this case left wall, right wall and corridor. These would constitute nodes in a two dimensional topological map of the environment and would be joined by links if it was physically possible to traverse from one to the other. A similar approach was developed in [58]. How-

ever, this strategy used the topological maps to extract the geometry of the local workspace so that the robot could localise itself with respect to any of the distinctive places identified in the workspace. The geometry was thus continuously extracted and averaged to minimise the metrical error. This approach, however, could not be considered a hybrid approach as the robot did not maintain an absolute estimate of its own position, but a relative estimate with respect to the nodes in the topological map.

Subsequent work compiled Markov chains from *existing* topological maps [18, 49, 83, 93, 105]. Although this approach did not allow the mapping of new environments it provided a framework for localising robots within buildings given large sensing and dead-reckoning uncertainty. The Markov chain maintains the position and orientation of the robot in terms of probability distributions over the states of the Markov Chain. The information is updated using Bayes' rule as the robot explores the workspace, and the new update is only dependent on the previous robot state. The robot is controlled by associating actions to each Markov state. At each update of the Markov chain the total probability mass for each action is calculated, and the action with the highest probability mass is executed.

Probabilistic methods have subsequently been improved also to perform CML [90, 107]. The new technique, known as the *Baum Welch* or *alpha beta algorithm*, alternates between two steps: the expectation step and the maximisation step. In the expectation step, the robot's position through time is estimated as the normalised product of the α and β probabilities. In this step, α is computed using the Markov localisation approach. The β value is analogous to α, but backwards in time. The expectation step thus provides an estimate of the robot's locations at various points in time. The maximisation step computes the most likely map based on the probabilities computed in the expectation step. The Baum Welch algorithm is a batch processing algorithm and the computation time can become prohibitive.

Neural-networks methods have also been developed for CML purposes. A good example is [45] a method that relies heavily on video information. This approach finds Cornered-centred Geometric Histograms (CGH) and uses these to build maps. The maps are in fact neural-networks consisting of three layers: a feature layer, an intermediate layer and a location layer. The network is known as Contextual

Layered Associative Memory (CLAM).

2.1.2 Geometric Maps

Geometric maps have been developed using either grids or landmarks. The attraction of grid maps methods is the fact that sensor fusion becomes a simple matter. Localisation using this type of approach is dependent on the processing of all the available data, making real-time mapping and localisation a real problem. To overcome some of these problems [91] developed a system which creates local maps which will be used for localisation by comparing them to an *a priori* obtained global map. The local maps are continuously being updated until they reach a limit in the amount of positional error that may have accumulated. At this point the *mature* maps are used for correction of the robot's position error, accumulated by dead-reckoning, and then they are discarded. This system allows for better memory management and, by regularly updating the position of the robot, it also allows for less positional errors. The aforementioned method is improved in [120] by including a means for mapping the environment as well as localising the robot. In this system, the mature maps are not discarded but are used to form a map of the vehicle surroundings. The vehicle maps the room by moving towards frontiers, which are regions of explored territory adjacent to unexplored territories.

As with topological maps Markov localisation has also been developed within the grid map framework. In this case the states of the Markov chain are the discrete cells of the map itself [16]. The advantages of this approach over its topological cousin are that it provides accurate position estimates of the robot's position. The disadvantage of using this approach is the added number of possible discrete states, which results in an added computational burden. To counter this, the dynamic Markov localisation approach was subsequently developed [15]. In this approach the map is an octree representation of the state space, permitting the refinement according to the degree of belief, thus focusing on the relevant part of the state space. A further development, termed Monte Carlo localisation, represents the density by a set of samples or particles drawn from it [30, 108]. This is possible because the density can be approximately reconstructed from these samples. The algorithm works

by sampling the density and applying the robot's motion model in the prediction step. In the update step the samples are weighted by the likelihood of the state (of the sample) given the observation. The new samples are used to approximate the new density, which will be used in the next iteration of the algorithm. The algorithm can be updated in $O(N)$ time, where N is the number of samples. This approach was used experimentally in [55] to compare the performance of different landmarks; sonar triangulation-based landmarks [114] and laser extracted line and door landmarks.

The grid-based solutions to CML presented above can be used to incorporate complex density distributions. However, the computational burden incurred in processing all the data has led a large part of the robotics community to research geometric landmark maps. The *stochastic map* can be thought of as the forefather of the Kalman based approaches [99], where the motion and observation models densities are assumed Gaussian. This approach provides a simple method for incorporating newly observed landmarks into the map, whilst also maintaining the robot-to-landmark and the landmark-to-landmark correlations. In the stochastic map the landmarks (referred to as *features* in some of the literature) can either be natural (rocks, trees, ...) or artificial (doors, beacons, ...). Systems that perform this type of mapping have been developed with a variety of sensors. A successful implementation [64] reports a system which uses returns from a Polaroid sonar to identify cylinder, planar and corner landmarks. The method they used to identify the landmarks is termed as *Regions of Constant Depth* (RCD). These landmarks are subsequently tracked by means of an EKF with a single state vector holding the vehicle and landmark states. The data association problem is simplified by taking into account only landmarks which have been successfully tracked for a given number of samples. Vision systems have also been proposed. In [29] a camera acquires corner features. These corner features constitute a set the landmarks that have been successfully used to develop a stochastic map. In [19] a system which fuses information from both a CCD camera and a laser range finder is described. The laser range finder identifies corners and semi-planes while the vision system finds vertical edges. These landmarks are fused by means of the χ^2 compatibility measure based on the squared Mahalanobis distance D^2 and incorporated into the stochastic

map. The problem associated with these approaches is that as the number of landmarks increases, the computational burden increases in $O(N^3)$ time, where N is the number of states in the filter. This has motivated a number of research groups to decouple the filter, effectively ignoring the correlations. Some of these efforts have yielded good approximations of the full stochastic map. The most relevant of these are the *covariance intersection* [112, 118] and the *decoupled stochastic map* [36]. These efforts show promising results. However, they are approximations to the full map, and some recent telling work shows that ignoring the correlations can be very much counterproductive [20]. Another more recent effort, the *geometric projection filter* [82], achieves the performance of the stochastic map whilst simplifying the overall processing. This implementation stores not the landmarks, but the relative distances between them. This implicitly takes into account the correlations without the need of the added computational burden. The system, however, requires that the relative distances between the landmarks can be observed with one view of the sensor.

Other than the above mentioned methods, researchers have also looked at further possibilities. For instance [69] combines a grid with a landmark approach for the purposes of outdoor localisation. The authors use stereo-vision data to create an occupancy grid of the environment. They then use this information to find a landmark in the environment, such as a rock. With this landmark they extract a polygon that fits round it. This is the feature that they will subsequently use for the purposes of localisation.

2.1.3 Hybrid Maps

Recent work has seen the development of topological maps where the nodes are represented by histograms of local geometric grid maps [34]. This type of approach attempts to extract precise position information and provide a solid framework for localisation. Each node has two histograms representing the x and y coordinate in Cartesian world coordinate. The robot maintains a set of hypotheses of its real position. As it moves and senses the environment, the observations are matched to the stored histograms, a new set of hypotheses is built, and the innovation is used

to update a Kalman filter storing the position of all the hypotheses. This system has been extended to map also new unknown nodes [35]. This new approach uses a neural network to predict which nodes might have links to other unexplored nodes. As the vehicle approached a potentially new node, it would scan the area and store the histogram description of the new node. Links in this instance had a distance and orientation measure relating the nodes. Consistency was kept by minimising an energy function built under the constraint that the distance and orientation between two nodes must be the same and opposite respectively.

2.1.4 Mapping and Localisation in Underwater Robotics

Much of the recent literature reports on techniques for mapping the sea floor. Most of the systems reported do not perform concurrent mapping and localisation. Typical techniques for mapping the sea bed are costly as they involve the deployment of ships. In the context of mapping in deep waters, not only the cost increases, but so does the engineering challenge as one must deploy UUVs. It is well known that sonar data depicts time events. The problem is converting from time information to spatial information. This requires navigation and bathymetry information. A reconstruction can be made by fusing the data provided by these sensors. In practice, optimising position accuracy represents a great challenge involving a number of surface vessels and subsea vehicle navigation systems and sensors.

One such technique is that used by the HUGIN UUV [53]. This system maps the sea bed using a Konsberg Simrad EM3000 multibeam echo sounder. The positioning of the UUV is achieved by means of integrating the inertial navigation readings with an absolute positioning measurement provided by an acoustic positioning system which communicates with a surface vessel. This vessel will be equipped with either Differential GPS or a Real-Time Kinematic Global Positioning System(RTK GPS). Mapping of the sea bed using such systems involves a considerable cost. The development of an inexpensive and yet reliable positioning system is therefore desirable. To achieve this goal one must break the existing link between surface vessels and UUVs. The published research aimed at achieving this goal is limited.

One of the earliest approaches was proposed in [43]. This effort demonstrates a

system that tracks point-landmarks by means of a single Kalman Filter. This system can deal with moving landmarks, both translating and rotating, and would be used to identify the position of a UUV. The system was demonstrated with encouraging simulation results.

Since then a number of different strategies have been proposed. Some of these have used *a priori* maps. An innovative approach towards terrain referenced underwater navigation which uses a map is reported in [67, 68]. This system deals with matching high resolution depth maps with a large, on-board, low resolution reference map. The algorithm uses *cliff maps* which are steep-gradient contours extracted from both the local and the reference maps. These maps allow for the extraction of critical points which are defined as high curvature values. The navigation problem is reduced to a point-based matching algorithm. In order to deal with differences in scale, a scale space technique is employed. The sensor used is a SIMRAD-EM12 multibeam echo-sounder bathymetric sonar. The results shown are promising, but the need of a reference map does not allow this type of system, as it stands, to be employed in exploratory missions. The latest results are reported in [96].

Another approach which matches returns from a sonar to a high resolution on-board map is that presented in [31]. Here a bathymetric profile is compared to a depth map by means of a *coarse-to-fine* image matching algorithm. Once the best match is found a validation gate is placed around the position estimate based on the navigation uncertainty. A *Probabilistic Data Association Filter with Amplitude Information* (PDAFAI) [65] is then used to probabilistically weigh each good match that lies within the validation gate. Simulation results show that the system can perform well over regions with high bathymetric variability.

Several vision based approaches have also been reported [52, 80, 118]. These approaches build a mosaic from a video sequence and then make use of this mosaic to navigate. As with any vision system, these methods are heavily constrained by the environment in which they operate, and poor visibility and murky waters will limit their applicability. These approaches present reasonable results obtained in test tanks. Another major constraint is that the memory requirements for storing a mosaic of a significant size might prove prohibitive.

Inspired by some of the earlier work on tracking [59] by the Ocean Systems

Laboratory, a navigating system has been developed which can localise the vehicle by observing the *acoustic flow* of a sequence of sonar scans. The research reported in [27] shows good results. This type of approach requires fast image updates which a forward-looking mechanically scanned sonar will not be able to produce. The author's experience also shows that it is very expensive in terms of CPU processing time, and for real-time operation, specialised hardware will be essential. One must also note the fact that this system does not create a map and it, therefore, behaves as a dead-reckoning sensor.

Some efforts to develop CML algorithms have been developed and tested in water tanks. A good example is the system demonstrated in [98] which uses separate Kalman filters for the landmarks and vehicle states. The system has been termed as a *bounded filter*. The different filters are designed so the equations take into account the inter object correlations. The sensor used is an Echo Sounder mounted on a pan and tilt. The sonar is directed to a target and it performs tracking on this single target. If the target is lost it is mapped for future reference. Results are very promising although limited, as only a single target can be tracked.

To the author's knowledge only two efforts have made the journey from the tank to the sea. The first effort was carried out using an approximation to the stochastic map [17]. This effort used a forward-looking sonar developed by the Naval Underwater Warfare Center Division Newport. The data was obtained by fitting a suite of sensors over the side of a surface craft. These sensors were at approximately 5.5 metres depth. The sensors included an INS, a DVL and updates from a DGPS. These sensors were used to assess the output from the CML algorithm. The same data set was later used to test a full stochastic map implementation [63]. The other effort [116] was the result of work carried out off the coast of Sydney. In this effort the ROV Oberon was deployed in a natural inlet and artificial targets were used to simplify the landmark extraction process. This effort has been the first to be tested with data gathered from a UUV. Ground truth was not available at the time of the experiment and the validity of the results remains to be verified.

2.1.5 Summary of CML Methods

The decision on which CML strategy to adopt will depend on many factors. Of these the most important factors to take into account will be the type of missions that are to be carried out by the autonomous agent (be it a robot or an AUV) and the environment in which those missions will take place. Other factors, such as hardware requirements, should be relaxed and *where possible* should be dictated by the chosen CML strategy and not vice-versa. Two questions must then be answered to decide on the strategy,

- Which are the most common missions that an AUV will carry out?
- Which environments are an AUV most likely to encounter?

Given the relative infancy of AUV development the first of these questions has not yet been answered by the underwater community. Most of the current efforts suggest that surveys are the most likely missions for these vehicles. Survey missions require high precision positional information. Whether the interest lies in surveying a minefield, the coast or oceanographic phenomena, the UUV is required to know its own position with enough accuracy as to provide the ensuing survey a certain degree of adequacy. Geometric maps should provide the degree of accuracy required. Further, most of the world's sea bed is still largely unexplored and to characterise it will be no easy task. The use of topological maps requires either large structures or places to be characterised *a priori*. This task will be hard if not impossible to implement for most AUV missions. The choice of which geometric map to use will be dictated by hardware capabilities. Storing a grid map will not be difficult to achieve. In the case of a bathymetric surveys it is commonly done. However, to *consistently* process this map and localise the vehicle within it will be *impossible* given the duration of typical missions, several kilometres, and the available processing hardware. Landmark maps, on the other hand, present an elegant manner of compressing the information and can be used by the AUV to perform CML. Of the geometric CML strategies that use landmarks the most popular approach has been the stochastic map. It will thus make sense to adopt this strategy for the purpose of this thesis.

2.2 Underwater Mapping Sensors

The choice of sensor to be used for constructing a stochastic map will, amongst other things, directly affect: the precision, update rate and span of the observable environment. In water, acoustic sensors have proved by far the most popular choice. Electromagnetic waves attenuate far more rapidly and the working range for this type of sensors is greatly reduced. Although cameras and lasers are extensively used for certain applications, their working ranges are typically well below five meters and their functionality is seriously affected in adverse circumstances, such as murky water. This has not deterred a number of researchers and, recently, great effort has focussed on this field. The following tasks have been examined: feature tracking [109]; pipe-line following [14, 37, 121]; photomosaicing [41, 94]; 3D reconstruction [87]; object recognition [86] and laser triangulation [21].

Sonar (SOund Navigation And Ranging) is an acoustic sensor used for sensing the environment. Sonar sensors can be divided into two main categories: *passive* and *active*. The passive sonar is a very sophisticated apparatus which senses acoustic energy in the environment. The active sonar emits pulses of acoustic energy which will be reflected back to the sonar as they collide with surfaces within the sonar's range. Passive sonars are mainly used in military applications, *stealth* being a major constraint for this type of operation. Active sonars are used in a wider range of applications such as charting or surveying for the offshore oil industry.

Given the physiognomy of the sea bed and the task at hand, that of localising an underwater vehicle, sonar is the most appropriate choice for sensing the surroundings. This can be explained in the context of localisation. Certain landmarks which can be tracked as the vehicle moves must be found in the scene. Having then found the relative position of these landmarks with respect to the vehicle, finding the position of a vehicle is a matter of reverse engineering (providing the landmarks remain in the same position in the environment). The problem with the sea bed is that, due to the erosion caused by the constant friction between the surface and the water, it is over vast areas absent of landmarks. This being the case, the longer the range of a sensor, so that it can find landmarks to lock on to (such as rocks, coral reefs, or even man-made structures), the more suitable the sensor.

Having established that sonar is the best option for our purposes, the most common types of active sonars available will now be listed and also explained. A reasoned argument as to why the *forward-looking* option has been chosen will also be given. Note that the terminology used below is not always upheld by the rest of the community. For instance a *forward-looking* sonar is sometimes also referred to as a *sector scanning sonar*.

2.2.1 Echo Sounder Sonar Transponder

This is the most common and widely available commercial sonar. This sonar emits a pulse at a given frequency, the pulse reflects on a surface and is reflected back to the receiver unit of the sonar. By working out the time gap between the emission and the reception of the pulse, the distance between that surface and the sonar can be found. Normally, this type of sonars are used in boats or UUVs for finding the distance from the sea bed to the lowermost part of the vehicle.

2.2.2 Side-scan Sonar

This is an acoustic imaging device, which is towed by a survey vessel, to provide wide-area images of the sea bed. The images are generated in sequence as the acoustic energy is transmitted to the side of the sonar, and the sound which is reflected back is used to create an image. For a better description of this type of sonar the reader is referred to [8]. Side-scan sonar has been used as a tool for mapping in many commercial applications. Slant-range and geometric corrections of images can be used as a means for working out the position of a vehicle, but too many constraints are placed in such systems, such as the assumption of a flat sea bed.

2.2.3 Bathymetric Sonar

Also known as a *Multibeam Echo Sounder*, this sonar is similar in operation to the Echo Sounder Sonar Transponder, except that it uses an array of hydro-phones which allows for multiple beams, as opposed to a single one. The result is a profile (cross-section) view of the sea bed. This type of sonar is commonly used to build maps.

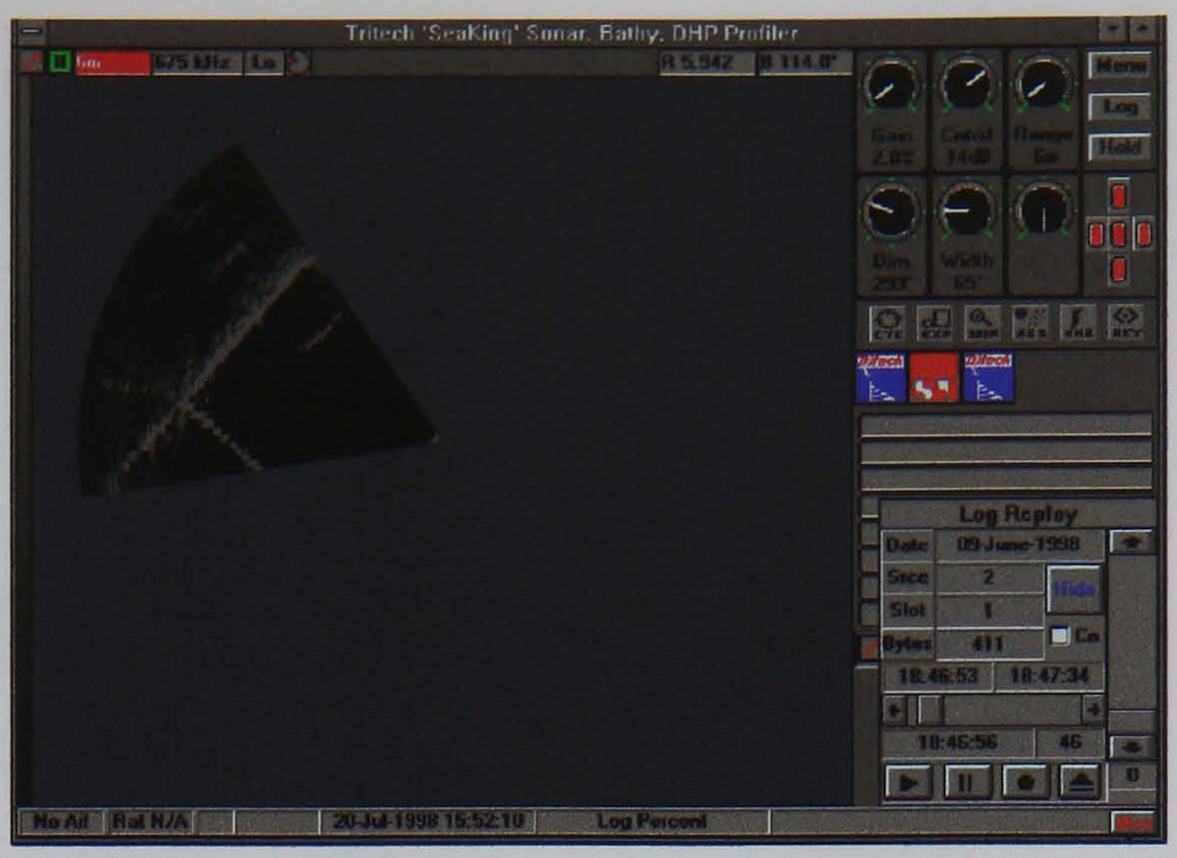

Figure 2.1: Forward-looking mechanically scanned sonar image, obtained with a SeaKing DFS, in the Ocean Systems Laboratory

2.2.4 Forward-looking Mechanically Scanned Sonar

This active sonar has a variety of applications, such as obstacle avoidance, mid-water mine detection and surveillance. The sonar consists of a single hydro-phone which is mechanically scanned along the horizontal axis. The returns from this sonar are then used to create an image. Most systems provide the user with the option of choosing the size of the sector they would like to scan and some degree of control on the resolution. In most cases higher resolution results in a slower refresh rate. Typical ranges are up to 200m, but this can be altered by the user. Again a longer range will also result in a slower refresh rate. The major advantage of this type of sonar is its apability to detect objects or sea bed features, such as protruding rocks, at large distances. These can be observed in subsequent scans and tracked, providing the UUV is moving at slow speeds. Another advantage is its price when compared to its more advanced *cousins* described bellow. Figure 2.1 shows an image obtained with the SeaKing Dual Frequency Sonar (DFS).

2.2.5 Forward-looking Multibeam Sonar

This type of sonar uses a fixed array of hydro-phones which allows for much faster updates of sectors (e.g. the Seabat 6012 can update a sector 30 times a second). These sonars are around ten times more expensive than mechanical systems. This has meant that their mechanical *cousin* has remained a more popular choice within the subsea technical community. Figure 2.2 shows an image obtained with the

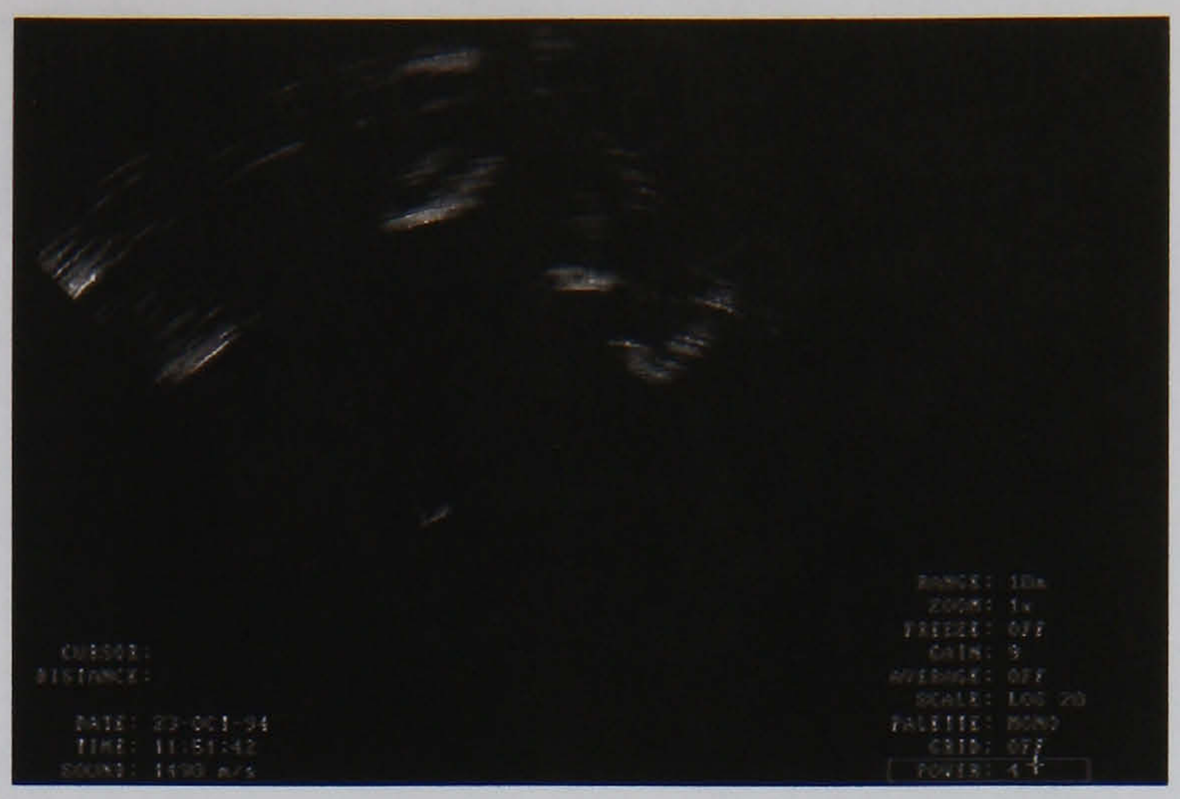

Figure 2.2: Forward-looking multibeam sonar image, obtained with a Seabat 6012, at a pier off the coast of Oban

Figure 2.3: 3D Acoustic camera image of an oil rig, obtained with an EchoScope 1600. *Figure courtesy of Omnitech*

Seabat 6012.

2.2.6 3D Acoustic Cameras

This type of sensor has recently been made available in the shape of EchoScope 1600 [44]. This sensor allows 3D data visualisation as it uses a 2D array of hydrophones. The cost of the sensor (latest figures stand at almost three times the cost of a Multibeam forward-looking sonar), its weight (40 kgs in air) and its size makes it prohibitive for certain applications, especially those involving AUVs. Figure 2.3 shows an image obtained with the EchoScope 1600.

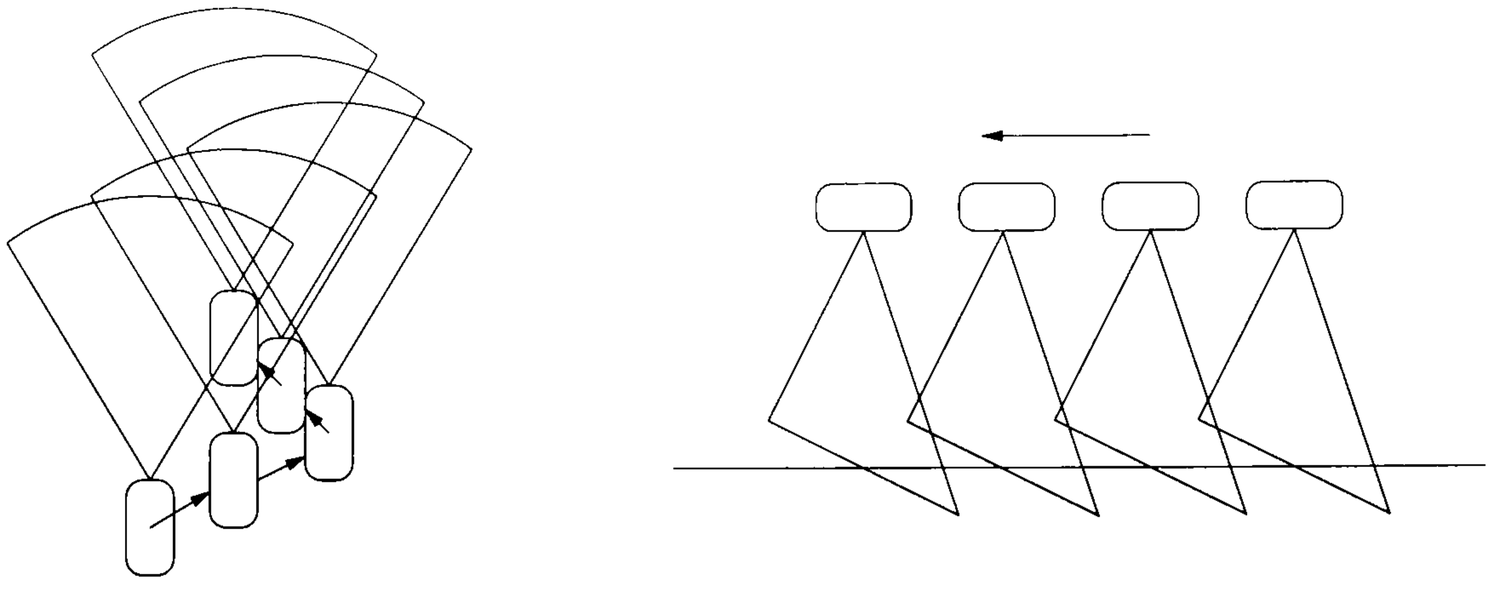

a) As Vehicle moves forward the areas covered by the sonar overlap.

b) No overlap occurs when using a bathymetric or a side-scan sonar.

Figure 2.4: Forward-looking and downward-looking sonars

2.2.7 Why Use a Forward-looking Sonar?

The advantage of using a forward-looking sonar is that it allows the user to scan an area ahead of the vehicle, which in successive frames, might be overlapped. This helps considerably the CML process, see Figure 2.4 (a). Side-scan and bathymetric sonars build a map of the sea floor as the UUV travels over the sea bed. Corrections to the output bathymetry or image are normally made by using positional information from an INS system, but there is no overlap, see Figure 2.4 (b). This will mean that the vehicle must have an *a-priori* built map of the area if it desires to perform localisation using this type of sonar. Alternatively it would have to re-observe the workspace a significant number of times.

This thesis will thus demonstrate CML using forward-looking sonars. Mechanically scanned sonars are of smaller size and weight and their reliability is proven. The problems associated with the mechanically scanned sonar is its slower update. Current ROV speeds (around 1.5 knots) are sufficiently slow for the mechanically scanned sonar update rate not to be a hindrance. However, predicted speeds for AUVs will surely lead the way to the use of multibeam sonars.

The following section examines the stochastic map for the case range and bearing observations typical of a sonar. It is meant to provide an introduction for the reader.

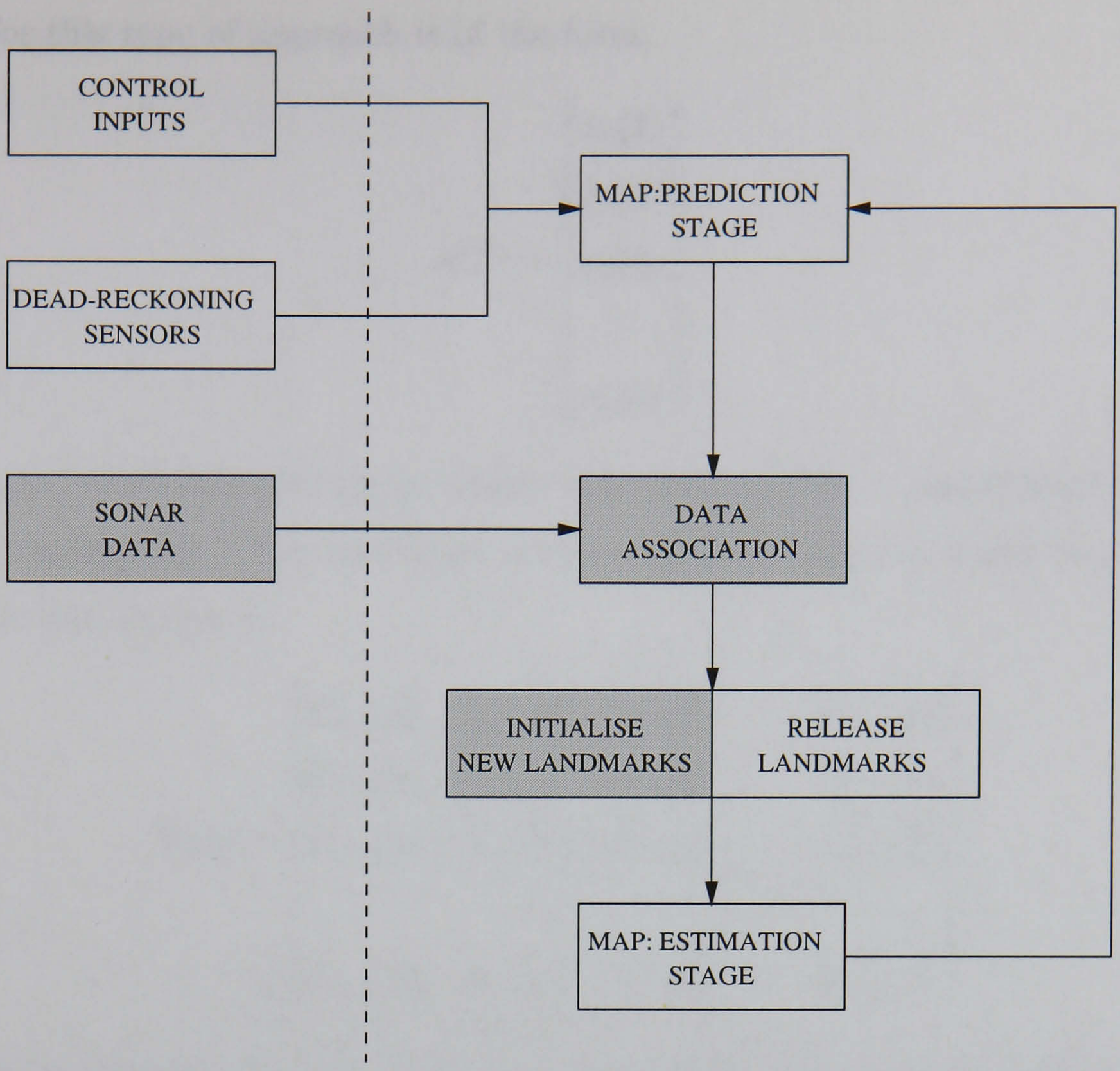

Figure 2.5: Overview of the stochastic map algorithm

2.3 Stochastic Mapping

The stochastic map was first introduced by R. Smith, M. Self, and P. Cheeseman [99]. It is a tool which allows concurrent mapping of landmarks and localising a vehicle with respect to these landmarks using an EKF architecture, see appendix A. The stochastic map is essentially an augmented extended Kalman filter, where the observed landmarks states are stored in the filter's state vector along with the vehicle states. A typical underwater implementation of a 2D stochastic mapping and localisation algorithm will closely resemble figure 2.5.

The success of this approach lies in the fact that the correlations between all the landmarks and the vehicle are stored and maintained by the filter. A typical state

vector for this type of approach is of the form,

$$\mathbf{x}(k) = \begin{bmatrix} \mathbf{x_v}(k) \\ \mathbf{x_1}(k) \\ \mathbf{x_2}(k) \\ \vdots \\ \mathbf{x_n}(k) \end{bmatrix} \tag{2.1}$$

where $\mathbf{x_v}(k)$ holds the state of the vehicle and $\mathbf{x_1}(k), \mathbf{x_2}(k), \ldots, \mathbf{x_n}(k)$ hold the states of the n landmarks. The estimated error covariance (approximated mean-square error) for this system is,

$$\mathbf{P}(k) = \begin{bmatrix} \mathbf{P_{vv}}(k) & \mathbf{P_{v1}}(k) & \mathbf{P_{v2}}(k) & \ldots & \mathbf{P_{vn}}(k) \\ \mathbf{P_{1v}}(k) & \mathbf{P_{11}}(k) & \mathbf{P_{12}}(k) & \ldots & \mathbf{P_{1n}}(k) \\ \mathbf{P_{2v}}(k) & \mathbf{P_{21}}(k) & \mathbf{P_{22}}(k) & \ldots & \mathbf{P_{2n}}(k) \\ \vdots & \vdots & \vdots & \ddots & \vdots \\ \mathbf{P_{nv}}(k) & \mathbf{P_{n1}}(k) & \mathbf{P_{n2}}(k) & \ldots & \mathbf{P_{nn}}(k) \end{bmatrix} \tag{2.2}$$

where the submatrices $\mathbf{P_{vv}}(k)$, $\mathbf{P_{vi}}(k)$ and $\mathbf{P_{ii}}(k)$ are the vehicle-to-vehicle, vehicle-to-landmark and landmark-to-landmark covariances respectively.

The reader will now be guided through the different steps followed by the algorithm to achieve its goal.

2.3.1 Prediction Stage

Prediction of Vehicle State

The equations used to update the vehicle state and its associated covariance are those used in the EKF, i.e. equations A.21 and A.22. Stochastic mapping assumes fixed landmarks and the resulting state transition will be obtained from,

$$\hat{\mathbf{x}}_\mathbf{v}(k) = \mathbf{f_v}[\hat{\mathbf{x}}_\mathbf{v}(k-1), \mathbf{u}(k), \mathbf{0}, k] \tag{2.3}$$

where $\hat{\mathbf{x}}_\mathbf{v}(\cdot)$ is the vehicle's state and $\mathbf{f_v}[\hat{\mathbf{x}}_\mathbf{v}(\cdot), \mathbf{u}(k), \mathbf{0}, k]$ is the vehicle's dynamic model. The transition model uses deterministic control input functions $\mathbf{u}(k)$ if available. These functions are normally the output's from the vehicle controller (thrust values, voltages, currents, ...).

Its associated covariance, strictly speaking the approximated mean-square error as $\hat{\mathbf{x}}(k)$ is not the exact conditional mean, is obtained as follows,

$$\mathbf{P}(k) = \mathbf{E}[\tilde{\mathbf{x}}(k)\tilde{\mathbf{x}}'(k)] \tag{2.4}$$

where $\tilde{\mathbf{x}}(\cdot)$ is the error in the estimate, which will be equivalent to the true state, $\mathbf{x}(k)$, minus the estimate, $\hat{\mathbf{x}}(k)$, i.e.

$$\tilde{\mathbf{x}}(k) = \mathbf{x}(k) - \hat{\mathbf{x}}(k) = \mathbf{f}_{\mathbf{x}}[\mathbf{x}(k-1), \mathbf{u}(k), \mathbf{w}(k), k] - \mathbf{f}_{\mathbf{x}}[\hat{\mathbf{x}}(k-1), \mathbf{u}(k), \mathbf{w}(k), k] \tag{2.5}$$

where the true state can be defined as

$$\mathbf{x}(k) \approx \begin{bmatrix} \mathbf{f}_{\mathbf{v}}[\hat{\mathbf{x}}_{\mathbf{v}}(k-1), \mathbf{u}(k), \mathbf{0}, k] + \mathbf{F}_{\mathbf{x}_{\mathbf{v}}}(k-1)\tilde{\mathbf{x}}_{\mathbf{v}}(k-1) + \mathbf{F}_{\mathbf{w}_{\mathbf{v}}}(k-1)\mathbf{w}(k-1) \\ \mathbf{x_1}(k) \\ \vdots \\ \mathbf{x_n}(k) \end{bmatrix} \tag{2.6}$$

where $\mathbf{F}_{\mathbf{x}_{\mathbf{v}}}(k-1)$ is the Jacobian of the vehicle model with respect to the vehicle state, used to linearise the state of the vehicle error $\tilde{\mathbf{x}}_{\mathbf{v}}(k-1)$, and $\mathbf{F}_{\mathbf{w}_{\mathbf{v}}}(k-1)$ is the Jacobian of the vehicle model with respect to the process noise. The prediction can be shown to be

$$\hat{\mathbf{x}}(k) \approx \begin{bmatrix} \mathbf{f}_{\mathbf{v}}[\hat{\mathbf{x}}_{\mathbf{v}}(k-1), \mathbf{u}(k), \mathbf{0}, k] \\ \hat{\mathbf{x}}_{\mathbf{1}}(k) \\ \vdots \\ \hat{\mathbf{x}}_{\mathbf{n}}(k) \end{bmatrix} \tag{2.7}$$

therefore $\tilde{\mathbf{x}}(\cdot)$ is found to be

$$\tilde{\mathbf{x}}(k) \approx \begin{bmatrix} \mathbf{F}_{\mathbf{x}_{\mathbf{v}}}(k-1)\tilde{\mathbf{x}}_{\mathbf{v}}(k-1) + \mathbf{F}_{\mathbf{w}_{\mathbf{v}}}(k-1)\mathbf{w}(k-1) \\ \tilde{\mathbf{x}}_{\mathbf{1}}(k) \\ \vdots \\ \tilde{\mathbf{x}}_{\mathbf{n}}(k) \end{bmatrix} \tag{2.8}$$

from which it follows that,

$$\mathbf{P}(k) = \begin{bmatrix} \mathbf{F_{x_v}}(k-1)\mathbf{P_{v\,v}}(k)\mathbf{F'_{x_v}}(k-1) & \mathbf{F_{x_v}}(k-1)\mathbf{P_{v\,1}}(k) & \dots & \mathbf{F_{x_v}}(k-1)\mathbf{P_{v\,n}}(k) \\ \mathbf{P_{1\,v}}(k)\mathbf{F'_{x_v}}(k-1) & \mathbf{P_{1\,1}}(k) & \dots & \mathbf{P_{1\,n}}(k) \\ \vdots & \vdots & \ddots & \vdots \\ \mathbf{P_{n\,v}}(k)\mathbf{F'_{x_v}}(k-1) & \mathbf{P_{n\,1}}(k) & \dots & \mathbf{P_{n\,n}}(k) \end{bmatrix}$$
$$+ \begin{bmatrix} \mathbf{F_{w_v}}(k-1)\mathbf{Q}(k)\mathbf{F'_{w_v}}(k-1) & \mathbf{0} & \dots & \mathbf{0} \\ \mathbf{0} & \mathbf{0} & \dots & \mathbf{0} \\ \vdots & \vdots & \ddots & \vdots \\ \mathbf{0} & \mathbf{0} & \dots & \mathbf{0} \end{bmatrix} \tag{2.9}$$

Prediction of Landmark States

For a vehicle using a sonar, essentially a range sensor returning range and angle with respect to the vehicle frame, the observation vector for a single landmark will be $\mathbf{z_i}(k) = [r \;\; \theta]'$. The full observation landmark vector will be of the form,

$$\mathbf{z}(k) = \begin{bmatrix} \mathbf{z_1}(k) \\ \mathbf{z_2}(k) \\ \vdots \\ \mathbf{z_n}(k) \end{bmatrix} \tag{2.10}$$

The prediction for landmark $\mathbf{x_i}(k)$ will be,

$$\hat{\mathbf{z}}_\mathbf{i}(k) = \begin{bmatrix} \sqrt{\bar{x}_i(k)^2 + \bar{y}_i(k)^2} \\ tan^{-1}(\bar{y}_i(k)/\bar{x}_i(k)) + \phi_v(k) \end{bmatrix} \tag{2.11}$$

where $\phi_v(\cdot)$ is the orientation of the vehicle with respect to the world frame and $\bar{x}_i(\cdot)$, $\bar{y}_i(\cdot)$ are respectively

$$\bar{x}_i(k) = x_i(k) - x_v(k) \tag{2.12}$$

$$\bar{y}_i(k) = y_i(k) - y_v(k) \tag{2.13}$$

The coordinates with respect to to the world frame of landmark i and of the vehicle are $[x_i(k)\, y_i(k)]$ and $[x_v(k)\, y_v(k)]$ respectively.

Dead-reckoning Sensors

Vehicle state data can be incorporated as an independent observation of a vehicle state or states. The extended Kalman filter architecture allows such measurements to be readily incorporated. Dead-reckoning sensors include Doppler Velocity Logs (DVL), angular rate sensors (gyros), accelerometers, odometers, etc. Absolute sensor measurements, such as compasses, GPS fixes and acoustic positioning fixes, can also be accommodated. The first order measurement predictions in these cases will be made according to,

$$\hat{\mathbf{z}}_j(k) = \mathbf{h}_j[\hat{\mathbf{x}}_\mathbf{v}(k), k] \tag{2.14}$$

where $\mathbf{h}_j[\hat{\mathbf{x}}_\mathbf{v}(k), k]$ is a nonlinear function of the state, which models the behaviour of sensor j. The innovation is found according to

$$\upsilon_\mathbf{j} = \hat{\mathbf{z}}_\mathbf{j}(k) - \mathbf{z}_\mathbf{j}(k) \tag{2.15}$$

And the innovation covariance is

$$\mathbf{S}(k) = \mathbf{H}(k)\mathbf{P}(k)\mathbf{H}'(k) + \mathbf{R}(k) \tag{2.16}$$

where $\mathbf{H}(k)$ is a matrix that holds the Jacobian of the observation with respect to the predicted map state. Once the innovation has been calculated the new estimate is found by finding the filter gain, equation A.26, and implementing the extended Kalman filter estimate update, equations A.27 and A.28. This architecture assumes that the noise is white, Gaussian and unbiased.

2.3.2 Data Association

Not all landmarks will be observed by the vehicle at each iteration. Those which are observed must be associated to the landmarks on the stochastic map state vector $\mathbf{x}(k)$. This is known as data association. The stochastic map works under the assumption that new observations are associated to the correct landmarks stored in the map. The extent to which the map will be affected by errors in the data association can be considered as a function of the actual error and the certainty of the map's and vehicle's states. However, consistent errors in this module will eventually cause map divergence. The data association implemented in this thesis will be examined in detail in chapter 4.

2.3.3 Initialising New Landmarks

Observations that were not associated to an existing landmark will be added to the stochastic map state and covariance. The new observation $\mathbf{z_{new}} = [r \;\; \theta]'$ is estimated with respect to the vehicle's reference frame,

$$\mathbf{x_{n+1}}(k) = \begin{bmatrix} x_v(k) + r\cos(\phi + \theta) \\ y_v(k) + r\sin(\phi + \theta) \end{bmatrix} \tag{2.17}$$

The new map state and associated covariance will be

$$\mathbf{x}(k) \leftarrow \begin{bmatrix} \mathbf{x}(k) \\ \mathbf{x_{n+1}}(k) \end{bmatrix} \tag{2.18}$$

$$\begin{aligned} \mathbf{P_{n+1\,n+1}}(k) &= \mathbf{H_{\hat{x}_v}}(k)\mathbf{P_{v\,v}}(k)\mathbf{H'_{\hat{x}_v}}(k) + \mathbf{H_{z_{new}}}(k)\mathbf{R}(k)\mathbf{H'_{z_{new}}}(k) \\ \mathbf{P_{n+1\,v}}(k) &= \mathbf{P_{v\,n+1}}'(k) = \mathbf{H_{\hat{x}_v}}(k)\mathbf{P_{v\,v}}(k) \end{aligned} \tag{2.19}$$

where $\mathbf{L_{\hat{x}_v}}(k)$ and $\mathbf{L_{z_{new}}}(k)$ are the Jacobian of equation 2.17 with respect to the robot vehicle state $\mathbf{\hat{x}_v}$, evaluated at $\mathbf{\hat{x}_v}(k)$, and to the new observation $\mathbf{z_{new}}$, evaluated at $\mathbf{z_{new}}$. Given an observation it is thus possible to incorporate it onto the map following this simple procedure. The question that must be answered is which observations to consider. This will very much depend on the sensor being used. Such issues will be thoroughly examined in this thesis.

2.3.4 Releasing Landmarks

The deletion of a landmark $\mathbf{x_i}$ from the state vector, and corresponding rows and columns from the state covariance matrix, has no effect on the updates of the vehicle and other landmark states [32]. However, a landmark which has been removed must be reinitialised upon re-observation [32]. This property of the stochastic map can be used to limit the number of landmarks included in the state vector. By doing this the stochastic map can be computationally efficient. Research into successful strategies for releasing landmarks falls outside of the scope of this thesis. The version of the stochastic map implemented simply releases those landmarks which are not re-observed a sufficient number of times through a predetermined period of time (function of the sensor update rate). This ensures that noisy landmarks (not uncommon when using sonar) are released by the filter.

2.3.5 Estimation Stage

The new set of measurements is used to build a new estimate of the state of the stochastic map and its associated covariance. The algorithm maintains the correlations between the errors of the vehicle and all the landmarks. The new state estimate is found according to the following equation,

$$\hat{\mathbf{x}}(k+1) = \hat{\mathbf{x}}(k) + \mathbf{K}(k)\upsilon(k) \tag{2.20}$$

where $\mathbf{K}(k)$, the gain matrix, is found to be

$$\mathbf{K}(k) = \mathbf{P}(k)\mathbf{H}'(k)\mathbf{S}^{-1}(k) \tag{2.21}$$

The innovation matrix, $\mathbf{S}(k)$, is defined as

$$\mathbf{S}(k) = \mathbf{H}(k)\mathbf{P}(k)\mathbf{H}'(k) + \mathbf{R}(k) \tag{2.22}$$

where $\mathbf{H}(k)$ is a matrix that stacks the Jacobians of the observed landmarks with respect to the estimated map state. The stochastic map's covariance will be updated according to

$$\mathbf{P}(k+1) = \mathbf{P}(k) - \mathbf{K}(k)\mathbf{H}(k)\mathbf{P}(k) \tag{2.23}$$

2.4 Properties of the Stochastic Map

The structure of the stochastic map is such that all correlations between the uncertainties of the states are kept and maintained by the filter. Work by M. Dissanayake et al. [33] has highlighted a number of benefits obtained when implementing the stochastic map using linear models for both the vehicle and observation. These benefits are summarised by the following three theorems:

- Theorem 1: The determinant of any submatrix of the map covariance matrix decreases monotonically as observations are made successively.
- Theorem 2: In the limit, as the number of observations increases, the landmark estimates become fully correlated.
- Theorem 3: In the limit, given that $\mathbf{Q(k)} \neq \mathbf{0}$, the covariance associated with any single landmark location estimate is determined only by the initial covariance in the vehicle location estimate.

Proof for these theorems can be found in [33] and [82]. These theorems show the importance of maintaining the correlations between the states. In fact, as the vehicle progresses through the environment, the estimates between any pair of landmarks become more and more correlated. In the limit, the errors in the estimates become fully correlated. At this stage, if the exact position of any landmark is found, the location of any other landmark on the map can also be determined with absolute certainty.

2.5 Aims and Objectives

This thesis aims to,

Develop a framework for *enhanced* CML using forward-looking sonar for *consistent* AUV navigation.

In order to achieve this aim, the stochastic map strategy will need to be *enhanced*, essentially by working on the modules of the CML strategy shown by the shaded boxes in figure 2.5. The sonar data must be interpreted and then used to update the stochastic map. The data must be correctly assigned to the stored landmarks. The data association algorithm plays a fundamental part in this process. The properties of the stochastic map outlined in the previous section will only hold given perfect data association. Therefore improving the interpretation and data association capabilities will provide a robust CML strategy.

The definition of consistent is taken from the standard estimation theory definition [72]: "*... a solution that converges in probability to the true value of the variables as the number of sample elements grows without bounds*". The most common criteria for consistency are [6]:

- *"The state errors should be zero-mean (unbiased) and compatible with their covariance as yielded by the filter".*
- *"The innovations should have the same property".*
- *"The innovations should be white (uncorrelated in time)".*

To enhance the CML process so that the aforementioned properties will be maintained, when using a forward looking sonar mounted on an AUV, the work presented here has the following research objectives:

1. To develop a landmark state vector which, in addition to the landmark's coordinates, includes landmark descriptors.

2. To use the new landmark state vector to improve the data association process.

3. To demonstrate the enhanced CML capabilities using data obtained from a sonar mounted on a real AUV.

2.6 Summary

This chapter has provided the essential background for the understanding of the work done in this thesis. The most common CML strategies have been examined in section 2.1. This chapter has identified the stochastic map as the most suitable tool for CML in an underwater environment. The different sensors which can be adopted to observe the environment have been studied in section 2.2, and forward-looking sonars have been found to provide the appropriate range and span required for an underwater CML strategy to work. A typical stochastic map architecture designed to work with a forward-looking sonar was thus presented in section 2.3. The aim of this thesis will be to enhance the design of this architecture so that CML will be truly possible. The stochastic map is a well proven strategy, section 2.4. However, the interpretation of the sonar data must be better carried out and the data association strategies must be improved for CML to become a reality.

Chapter 3

Extraction of Descriptors from Landmarks

The stochastic map described in the previous chapter is used to concurrently build a landmark map of the environment and localise the vehicle. Landmarks are defined as stationary features of the environment. The sensor returns must therefore qualify as landmarks to be included in the map. This process will be referred to as *segmentation*. Segmentation of sonar data will be examined in section 3.3. The segmentation algorithm developed for this thesis will be outlined in section 3.3.2. The association of segmented landmarks to tracked landmarks is fundamental to the consistency of the stochastic map. The stochastic map is updated under the presumption that the innovations correspond to the right set of tracked landmarks. Errors in data association will, eventually, produce a divergent map. The data association can be significantly simplified by the right choice of landmarks. Section 3.4 will focus on the choice of landmarks and a set of descriptors assigned to these. Descriptors are nothing more than quantitative features. The chapter will then provide a full statistical analysis of the chosen descriptors that will demonstrate their discriminatory capabilities, section 3.4.3, and a thorough discussion in section 3.5.

3.1 Landmarks

The importance of finding reliable landmarks is stressed in [106]. Here a system is described which, given a few sensor snapshots of the environment, will work out which landmarks to use by means of a neural network, as long as the position at which the snapshots were taken is known. This segmentation algorithm has been termed Bayesian Landmark Learning. The choice of suitable landmarks emerges by minimising the localisation error. This innovative approach relies on *a priori* infor-

mation in the form of sensor snapshots of the environment. In fact, any landmark driven approach relies to some extent on *a priori* information. In most cases these landmarks will be tied to the sensor and the environment. For instance, when localising indoor robots using a camera, landmarks such as vertical edges are normally found to be good candidates [19, 79]. Given a sufficient vertical edge distribution in the workspace, CML will be implementable. The use of one specific landmark type will lead to a simpler data association scheme where the measurements can be assigned to an existing landmark, initialise a new landmark or be considered a false alarm.

Similarly, in [1, 78, 119] the landmarks of choice are lines along the horizontal axis, found with either scanning laser range finders or ultrasonic sensors. More complex representations of the workspace have also been proposed. These methods use different types of landmarks to represent the environment, relaxing the constraint on the density and distribution of one type of landmark. In [64] a Polaroid sonar sensor model was implemented to extract a set of landmarks: cylinders, planes, edges and corners. The method was coined *Regions of Constant Depth (RCD)*. The landmarks, commonly found in indoor environments and extracted using RCD, were used in a stochastic map. This choice of landmarks posed a problem in that the system had to decide first which type of landmark it was observing before the stochastic map could be updated. The data association algorithm therefore needed to decide if a measurement belonged to a mapped landmark or a new landmark and, in the case of the latter, which type of landmark. The data association thus requires a more complex strategy and, in most circumstances, added computational power. Nevertheless, many in the indoor robotics community have also extracted all, or a set, of these landmarks using different models and methods to the aforementioned RCD [2, 4, 25, 88].

A further level of abstraction is encountered when constructing topological maps. Landmarks in topological maps are distinguishable patterns. These maps are constructed with no metric information. However they are only made possible due to a good *a priori* understanding of the workspace. A usual representation consists of a graph where each node corresponds to a landmark. A node is linked to another if they are adjacent. An example would be a corridor leading to the door of a room.

The landmark corridor will be linked to the landmark door, but not to the landmark room behind the door. This method can be thought of as a *place recognition* problem. The approach is popular in indoor robotics, where places and their interfaces can be easily defined [3, 34, 49, 57, 58, 70, 93].

3.2 Underwater Landmarks

Most of the above landmarks do not lend themselves well to underwater environments. Man-made structures are uncommon and, if present, do not normally resemble those encountered indoors, unless the vehicle is inside or around a harbour. It is therefore necessary to find strategies for defining landmarks that can be implemented on natural terrain. This section will explore some of the existing strategies. Section 3.2.1 will look at work done on finding landmarks in bathymetric maps. These efforts reassert the importance of compressing data so that data association is simplified and data storage is manageable. Section 3.2.2 examines landmarks used in developing forward-looking CML maps. This section is directly relevant to the thesis due to the choice of sensor. The work done by the community will be examined. This review will lead the reader into the proposed solution.

3.2.1 Bathymetric Landmarks

Although work on terrain-based navigation using bathymetry normally attempts to find a match for the new contour by finding an appropriate function to compare it to a section of the bathymetric map [7, 11, 31, 67], some systems have also found landmarks to be convenient. Indeed [67] reports on a system which extracts landmarks from an existing bathymetric map and matches them to those extracted from a locally created map to estimate an AUV's position. The landmarks used in this case are created by applying a Laplacian-of-a-Gaussian filter and detecting the zero-crossings. These crosses are essentially the strongest intensity (depth) changes in the image. The outcome would generate a contour map. The landmarks were created by extracting the highest curvature points in the contours. Future work used all the points in the contour maps as landmarks [95, 96]. Features were also ex-

tracted from these points. The features represented differential attributes invariant to rotation and translation, namely: depth, Gaussian curvature, gradient norm and the Laplacian. The landmarks and features assigned to them were then fed to the matching algorithm for updating. The system thus ensures both; reduced storage capabilities, only the *a priori* processed landmark map and the newly formed local landmark map must be stored; and a simpler data association strategy.

3.2.2 Forward-looking Sonar Landmarks

Given the hardships, and prospective processing cost, in reliably modelling natural terrain, most research done with forward-look sonar has assumed point landmarks [36, 43, 116]. These landmarks are obtained by segmenting the highest returns from the sonar and applying geometric inversion to find their world reference map coordinates. The landmarks will thus be represented as a pair of coordinates. These approaches trade much of the information on the map for a reliable, if simplistic, landmark extraction approach. To our knowledge, only the efforts reported by B. Moran and R. Carpenter have attempted richer representations of the environment when using a forward-looking sonar. Both of these approaches will now be examined in detail.

Bradley Moran: Regions of Constant Depth

The RCD approach defines circular arcs as the basic features inherently found in sonar data. This choice take its roots in the underlying physics of echo formation and beam patterns. Smooth reflectors, reflectors whose surface heights are much smaller than the range wavelength of the emitted pulse, will reflect maximum energy at normal incidence with the emitter. This reflected energy will decay rapidly as the incidence angle is increased. For an incidence beyond half the beam-width of the sensor on a smooth surface it will be undetectable [13]. Thus, for a polar plot of a sonar scan incident on a smooth planar surface the returns will have constant range throughout the detected bearing span. The RCD provide bearing and range measurements which are combined to determine the location of targets. These targets are grouped with prior targets to form the landmarks.

Bradley A. Moran [76] extends the RCD approach by incorporating a new landmark; the sculpt. This landmark represents a free-form sculpted shape. This new descriptor allows the inclusion of natural-terrain features as landmarks for the filter. The downfall is the subsequent added complexity in the data association, which now has an extra landmark to contend with.

Robert Carpenter: Landmark Descriptors

The approach reported by Robert N. Carpenter [17] uses an electronically scanned multibeam sonar. The approach creates landmarks based on compact regions of high-level bottom scatter. The landmarks are subsequently characterised by geometric descriptors. These descriptors are the landmarks perimeter, area, area-to-perimeter ratio, and radial signature. For a description of area and perimeter the reader is directed to section 3.4.1. Area-to-perimeter ratio is self-explanatory. Radial signature is a graph of distance between the landmark's centre of mass and its boundary versus angle. This last descriptor, in fact, stores the shape of the object as a discrete one-dimensional string. These descriptors are used in conjunction with the landmark's coordinates to represent the environment and form the input into the data association.

The approach is similar to work done in the Ocean Systems Laboratory to classify sonar returns from a RESON Seabat 6012 sonar [23, 61]. The descriptors used then included gray-level descriptors, i.e. signal strength. However, a set of robust features which allowed for robust classification was subsequently identified and the gray-level descriptors were discarded [101]. Robert Carpenter's approach is also similar to the approach proposed in this thesis.

3.3 Segmentation of Landmarks

The process by which prospective landmarks are extracted from the sonar returns is commonly referred to as segmentation. This module will extract every possible landmark given a single sector scan of the sonar. These possible landmarks will be referred to as observations. They will serve as an input into the data association module which will then decide if the observation is in fact a landmark, and, if so, if

it originates from an existing landmark or if it is a new landmark. This will be discussed further in the next chapter. The choice of landmark is closely related to the environment and the sensor chosen to observe the environment. The choice of the segmentation process is related to both the environment and the landmarks themselves. For instance, while it will be sufficient for a robot in an office environment to extract visual vertical edges from camera input [79], this will not be appropriate for an underwater vehicle where the limitations of cameras are well understood and where there exists a distinct absence of structured visual edge features.

The choice of landmarks proposed in this thesis is inspired by experience in the Ocean Systems Laboratory in processing sonar data. The laboratory has built a good understanding of such data when developing a variety of implementations. Originally, as mentioned previously, the work was geared towards classifying sonar returns [23, 61, 101]. Since then, work has also been done for the purposes of tracking returns [102, 111], obstacle avoidance [85] and, more recently, on CML [103]. For all this work, compact regions of high-level bottom scatter, as used by R. N. Carpenter and discussed in the previous section, were found to be robust and sufficiently distinct. Other researchers have also used these landmarks when working with sonar returns. However these were not necessarily defined as landmarks. The terminology includes targets (in the field of mine-hunting), objects (in the field of classification) and obstacles (in the field of obstacle avoidance). The following section will examine the methods proposed by these researchers for the purposes of segmenting these returns. The method proposed in this thesis will be covered in section 3.3.2.

3.3.1 Literature on the Segmentation of Landmarks from Sonar Returns

Work on segmenting underwater sonar returns has received somewhat limited attention, focusing on two different approaches. The first of these divides the scene into three regions: echo, shadow and reverberation. This approach is favoured when attempting to reconstruct the bathymetry from an imaging sonar [122], although other applications include side-scan image fusion [28] and classification of the sea

bed [74]. The main motivation is that the echoes and, in particular, the shadow areas behind them can provide a good indication of the geometry of the scene. Figure 3.1 provides a simple diagram illustrating a sonar insonifying the scene. If the beam is thought of as composed of rays [8], the area behind the protruding regions of the scene will not be insonified. The size of the shadow and the intensity of the returns will be a function of the geometry and the physics of the scene. An example of this work can be found in [122]. The second approach, referred to as the *two regions approach*, divides the scene into two regions: echo and background. This approach has been developed mainly to work with forward-looking sonar, where shadows are not always present. The echoes are regions in the returns of higher intensity. Segmenting these regions is a integral part of any classification [101] or obstacle avoidance [48, 85] strategy.

The different approaches are motivated by the application. Whichever the aim, the algorithms used for segmenting the data share a common purpose: to separate the data into distinct regions. All of the algorithms can, therefore, easily adapt to either method. Most segmentation algorithms are preceded or followed by a low pass filter. Such procedure will now be examined along with the most common segmentation algorithms found in the literature to segment sonar returns.

Low Pass Filtering: The speckle noise present in sonar data comes from a variety of sources. These include sea-bottom scatter, surface returns and multipath. The interface between the sonar and the surrounding medium is still a subject of study and, although studies in air ultrasonics [13] and underwater sonar [8] have demonstrated considerable progress, many questions must still be answered. It is for this reason that sonar data is commonly low passed filtered, under the somewhat obvious, and not necessarily true, assumption that the noise is of higher frequency and uncorrelated. The tools for smoothing the data are various and well documented in the signal and image processing literature [40]. Popular methods include median, Gaussian and other smoothing filters. Another popular approach uses morphological operators on thresholded binary images. Finally the simpler of the approaches ignores regions according to their size, location or some other descriptor. Low pass filtering can be done before or after the segmentation process.

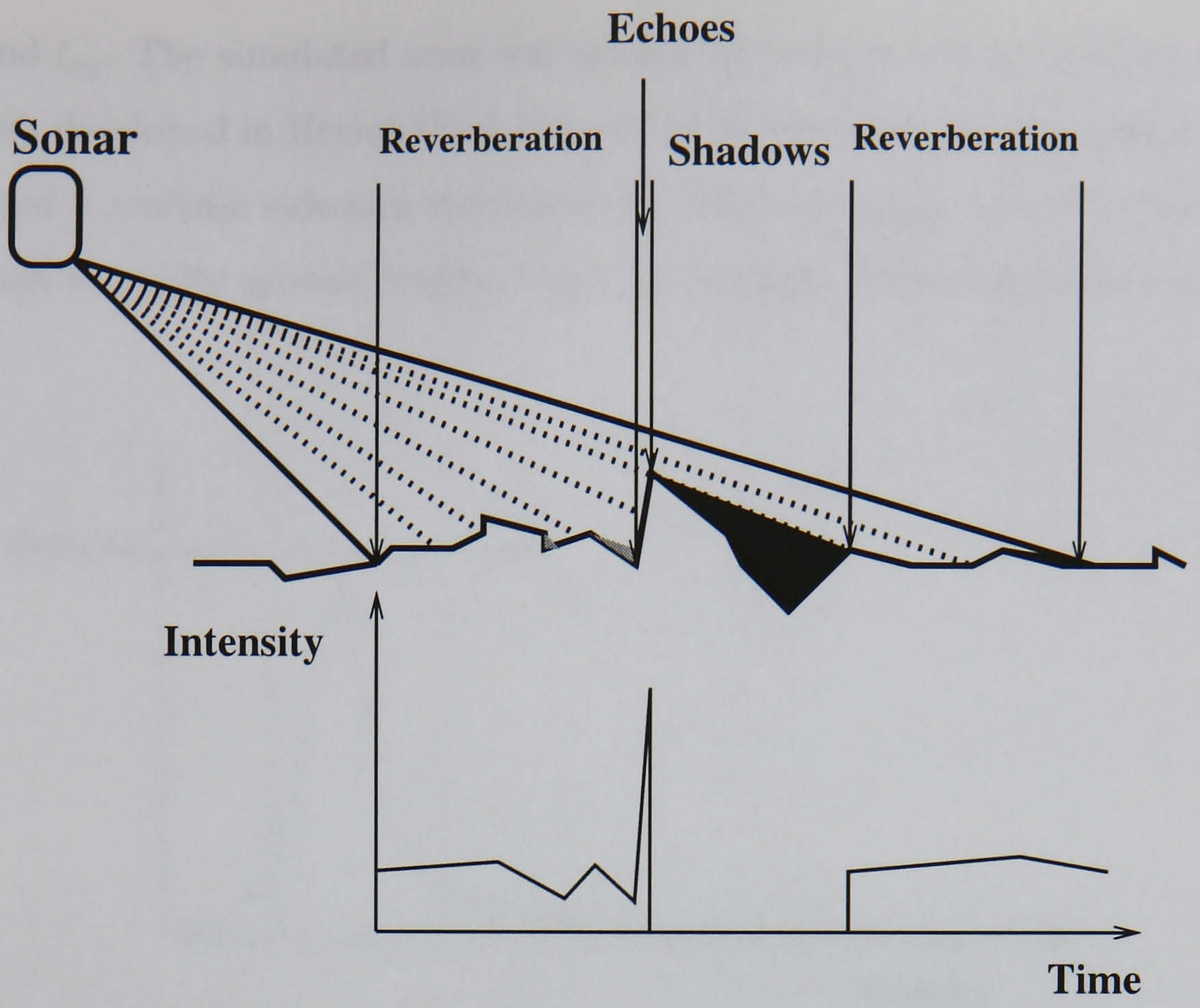

Figure 3.1: Simplistic diagram illustrating the side view of a sonar observing a scene and the resulting time-intensity return.

Thresholding: A well documented segmentation technique [40]. These implementations normally apply two thresholds when segmenting the scene into three regions, or one threshold if segmenting the scene into two regions. The shadow threshold t_s segments returns of a lower value as shadows and the echo threshold t_e segments returns of a higher value as echoes, see figure 3.3. These thresholds can be fixed *a priori* if the performance characteristics of the sonar and the type of scene are known. If this is not the case, histogram based techniques can be implemented to automatically adapt the thresholds. The assumption that only returns $> t_e$ are assumed to be part of a landmark is a weakness of this method. In some instances it will be necessary to segment regions $> t_{e_2}$, provided some of the returns in the connected region are $> t_{e_1}$. This technique is known as the double threshold algorithm. The implementation of thresholds for scene segmentation has proven popular due to their simplicity [28, 47, 48, 115, 122].

Figure 3.2 depicts a simulated scan and its associated histogram, with two possible thresholds t_{e_1} and t_{e_2}. Figure 3.4 depicts the outcome of the segmentation for both (a) the threshold algorithm, using t_{e_1} and (b) the double threshold algorithm,

using t_{e_1} and t_{e_2}. The simulated scan was generated using a forward-looking sonar simulator [9], developed in Heriot-Watt University, as an extension to previous work which created a realistic sidescan simulator [8]. The advantage of using this data is that it can be easily ground truthed and the Kalman filter consistency can be tested.

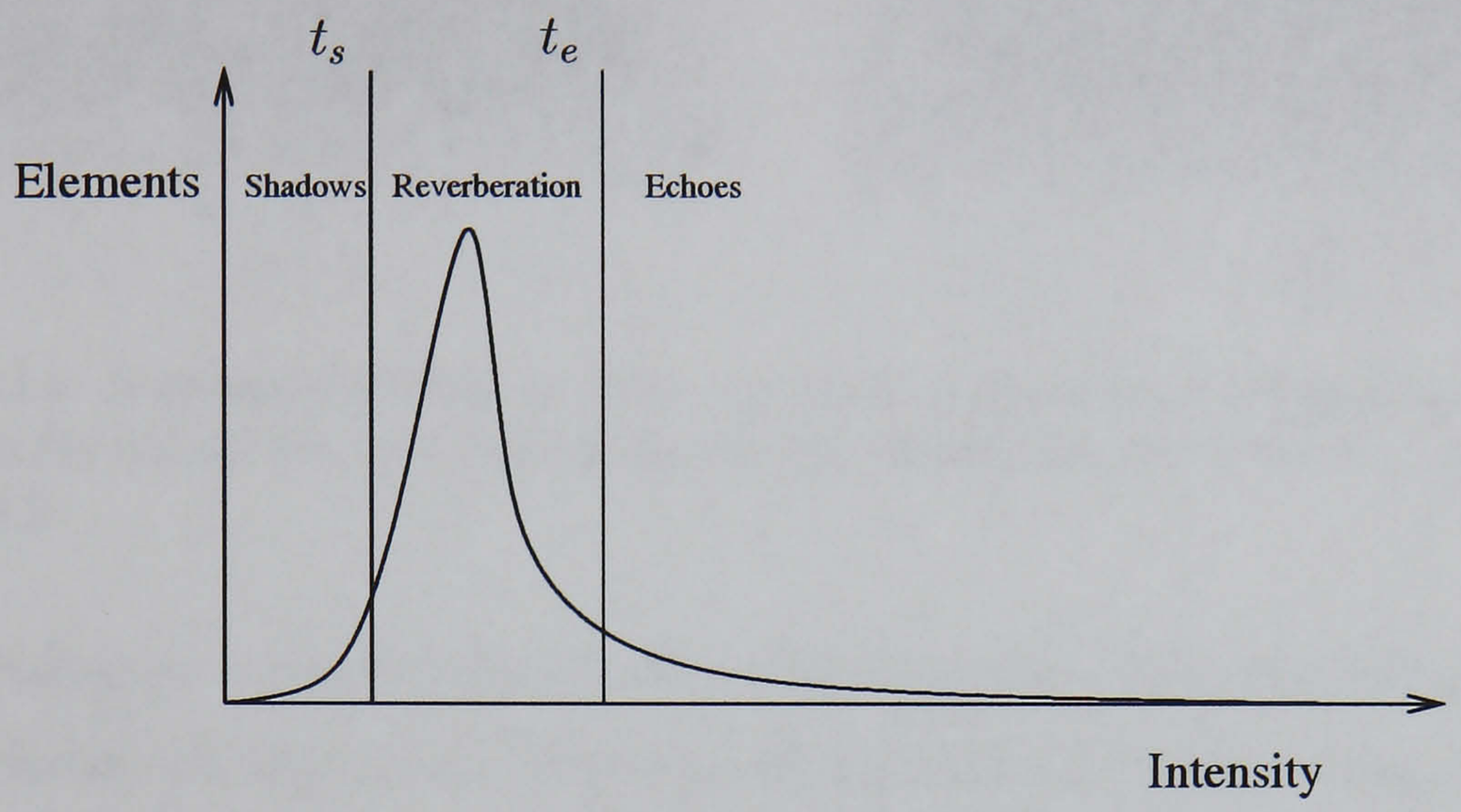

Figure 3.2: A histogram holds the shadows on the lower level intensities and the echoes on the higher intensity. Appropriately located thresholds allow the segmentation of the relevant data.

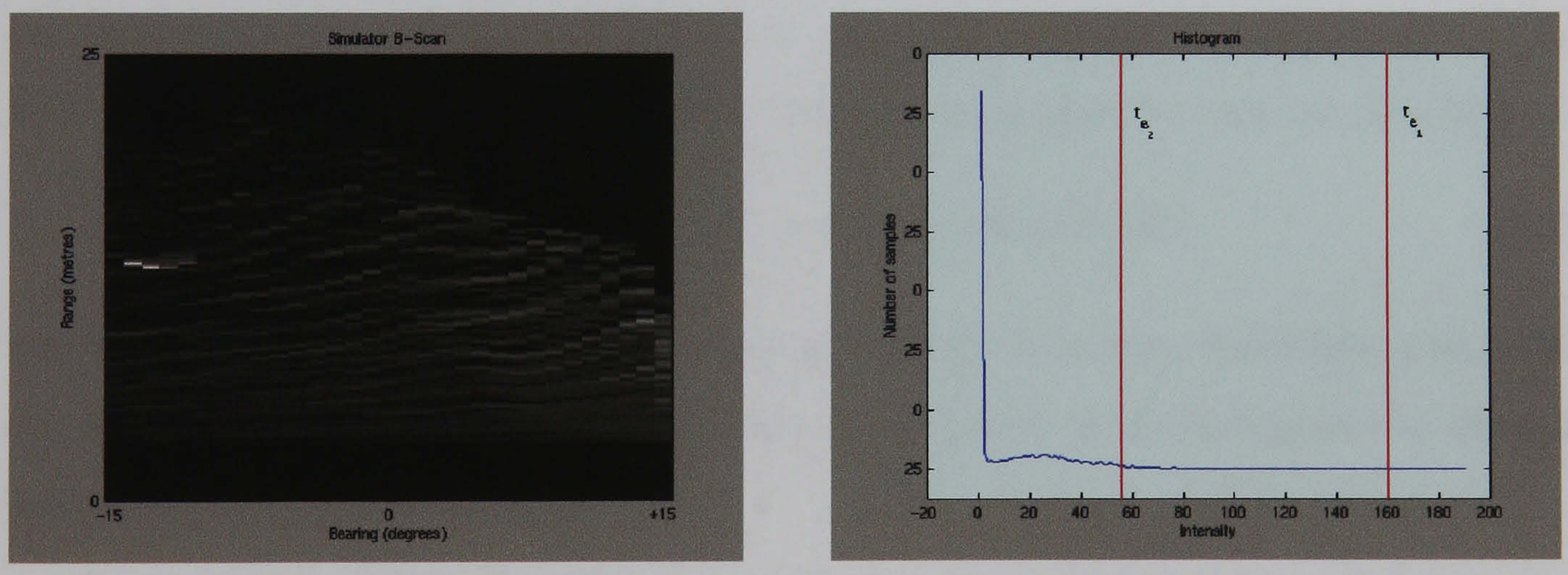

(a) (b)

Figure 3.3: Simulator data (a), depicting a sphere lying on the sea bed, and typical histogram (b). Finding the high intensity regions is not always trivial. The thresholds t_{e_1} and t_{e_2} must be fined tuned.

Clustering: These techniques slide local windows over the sonar data and extract descriptors, mean and variance of the signal in the window for Gaussian distributions. These samples are then clustered into a number of predefined regions, K,

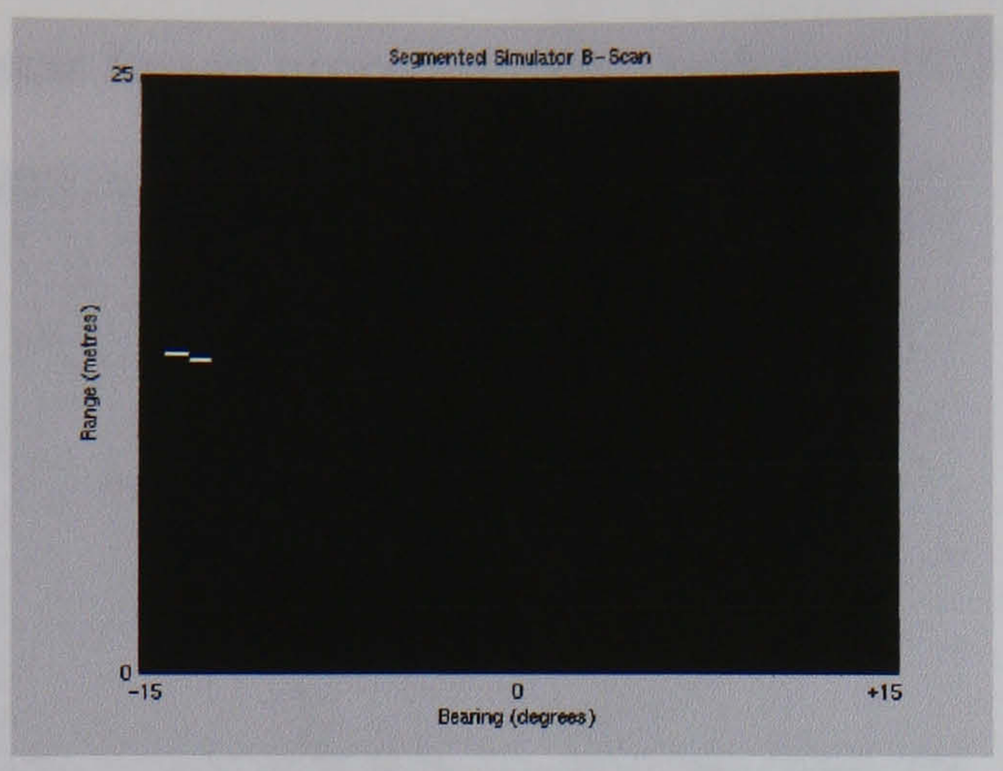

(a) (b)

Figure 3.4: Segmented simulator data: (a) shows the outcome of applying threshold t_{e_1}, and (b) shows the outcome of the double threshold with values t_{e_1} and t_{e_2}, see figure 3.3

by minimising an *a priori* defined scattering criterion. The clustering can be done with a K-means [5] algorithm. This type of algorithm returns a mean and standard deviation for the intensity of the selected regions. Unless the scattering criterion is properly defined, again according to the characteristics of the sonar and the scene, segmentation using only this information will be poor. It is possible however to refine the segmentation by applying statistical theory. Assume a return $y = x + n$, i.e. the return has a component due to the region, x, and a noise component n. The following maximum-likelihood criterion can now be applied to segment the data,

$$\hat{x} = \arg\max_{x}(p_{Y|X,\Phi_y}(y|x = \mu_k))\forall k \in [1...K] \tag{3.1}$$

where μ_k is the mean of region k, obtained from the K-means algorithm, and p the density of probability of $Y|X$, which can be obtained by assuming one of several laws: Gauss, Rayleigh, Rice, etc.

An example of this algorithm, without the statistical refinement, can be seen in figure 3.5 (a). The number of chosen classes is three. The highest class is assumed to be the landmark returns. The algorithm can be fine-tuned by adjusting the number of classes. However for this particular implementation, much of the sea floor is mistakenly segmented as a landmark. Also in figure 3.5, the same K-means serves as the input to a statistical segmentation algorithm assuming a Gaussian distributed noise model. This provides much more valuable results, although some of the sea floor returns are still miss-segmented. An example of K-means applied to side scan

sonar image processing can be found in [42].

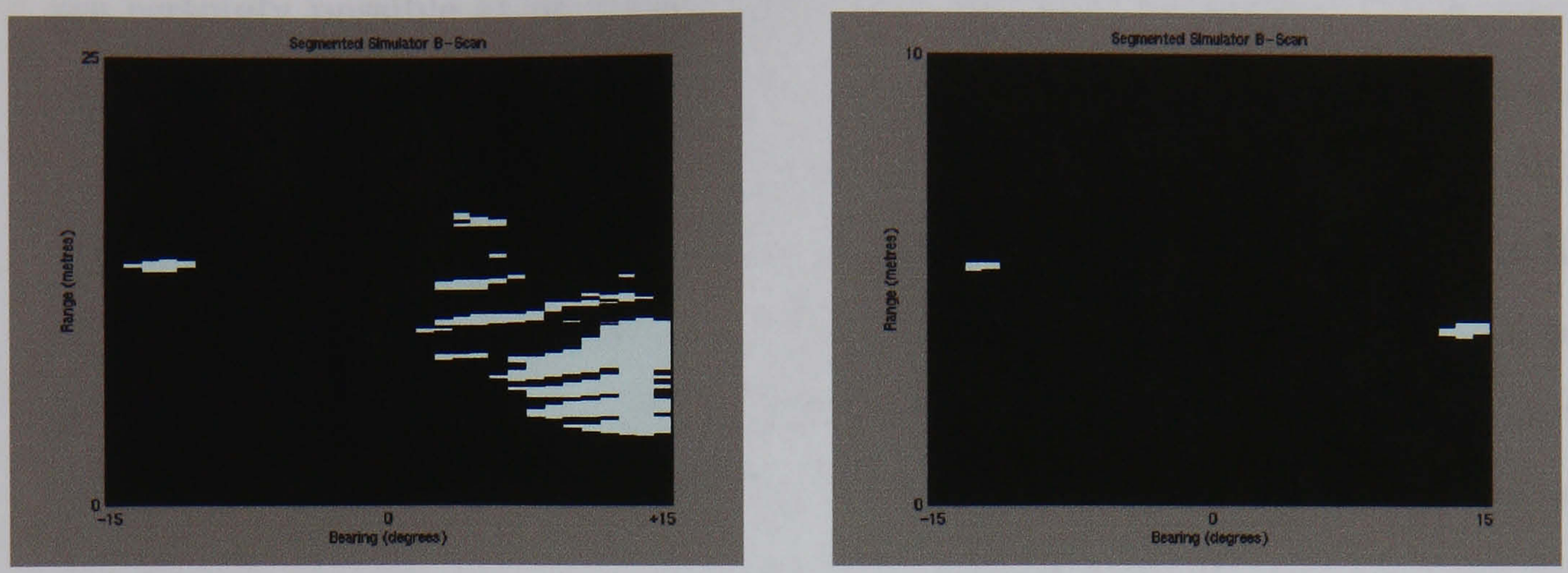

(a) (b)

Figure 3.5: Segmented simulator data: (a) shows the outcome of applying a K-means segmentation with three classes, and taking the highest class as the landmark returns. The same output is fed onto a statistical segmentation algorithm to produce a better output(b)

Markov Random Fields: The Markov random field, $M = (Z, R)$, holds the observation field, $Z = \{Z_s, s \in S\}$, and region field, $R = \{R_s, s \in S\}$, defined on a lattice S of N sites s. The Markov random field is obtained with respect to a chosen neighbourhood system $G = \{G_s, s \in S\}$ and the true realisation of R, $r = \{r_s, s \in S\}$, is estimated by minimising a global energy function $U(z, r)$, given z a realisation of the observation field Z. The energy functions vary in nature and the minimisation techniques are not always trivial. The literature offers many examples of Markovian segmentation of sonar returns, mostly of side-scan sonar [50, 73, 75, 84]. This technique uses the information of the neighbourhood pixels when segmenting the data.

3.3.2 Proposed Segmentation

As discussed earlier, the purpose of the segmentation is to extract landmarks and minimise the number of false alarms to simplify the data association process. It is for this reason that information, from landmarks stored on the map, is used to aid the segmentation process. The following implementation is a compromise between quality and performance. The goal of the algorithm is to discard as many false alarms

as is feasible. Note, however, that by using Markov random fields, improved results are certainly possible at an added processing cost. An overview of the segmentation process can be seen in figure 3.6. The algorithm performs two segmentation procedures, coarse segmentation and segmentation of the *Regions of Interest* (ROI). The coarse segmentation is intended to extract possible new landmarks. The ROI are used to extract expected landmarks. The landmark descriptor extraction process, which will be covered in detail in section 3.4, will extract descriptors from the segmented landmarks, these descriptors will aid the data association process and will also be used to define the ROI. Previous work tracking returns in multibeam sonar images has demonstrated the capabilities of this system [102, 111]. In this section both segmentation modules will be examined along with the ROI and their creation. The implementation assumes returns from a forward-looking multibeam sonar. These returns will be thought of as images.

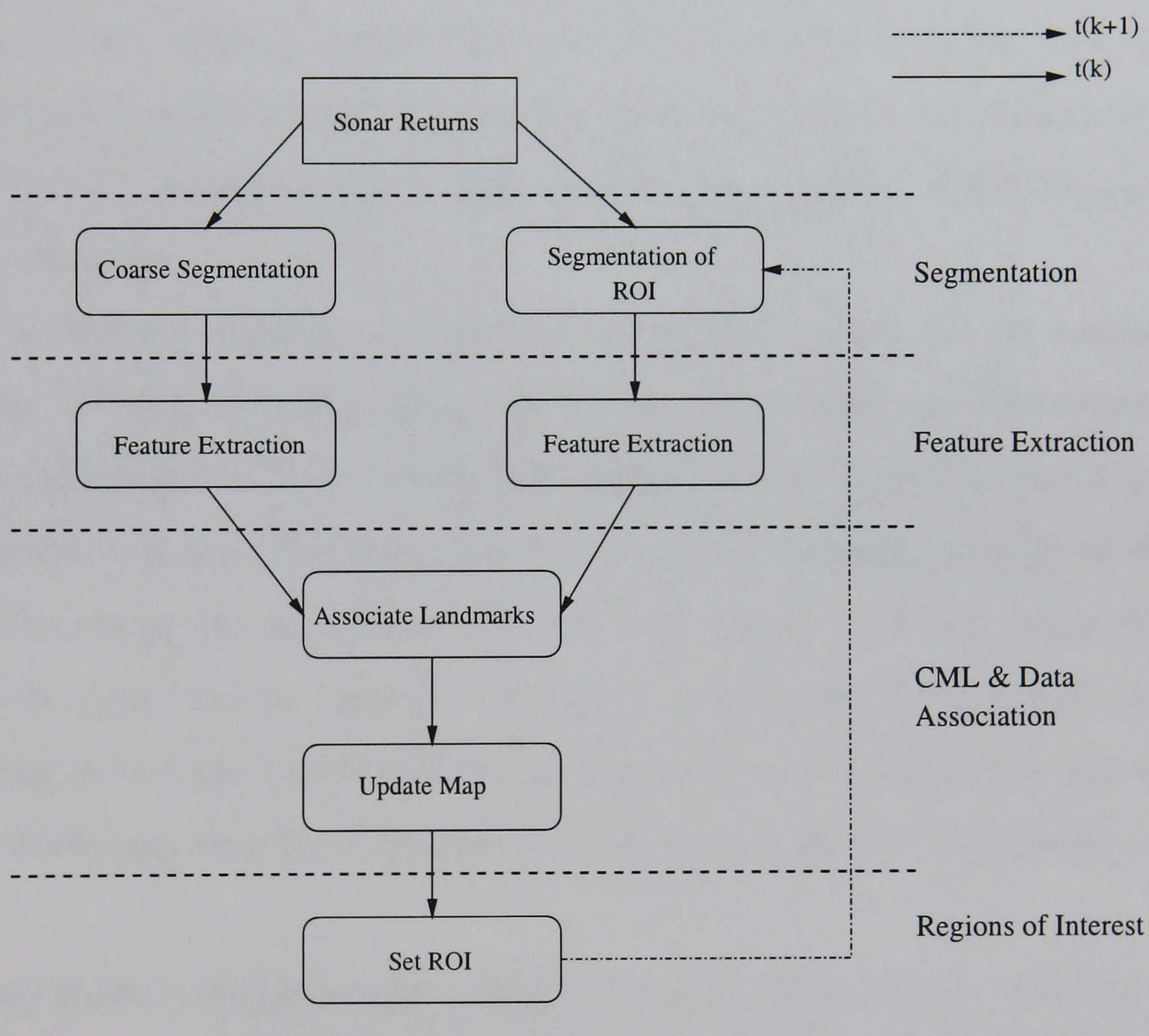

Figure 3.6: Overview of the segmentation process

Coarse Segmentation

Filtering for noise smoothing is an absolute necessity in the case of sonar images as *salt-and-pepper* noise is common, especially in the case of multi-beam sonar images. The filtering part is also generally very time consuming. Several techniques have been tested, including mean, median and Gaussian filters, and it was found that a good compromise between quality and speed was reached using a Gaussian filter which yields results almost as good as the median filter, even on noisy images, but at a reduced computational cost [40]. Once the image has been smoothed, the detection of landmarks can be initiated.

A single, fixed threshold generally gives results which are highly dependent on the background level. A better alternative is to use an adaptive thresholding technique based on the image histogram which is independent of the actual signal level. This algorithm estimates the noise probability density function assuming that the histogram of the image is a good estimate of it (thus assuming that new landmarks to be detected occupy a relatively small number of pixels in the image). It must be noted that the calculation of the histogram is done on the original image and not the filtered image.

The predicted locations of previously identified landmarks are removed from histogram calculation. A false alarm rate (FAR) is then fixed and used in conjunction with the histogram to derive the threshold value. If a landmark is part of the image on which the histogram has been derived, it contributes most probably to the higher part of the histogram and will be selected even with a high false alarm rate, while most of the noise will be rejected. The noise that should be tolerated corresponds to backscatter returns which are at the same level as the landmarks present in the image. Removing this kind of noise would also remove the landmarks or part of them.

A final check is performed by tuning a threshold with respect to the sonar characteristics. If the intensity of the landmarks extracted using the above strategy is less than this pre-determined threshold, they will be discarded. The algorithm thus ensures that only the highest intensity returns will be considered, disregarding the weakest returns by means of the adaptive thresholding technique. Finally, it checks

their feasibility by means of a predetermined threshold. In figure 3.7 both data from a Florida Atlantic University sonar scan and its associated histogram are displayed. The coarse segmentation of this scan is shown in figure 3.8 (a).

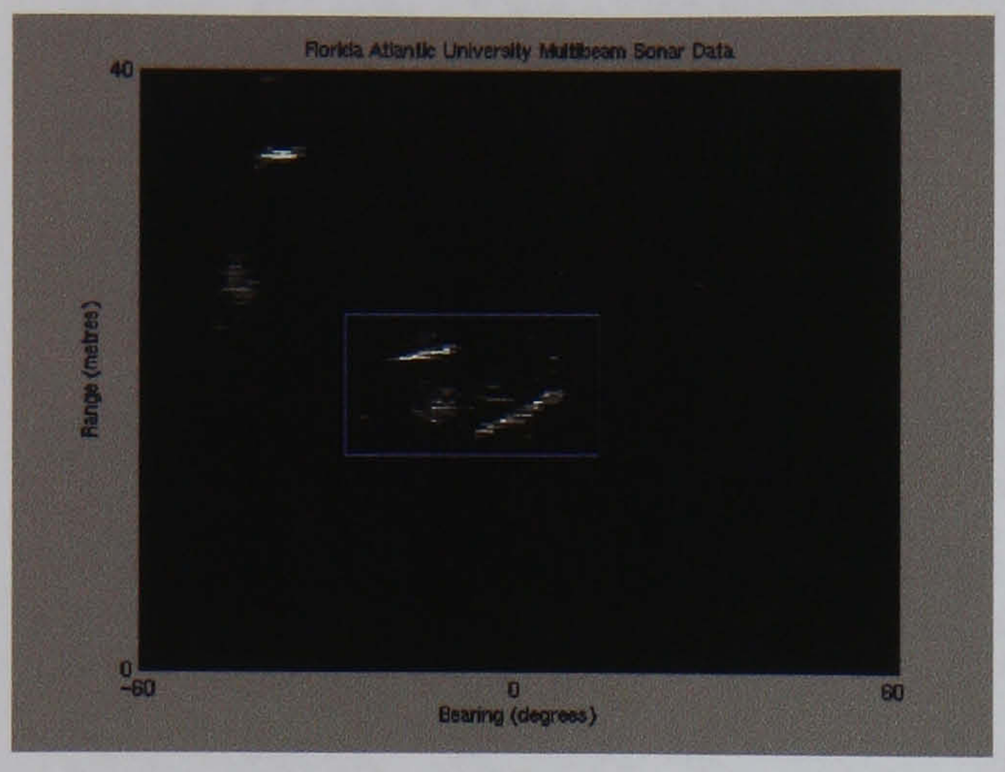

(a)

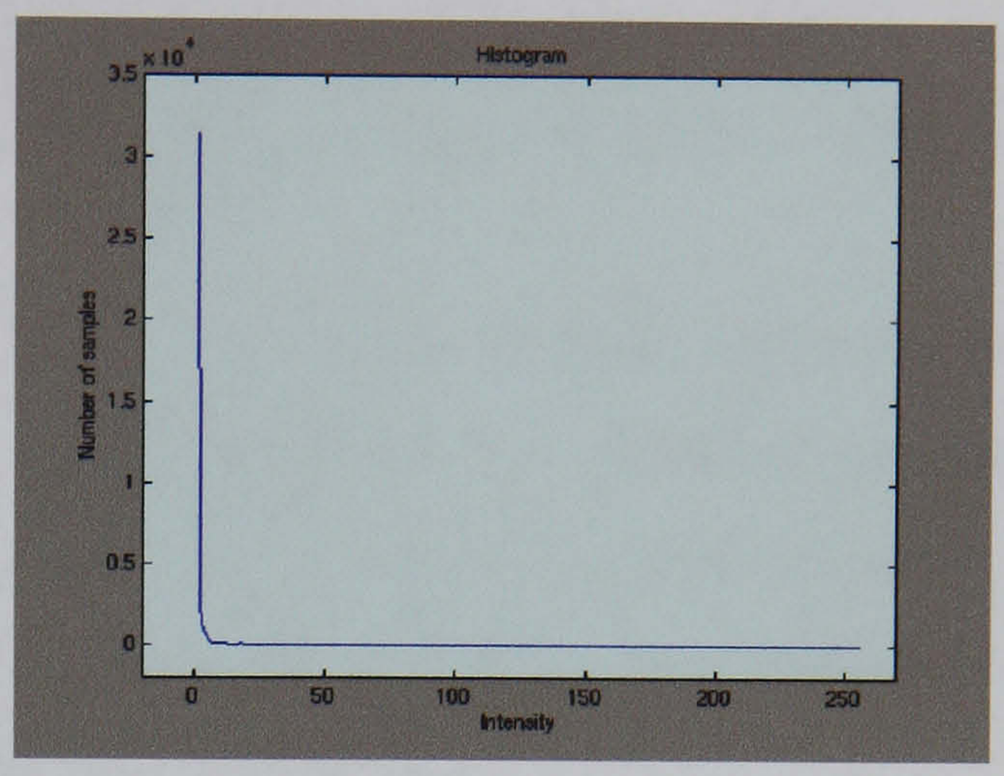

(b)

Figure 3.7: (a) Data from the Florida Atlantic University forward-looking electronically scanned sonar with ROI, and (b) associated histogram.

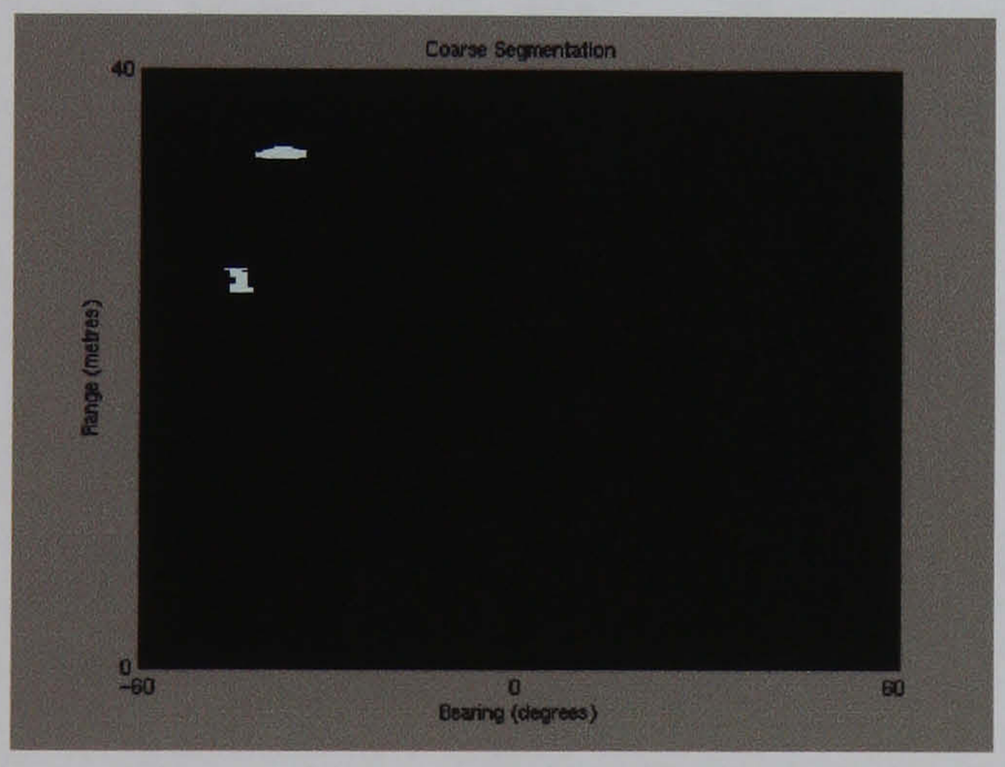

(a)

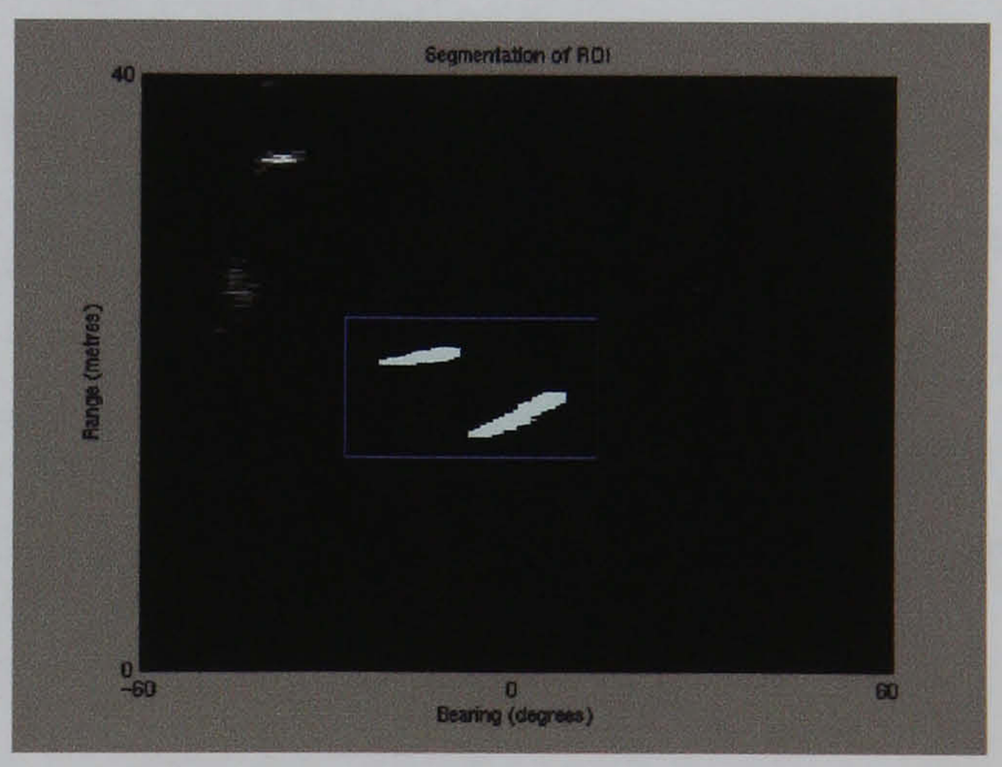

(b)

Figure 3.8: (a) Coarse segmentation, and (b) segmentation of ROI

Segmentation of ROI

The process uses the output of the stochastic map (see chapter 2) which estimates the absolute landmarks' positions. These estimates are used to predict their location in the local sonar reference frame.

The landmark extraction algorithm is again based on the histogram of the original image, previously computed, to set the thresholds. The ROI are filtered using a

Gaussian filter and a double threshold is applied. The first (higher) threshold selects the parts of the image that are to be taken into account while the second threshold (lower) selects the areas above it which are connected to the regions selected by the higher threshold by a continuous chain of pixels above the lower threshold. Eight or four-connectivity can be used to define the neighbourhood of a pixel. This work uses eight-connectivity.

The first interest of this algorithm is to discard middle value peaks, not connected to high returns, which would be kept by a simple thresholding technique, generally due to noise. This algorithm also keeps relatively low intensity pixels connected to high returns which correspond to less reflective parts of a landmark. Figure 3.8 (b) illustrates the outcome of segmenting the ROI from figure 3.7.

Extraction of ROI

Define $\mathbf{Z}(k)$ as the set of possible landmarks currently present in the scene. This set can be decomposed in two subsets $\mathbf{Z}_{new}(k)$ and $\hat{\mathbf{Z}}_{map}$ which respectively represent the landmarks which just appeared in the scene and the predicted position in the scene of landmarks stored on the map. For each landmark in $\mathbf{Z}_{new}(k)$, an ROI is set which matches exactly the labelled landmark resulting from the coarse segmentation. For each landmark in $\hat{\mathbf{Z}}_{map}$, an ROI is set which matches that of the landmark stored on the map, and is positioned using the stochastic map prediction and innovation uncertainty.

Illustrative Results

This section illustrates the outcome of the segmentation procedure proposed in this chapter. However, at this stage the tracking is performed by means of a single Kalman filter on each landmark. Chapter 5 will introduce this strategy in the stochastic map architecture. Figure 3.9 illustrates the outcome of data obtained with the Heriot-Watt University simulator. The simulator data depicts a sphere moving towards the sonar. This sequence depicts the ROI following the sphere. In figure 3.10 the tracked target is a diver. The sequence was obtained using the Seabat 6012, see appendix C. Finally, figure 3.11 illustrates a sequence obtained using the

Florida Atlantic University electronically scanned concept sonar, see appendix E. This sequence was obtained from an AUV and will be used in chapter 5 to test the enhanced stochastic map.

3.4 Landmark Descriptor Extraction

The set of descriptors used to characterise the landmarks must demonstrate a behaviour which will provide a certain degree of robustness. Descriptors based on the intensity level of the landmarks will be affected by changes in the settings of the sonar and the segmentation [101]. The thesis assumes a two-dimensional map, and, as such, the extracted landmarks will be assigned two dimensional descriptors. The choice of suitable descriptors will aid the data association process. This section examines a number of feasible descriptors. The list, examined below, is by no means exhaustive. It does however include a suitable range of parameters to define the landmarks.

3.4.1 Landmark Descriptors

The descriptors now described are commonly found in image and computer vision literature [100]. The descriptors are two-dimensional features which operate in Cartesian coordinates. The data, once segmented, must therefore be converted from polar to Cartesian coordinates, see figure 3.12.

The Ocean Systems Laboratory has built a good understanding of the use of both qualitative and quantitative descriptors for the purpose of classifying sonar returns [23, 61]. This experience has motivated the choice of six descriptors: size, perimeter, compactness, maximum dimension, centroids and invariant moments. Recent work [101] has shown that, in the case of moving targets, these descriptors form a robust framework to build inter-frame feature measures. These inter-frame feature measures were found to be suitable for classifying targets under varying conditions. It is thus hoped that the descriptors will provide sufficient discrimination to aid the data association. This will be examined next in section 3.4.3. The descriptors are summarised below.

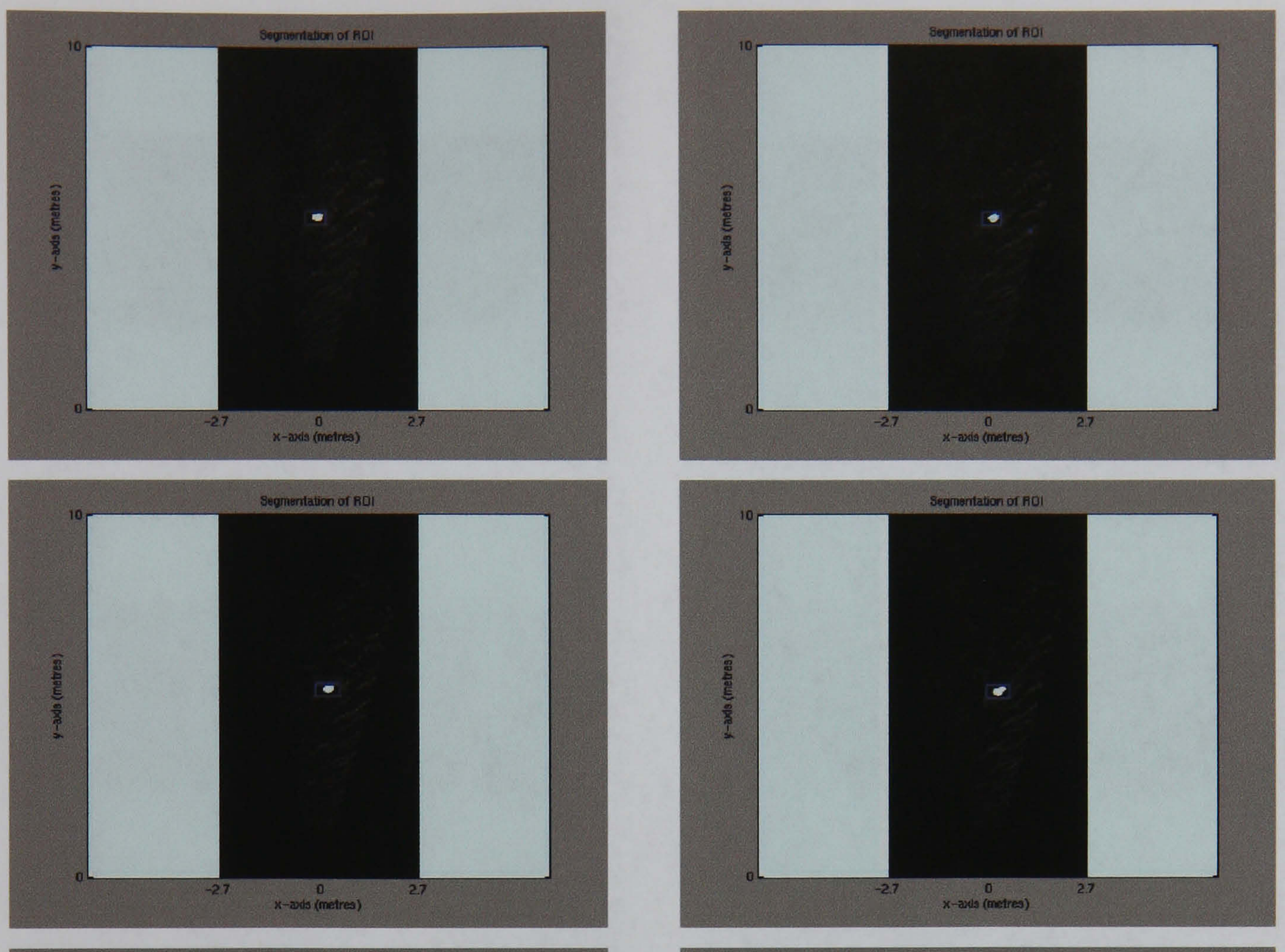

Figure 3.9: Sequence of ROIs: Simulator data

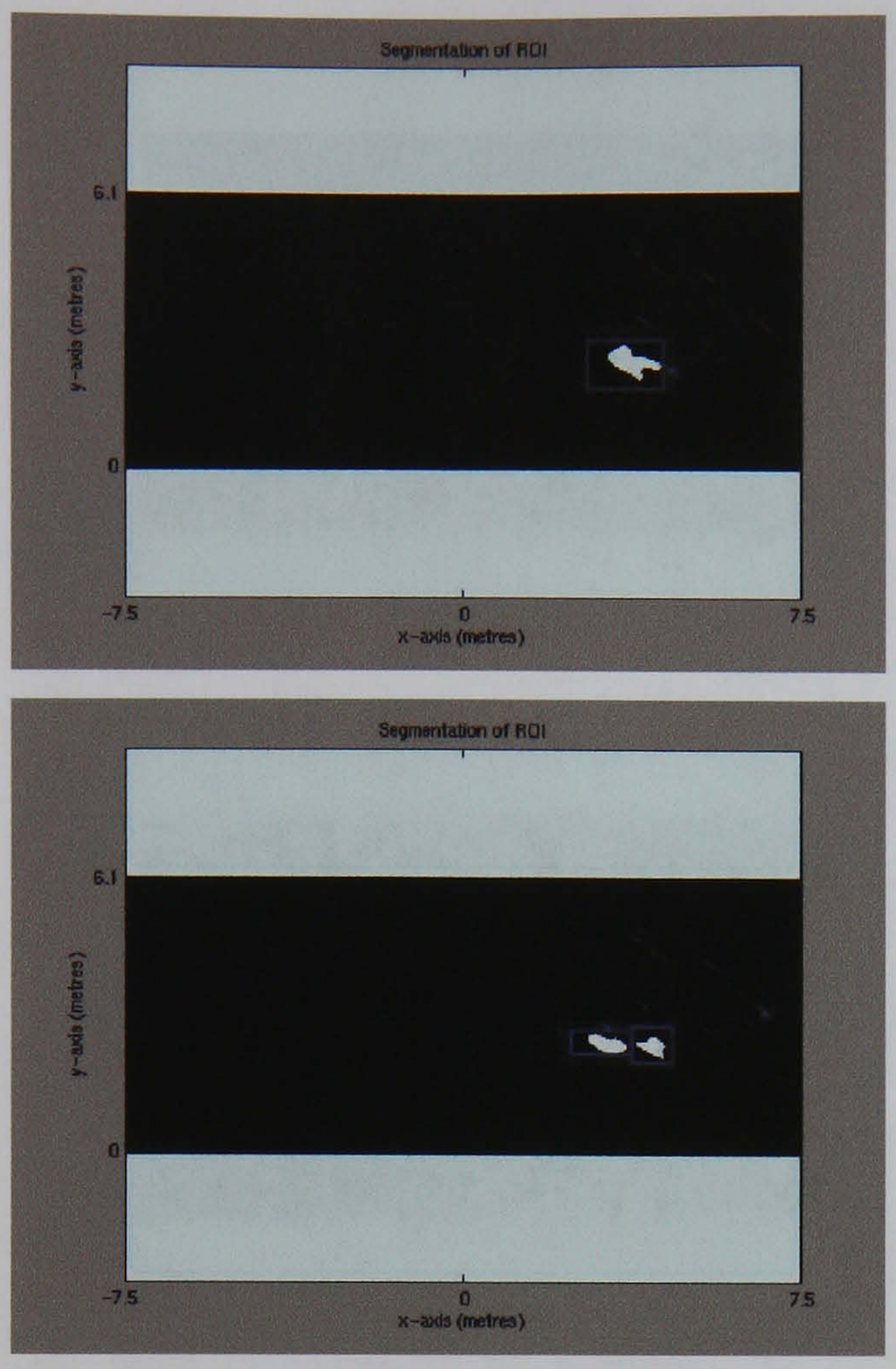

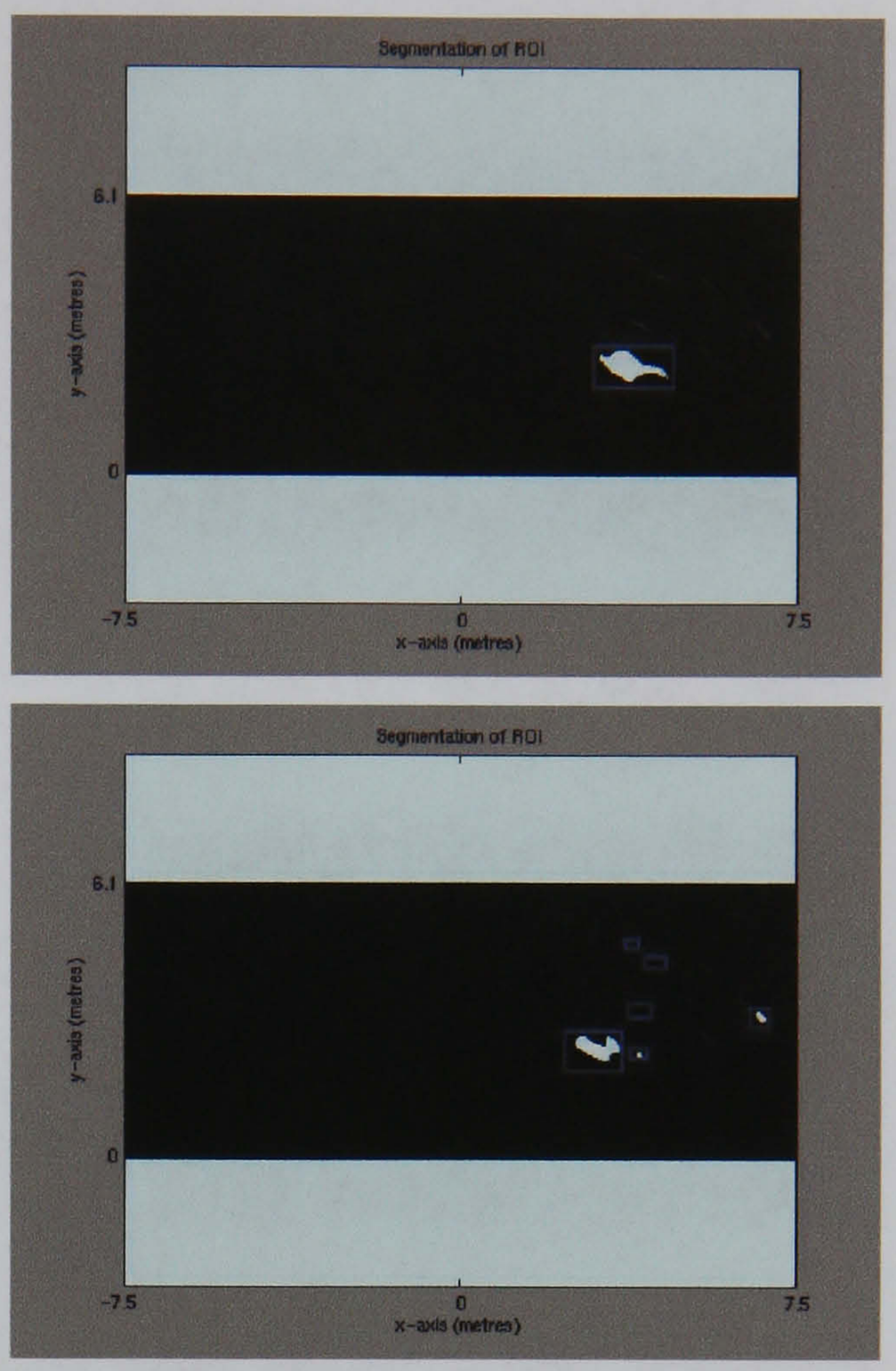

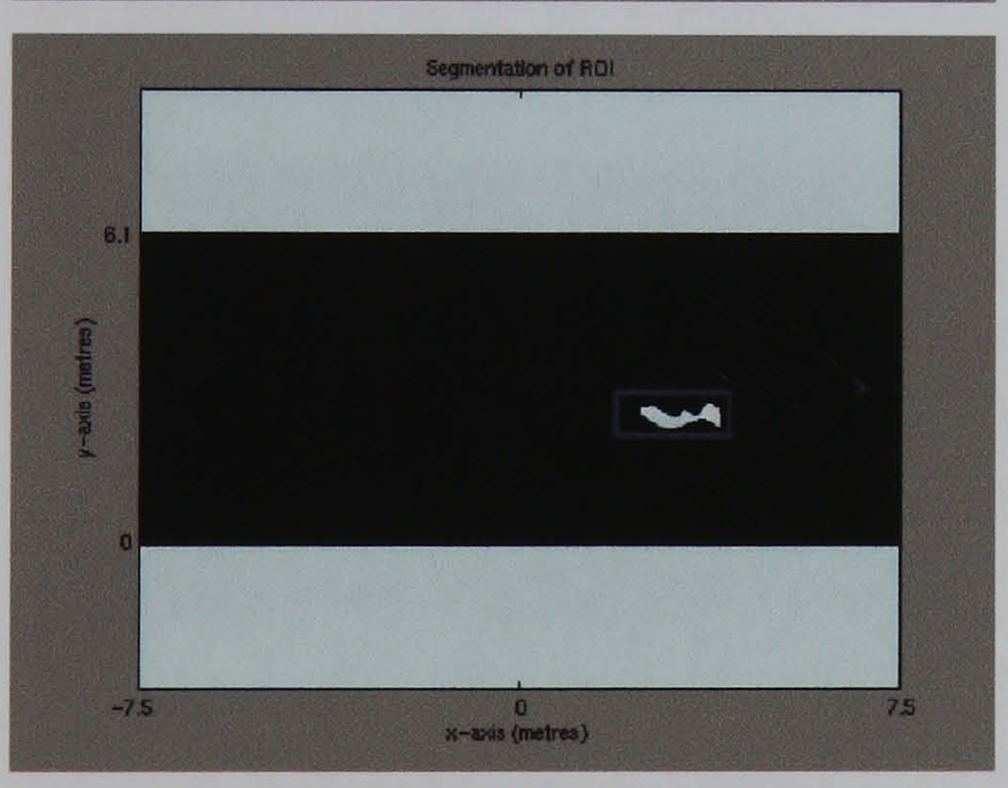

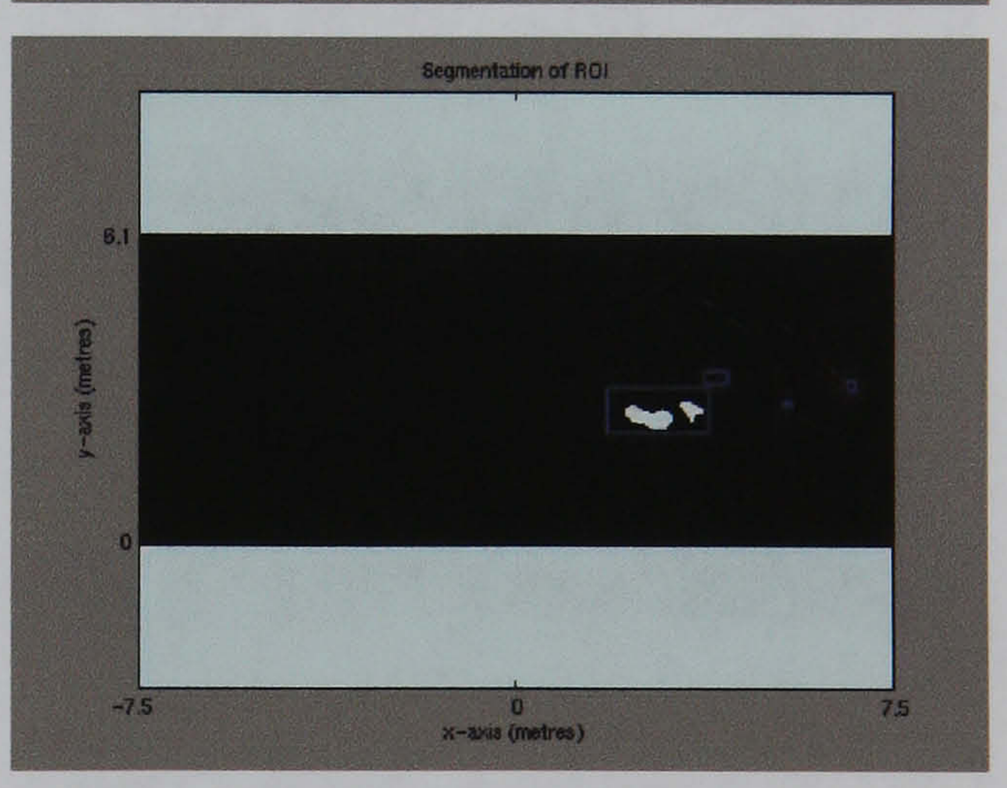

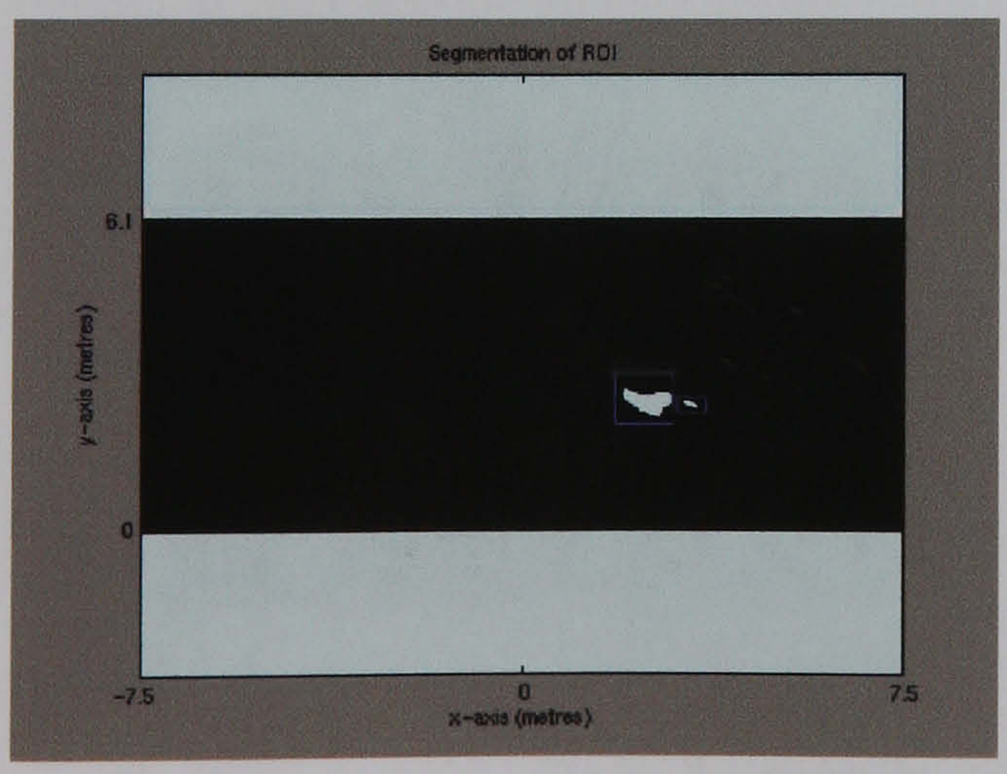

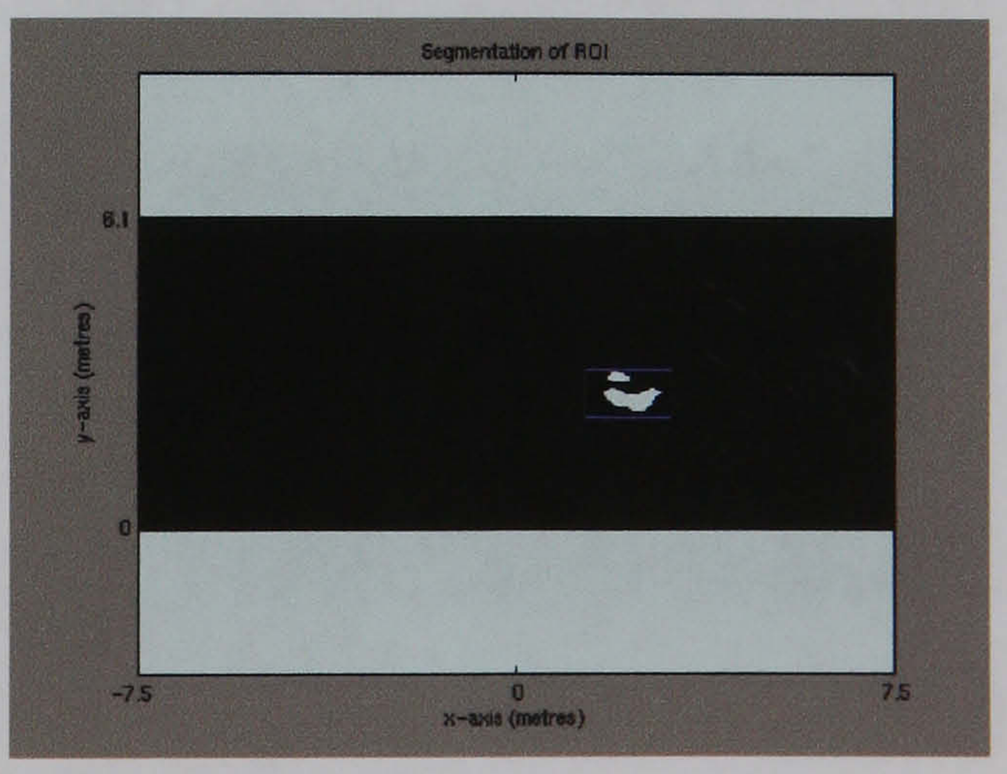

Figure 3.10: Sequence of ROIs: Seabat data

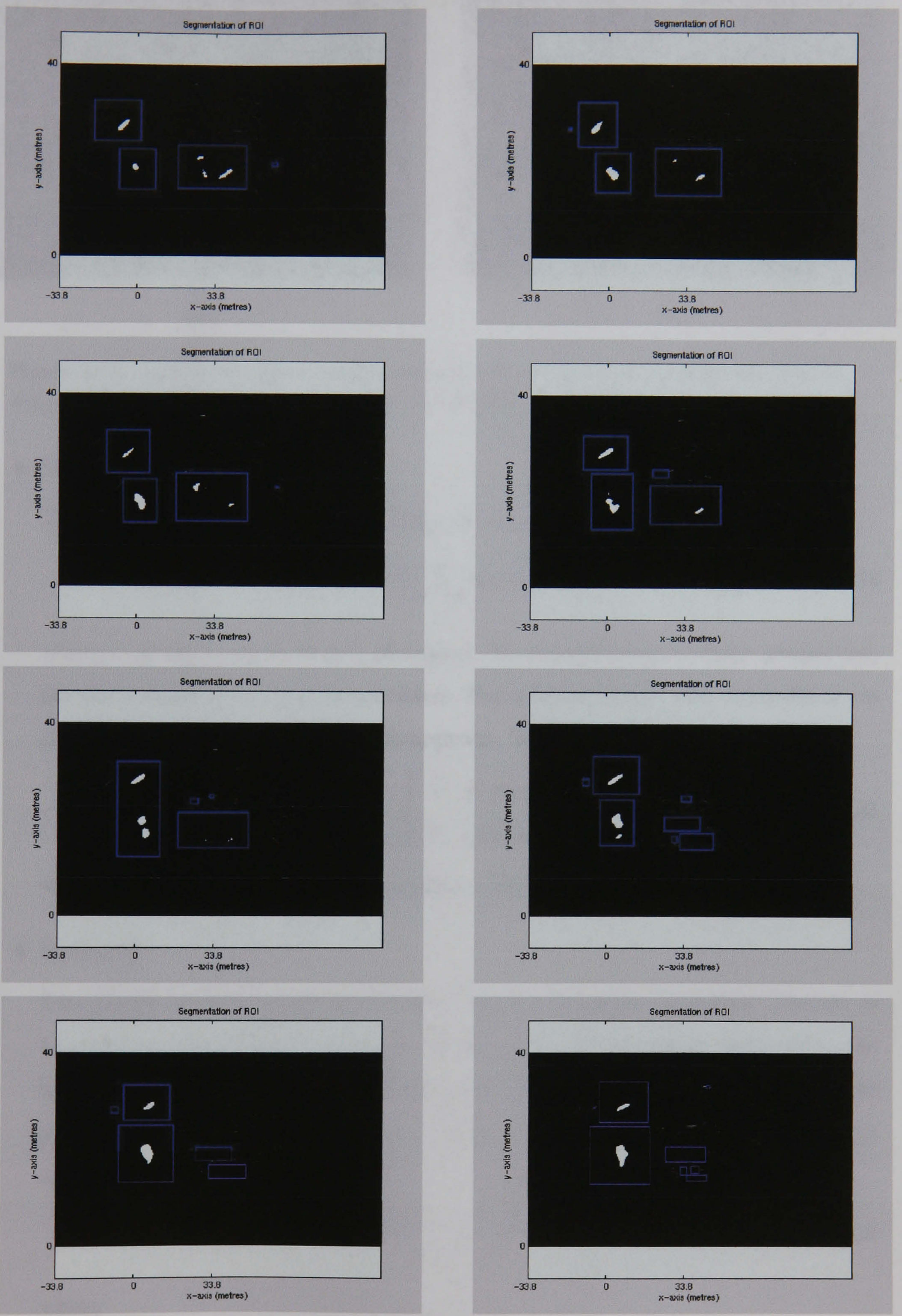

Figure 3.11: Sequence of ROIs: Florida Atlantic University sonar data

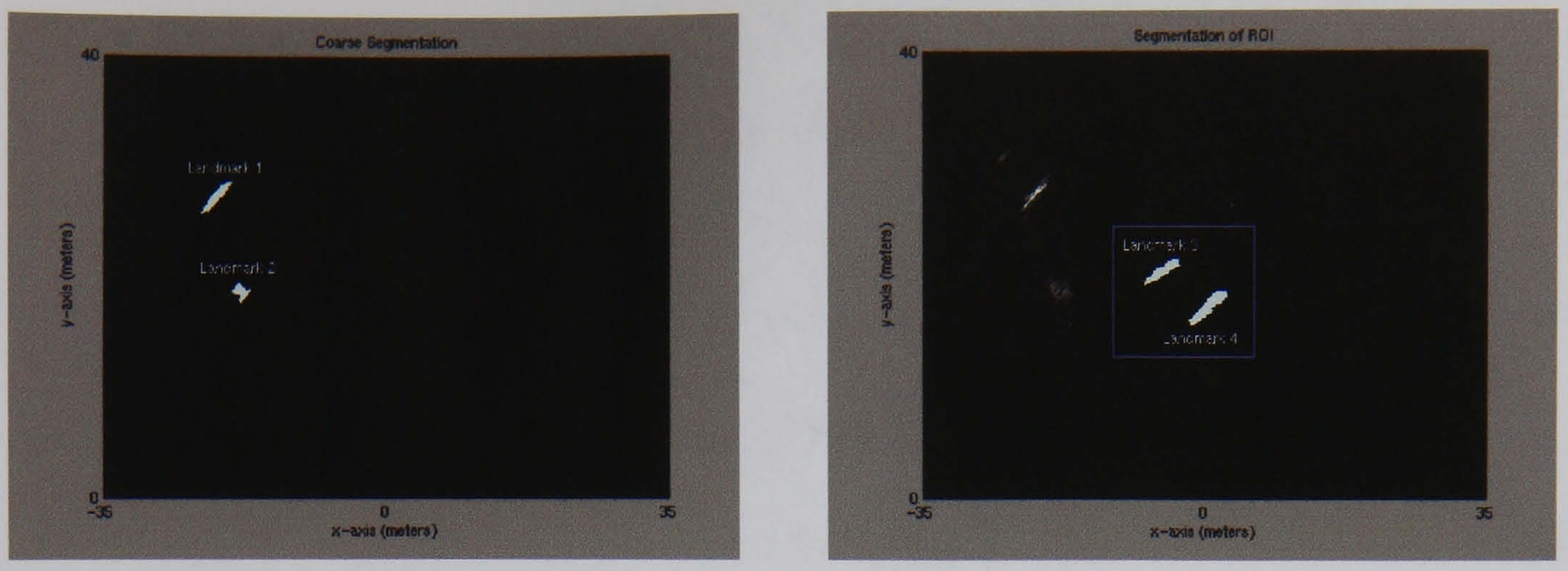

(a) (b)

Figure 3.12: (a) Coarse segmentation transformed to Cartesian coordinates, and (b) segmentation of ROI also in Cartesian coordinates

- Size:

  The size, the surface area of a landmark measured in m^2, can be defined as,

$$S = \sum_i \sum_j b(i,j) \times t_a \tag{3.2}$$

  where t_a is the surface, in m^2, of a pixel. To describe region shape properties, the data input, $f(i,j)$, is thresholded. For a binary input the dependence on the linear grey-level transform disappears. Therefore,

$$b(i,j) = \begin{cases} 1 & \text{if } f(i,j) \in T \\ 0 & \text{otherwise} \end{cases} \tag{3.3}$$

  where T is the set of pixels belonging to the landmark.

- Perimeter:

  Two pixels are four-neighbours if they share a common boundary. The set of boundary pixels, B, of a landmark consists of the set of pixels belonging to the landmark which have four-neighbours with the set of background pixels. The perimeter, P, can thus be defined as the addition of pixels in the boundary and will be measured in m^2,

$$P = \sum_i \sum_j p(i,j) \tag{3.4}$$

  where

$$p(i,j) = \begin{cases} 1 & \text{if } f(i,j) \in B \\ 0 & \text{otherwise} \end{cases} \tag{3.5}$$

- Compactness:

  The compactness of a geometric figure is measured by the isoperimetric inequality

$$\frac{P^2}{S} \geq 4\pi \tag{3.6}$$

  such that the measure of compactness, C, can be described as,

$$C = \frac{4\pi \cdot S}{P^2} \tag{3.7}$$

  A circle is the most compact figure ($C = 1$).

- Maximum Dimension:

  The length of the maximum chord, also known as the major axis. The descriptor can be defined as,

$$MD = \max_{m,p \in B} \left(\sqrt{(i_m - i_p)^2 + (j_m - j_p)^2} \right) \tag{3.8}$$

  where i and j are the coordinates of boundary pixels.

- Centroids

  The moments of a landmark can be obtained from,

$$m_{pq} = \sum_i \sum_j i^p j^q b(i,j) \tag{3.9}$$

  where p and q represent the order and $b(i,j)$ is found using equation 3.3. The centroids can be found to be

$$X = \frac{m_{10}}{m_{00}} \qquad Y = \frac{m_{01}}{m_{00}} \tag{3.10}$$

  The centroids are used in the calculation of the invariant moments.

- Invariant Moments

  These descriptors are derived from the second order normalised central moments of the landmarks and are invariant to translation, rotation and scale [51]. The central moments can be defined as,

$$\mu_{pq} = \sum_i \sum_j (i - X)^p (j - Y)^q b(i,j) \tag{3.11}$$

where $\bar{x}$ and $\bar{y}$ are the coordinates of the centre of mass of the landmark defined in equation 3.10.

The normalised central moments, n_{pq}, are

$$\eta_{pq} = \frac{\mu_{pq}}{\mu_{00}^{\gamma}} \tag{3.12}$$

where

$$\gamma = \frac{p+q}{2} + 1 \tag{3.13}$$

The first invariant moment is defined as,

$$M_f = \eta_{20} + \eta_{00} \tag{3.14}$$

The second invariant moment is,

$$M_s = (\eta_{20} - \eta_{02})^2 + 4\eta_{11}^2 \tag{3.15}$$

For the four possible landmarks identified in figure 3.12 the descriptor outputs are given in table 3.1.

Landmarks:	1	2	3	4
Size (m^2):	3.50	2.20	3.80	5.45
Perimeter (pixels):	119	89	114	138
Compactness:	54.6	49.2	46.2	47.6
Maximum Dimension (pixels):	40.8	22.4	41.2	46.6
Centroids (pixels):	16.6	12.0	20.7	21.6
	12.7	8.8	8.5	11.6
First Invariant Moment:	0.430	0.204	0.443	0.398
Second Invariant Moment:	0.158	0.003	0.169	0.129

Table 3.1: Descriptor Measures of Landmarks in Figure 3.12

3.4.2 Descriptors' View Dependency

The values of the geometrical descriptors, described above, will be dependant, not only on the target's own geometry and reflective properties, but on the range and

angle of view between the sonar and the target. The attenuation of sound accounts for the differences as the range is increased. The incidence angle and the target's surface type also determine the energy of the return, as was observed in section 3.2.2.

To take into account the sonar's view dependecy, the indoor robotic community has developed models of the sonar to match segmented returns to appropiate environment descriptors. The RCD approach, mentioned in section 3.1, is one such method inspired by this work. This method assumes perfectly specular reflections. The implementation of other models has also been proposed. In [39] a diffuse reflector is assumed. Models have also been developed for *Continuous Transmission Frequency Modulated (CTFM)* sonar [88]. All of these methods provide models for the environment such that dense scans can classify the returns into planes, edges, corners and/or cylinders. However, when faced with natural terrain the absence of planes, edges, corners and/or cylinders can be guaranted for most cases. This thesis has thus opted not to model the returns. This will mean that targets will look different when observed from different view points. Therefore, the descriptors will vary as the objects are observed from different view points.

The structure of the stochastic map presented in this thesis will initisalise a new landmark for any observation which is not matched to any stored landmark, as mentioned in section 2.3.3. The descriptors used in the data association process, see chapter 4, should remain fairly constant for similar ranges and angles of view. At the point where the range and angle of view change considerably, a new landmark will be initialised for the target's new look. As will be seen later, in section 4.6, this technique averts the introduction of errors caused by ignoring the descriptor data.

3.4.3 Descriptor Selection

The descriptors can be used to build a description of a landmark. They can also be used to reduce the spatial ambiguity between landmarks which are close together, and to ignore false alarms in close proximity. However, the usefulness of these descriptors will be dictated by their discriminatory capabilities. Descriptors with poor discriminatory capabilities will hinder the data association process. It is important that the descriptors taken on board to aid the data association process have

a large *between-landmark distance* and a small *within-landmark variance.* This is represented in figure 3.13. The aim will thus be to ensure that the descriptors used will maximise the between-landmark distance and minimise the within-landmark variance in descriptor space. By doing this, not only will the resulting descriptors be better, but processing time will be saved by limiting the size of the descriptor space. A number of different methods, all of them well documented in classification literature [104], can be used to achieve this. One approach examines the descriptors individually and removes from further processing those with little discriminatory capabilities. Another, better approach, takes combinations of descriptors, thus ensuring that correlations between descriptors are taken into account.

The following sections will investigate the separability of landmarks using both approaches. The first approach will identify the performance of each individual descriptor. The combinatory approach will be performed to select the final optimal set of descriptors, disregarding, if necessary, descriptors which are highly correlated to others, and therefore fail to bring benefits.

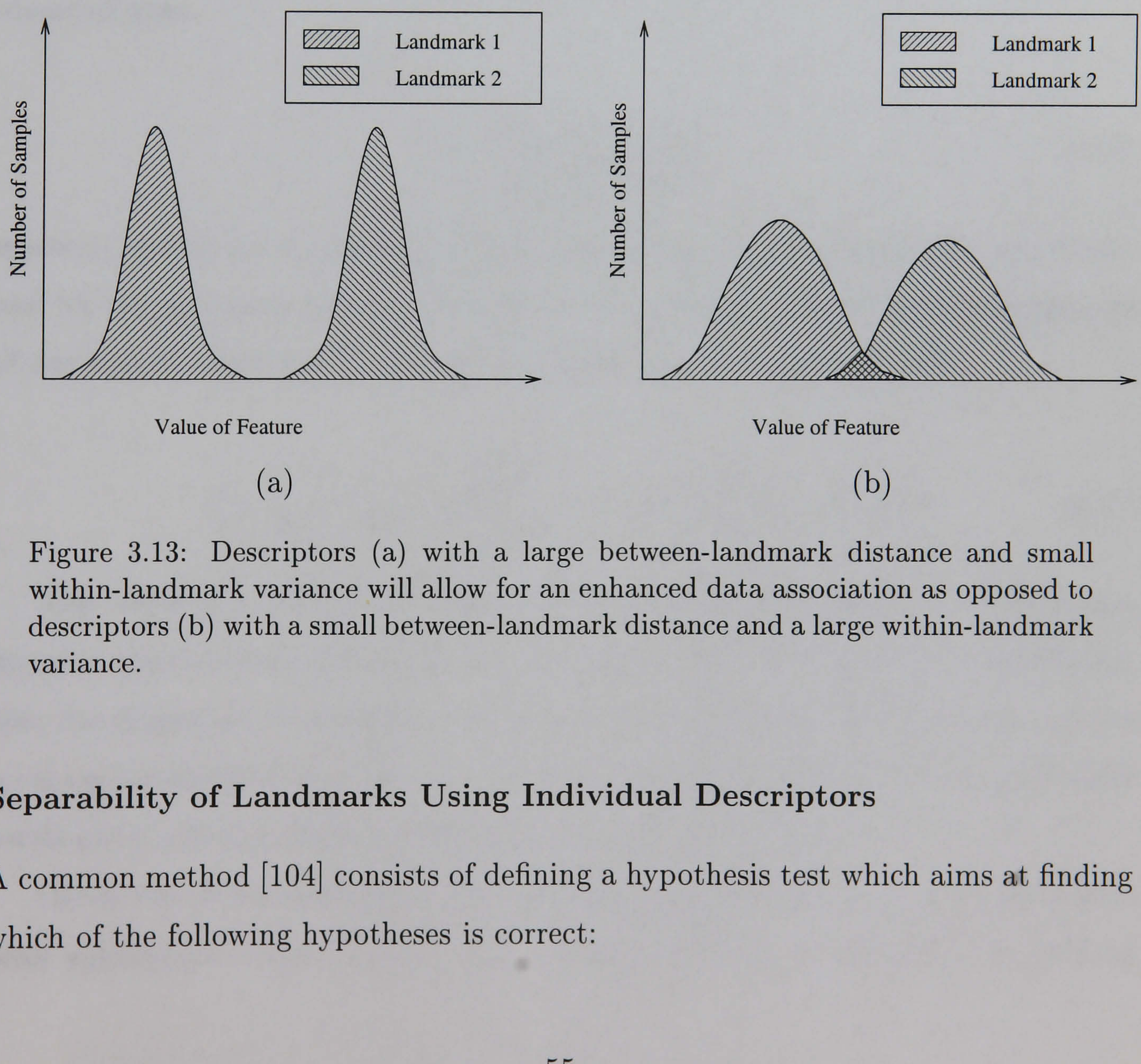

Figure 3.13: Descriptors (a) with a large between-landmark distance and small within-landmark variance will allow for an enhanced data association as opposed to descriptors (b) with a small between-landmark distance and a large within-landmark variance.

Separability of Landmarks Using Individual Descriptors

A common method [104] consists of defining a hypothesis test which aims at finding which of the following hypotheses is correct:

N	$1-\rho$	0.975	0.99	0.995
10		2.228	2.764	3.169
30		2.042	2.457	2.750
50		2.009	2.403	2.678

Table 3.2: Interval values for various significance levels, $1-\rho$, and different degrees of freedom, N, given a t-distribution.

- H_0 - $\Delta\mu = 0$, the values of the descriptor do not differ significantly.
- H_1 - $\Delta\mu \neq 0$, the values of the descriptor differ significantly

where $\Delta\mu = \mu_1 - \mu_2$ is the test in the difference between the means of the values taken by a descriptor in two landmarks.

The decision will be taken by exploiting statistical information obtained from experimental results. The *null hypothesis*, H_0, will be said to be met if a chosen statistic q falls within an acceptable region given a t-distribution. The statistic is obtained from,

$$q = \frac{(\bar{\omega}_1 - \bar{\omega}_2) - (\Delta\mu)}{s_z \sqrt{\frac{1}{N_{\omega_1}} + \frac{1}{N_{\omega_2}}}} \tag{3.16}$$

where $\bar{\omega}_1$ and $\bar{\omega}_2$ are the means for both landmarks, $\Delta\mu$ is the test for the hypothesis and for the null hypothesis it will be zero, N_{ω_1} and N_{ω_2} are the number of samples of descriptors respectively for both landmarks and, s_z is derived from,

$$s_z^2 = \frac{1}{N_{\omega_1} + N_{\omega_2} - 2} \left(\sum_{j=1}^{N_{\omega_1}} (\omega_{1_j} - \bar{\omega}_1)^2 + \sum_{j=1}^{N_{\omega_2}} (\omega_{2_j} - \bar{\omega}_2)^2 \right) \tag{3.17}$$

The statistic q can now be compared to the interval values in a t-distribution given an appropriately defined significance level ρ. This follows from the assumption that the descriptor measures for both landmarks are normally distributed and s_z^2 has a chi-square distribution. Table 3.2 shows the interval values for various significance levels given different degrees of freedom, $N = N_{\omega_1} + N_{\omega_2} - 2$.

Given the above definitions, the most suitable descriptors can now be found, with appropriate sonar returns. The following results were obtained by tracking

Hypotheses:	H_0	H_1
Size:	15.42%	84.58%
Perimeter:	16.90%	83.10%
Compactness:	17.78%	82.22%
Maximum Dimension:	14.68%	85.32%
First Invariant Moment:	22.16%	77.84%
Second Invariant Moment:	24.38%	75.62%

Table 3.3: Percentage of the 1485 t-Tests carried out for each descriptor satisfying the null hypothesis, H_0, or the alternative hypothesis, H_1.

landmarks in sequences of scans obtained from a sonar developed by Florida Atlantic University. The sonar has 120 beams of width 1° horizontally and 30° vertically and a range of 40 metres. The scans were obtained at a 9 Hz sample rate. The scans were divided into 5 sets, each set consisting of 150 scans. The number of landmarks in all sets was 55. These were not always tracked for the whole duration of a set as the sonar was mounted on an AUV and was moving. Landmarks were tracked for a minimum of 12 observations (equivalent to 1.33 seconds) to a maximum of 128 observations (equivalent to 14.2 seconds). As there exists the possibility that a landmark might have the same, or similar, descriptor measure to another landmark, the hypothesis test was conducted by checking all landmarks versus each other. Table 3.3 shows the number of tests which fall within the null hypothesis against the number of tests which fall within the *alternative hypothesis*, H_1, for all descriptor measures given a significance level, $\rho = 0.005$. From the table it can be clearly seen that the maximum dimension descriptor is the most discriminating one, and thus the best candidate if only one descriptor were to be used, whilst the second invariant moment is the worst descriptor. However, 75.62% is a high figure and, used in combination with other descriptors, it might serve to provide a better performance. This will now be examined.

Separability of Landmarks Combining Descriptors

The aim in this section will be to examine the different discrimination values obtained for the different landmarks with different combinations of descriptors. There is a chance that some descriptors will be highly correlated with each other and their inclusion in the final descriptor vector will not be of benefit to the data association. This section will also use standard classification algorithms [104]. Given that the set of descriptors under examination is small. It will be feasible to examine all possible combinations of descriptors. This will require $2^6 - 1 = 63$ operations. Such a procedure carried out off-line is by all means feasible. Now follows a detailed insight into the process by which the data will be compared. The following section will introduce the adopted data normalisation procedure. The section after that will describe the different distance measures examined: divergence, Brattacharyya and scatter matrices criteria. The results obtained using all these methods will be shown in the final section.

Data Normalisation: One of the problems encountered when combining different descriptors is that their values might lie in different dynamic ranges. Descriptors will therefore influence the cost function according to these values. However, this does not mean that a descriptor with small values will be less useful, in a classifying sense, than a descriptor with a higher value. It is for this reason that the data must be normalised. The normalisation strategy adopted in these experiments is [104],

$$\mathbf{x}_{nl} = \frac{\mathbf{x}_l - \bar{\omega}_l}{\max \mathbf{x}_l - \min \mathbf{x}_l} \tag{3.18}$$

where $\bar{\omega}_l$ is the mean taken from all the measures, $\mathbf{x}_l$, of descriptor l under consideration across all landmarks, and $\mathbf{x}_{nl}$ is the normalised data. This procedure centres all the descriptor measures around zero and limits their values to a range of $[-1, 1]$.

Separability Measures: Once the data has been normalised, the separability of the different descriptor combinations must be analysed. Five standard distance measures [104]have been implemented in this thesis.

Divergence: The ratio $\ln \frac{p(\mathbf{x}|\omega_1)}{p(\mathbf{x}|\omega_2)} \equiv D_{12}(\mathbf{x})$ is a discriminatory measure associated to descriptor vector $\mathbf{x}$ with respect to two landmarks ω_1, ω_2. Given two overlapping classes, D_{12} will be zero. Since the vector $\mathbf{x}$ takes different values, the mean value over both class ω_1 and class ω_2 will be considered,

$$D_{12} = \int_{-\infty}^{+\infty} p(\mathbf{x}|\omega_1) \ln \frac{p(\mathbf{x}|\omega_1)}{p(\mathbf{x}|\omega_2)} d\mathbf{x} \qquad D_{21} = \int_{-\infty}^{+\infty} p(\mathbf{x}|\omega_2) \ln \frac{p(\mathbf{x}|\omega_2)}{p(\mathbf{x}|\omega_1)} d\mathbf{x} \tag{3.19}$$

The divergence is the sum of both ratios,

$$d_{12} = D_{12} + D_{21} \tag{3.20}$$

Assuming data with Gaussian density functions, the divergence measure takes the following form,

$$d_{ij} = \frac{1}{2} trace \left\{ \mathbf{P}_i^{-1}\mathbf{P}_j + \mathbf{P}_j^{-1}\mathbf{P}_i - 2I \right\} + \frac{1}{2}(\bar{\omega}_i - \bar{\omega}_j)'(\mathbf{P}_i^{-1} + \mathbf{P}_j^{-1})(\bar{\omega}_i - \bar{\omega}_j) \tag{3.21}$$

It is clear that divergence depends on both the mean values $\bar{\omega}$ and the covariances $\mathbf{P}$ associated to each class. The average class separability is just the average divergence for all classes,

$$D = \sum_{i=1}^{L} \sum_{i=j}^{L} P(\omega_i) P(\omega_j) d_{ij} \tag{3.22}$$

where $P(\omega_i)$ is the probability of the class (the number of samples of that class over the total number samples).

Brattacharyya: The *Chernoff bound* is an upper bound on the minimum attainable classification error of the Bayes classifier for two classes ω_1, ω_2. A special form of this bound is as follows:

$$\epsilon_{CB} = \sqrt{P(\omega_i)P(\omega_j)} \int_{-\infty}^{+\infty} \sqrt{p(\mathbf{x}|\omega_i)p(\mathbf{x}|\omega_j)} d\mathbf{x} \tag{3.23}$$

Given Gaussian distributions for both classes under consideration, this results in,

$$\epsilon_{CB} = \sqrt{P(\omega_i)P(\omega_j)} \exp -b_{ij} \tag{3.24}$$

where b_{ij} is the Brattacharyya distance,

$$b_{ij} = \frac{1}{8}(\bar{\omega}_i - \bar{\omega}_j)' \left(\frac{\mathbf{P}_j + \mathbf{P}_j}{2}\right)^{-1} (\bar{\omega}_i - \bar{\omega}_j) + \frac{1}{2} \ln \frac{|\frac{\mathbf{P}_i + \mathbf{P}_j}{2}|}{\sqrt{|\mathbf{P}_i||\mathbf{P}_j|}} \tag{3.25}$$

Again the average distance can be computed,

$$B = \sum_{i=1}^{L} \sum_{i=j}^{L} P(\omega_i) P(\omega_j) b_{ij} \tag{3.26}$$

where $P(\omega_i)$ is the probability of the class (the number of samples of that class over the total number samples).

Note that in the case of $\mathbf{P}_i = \mathbf{P}_j$ the Brattacharyya distance becomes proportional to the Mahalanobis distance between the means.

Scatter Matrices: The previous distance measures have assumed Gaussian distributions. Given the typical distribution of data, figure 3.14, this assumption is well founded. However, it will be of benefit to define also distances which are independent of this assumption. The scatter matrices do just that. The *within-class scatter matrix* $\mathbf{S}_w$ is

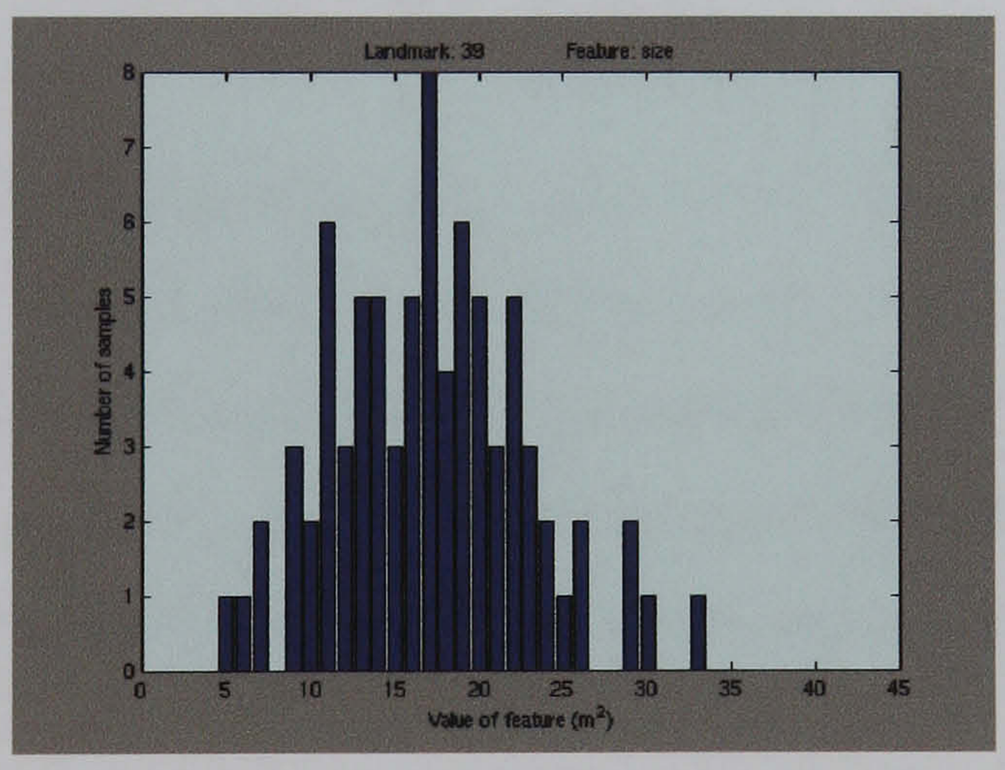

Figure 3.14: Typical distribution of descriptor data

$$\mathbf{S}_w = \sum_{i=1}^{L} P(\omega_i) \mathbf{P}_i \tag{3.27}$$

where $\mathbf{P}_i$ is the covariance matrix for class ω_i,

$$\mathbf{P}_i = E[(\mathbf{x} - \bar{\omega}_i)(\mathbf{x} - \bar{\omega}_i)'] \tag{3.28}$$

and $P(\omega_i)$ is the *a priori* probability of the class (the number of samples of that class over the total number samples). The $trace\{\mathbf{S}_w\}$ is a measure, over all classes, of the average variance of the descriptors. The *between-class scatter matrix* $\mathbf{S}_b$ is

$$\mathbf{S}_b = \sum_{i=1}^{L} P(\omega_i)(\mathbf{x} - \bar{\omega}_0)(\mathbf{x} - \bar{\omega}_0)' \tag{3.29}$$

where

$$\bar{\omega}_0 = \sum_{i=1}^{L} P(\omega_i)\bar{\omega}_i \tag{3.30}$$

The $trace\{\mathbf{S}_b\}$ is a measure of the average distance between each mean and the average global value $\bar{\omega}_0$. The *mixture scatter matrix* is the covariance matrix of the descriptor vector with respect to the global mean, and it is equivalent to,

$$\mathbf{S}_m = \mathbf{S}_w + \mathbf{S}_b \tag{3.31}$$

The $trace\{\mathbf{S}_m\}$ is the sum of variances of the descriptors around their respective global mean. Given these matrices, three different measurement criteria are defined.

$$J_1 = \frac{trace\{\mathbf{S}_m\}}{trace\{\mathbf{S}_w\}} \tag{3.32}$$

The J_1 criterion clearly takes large values when samples in the descriptor space are well clustered around their mean within each class, and the clusters are well separated. The $J1$ criterion also ignores the correlations between the descriptors (off-diagonal terms). Similarly, taking the determinant (the product of the eigenvalues) results in a measure of separability which also corresponds to the same criterion,

$$J_2 = |\mathbf{S}_w^{-1}\mathbf{S}_m| \tag{3.33}$$

Finally, an alternative is to take the trace of J_2,

$$J_3 = trace\{\mathbf{S}_w^{-1}\mathbf{S}_m\} \tag{3.34}$$

Results: The sets of scans used previously to obtain a measurement of the separability of each individual descriptor have also been used to develop measurements for the new criteria of separability described above. The data in this case has been normalised, and each of the criteria was examined for all possible combinations of the

Separability Distances:	D	B	J_1	J_2	J_3
Size:	1	1	1	1	1
Perimeter:	1	1	0	1	1
Compactness:	1	1	0	1	1
Maximum Dimension:	1	1	0	1	1
First Invariant Moment:	1	1	0	1	1
Second Invariant Moment:	1	1	0	1	1

Table 3.4: This table illustrates the results from the combinatory tests. All the possible descriptor combinations were tested. The table shows which combination of descriptors yields the best results for each test criteria. One indicates that the test criterion (columns) includes the descriptor (rows) in the final descriptor vector. Thus, according to J_1 the vector should only include the size descriptor.

descriptors with the whole descriptor set. Table 3.4 illustrates the outcome of the experiments for all the different criteria. It is clear from this table that a descriptor vector will be better suited to describe a landmark by using all descriptor measures. Only the case of the separability criterion J_1 shows a different outcome. This outcome is unexpected when compared to the results from table 3.3. However it is not unexplainable. When observing the value of the $trace\{\mathbf{S}_w\}$ for the size descriptor, it was found to be several orders smaller than any other individual descriptor, and that of $trace\{\mathbf{S}_m\}$ is comparable to that of the other individual descriptors. This indicates that the descriptor is well spread around the global mean and the variance for the landmarks are small. Cross-correlating this with the previous results means that the means of this descriptor for a small cluster of landmarks must fall close to each other, i.e. several landmarks have similar areas. In any case, given that on the stochastic map the position of the landmarks will also be used, if there is a need to reduce the number of descriptors, it will be reasonable to use only the size descriptor. In this thesis, real time implementation has not been a main contributing factor, and all the descriptors will therefore be used in the final system.

3.5 Discussion

The stochastic map is built by taking range and bearing measurements with respect to observable landmarks. The chosen sensor will thus play an important role in the accuracy and consistency of those measurements. Forward-looking sonar systems are noisy and the amount of work done to segment objects in their field of view has been rather limited. This chapter has reviewed the most common methods for segmenting objects from sonar data. Most of these methods have been developed with side-scan sonar in mind. The thesis proposes to segment objects using ROIs. These allow for a considerable decrease in processing time along with a more refined segmentation. The richness of forward-looking sonar data means that the landmarks found by the algorithm are not just limited to a range and bearing measurement. In fact previous work in the Ocean System Laboratory has segmented objects, defined as high intensity compact regions, and attributed descriptors to them. These descriptors have been successfully used to perform a variety of tasks such as tracking, classification and implementing a stochastic map. Work by R. N. Carpenter has also used descriptors to perform CML. In his case it was a sub-optimal adaptation of the stochastic map. Sub-optimal in the sense that the landmark-to-landmark correlations were ignored. His work did not provide a thorough discussion of how or why the descriptors (area, perimeter, area-to-perimeter ration and radial signature) were selected. This chapter, on the other hand, builds on the Ocean Systems Laboratory experience in using descriptors, and chooses six simple descriptors which are extracted along with the centroids from each landmark. The chapter also addresses the question of which descriptors will be more suitable to adapt to a data association algorithm. This chapter argues that descriptors with a large between-landmark distance and a small within-landmark variance should be used, section 3.4.3. Standard classification techniques have therefore been implemented to discern which of the descriptors are more suited to the task. The t-test showed good class separability for all descriptors. However it provided no notion of how the different descriptors were correlated and whether all of the descriptors should be used. It was necessary to perform different tests which considered all the possible combinations of descriptors. The chosen tests were: Divergence, Brattacharyya and scatter matrices criteria $J1$,

$J2$ and $J3$. Four of the tests propose the use of all the descriptors to discriminate between the landmarks. The only test which delivered a different result was that which implemented the J_1 criterion; the one criterion which ignores the correlations between descriptors. It will thus be reasonable to state,

> The vector of the landmark descriptors size, perimeter, compactness, maximum dimension, first invariant moment and second invariant moment has been found to provide good discrimination between forward looking sonar landmarks.

These findings will play a fundamental role in the development of the data association strategy outlined in the following chapter.

3.6 Summary

This chapter has examined the definition of landmark in the context of CML, focusing on the work carried out by other groups, both in land (office) robotics, section 3.1, and particularly underwater robotics, section 3.2. Given an appropriate choice of landmarks, for the purposes of stochastic mapping and localisation using an underwater sonar, the process by which these landmarks are segmented from the environment has been explored in section 3.3, and an approach has been put forward in section 3.3.2. This approach extracts landmarks which can be described as high intensity compact regions. These landmarks are the most common form of landmark found when using a forward looking sonar. The landmarks are characterised by having descriptors assigned to them, section 3.4. These descriptors will be used alongside the landmarks' world referenced positions to simplify the data association problem. This will be examined in the next chapter. A full statistical analysis of the chosen descriptors has proven their suitability as descriptors of the landmarks.

Chapter 4

Data Association

It has already been established that the stochastic map requires the segmented landmarks to be correctly assigned to the mapped landmarks in order for the filter to function properly. The process by which this operation is performed is termed *data association*. Data association is complicated by the uncertainty in the origin of the observations and inaccuracy of the observation's measurements. Multiple observations, including clutter, further complicate the problem. Research on multiple target tracking has addressed this problem [6]. Our proposed data association approach is inspired by such efforts. In section 4.1 of this chapter the main data association strategies proposed by the multiple target tracking literature will be outlined. Section 4.2 provides an overview of the methods that have been adapted to landmark based CML, and also reports on some innovative methods. This thesis proposes to solve the data association by introducing the landmark descriptors described in the previous chapter. Section 4.4 compares various data association strategies. The section illustrates how the performance of all of these can be improved by the introduction of the landmark descriptors. The major benefit gained by using these descriptors with real sonar data is detailed in section 4.6. The chapter finishes with a thorough discussion.

4.1 Data Association in the Context of Multiple Target Tracking

Techniques for tracking a single target amongst clutter are well established [6]. It is a good exercise to refresh the memory of the reader as these techniques will form the basis for many of the algorithms that are used to track multiple targets. The next section will briefly cover these techniques. Section 4.1.2 will cover techniques

used for tracking multiple targets in more detail.

4.1.1 Tracking a Single Target in Clutter

Techniques for tracking a target use the prediction of the target state to limit the search space. The procedure defines a *validation region.* This validation region is an ellipse, or ellipsoid, which represents the uncertainty in the state's prediction. It is the minimum volume that contains a minimum probability mass under the Gaussian assumption. It is obtained by normalising the error between the prediction and the measurement and making sure that it falls within acceptable bounds,

$$\upsilon_i' \mathbf{S}_i^{-1} \upsilon_i \leq \gamma \tag{4.1}$$

where the innovation, $\upsilon_\mathbf{i}$, is defined as

$$\upsilon_i = \hat{\mathbf{z}}_i(k) - \mathbf{z}_i(k) \tag{4.2}$$

and the innovation matrix, $\mathbf{S_i}$, as

$$\mathbf{S}_i = \mathbf{H}_i(k)\mathbf{P}_i(k)\mathbf{H}_i'(k) + \mathbf{R} \tag{4.3}$$

where $\mathbf{H}_i$ is a matrix that holds the Jacobian of the observed target with respect to the estimated target, i.e. the linearised transformation from world coordinates to measurement space. Finally γ is a threshold parameter obtained from the chi-square, χ^2, distribution. The number of degrees of freedom of the chi-square distribution will be equal to the dimensionality of the measurements.

Nearest Neighbour Standard Filter

The *Nearest Neighbour standard filter (NN)* simply assigns the closest validated measurement to the predicted measurement. In figure 4.1 both z_1 and z_2 are validated, and the filter will simply decide which one falls closer to the prediction by minimising the following distance measure,

$$d_i^2(k) = \upsilon_i'(k)\mathbf{S}_i^{-1}(k)\upsilon_i(k) \tag{4.4}$$

This distance is commonly referred to as the Mahalanobis distance.

The approach is thus a two step approach. The first step validates the observations and the second step associates the validated observations.

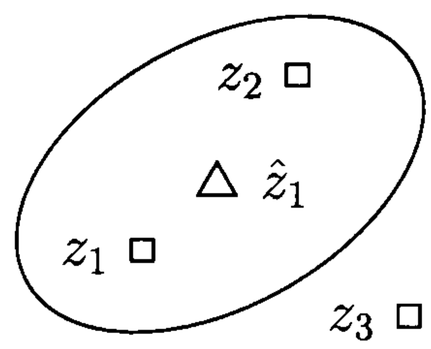

Figure 4.1: This illustration depicts the prediction for the state estimate x_1 at time k. The uncertainty of this prediction is represented by the elliptical gate (validation region). Observations z_1 and z_2 fall inside this gate and will be considered by the NN algorithm.

Track-Splitting Filter

The track-splitting filter postulates multiple hypotheses when more than one measurement falls within the validation region. Each new hypothesis initiates a new track. A log-likelihood function is computed for each track and the least likely ones are 'pruned' by the algorithm. The likelihood function can be found recursively [6],

$$\begin{aligned} \lambda(k) &= \lambda(k-1) + \upsilon'(k)\mathbf{S}^{-1}(k)\upsilon(k) \\ &= \lambda(k-1) + d_z^2(k) \end{aligned} \tag{4.5}$$

The main problem associated to this type of algorithm is the fact that the memory and computation requirements grow with time, especially in cluttered environments.

Probabilistic Data Association Filter

The probabilistic data association filter assigns probabilistically to a target all the measurements falling within the validation region. The conditional mean estimate (target's state) is obtained from the combined innovation υ,

$$\hat{\mathbf{x}}(k+1) = \hat{\mathbf{x}}(k) + \mathbf{K}(k)\upsilon \tag{4.6}$$

for

$$\upsilon = \sum_{i=1}^{m} \beta_i(k)\upsilon_i(k) \tag{4.7}$$

where m is the number of validated measurements, $\beta_i(k)$ is the posterior probability that measurement i originates from the target, an expression for this probability is given in [6], and for each validated measurement,

$$\upsilon_i(k) = \mathbf{z}_i(k) - \hat{\mathbf{z}}(k) \tag{4.8}$$

The filter's associated error covariance is updated according to,

$$\begin{aligned}\mathbf{P}(k+1) &= \beta_0(k)\mathbf{P}(k) + (1-\beta_0)(\mathbf{I}-\mathbf{K}(k)\mathbf{H}(k))\mathbf{P}(k) \\ &\quad \times \mathbf{K}(k)\left[\sum_{i=1}^{m}\beta_i(k)\upsilon_i(k)\upsilon_i'(k) - \upsilon(k)\upsilon(k)\right]\mathbf{K}'(k) \end{aligned} \tag{4.9}$$

where β_0 is the posterior probability that no measurement is correct.

The filter works under the assumptions that:

- a false alarm can be modelled as independent identically distributed random variables with spatially uniform distributions and
- the state is normally distributed according to the latest estimate and covariance matrix [6],

$$p[\mathbf{x}(k)|Z^{k-1}] = N[\mathbf{x}(k); \hat{\mathbf{x}}(k|k-1), \mathbf{P}(k|k-1)] \tag{4.10}$$

This approach is suboptimal as it only examines the latest set of measurements at each iteration.

Optimal Bayesian Filter

This algorithm associates probabilistically all the possible measurement histories, from the start of the tracking sequence to the last iteration. This filter, although optimal in a Bayesian sense, soon saturates the computing capabilities of any machine as the number of measurement histories increases exponentially.

4.1.2 Tracking Multiple Targets in Clutter

The problem of data association has been the subject of major research in the multiple target tracking literature. A good summary of methods can be found in [6]. When tracking multiple targets it is customary to consider all the targets simultaneously as the association possibilities become highly coupled. Figure 4.2 illustrates some of the problems encountered when tracking more than one target. The techniques examined in this section, as with the single target strategies, also use the validation region, section 4.1.1.

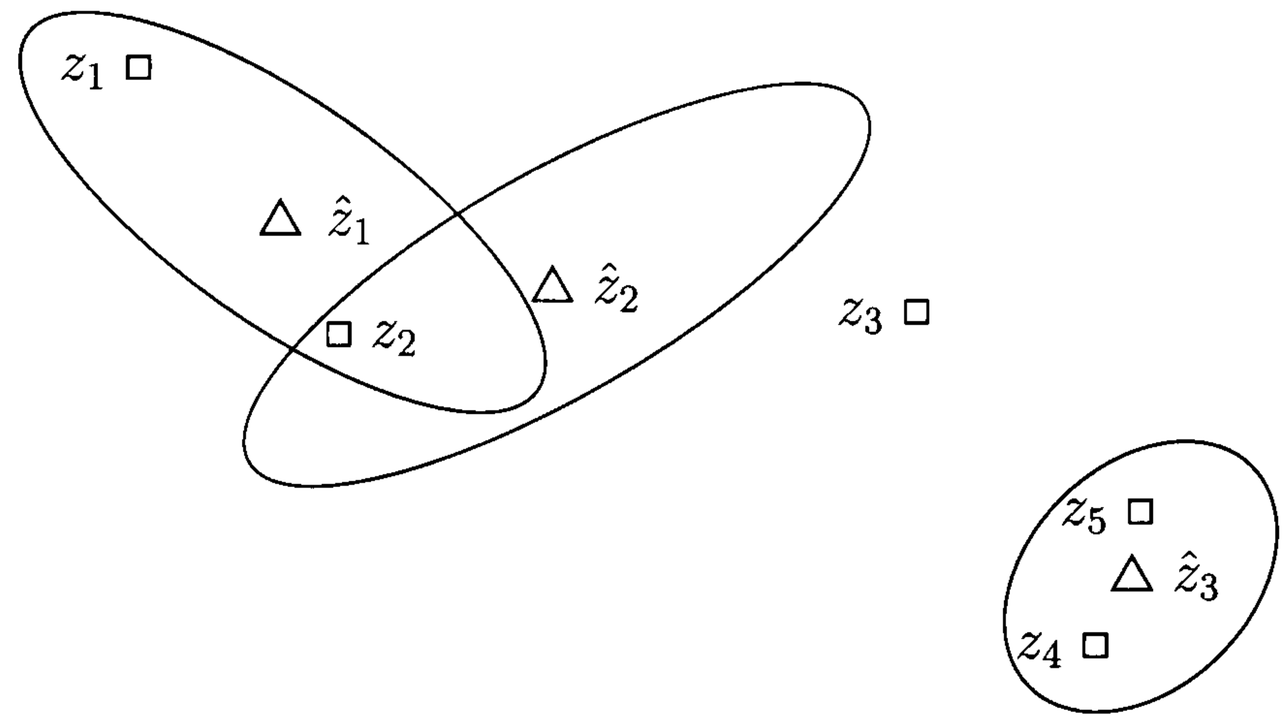

Figure 4.2: This example illustrates some of the problems that a multiple target tracking algorithm in clutter will have to contend with. Observation z_2 is closer to the prediction of target x_1 than observation z_1, however it also falls under target's x_2 validation region. So which target did it originate from? Observation z_3 doesn't fall inside any validation region. Is it a false alarm caused by clutter or a new target? And which observation originates from target x_3, is it z_4 or z_5?

Joint Likelihood Method for Track Formation

This algorithm requires no knowledge of the number of targets, only their dynamic models. Through batch calculation it is able to initiate tracks for several targets. It is essentially a Bayesian decision theory pattern classifier [77]. The patterns under consideration are the measurements, which are to be arranged into tracks given their trajectory models. The l^{th} sequence of measurements up to time k is thus,

$$Z^{k,l} \triangleq \left\{ \mathbf{z}_{i_{1,l}}(1), \cdots, \mathbf{z}_{i_{k,l}}(k) \right\} \tag{4.11}$$

The technique consists of creating a set of feasible partitions. Each partition is built of measurement sequences, under the constraints that each measurement belongs to some track, and each measurement belongs only to one track,

$$\phi \triangleq \left\{ Z^{k,l_i} \right\}_{i=0}^{I} \tag{4.12}$$

The set $Z^{k,0}$ holds all the measurements not associated to any track in a particular partition. To each partition corresponds an event,

$$\theta(\phi) = \{\text{partition } \phi \text{ is true}\} \tag{4.13}$$

Having obtained all the possible partitions,

$$\Phi \triangleq \{\phi\} \tag{4.14}$$

the most likely one is found by maximising the joint likelihood function of all the measurements over all of the partitions into acceptable trajectories,

$$\max_{\phi \in \Phi} p\left[Z^k | \theta(\phi)\right] \tag{4.15}$$

This can be performed by means of 0-1 programming by minimising the following,

$$\min_{\rho} \rho' \mathbf{c} \tag{4.16}$$

subject to the following constraint

$$\mathbf{A}\rho \leq \mathbf{1} \tag{4.17}$$

where ρ is a binary vector which indicates which of the acceptable tracks belong to a feasible partition. Matrix $\mathbf{A}$ is binary and each column corresponds to a set Z^{k,l_i} and the elements of each column indicate which measurements belong to the corresponding set. And $\mathbf{c}$ denotes the vector which holds the log-likelihood ratios, $\tilde{\lambda}^{k,l_i}$, for all the sets,

$$\tilde{\lambda}^{k,l_i} = \lambda^{k,l_i} + N_l \log V^{-1} \tag{4.18}$$

where N_l is the total number of measurements in the set, the hyper-volume is V^{-1} and λ^{k,l_i} is equivalent to the log-likelihood used in the track-splitting filter described in the previous section. For a full derivation examine [6] or [77].

Joint Probabilistic Data Association Filter

This filter [38] has been developed as an extension to the probabilistic data association filter mentioned in section 4.1.1. The algorithm works under the constraint that the number of targets is known. It assigns at each iteration the latest measurements to the tracked targets. The algorithm averages the innovations of each measurement for each target, weighing them according to the probability that the measurement originates from the target. The update equations for the targets are as equations 4.6 and 4.9. The probabilities are found according to the following criteria,

$$\beta_{it} \triangleq P\{\theta_{it} | Z^k\} = \sum_{\theta \in \Theta} P\{\theta | Z^k\} \hat{\omega}_{it}(\theta) \tag{4.19}$$

where θ is a feasible joint association event. An event is said to be feasible if each measurement has one source and no more than one measurement originates from

a target. Each event is represented by a binary matrix, whose elements $\hat{\omega}_{it}(\theta)$ are one if the measurement i has been assigned to target t and zero otherwise. And the conditional probability of the joint association event $P\{\theta|Z^k\}$ assuming a Poisson model for the probability mass function can be found to be [6],

$$P\{\theta|Z^k\} = \frac{\lambda^\phi}{c'} \prod_{i=1}^{m_k} \left[N_{t_i}\left[\mathbf{z_i}(k)\right]\right]^{\tau_i} \prod_{t=1}^{T} (P_D^t)^{\delta_t} (1 - P_D^t)^{1-\delta_t} \tag{4.20}$$

where λ is the spatial density of false measurements, the number of false measurements in the event under consideration is ϕ, m_k is the total number of measurements in the scan, N signifies the normal law and τ_i is an indicator variable of value one if measurement $\mathbf{z_i}(k)$ has been assigned to an established track and zero otherwise, t is the number of targets, P_D^t is the probability of detecting prior targets and δ_T is an indicator variable which is of value one if target t is detected at time k and zero otherwise.

Multiple Hypothesis Filter

The *Multiple Hypothesis Filter (MHF)* measurement-oriented approach, described in [89], calculates the probability that each established target, or a new target, gives rise to a certain observation. The filter works by evaluating hypotheses of all the possible associations, $\Omega(k)$, up to time k.

Hypotheses are made by associating to $\Omega(k-1)$ each observation, $\mathbf{z}_i(k)$. For each observation, $\mathbf{z}_i(k)$, there are three possible associations:

- it belongs to an existing target,
- it is a new target or
- it is a false alarm.

A hypothesis matrix is built where all the possible configurations are considered.

The joint cumulative event, $\Theta(k)_l$, at time k is made up of the joint event, $\Theta(k-1)_s$, and the current association event, $\theta(k)$. The conditional probability of a cumulative event at time k can be written as,

$$P\left\{\Theta(k)_l|Z(k)\right\} = P\left\{\theta(k), \Theta(k-1)_s|Z(k), Z(k-1)\right\} \tag{4.21}$$

from this a recursive relationship may be written,

$$P\{\Theta(k)_l|Z(k)\} = \frac{1}{c}p[Z(k)|\theta(k),\Theta(k-1)_s|Z(k-1)] \times P\{\theta(k)|\Theta(k-1)_s,Z(k-1)\}P\{\Theta(k-1)_s|Z(k-1)\} \quad (4.22)$$

This can be shown to be [6],

$$P\{\Theta(k)_l|Z(k)\} = \frac{1}{c}\frac{\phi!\nu!}{m_k}\mu_F(\phi)\mu_N(\nu)V^{-\phi-\nu}\prod_{i=1}^{m_k}[N_{t_i}[\mathbf{z}_i(k)]]^{\tau_i} \times \prod_t (P_D^t)^{\delta_t}(1-P_D^t)^{1-\delta_t}P\{\Theta(k-1)_s|Z(k-1)\} \quad (4.23)$$

where ϕ, τ and m_k are respectively the number of false alarms, new targets and measurements in the event $\theta(k)$, $\mu_F(\phi)$ and $\mu_N(\nu)$ are the densities of false and new targets respectively, V is the hyper-volume of the surveillance region, N signifies the normal law and τ_i is an indicator variable of value one if measurement $\mathbf{z}_i(k)$ came from an established track and zero otherwise, t is the number of targets, P_D^t is the probability of detecting prior targets and δ_T is an indicator variable which is of value one if target t is detected at time k and zero otherwise.

The algorithm can produce a exponential growth of hypotheses in time. To limit this behaviour a common procedure is to combine all hypotheses that have identical histories for the past k scans. This procedure is known as the N-scan-back filter. To reduce the number of hypotheses created at each iteration the algorithm uses both *clusters* and *superclusters* [6]. A cluster is formed for a measurement that falls within the validation region, equation 4.1, of an established target. Any subsequent measurements that fall within that region will belong to the same cluster. If a measurement falls inside two clusters, those clusters will form a supercluster. Hypotheses will be formed such that measurements will only be associated to targets belonging to the same cluster or supercluster. This allows for a dramatic reduction in the amount of computation required to find the most probable cumulative event.

4.2 Data Association in the Context of Concurrent Mapping and Localisation

Multiple target tracking literature is normally concerned with multiple targets, with possibly different dynamic models, surrounded by clutter and, in most cases, a static

sensor. CML must also deal with multiple targets (landmarks) and two of the algorithms described in section 4.1 have been adapted for this purpose. This section will give an overview of the work done by researchers in implementing these methods under the CML structure, where the targets (landmarks) are now assumed static and it is the sensor that moves according to a dynamic model. This section will also give an overview of methods reported in the CML literature designed with the sole purpose of solving the data association problem solely for CML applications.

4.2.1 Adaptation of Multiple Target Tracking Methods

Of all the methods previously examined, researchers have adapted two of them to the CML architecture. These are the NN and the MHF. We will now examine these adaptations in detail.

Adaptation of the NN

J. J. Leonard and H. Durrant-Whyte [64] identified the importance of data association within a stochastic mapping scheme. They implemented a simple solution based on the NN. Their method aimed at avoiding false matches and augmenting the state of the stochastic map with false landmarks. They introduced a scheme by which each new observation will be qualified as a *tentative* landmark if it meets a certain criteria, and will only be *confirmed* as a landmark if the criteria is met consecutively through a specified number of iterations. This method is also favoured by R. Smith [98]. A similar method is used by J. H. S. Feder [36]. Termed as delayed nearest neighbour, it also waits for the confirmation of landmarks. In addition, landmarks which are lost in subsequent iterations are removed, allowing for limited robustness towards changes in the environment. All these methods work well in uncluttered environments.

A simple solution when working in cluttered environments associates a landmark to an observation when this observation is the only one that falls within the validation region. This implementation by S. B. Williams et al. [116] avoids most false matches. However, many good matches are also ignored.

Although most research groups only exploit positional information, there is much

to be gained by using more accurate descriptors of the landmarks. R. N. Carpenter used the descriptors mentioned in the previous chapter 3 to feed a perceptron algorithm, providing an added measure of robustness in the selection of observations. The observations are initially selected using a validation gate, see equation 4.1. Work in the Ocean Systems Laboratory has demonstrated the success of using descriptors for tracking landmarks in sonar image sequences [85, 102], and also for the purposes of CML [103].

Adaptation of the MHF

The work presented by I. J. Cox and J. J. Leonard [26] presented an implementation of the MHF used to model the environment. The approach was used to store and maintain different hypotheses of the environment, built using an ultrasonic sensor and RCD landmarks. The algorithm was adapted to incorporate different landmark (target) models. This was done simply by initialising all the possible landmarks in different hypotheses as and where new landmarks were detected. Later, B. A. Moran [76] adapted this implementation to an underwater environment. Although these implementations assumed the position of the vehicle was precisely known, their architecture would be ideally suited for CML.

Similarly, work by C. M. Smith [97] presents a hybrid solution to the CML problem. Inspired by the aforementioned work the basis for the algorithm is the MHF. The integrated mapping and navigation algorithm developed holds various possible states of the vehicle at any discrete time step along with all the possible landmark states, ignoring correlations between the states. A MHF is used to associate the new observations to all the states held by the algorithm, postulating new possible states. The decision making as to which are the most likely states, both for the vehicle and the landmarks, is deferred.

4.2.2 Data Association Designed for CML

The relative infancy of the subject means that original work on data association inspired by CML is limited. Three methods have been reported in the literature. These methods will now be examined.

Joint Assignment Matrix

The method proposed by J. K. Uhlmann [112] is a strategy for generating multiple hypotheses. The method maximises the product of the prior probabilities of its component pairs, in an attempt to find the most probable assignments. The prior probabilities can be obtained from,

$$p_a(\mathbf{z}, \hat{\mathbf{z}}) = \frac{1}{\sqrt{|2\pi\mathbf{S}|}} \exp\left(-\frac{1}{2}(\mathbf{z}-\hat{\mathbf{z}})\mathbf{S}^{-1}(\mathbf{z}-\hat{\mathbf{z}})'\right) \tag{4.24}$$

which is a measure of the probability that $\mathbf{z}$ originated from $\hat{\mathbf{z}}$, i.e. a measure of the probability of the innovation, under the assumption that it is a Gaussian distributed random variable with covariances $\mathbf{S}$.

The joint assignment matrix is created by constraining the probability that measurement z_i is assigned to landmark x_j as the sum of the probabilities of all the assignments containing the pair, normalised by the sum of the probabilities of all the assignments,

$$p_a(\mathbf{z}_j, \hat{\mathbf{z}}_i | \text{assignment constraint}) = \frac{1}{\sum_\sigma \prod_k a_{k\sigma_k}} \sum_{\{\sigma|\sigma_i=j\}} \prod_m a_{m\sigma_m} \tag{4.25}$$

where a_{ij} is the matrix element giving the probability that landmark i gave rise to measurement j, and σ_i are the assignments.

Assuming the following matrix of prior probabilities,

	$\hat{\mathbf{z}}_1$	$\hat{\mathbf{z}}_2$	$\hat{\mathbf{z}}_3$
$\mathbf{z}_1$	0.5	0.6	0.4
$\mathbf{z}_2$	0.2	0.5	0.2
$\mathbf{z}_3$	0.3	0.2	0.1

there are six possible assignments sets,

$$\begin{aligned}
\sigma_1 &= \{\hat{\mathbf{z}}_1\mathbf{z}_1, \hat{\mathbf{z}}_2\mathbf{z}_2, \hat{\mathbf{z}}_3\mathbf{z}_3\} \\
\sigma_2 &= \{\hat{\mathbf{z}}_1\mathbf{z}_1, \hat{\mathbf{z}}_2\mathbf{z}_3, \hat{\mathbf{z}}_3\mathbf{z}_2\} \\
\sigma_3 &= \{\hat{\mathbf{z}}_1\mathbf{z}_2, \hat{\mathbf{z}}_2\mathbf{z}_1, \hat{\mathbf{z}}_3\mathbf{z}_3\} \\
\sigma_4 &= \{\hat{\mathbf{z}}_1\mathbf{z}_2, \hat{\mathbf{z}}_2\mathbf{z}_3, \hat{\mathbf{z}}_3\mathbf{z}_1\} \\
\sigma_5 &= \{\hat{\mathbf{z}}_1\mathbf{z}_3, \hat{\mathbf{z}}_2\mathbf{z}_1, \hat{\mathbf{z}}_3\mathbf{z}_2\} \\
\sigma_6 &= \{\hat{\mathbf{z}}_1\mathbf{z}_3, \hat{\mathbf{z}}_2\mathbf{z}_2, \hat{\mathbf{z}}_3\mathbf{z}_1\}
\end{aligned}$$

The normalising factor is thus,

$$\begin{aligned}\sum_{\sigma}\prod_{k} a_{k\sigma_k} &= a_{11}\times a_{22}\times a_{33} + a_{11}\times a_{23}\times a_{32} + \\ &\quad a_{21}\times a_{12}\times a_{33} + a_{21}\times a_{32}\times a_{13} + \\ &\quad a_{31}\times a_{12}\times a_{23} + a_{31}\times a_{22}\times a_{13} \\ &= 0.169\end{aligned}$$

and the posterior probability for a_{11} is thus,

$$\begin{aligned}p_a(\mathbf{z}_1, \hat{\mathbf{z}}_1|\text{assignment constraint}) &= \frac{1}{0.169}\times(a_{11}\times a_{22}\times a_{33} + a_{11}\times a_{23}\times a_{32}) \\ &= 0.266\end{aligned}$$

the joint assignment matrix is simply found by performing this operation for all elements in the prior probability matrix,

	$\hat{\mathbf{z}}_1$	$\hat{\mathbf{z}}_2$	$\hat{\mathbf{z}}_3$
$\mathbf{z}_1$	0.266	0.284	0.450
$\mathbf{z}_2$	0.166	0.503	0.331
$\mathbf{z}_3$	0.568	0.213	0.219

Clearly the outcome of the posterior probabilities significantly changes the probabilities of association. In this case, the hypothesis worth examining is that proposed by assignment σ_6.

The joint assignment matrix thus works as a tool for reducing the amount of possible hypotheses stored by a tracking filter. It can be used in conjunction with the MHF and in the context of both multiple target tracking and CML.

Joint Compatibility Test

The *Joint Compatibility Test (JCT)* method, proposed by Neira and Tardós [81], evaluates incrementally an association event $\theta(k)$. The association event is made up of a set of possible associations $\theta(k) = \{j_1, j_2, \ldots, j_i\}$ at sample period k. It is built by iteratively checking the map's consistency for each association included in the event. The compatibility test which guarantees consistency is the Mahalanobis distance,

$$d_i^2(k) = \Upsilon_i' \mathbf{S}_i^{-1} \Upsilon_i \tag{4.26}$$

where Υ_i is the innovation vector for the association event $\theta(k)$

$$\Upsilon = [\upsilon_{j_1} \upsilon_{j_2} \cdots \upsilon_{j_i}]' \tag{4.27}$$

and $\mathbf{S}_i$ is the innovation covariance for that same event,

$$\mathbf{S}_i = \mathbf{H}_i \mathbf{P} \mathbf{H}_i' + \mathbf{R} \tag{4.28}$$

where

$$\mathbf{H}_i = \left. \frac{\partial \mathbf{h}[\mathbf{x}, i]}{\partial \mathbf{x}} \right|_{\mathbf{x}=\hat{\mathbf{x}}} \tag{4.29}$$

Now for each new association, the innovation $\upsilon_{j_{i+1}}$ and corresponding covariance,

$$\mathbf{S}_{j_{i+1}} = \mathbf{H}_{j_{i+1}} \mathbf{P} \mathbf{H}_{j_{i+1}}' + \mathbf{R} \tag{4.30}$$

where

$$\mathbf{H}_{j_{i+1}} = \left. \frac{\partial \mathbf{h}[\mathbf{x}, j_{i+1}]}{\partial \mathbf{x}} \right|_{\mathbf{x}=\hat{\mathbf{x}}} \tag{4.31}$$

can be used to obtain an updated Mahalanobis distance. Given,

$$\mathbf{S}_{i+1} = \begin{bmatrix} \mathbf{S}_i & \mathbf{w}_{i+1}' \\ \mathbf{w}_{i+1} & \mathbf{S}_{j_{i+1}} \end{bmatrix} \tag{4.32}$$

where

$$\mathbf{w}_{i+1} = \mathbf{H}_{j_{i+1}} \mathbf{P} \mathbf{H}_i' \tag{4.33}$$

Using the partitioning method for matrix inversion [46], the inverse innovation covariance for the new event can be found to be,

$$\mathbf{S}_{i+1}^{-1} = \begin{bmatrix} \mathbf{M}_{i+1} & \mathbf{L}_{i+1}' \\ \mathbf{L}_{i+1} & \mathbf{N}_{i+1} \end{bmatrix} \tag{4.34}$$

where

$$\mathbf{N}_{i+1} = (\mathbf{S}_{j_{i+1}} - \mathbf{w}_{i+1} \mathbf{S}_i^{-1} \mathbf{w}_{i+1}')^{-1} \tag{4.35}$$

$$\mathbf{L}_{i+1} = -\mathbf{N}_{i+1}\mathbf{w}_{i+1}\mathbf{S}_i^{-1} \tag{4.36}$$

$$\mathbf{M}_{i+1} = \mathbf{S}_i^{-1} + \mathbf{L}'_{i+1}\mathbf{N}_{i+1}^{-1}\mathbf{L}_{i+1} \tag{4.37}$$

Thus new Mahalanobis distance $d^2_{i+1}(k)$,

$$\begin{aligned} d^2_{i+1}(k) &= \Upsilon'_{i+1}\mathbf{S}_{i+1}^{-1}\Upsilon_{i+1} \\ &= \begin{bmatrix} \Upsilon'_i & \upsilon'_{j_{i+1}} \end{bmatrix} \begin{bmatrix} \mathbf{M}_{i+1} & \mathbf{L}'_{i+1} \\ \mathbf{L}_{i+1} & \mathbf{N}_{i+1} \end{bmatrix} \begin{bmatrix} \Upsilon_i \\ \upsilon_{j_{i+1}} \end{bmatrix} \\ &= \Upsilon'_i\mathbf{M}_{i+1}\Upsilon_i + 2\upsilon'_{j_{i+1}}\mathbf{L}_{i+1}\Upsilon_i \\ &\quad +\upsilon'_{j_{i+1}}\mathbf{N}_{i+1}\upsilon_{j_{i+1}} \\ &= d^2_i(k) + \Upsilon'_i\mathbf{L}'_{i+1}\mathbf{N}_{i+1}^{-1}\mathbf{L}_{i+1}\Upsilon_i \\ &\quad +2\upsilon'_{j_{i+1}}\mathbf{L}_{i+1}\Upsilon_i + \upsilon'_{j_{i+1}}\mathbf{N}_{i+1}\upsilon_{j_{i+1}} \end{aligned} \tag{4.38}$$

The association event can, therefore, be incrementally updated by this method. The aim is to find an event with the maximum number of pairings which maintains the overall consistency of the map. The NN approach proposed by other researchers has ignored the joint compatibility of the pairings and failed to take into account the importance of the correlations between the landmarks.

Graph-Based Data Association

Work by T. Bailey et al. [4] presented a system for performing data association between two batch observations. By batch observations it is meant that the perception of the environment allows for accurate measurements of the relative geometry between landmarks. The assumption the system makes is that if static landmarks exist in two batch observations, than the relative geometry of these will be unaltered in both observations. In this implementation landmarks were represented as nodes and the invariant relationship between the nodes has been termed as edges. Using this representation a graph is created for each observation. Figures 4.3 and 4.4 show two possible configurations for segmented landmarks from two scans and their corresponding graphs. The data association problem can then be considered as a

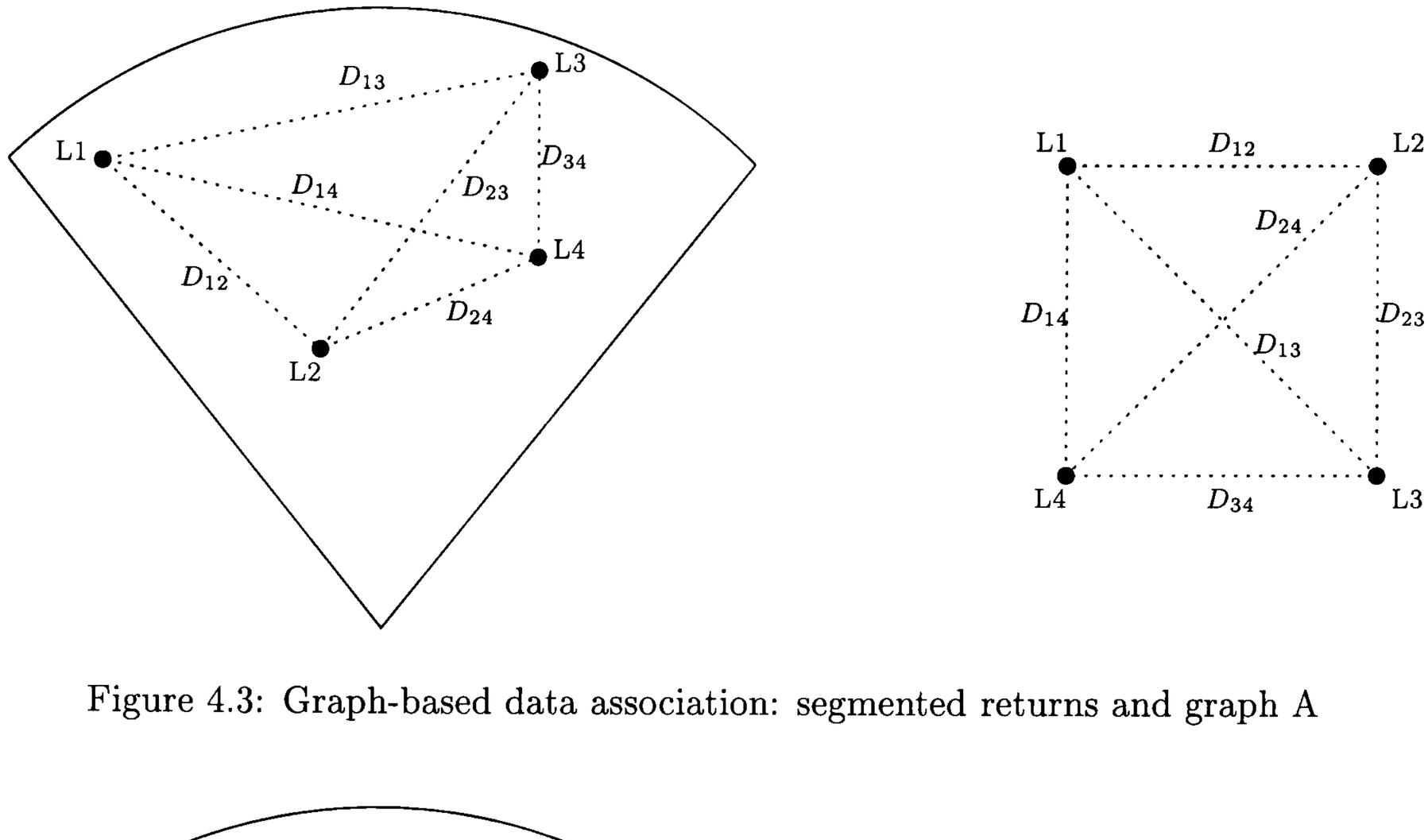

Figure 4.3: Graph-based data association: segmented returns and graph A

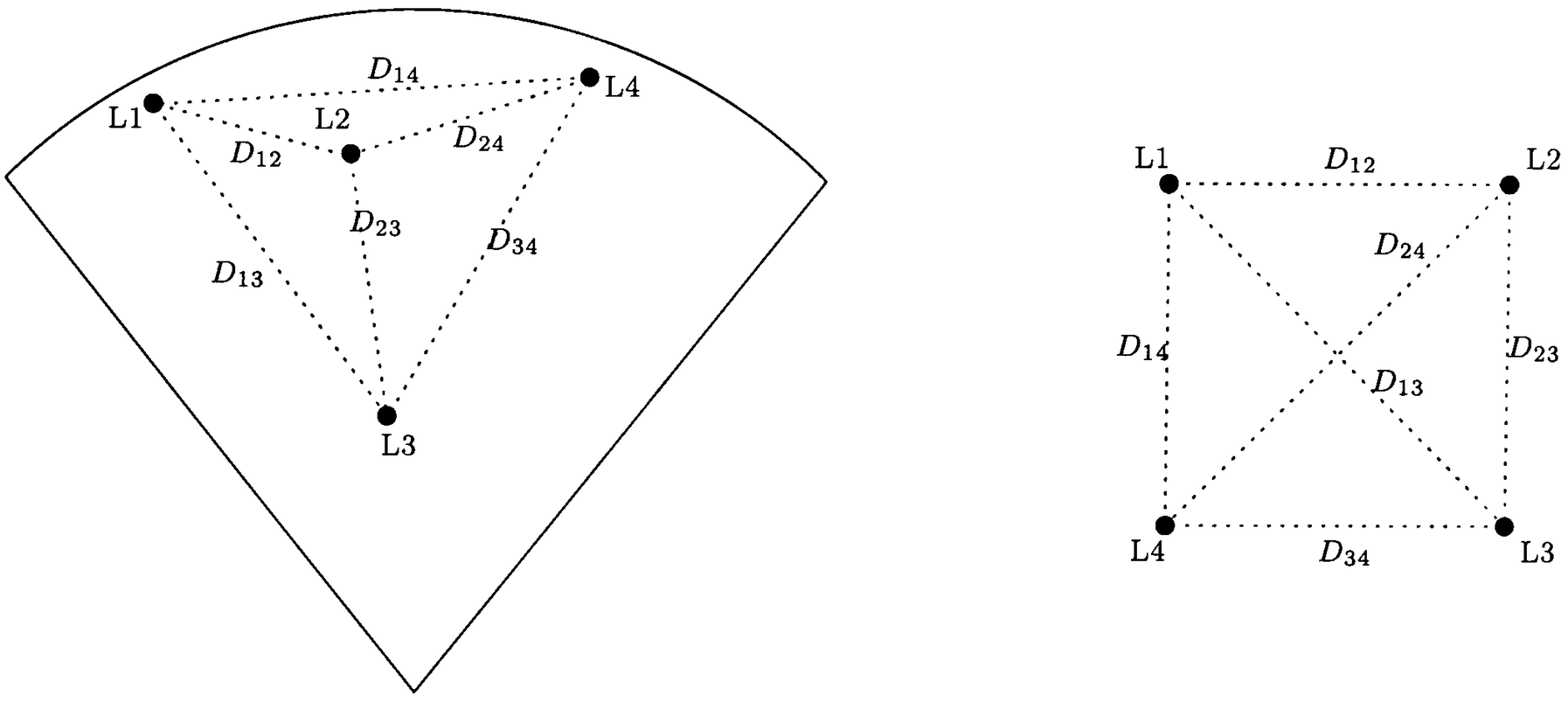

Figure 4.4: Graph-based data association: segmented returns and graph B

problem of finding the maximum common subgraph [24, 92], i.e. finding the common nodes to both graphs. The problem is solved by finding the correspondence between the landmarks in both graphs, figure 4.5 illustrates the correct outcome for the associations, and the correspondence graph where all the possible correspondences between landmarks are illustrated (dotted lines) and the three true edges are also shown (solid lines).

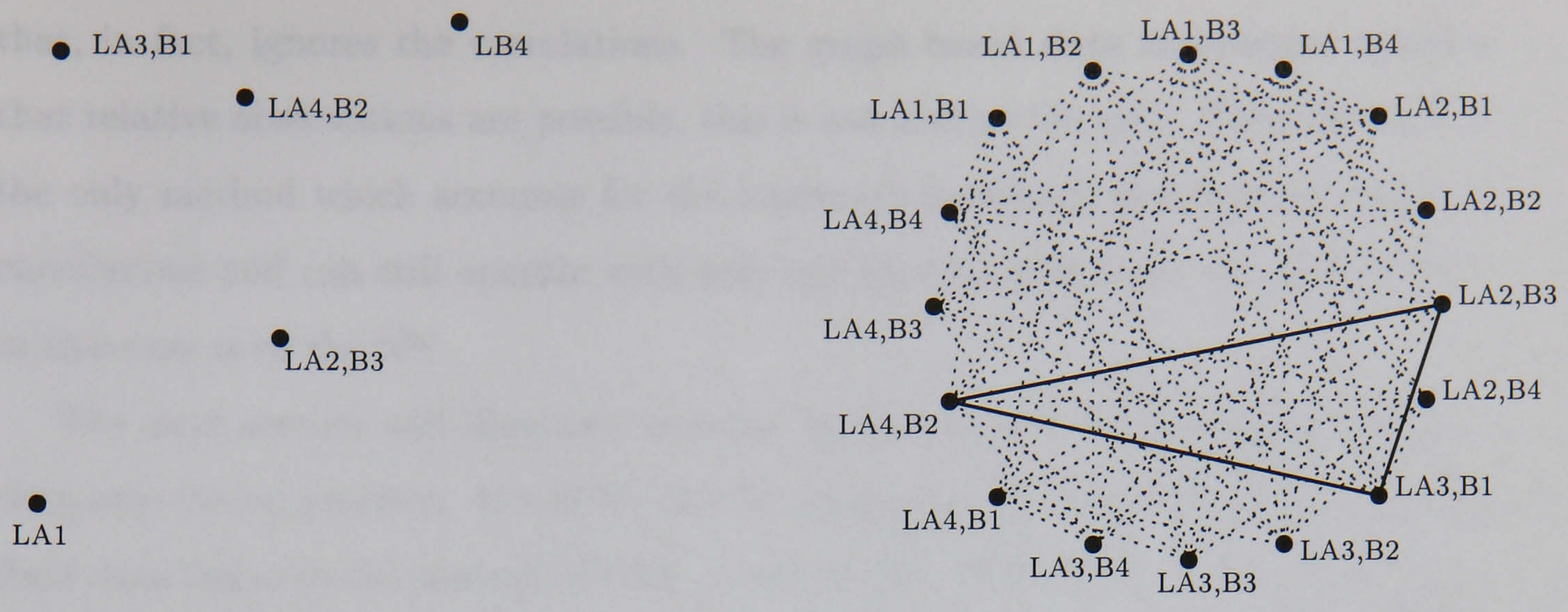

Figure 4.5: Graph-based data association: complete map and correspondence graph

4.3 Summary of Data Association Literature

This chapter has reviewed both the most popular strategies in the single/multiple target tracking and the more specialised strategies adopted in the context of CML. Of the methods adopted by the target tracking community, the NN and MHF have been adapted to solve the data association for CML. The NN method is by far the simplest and least computationally expensive method to implement. The MHF is well founded and, although greedier in computational terms, it provides a number of representations of the environment and the vehicle with a probability assigned to them. It allows for the most probable solution to, hopefully, surface amongst all the other possible solutions. The other methods in the target tracking literature are not as well suited to the CML context. The joint likelihood method for track formation is a batch approach and thus ineffective for the task at hand since CML requires a solution to the data association algorithm at each iteration. The joint probabilistic data association requires the number of targets to be known. This is not the case when concurrently building a map and localising a vehicle.

The data association strategies proposed with CML in mind have all considered the joint associations. Where the NN algorithm takes each measurement individually and assigns a landmark to it, these methods aim at obtaining a consistent solution by jointly examining all the possible associations. The joint assignment matrix, however, ignores the correlations between the landmarks as it was developed under the covariance intersection strategy for CML, a suboptimal approach

that, in fact, ignores the correlations. The graph-based data association requires that relative observations are possible, this is not always the case. Thus the JCT is the only method which accounts for the landmark-landmark and vehicle-landmark correlations and can still operate with only one landmark in sight. Its performance in this case is as the NN.

The next section will illustrate how the landmark descriptors can simplify the data association problem. It will do this by comparing three different strategies for data association in the context of CML: the NN, the MHF and the JCT. This thesis will show how the performance of these three approaches can be improved with the inclusion of landmark descriptors.

4.4 Data Association Using Landmark Descriptors

Most of the CML literature previous to this thesis has considered the data association problem as a problem of assigning range and/or bearing measurements to position estimates of landmarks. The problem, in the context of CML, can be thought of as localising oneself in a forest by mapping every tree through uncertain relative observations between them and one's own uncertain position. However, if the trees in the forest were given descriptors, be they qualitative (tall, large, old, ...) or quantitative, the whole process would be, to a certain extent, simplified. Man made forests where all the trees were planted at the same time could still pose some difficulty. Natural forests, on the other hand, where the trees have grown in a constant battle for sunlight and different species battle for the same territory will be much simpler to map and to localise oneself in. The work which now follows was inspired by this reasoning. Sonar scans, as seen in the previous chapter, allow for descriptors to be assigned to detected landmarks. Only the effort reported by R. N. Carpenter [17] and the author's own efforts [103] have used this information to aid the data association. The aim of this thesis has been to exploit the richness of the data. In the next section the work by Carpenter is explained. This work is fundamentally different to the author's own approach in the way it uses the feature

descriptors within its data association scheme. The method proposed by this thesis is subsequently detailed.

4.4.1 R. N. Carpenter's Modified NN Approach

This work uses feature descriptors essentially to improve the performance of the NN. The validation gate is bi-dimensional and the innovation vector and covariance are made with range and bearing predictions and observations. Observations which fall within the gate are then tested by means of a perceptron network algorithm. The feature descriptors are estimated to be equivalent to their last observation and the perceptron network is fed with similarity measures between the stored values and the new observations. Thus in the validation step the feature descriptors' values are ignored, therefore increasing the size of the gate. In the association step the range and bearing information is ignored; a naive measure if the certainty of the vehicle's position is high. The approach proposed in this thesis includes the landmark feature descriptors in the innovation vector and covariance. This multidimensional space will allow for all the available information to be used in both the validation and association steps. It will also allow for the feature descriptors to be ported into all other standard data association schemes.

4.4.2 A New Observation Model

In the approach presented in this thesis the landmark descriptors are formally introduced into the Kalman filter architecture for reasons which will become obvious. The new observation model will be a vector containing both the relative range and bearing observations, $\mathbf{z}_r$, and the observations of the features descriptors, $\mathbf{z}_f$. Thus,

$$\mathbf{z}(k) = \begin{bmatrix} \mathbf{z}_r(k) \\ \mathbf{z}_f(k) \end{bmatrix} \tag{4.39}$$

Given the following observation models,

$$\mathbf{z}_r(k) = \begin{bmatrix} r(k) & \theta(k) \end{bmatrix}' \tag{4.40}$$

and

$$\mathbf{z}_r(k) = \begin{bmatrix} S(k) & P(k) & C(k) & MD(k) & M_f(k) & M_s(k) \end{bmatrix}' \tag{4.41}$$

where r and θ are the range and bearing to the landmark, and S, P, C, MD, M_f and M_s are the landmark's size, perimeter, compactness, maximum dimension, first invariant moment and second invariant moment descriptors respectively. Not only do landmarks so described become more distinct, but these descriptors can be considered to be uncorrelated to the vehicle's estimate of its own position. The descriptors therefore continue to distinguish landmarks as the vehicle's certainty of its own position deteriorates. The Mahalanobis distance, given the lack of correlation between the feature descriptors and the other estimates in the filter, becomes,

$$\begin{aligned} d^2(k) &= d_r^2(k) + d_f^2(k) \\ &= \upsilon_r'(k)\mathbf{S}_r^{-1}(k)\upsilon_r(k) + \upsilon_f'(k)\mathbf{S}_f^{-1}(k)\upsilon_f(k) \end{aligned} \tag{4.42}$$

where the innovations are

$$\upsilon_r(k) = \mathbf{z}_r(k) - \hat{\mathbf{z}}_r(k) \tag{4.43}$$

and

$$\upsilon_f(k) = \mathbf{z}_f(k) - \hat{\mathbf{z}}_f(k) \tag{4.44}$$

and $\mathbf{S}_r(k)$ and $\mathbf{S}_f(k)$ are their respective covariances. It is thus clear by observing equation 4.42 that as the uncertainty of the vehicle's position increases $d_f^2(k)$ will become the predominant term,

$$\text{tr } \mathbf{S}_r(k) \gg \text{tr } \mathbf{S}_f(k) \tag{4.45}$$

then

$$d^2(k) \approx d_f^2(k) \tag{4.46}$$

the reverse is also true. Therefore a system with high uncertainty of the feature descriptors will revert to its typical behaviour. In most cases however the descriptors

will be a part of the innovation space and play a fundamental part in the validation process. Further, their inclusion in the Kalman filter architecture make them readily accessible as a part of any conventional data association scheme.

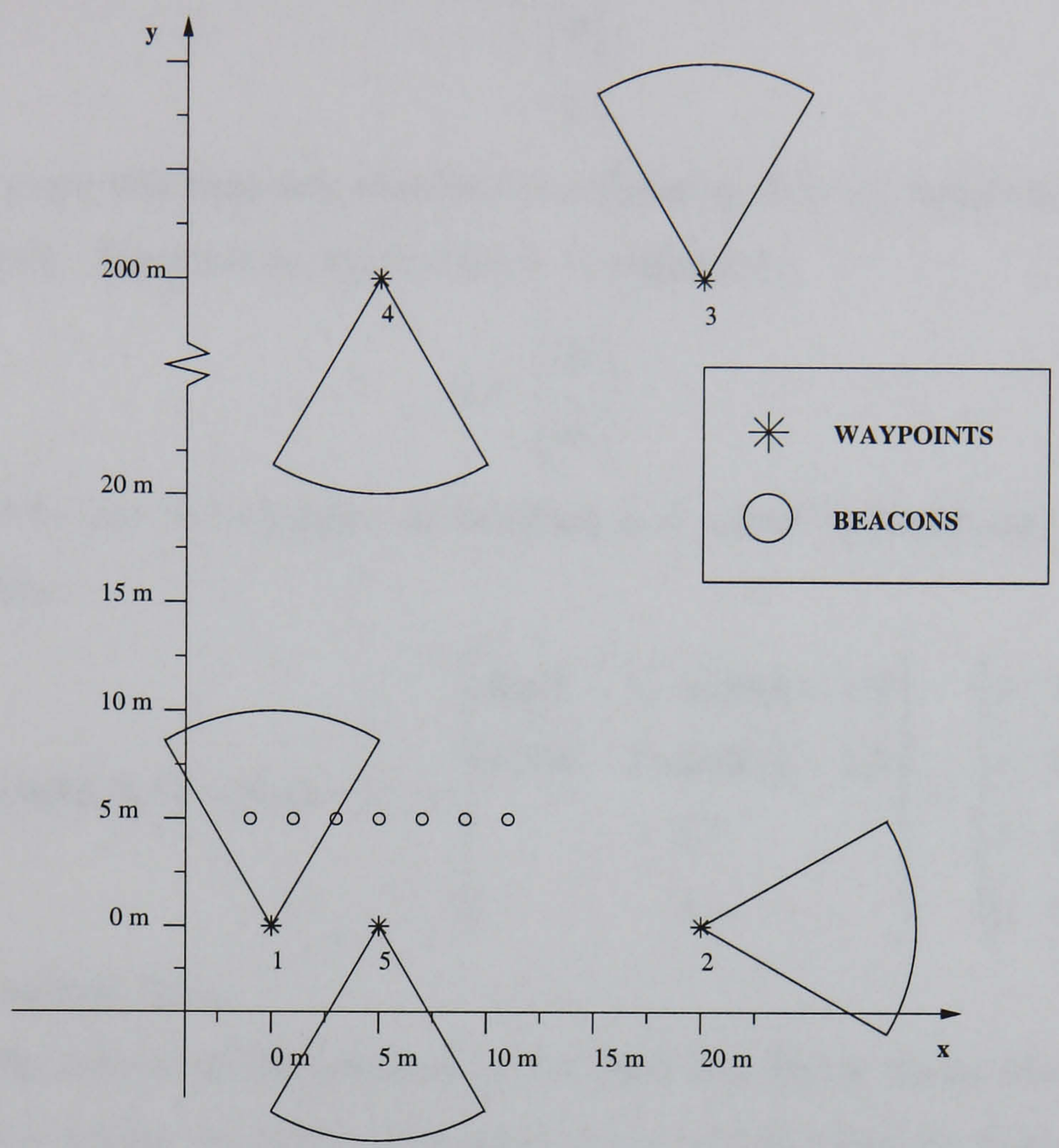

Figure 4.6: Example scene for comparison of data association with and without feature extraction

The following example illustrates the most obvious benefits of using descriptors. It is not a realistic experiment as the simulated sonar returns are assumed to be view independent. However, it illustrates well the benefits of the landmark descriptors. In the example a simulated vehicle travels through a predetermined set of waypoints and observes a set of seven landmarks (the scene is illustrated in figure 4.6) and the pie sectors show the predicted sectors scanned by the sonar upon arrival at the waypoints. Note that the uniform spacing between the landmarks will serve to confuse all the data association strategies. In this simulation the vehicle adopts a simple model [36],

$$\hat{\mathbf{x}}_{\mathbf{v}}(k) = \mathbf{f}_{\mathbf{v}}[\hat{\mathbf{x}}_{\mathbf{v}}(k-1), \mathbf{u}(k), \mathbf{0}, k] \tag{4.47}$$

where the state vector is equivalent to,

$$\mathbf{x} = \begin{bmatrix} x \\ y \\ \theta \\ v \end{bmatrix} \tag{4.48}$$

where x and y are the vehicle's absolute coordinates, θ is the heading of the vehicle and v the speed. The control input vector is defined as,

$$\mathbf{u} = \begin{bmatrix} \delta\theta \\ \delta v \end{bmatrix} \tag{4.49}$$

where $\delta\theta$ and δv are the changes in heading and speed respectively. The transfer function is thus,

$$\mathbf{f_v}[\hat{\mathbf{x}}_\mathbf{v}(k-1), \mathbf{u}(k), \mathbf{0}, k] = \hat{\mathbf{x}}_\mathbf{v}(k-1) + \begin{bmatrix} dtv(k-1)\cos(\theta(k-1)) \\ dtv(k-1)\sin(\theta(k-1)) \\ 0 \\ 0 \end{bmatrix} + \begin{bmatrix} 0 & 0 \\ 0 & 0 \\ 1 & 0 \\ 0 & 1 \end{bmatrix} \mathbf{u}(k) \tag{4.50}$$

where t is the sample time.

However, the vehicle model assumed by the filter is a linear model which assumes no knowledge of the vehicle dynamics. The state of the vehicle takes the following form,

$$\mathbf{x_v}(k) = \begin{bmatrix} x & \dot{x} & \ddot{x} & y & \dot{y} & \ddot{y} & \phi & \dot{\phi} & \ddot{\phi} \end{bmatrix}' \tag{4.51}$$

with the following dynamic model,

$$\mathbf{F_v}(k) = \begin{bmatrix} \mathbf{F_{v_x}}(k) & \mathbf{0} & \mathbf{0} \\ \mathbf{0} & \mathbf{F_{v_y}}(k) & \mathbf{0} \\ \mathbf{0} & \mathbf{0} & \mathbf{F_{v_\phi}}(k) \end{bmatrix} \tag{4.52}$$

where

$$\mathbf{F_{v_x}}(k) = \mathbf{F_{v_y}}(k) = \mathbf{F_{v_\phi}}(k) = \begin{bmatrix} 1 & dt & \frac{1}{2}dt^2 \\ 0 & 1 & dt \\ 0 & 0 & 1 \end{bmatrix} \tag{4.53}$$

And process noise,

$$\mathbf{Q_v}(k) = \begin{bmatrix} \mathbf{Q_{v_x}}(k) & \mathbf{0} & \mathbf{0} \\ \mathbf{0} & \mathbf{Q_{v_y}}(k) & \mathbf{0} \\ \mathbf{0} & \mathbf{0} & \mathbf{Q_{v_\phi}}(k) \end{bmatrix} \tag{4.54}$$

where,

$$\mathbf{Q_{v_x}}(k) = \begin{bmatrix} \frac{1}{4}dt^4 & \frac{1}{2}dt^3 & \frac{1}{2}dt^2 \\ \frac{1}{2}dt^3 & dt^2 & dt \\ \frac{1}{2}dt^2 & dt & 1 \end{bmatrix} \sigma_{v_x}^2 \tag{4.55}$$

Sonar Sector	60°
Sonar Angular Resolution	1°
Sonar Angular Accuracy	1°
Sonar Range	$20m$
Sonar Range Resolution	$0.05m$
Sonar Range Accuracy	$0.05m$
Sonar Update Rate	$1Hz$
Compass Resolution	0.08°
Compass Accuracy	4°
Compass Update Rate	$1Hz$
Velocity Log Resolution	$0.01m/s$
Velocity Log Accuracy	$0.06m/s$
Velocity Log Update Rate	$1Hz$

Table 4.1: Sensor Values for Data Association Experiment

The vehicle uses a compass and a velocity log to provide dead-reckoning. The parameters for the accuracies and resolution of the different sensors can be seen in table 4.1. This experiment has been run for three different data association schemes. For all the cases the experiment was initially run using only the range and bearing bi-dimensional innovation vector, $\upsilon_r(k)$. Later the experiment was also run for all cases using the multidimensional innovation vector, υ, using all feature information.

Experiment Using Only Range and Bearing Observations

In this part of the experiment the sonar would scan the environment and map the landmarks when travelling from the first to the second waypoint. Figure 4.7 illustrates the initial state of the stochastic map. This is the first iteration of the filter

and two landmarks have been found and correctly mapped. In the next iteration figure 4.8 shows the resulting scene using both NN and the most probable MHF event. Again the new landmarks have been found and the correct data association has been achieved. The result obtained using the JCT can be seen in figure 4.9. The approach has thus fallen at the first hurdle. The explanation is simple: the JCT searches for the maximum number of associations which fall within the validation region. This is not necessarily a measure of the most probable event. The uniform spacing between the landmarks has contributed to the confusion of the JCT approach. Using feature descriptors, as will be demonstrated later, the validation gate can be made more restrictive and failure can be avoided. The test is continued for the NN and the MHF. At iteration 306 the vehicle has reached the fourth waypoint and is travelling towards the fifth waypoint. The uncertainty of its position has grown considerably. It has only been using dead-reckoning sensors, see figure 4.10. Finally the vehicle re-observes the mapped landmarks. The reader is reminded that the observations are assumed view independent. However, the error in the vehicle's own position is such that it fails to correctly associate the observations to the stored landmarks. Figure 4.11 shows the results obtained by using NN and the result of the most probable map stored by the MHF. The implementation keeps the twenty most probable maps at each iteration. Thus the three systems have failed to correctly re-localise the vehicle and the result is an inconsistent map and a potentially disastrous situation as, given the absence of ground truth, it would be impossible to determine that this is indeed the case. The second part of the experiment introduces the feature descriptors for the same mission. The results are detailed below.

Experiment Using the Landmark Descriptors

Again the experiment follows the same pattern as before. The difference now being that the landmarks have descriptors assigned to them. Table 4.2 shows the value of these descriptors and table 4.3 shows the variances assigned to these. The values of these descriptors are typical values obtained from the experiments in the previous chapter. Throughout the experiment the sonar returns are still assumed to be view independent. In this experiment, the JCT, due to the more restrictive gate, performs well on the second and subsequent iterations. The initial results follow

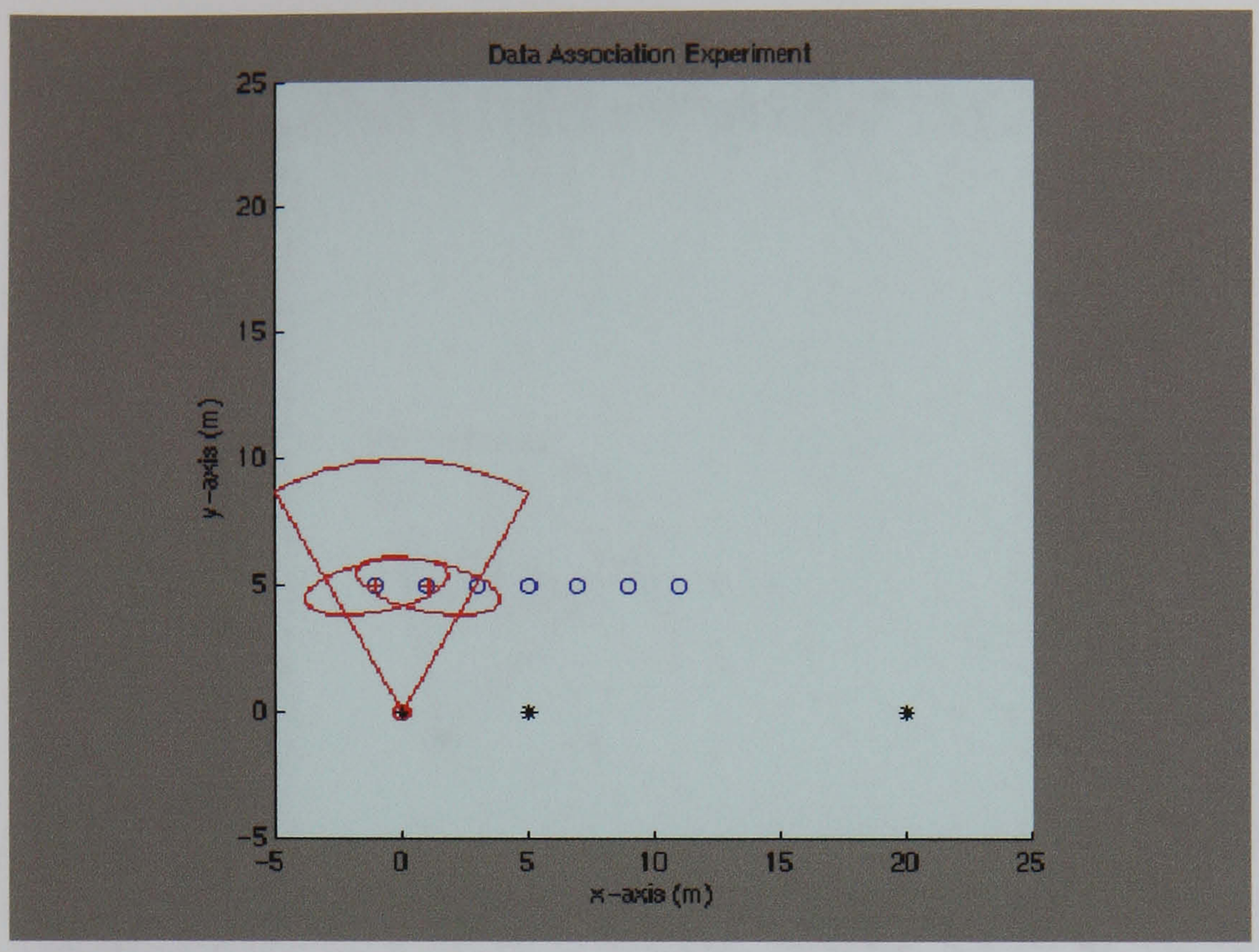

Figure 4.7: First Iteration: The red trail and sector are the estimated trajectory and the estimated field of view of the vehicle; the blue dashed trail and sector are the true trajectory and field of view of the vehicle; the blue circles show the true position of the landmarks; the magenta crosses and dashed ellipses represent their estimated position and uncertainty and the red crosses and ellipses represent their estimated position and uncertainty. Two landmarks have been observed and properly mapped.

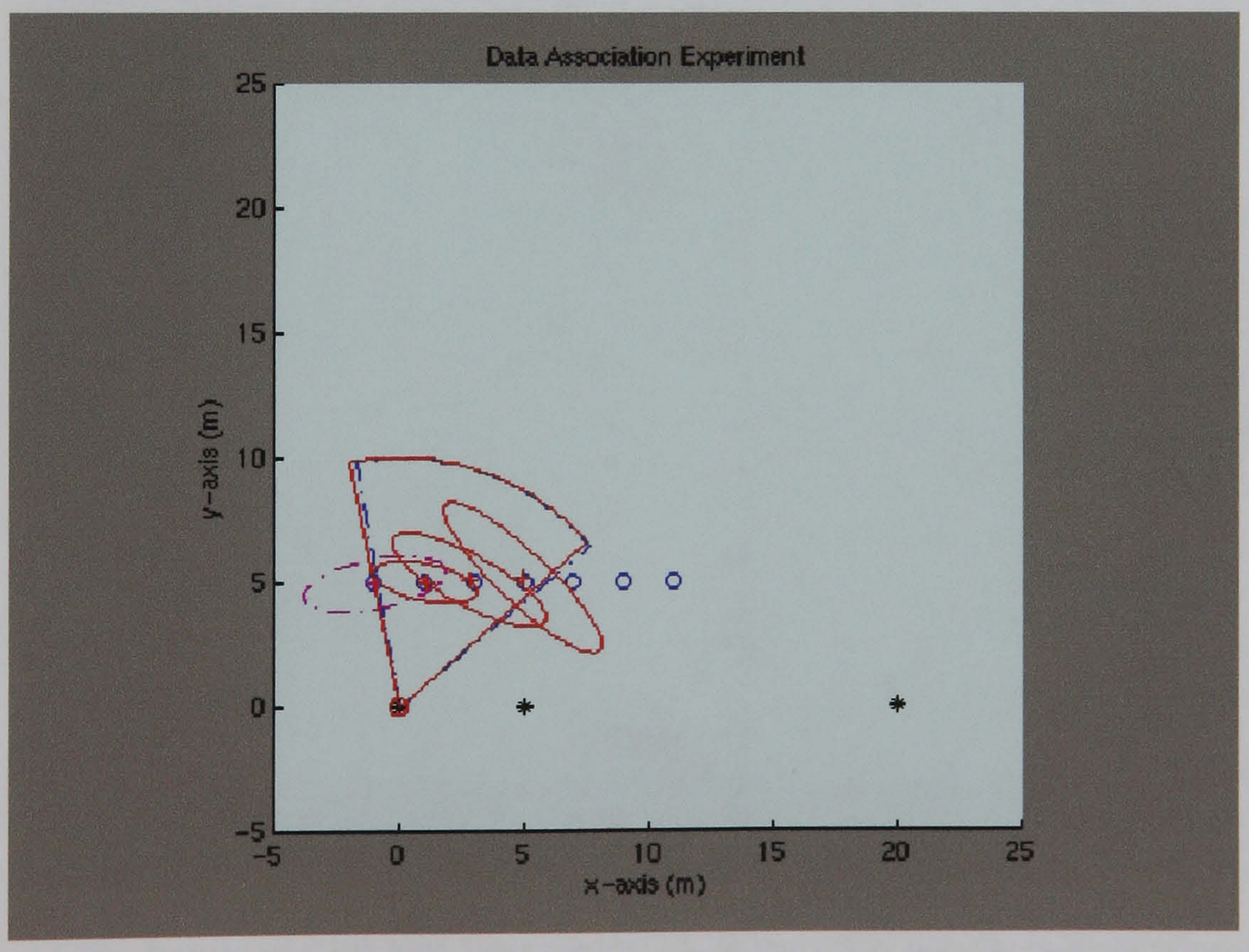

Figure 4.8: Second Iteration: NN and MHF. Two new landmarks and an old landmark have been observed and properly associated to existing landmarks on the map.

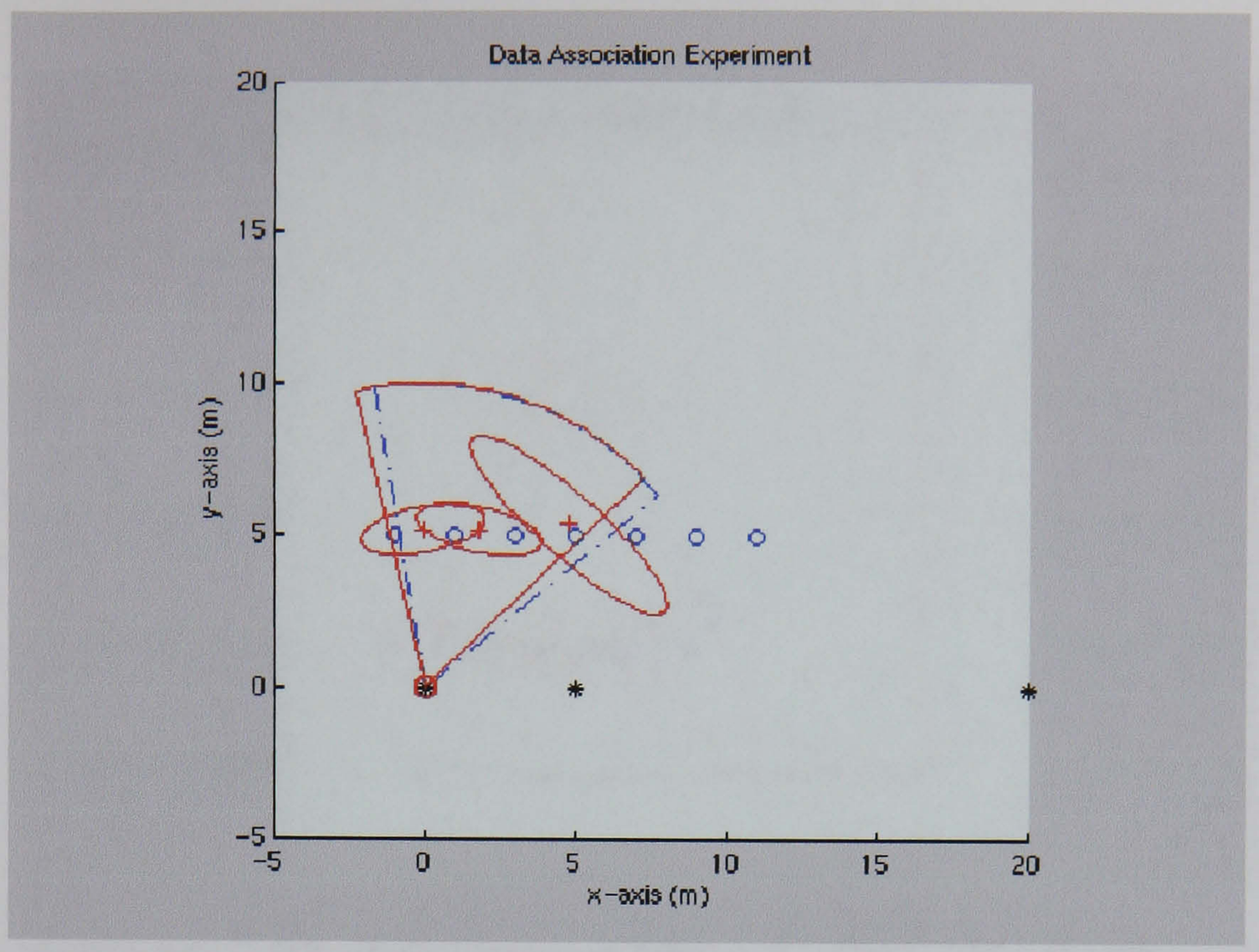

Figure 4.9: Second Iteration: JCT. Two new landmarks and an old landmark have been observed. Landmark two has been incorrectly assigned to landmark one. Landmark three to two and the fourth landmark has initialised the correct landmark

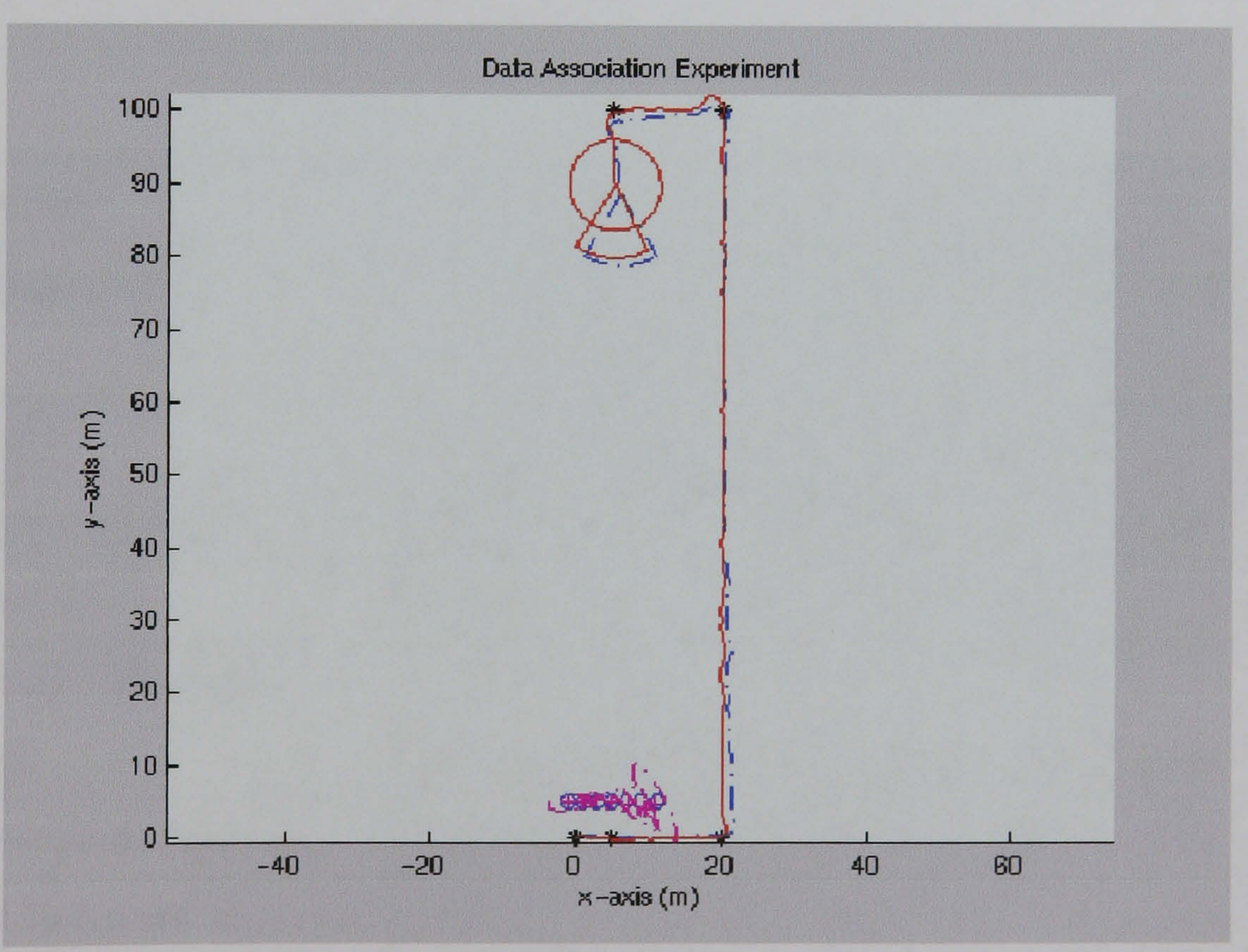

Figure 4.10: Iteration 306: NN and MHF. The filter has reached the fourth waypoint and is on its way to the last waypoint. The error in its position and the uncertainty have grown

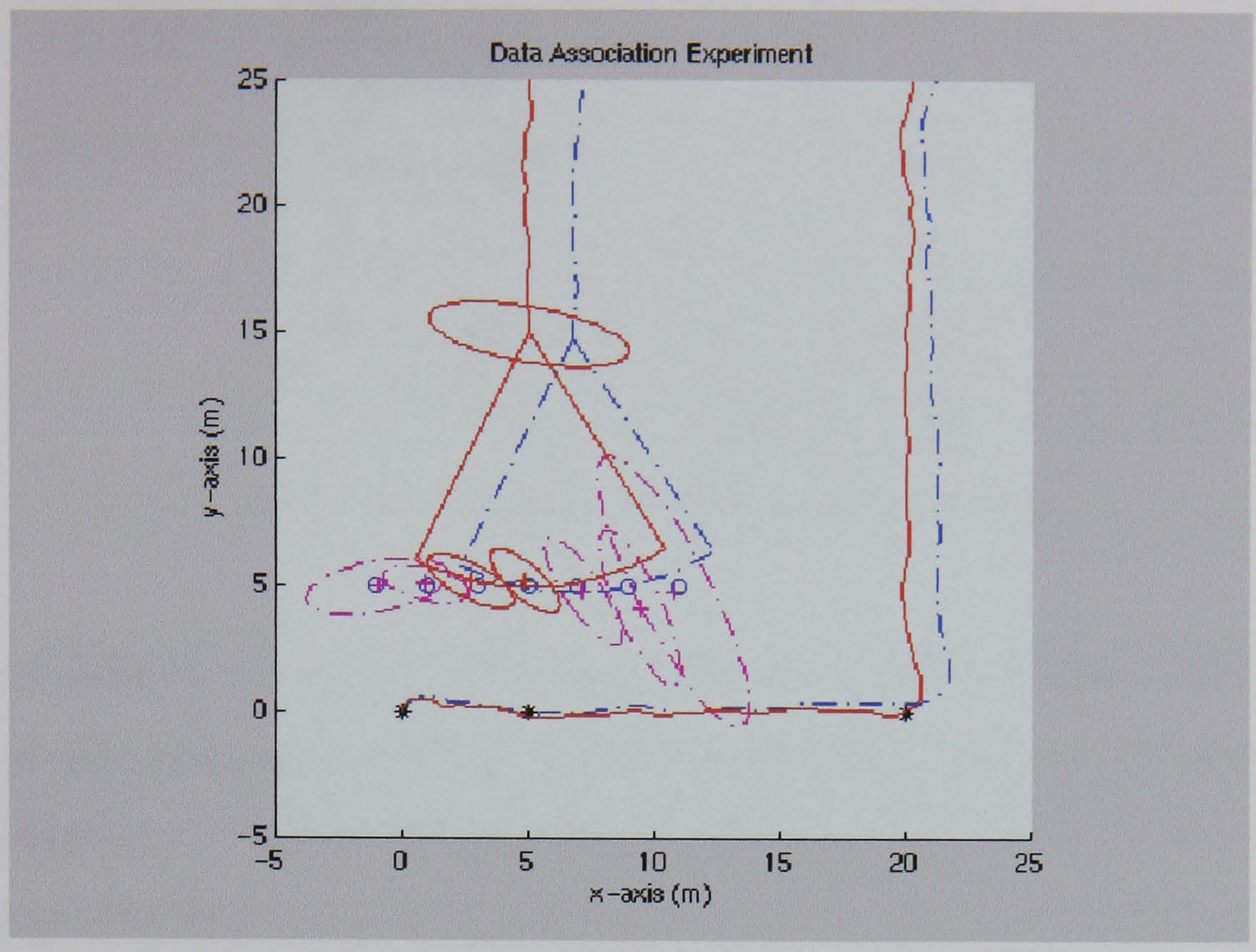

Figure 4.11: Iteration 448: NN and MHF. Landmarks four and five have been incorrectly assigned to landmarks three and four stored on the map.

Landmarks:	1	2	3	4	5	6	7
Coordinates (m):	-1.0 5.0	1.0 5.0	3.0 5.0	5.0 5.0	7.0 5.0	9.0 5.0	11.0 5.0
Size (m^2):	31.4	11.6	4.4	15.5	4.0	4.5	9.7
Perimeter (pixels):	538	235	150	426	127	118	195
Compactness:	130.0	66.0	71.0	160.4	55.4	43.8	54.5
Maximum Dimension (pixels):	100.9	73.6	58.4	96.8	43.1	42.6	59.3
First Invariant Moment:	0.306	0.398	0.771	0.533	0.447	0.378	0.344
Second Invariant Moment:	0.039	0.121	0.641	0.223	0.179	0.1198	0.097

Table 4.2: Landmark Descriptors and Coordinates for Landmarks

Descriptor	Variance
Size:	1.96
Perimeter:	441
Compactness:	104.4
Maximum Dimension:	49
First Invariant Moment:	0.0049
Second Invariant Moment:	0.0028

Table 4.3: Variances of Landmark Descriptors

the same pattern of good results as the experiments detailed earlier, figures 4.7, 4.8 and 4.10. However, upon re-observation the data association is successful for all three filters; figure 4.12. This simple experiment has shown how the addition of landmark descriptors can improve the data association capabilities of three different systems. In the next section a carefully prepared set of experiments will illustrate to what extent the performance is improved. It will also compare the three different data association strategies. It will show that, with the addition of landmark descriptors, the NN becomes a suitable data association strategy.

4.5 Data Association Comparison Experiments

The following experiments have been designed to compare the three different data association strategies, with and without landmark descriptors. The experiments simulate the case of a vehicle being placed in the middle of a previously mapped region. The vehicle must correctly match the new observed landmarks with those stored on the map. The experiments will be carried out using the three different association strategies for increasing uncertainty in the vehicle's position, the vehicle's orientation and the position of the landmarks. The size of the workspace is $30 \times 30m^2$. The vehicle is placed at random locations in the workspace. The landmarks are also randomly distributed in the workspace. Thus, there is more information held by the positional states than there was in the previous example. The spatial ambiguity caused by uniformly spaced landmarks has been eliminated.

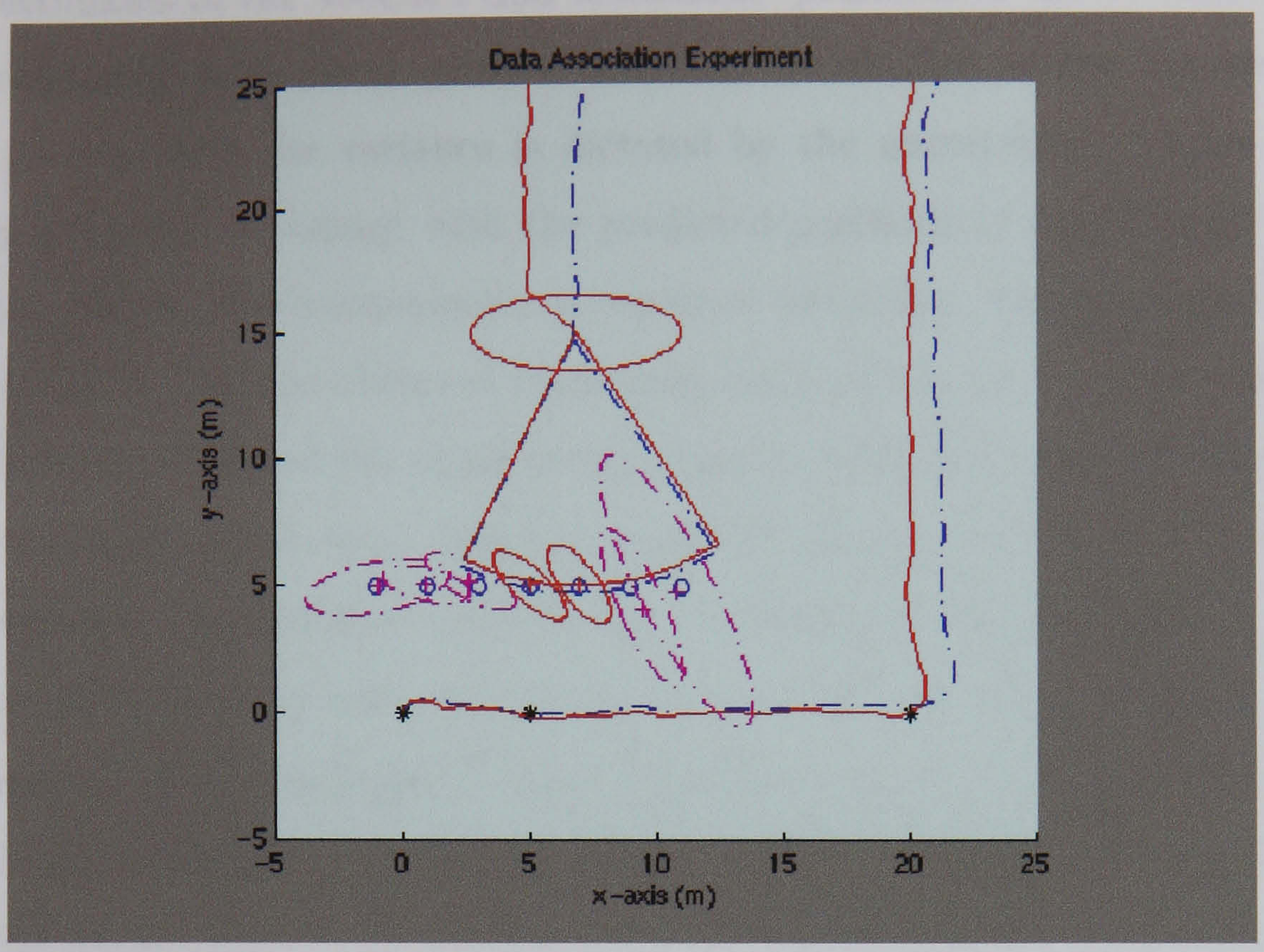

Figure 4.12: Iteration 448: NN and MHF. Landmarks four and five have been correctly assigned to landmarks four and five stored on the map.

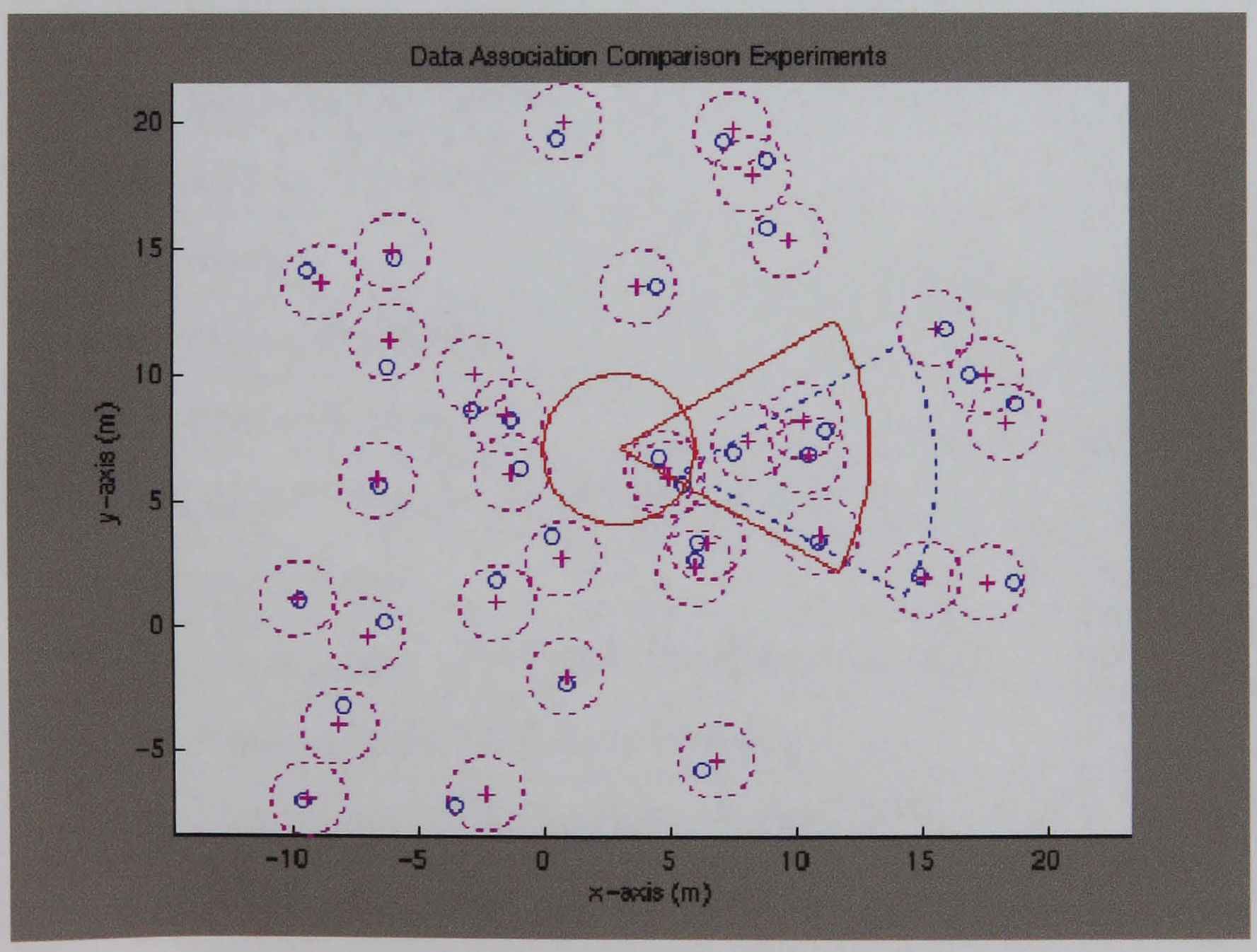

Figure 4.13: Data association comparison experiments typical workspace. The red sector is the estimated field of view of the vehicle; the red ellipse represents the vehicle's position uncertainty; the dashed blue sector is the true field of view of the vehicle; the blue circles show the true position of the landmarks; the magenta crosses and dashed ellipses represent their estimated position and uncertainty.

The estimates of the vehicle's and landmarks' positions in the stochastic map are also randomly determined, given a Gaussian distribution, where the mean is their true position and the variance is dictated by the uncertainty. Figure 4.13 illustrates a typical workspace with the predicted positions of the mapped landmarks and the vehicle. Each experiment is repeated 100 times. The experiment is said to be successful if all the observed landmarks are correctly matched. If any landmark is incorrectly matched the experiment is considered unsuccessful. If the experiment fails to match one or more observations to the mapped landmarks the experiment is considered unsuccessful but recorded. The common parameters for the experiments can be seen in table 4.4. In the first set of experiments only the positional information of the landmarks is used. The second set of experiments are made with positional information aided by one good quality landmark descriptor. Two good descriptors are used in the third set of experiments and the effects of bad quality descriptors are examined in the last set of experiments. All the experiments assume view independent returns.

Sonar Sector	60°
Sonar Angular Resolution	1°
Sonar Angular Accuracy	1°
Sonar Range	$10m$
Sonar Range Resolution	$0.05m$
Sonar Range Accuracy	$0.05m$
Probability Threshold for Validation Region	0.9
Landmark Density	$0.0378m^{-2}$
Initial Uncertainty of Vehicle's Position ($\sigma_{\mathbf{v}_x}$,$\sigma_{\mathbf{v}_y}$)	$0.1m$
Initial Uncertainty of Vehicle's Heading ($\sigma_{\mathbf{v}_\theta}$)	1°
Initial Uncertainty of Landmarks' Positions ($\sigma_{\mathbf{p}_x}$,$\sigma_{\mathbf{p}_y}$)	$0.1m$

Table 4.4: Common Parameters for Data Association Experiments

4.5.1 Data Association Experiments Using Only Position Information

This set of experiments are performed using only the range and bearing from the landmarks. The results obtained will serve as a means of comparing the three different association strategies. Table 4.5 shows the data association results obtained for instances of low uncertainty, as given by the standard deviation values in table 4.4. The next section explores the effects of increasing the uncertainty and error in the landmarks' positions estimates. The following section explores the effects of increasing the vehicle's position estimate. The final section explores that of increasing the vehicle's heading uncertainty.

	NN	MHF	JCT
Correct Associations (%)	99	99	99
Non-incorrect Associations (%)	100	100	100

Table 4.5: Data Association No Descriptors - Low Uncertainty: When all landmarks are correctly associated the experiment will be classed as *Correct Association*. When at least one observation was correctly associated and the rest were not associated to any other landmark the experiment will be classed as *Non-incorrect Association*.

Increasing Landmarks' Positions Uncertainty and Error

The results obtained for this part of the experiment show that the performance of the standard data association strategies quickly degrades as the uncertainty of the landmarks increases. Figure 4.14 (a) shows the outcome of the NN algorithm. For standard deviations beyond 1.5 metres for the x and y coordinates the algorithm's performance drops below 50 %. The results of the most probable associations proposed by the MHF are of less quality than those obtained by the NN algorithm, see figure 4.14 (b). Similar results to the NN are obtained with the JCT, figure 4.14 (c).

Increasing Vehicle's Position Uncertainty and Error

These results show that the strategies are also severely influenced by increases of the vehicle's position uncertainty. The NN algorithm, figure 4.15(a), drops below 50 %

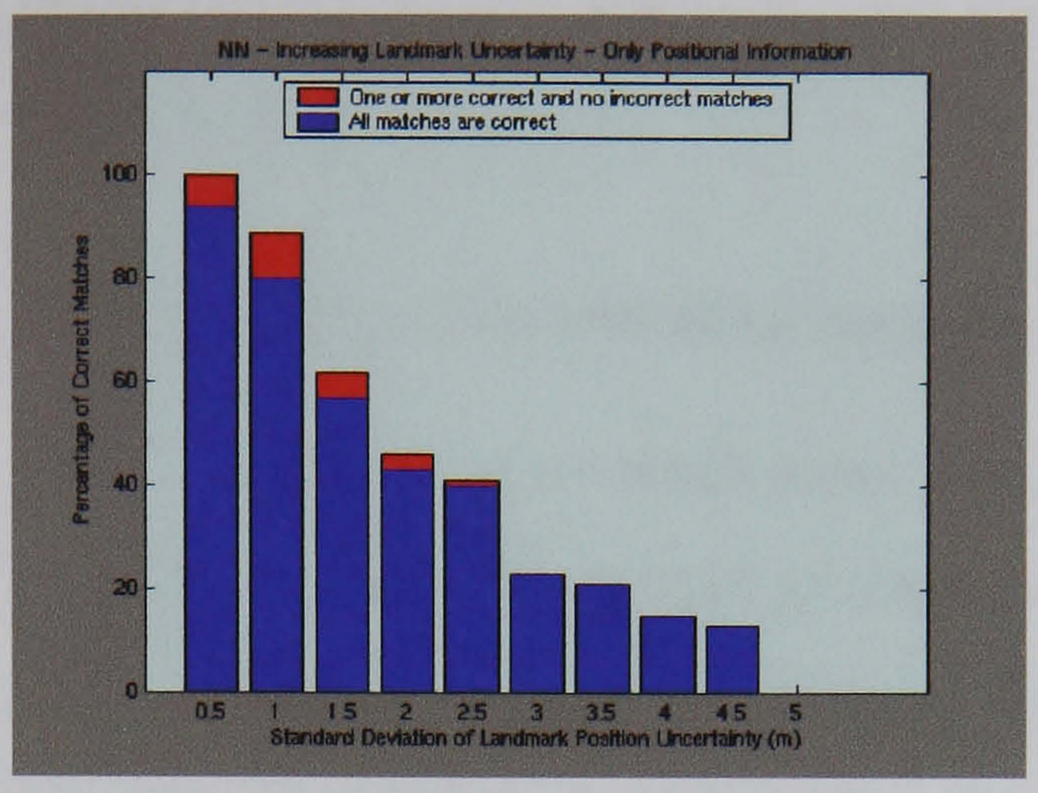

(a)

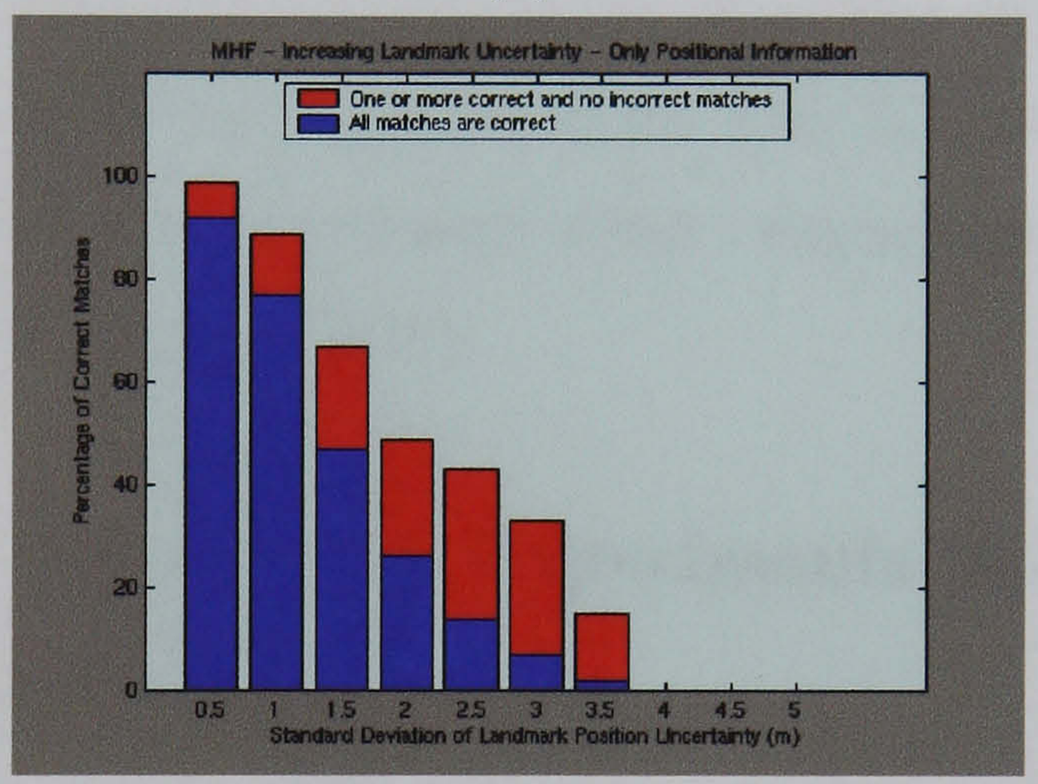

(b)

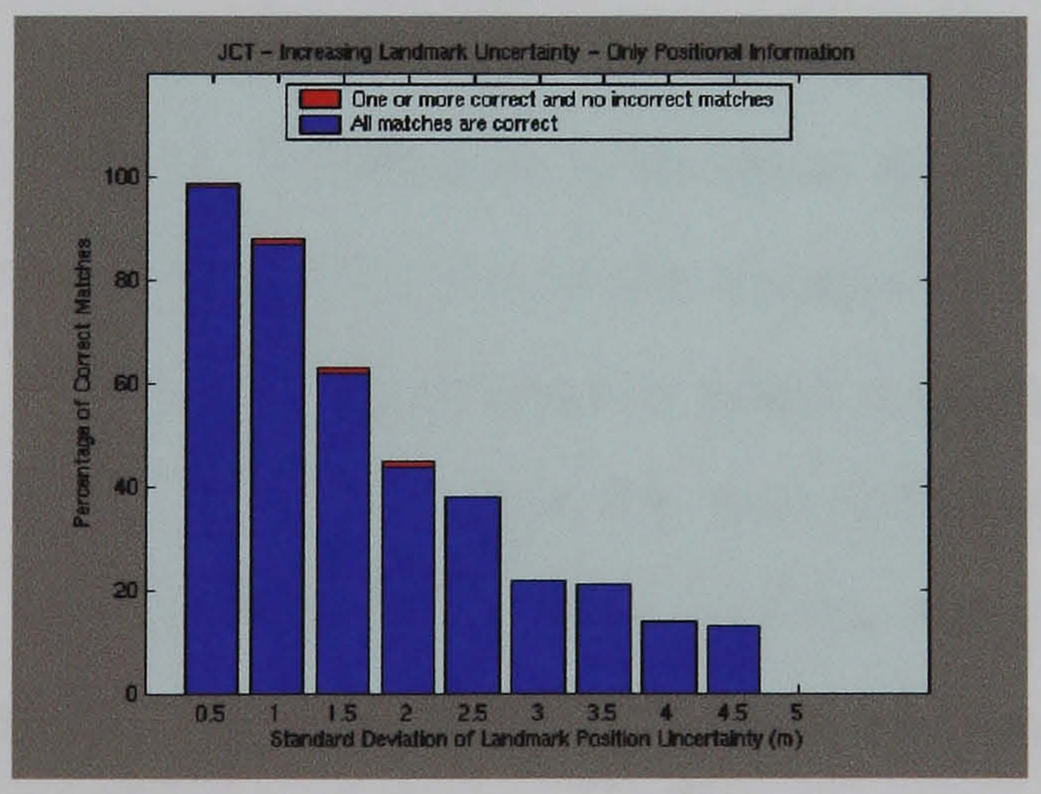

(c)

Figure 4.14: Results obtained only using range and bearing measurements, for (a) NN, (b) MHF and (c) JCT. Each column illustrates the correct associations obtained from 100 data association experiments (blue) and the associations where at least one observation was correctly associated and the rest were not associated to any other landmark (red). The increasing values of the columns are the 1σ values of the landmarks' positions.

success for standard deviations beyond 1 metre. The MHF, figure 4.15(b), doesn't provide a single correct association beyond 1.5 metres standard deviation. Only the JCT shows some degree of robustness, figure 4.15(c), dropping below 50 % success for standard deviations above 2.5 metres.

Increasing Vehicle's Heading Uncertainty and Error

The results show that the algorithms are much more robust to increased uncertainty and error in the heading estimate than would perhaps be expected. The NN algorithm, as can be seen in figure 4.16 (a), has a sharp drop in performance as the standard deviation of the uncertainty becomes 20°. As the uncertainty and error grow beyond 20°, the performance of the algorithm degrades only slightly. The MHF displays a similar performance, figure 4.16 (b). The JCT also experiences a sharp drop. However the performance doesn't degrade as the error and uncertainty increase beyond 20°, figure 4.16 (c).

4.5.2 Data Association Experiments Aided by Landmark Descriptor

In this set of experiments the data association incorporates one landmark descriptor into the landmarks' observations. The descriptor will be simulated and the values will not necessarily be in accordance with those found in the previous chapter. However it will give a clear indication of the changes of performance expected with its introduction. This landmark descriptor takes a uniformly distributed random value between 0 and 10. The map stores this value taking the true value as the mean and with a Gaussian random error of standard deviation 0.1. The descriptor should incorporate information into the filter and, given the uncertainty, it is considered a good descriptor. Again the three association strategies are examined and the new results will serve to compare the performance of these with respect to the performance observed in the previous set of experiments. Table 4.6 shows the data association results obtained for instances of low uncertainty, as given by the standard deviation values in table 4.4. Again the effects of increasing the uncertainty and error in the landmarks' positions estimates, the vehicle's position estimate and the

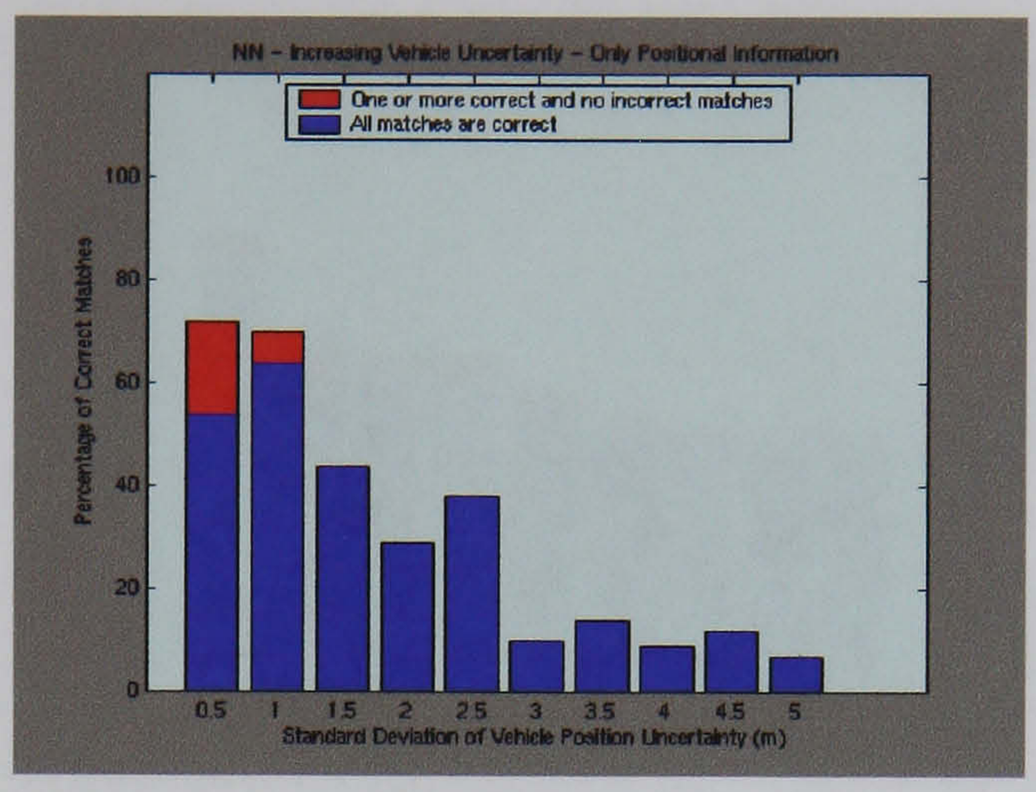

(a)

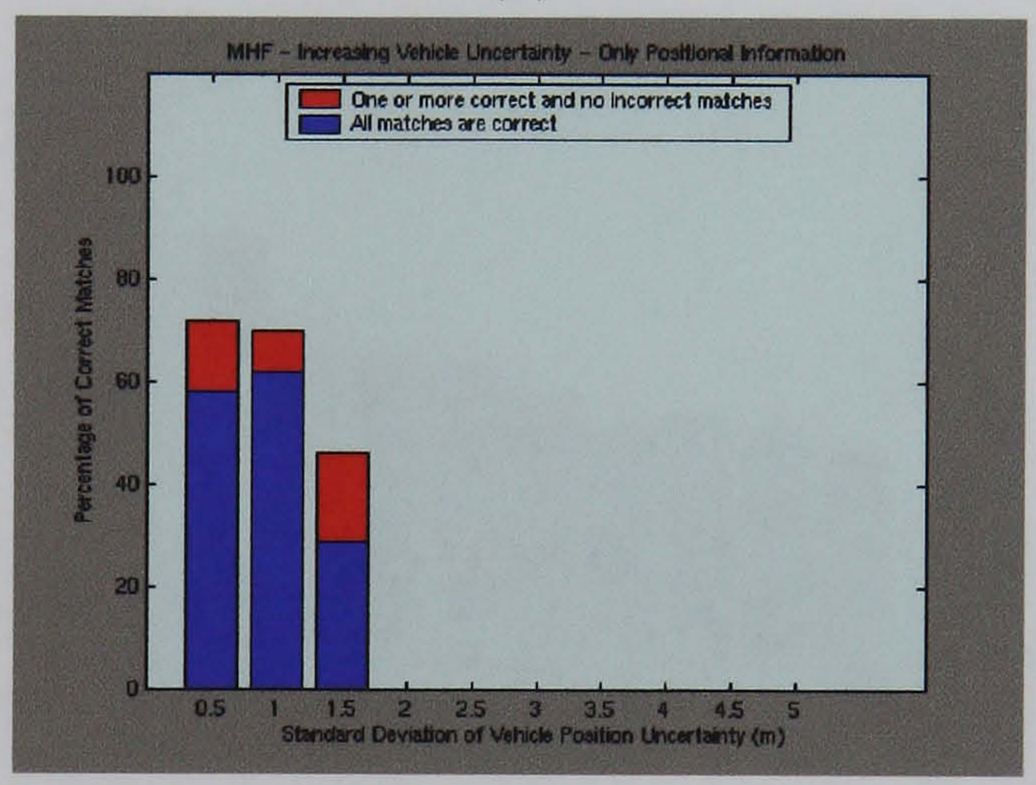

(b)

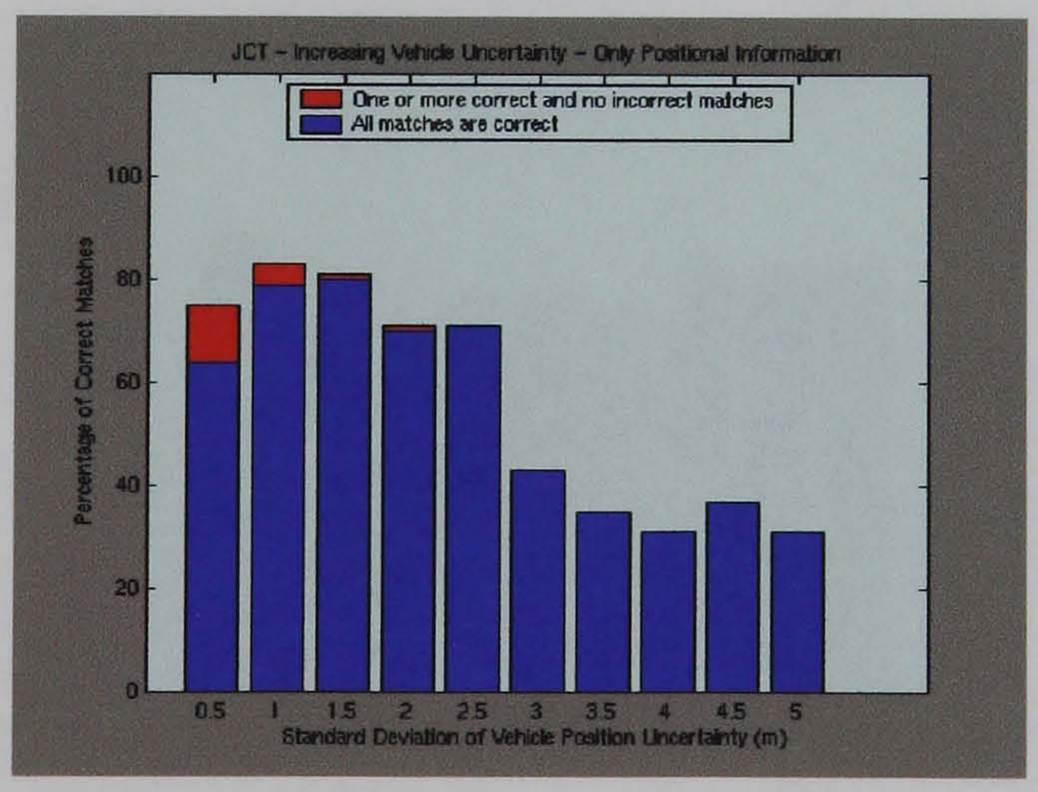

(c)

Figure 4.15: Results obtained only using range and bearing measurements, for (a) NN, (b) MHF and (c) JCT. Each column illustrates the correct associations obtained from 100 data association experiments (blue) and the associations where at least one observation was correctly associated and the rest were not associated to any other landmark (red). The increasing values of the columns are the 1σ values of the vehicle's position.

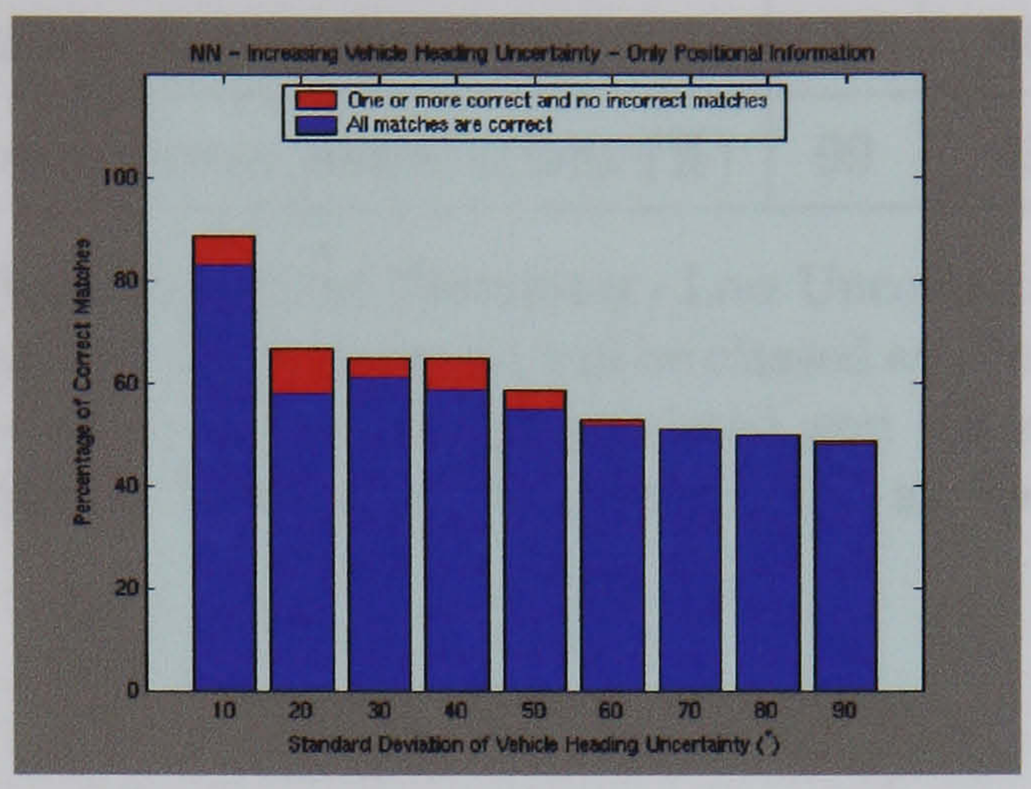

(a)

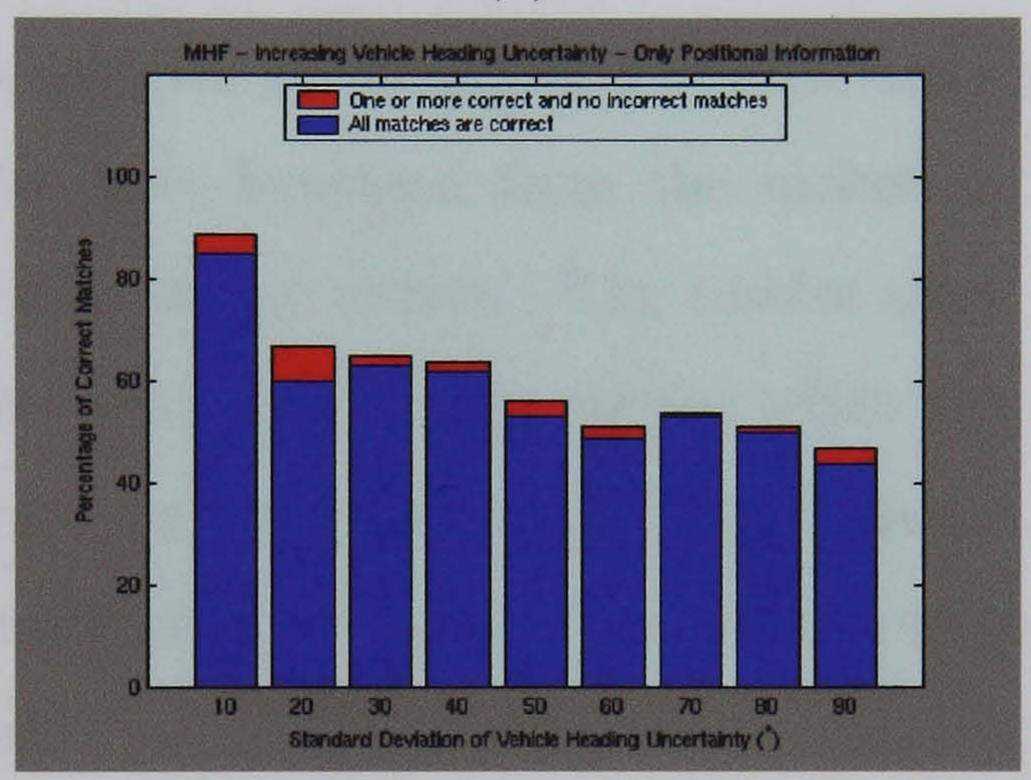

(b)

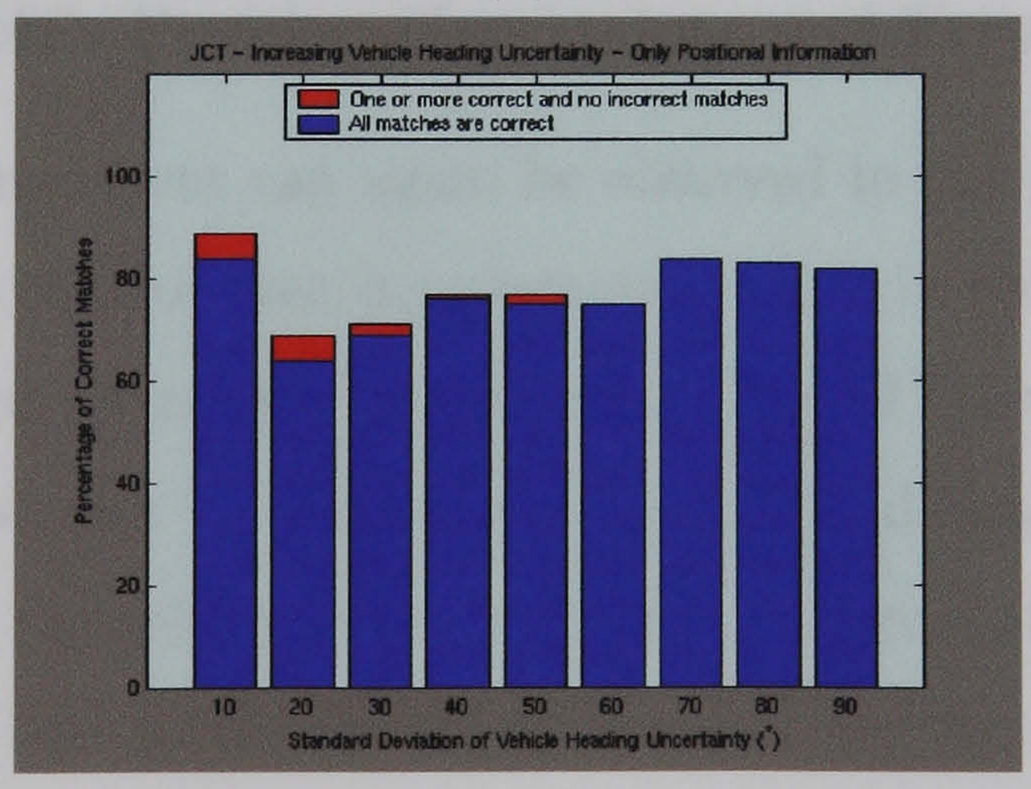

(c)

Figure 4.16: Results obtained only using range and bearing measurements, for (a) NN, (b) MHF and (c) JCT. Each column illustrates the correct associations obtained from 100 data association experiments (blue) and the associations where at least one observation was correctly associated and the rest were not associated to any other landmark (red). The increasing values of the columns are the 1σ values of the vehicle's heading.

vehicle's heading estimate are explored in the following sections.

	NN	MHF	JCT
Correct Associations (%)	96	96	98
Non-incorrect Associations (%)	99	99	99

Table 4.6: Data Association One Descriptor - Low Uncertainty: When all landmarks are correctly associated the experiment will be classed as *Correct Association*. When at least one observation was correctly associated and the rest were not associated to any other landmark the experiment will be classed as *Non-incorrect Association*.

Increasing Landmarks' Positions Uncertainty and Error

The positive effects achieved by introducing a single descriptor are clear, figure 4.17. The three strategies have benefited from the inclusion of an extra uncorrelated state in the landmarks' state vectors. The results show that the performance of the three association strategies is very similar when the error and uncertainty in the landmarks' positions increases, and the degradation, when compared to the association performance which resulted from a state vector without the descriptor, is much less affected.

Increasing Vehicle's Position Uncertainty and Error

A substantial improvement can again be observed in the performance of the three strategies, figure 4.18. However, a systematic feature in the algorithms performance can be observed for an error with 1σ uncertainty of $0.5m$. The results, although better than for the case of a state vector with no descriptor, are worse than for increased errors in the vehicle's position. Only for errors of 1σ uncertainty of $3m$ or higher, for the NN and MHF, and $3.5m$ or higher, for the JCT, do they deteriorate below that level. This phenomenon can be explained in terms of the respective weights of the different innovations in the validation region, equation 4.42. The predominant term for low vehicle uncertainties is that of the position, which in this case substantially degrades the algorithm performance. The increase of the vehicle's position uncertainty produces a shift in the dominance, such that the descriptor becomes dominant and consequentially the results are improved due to the better

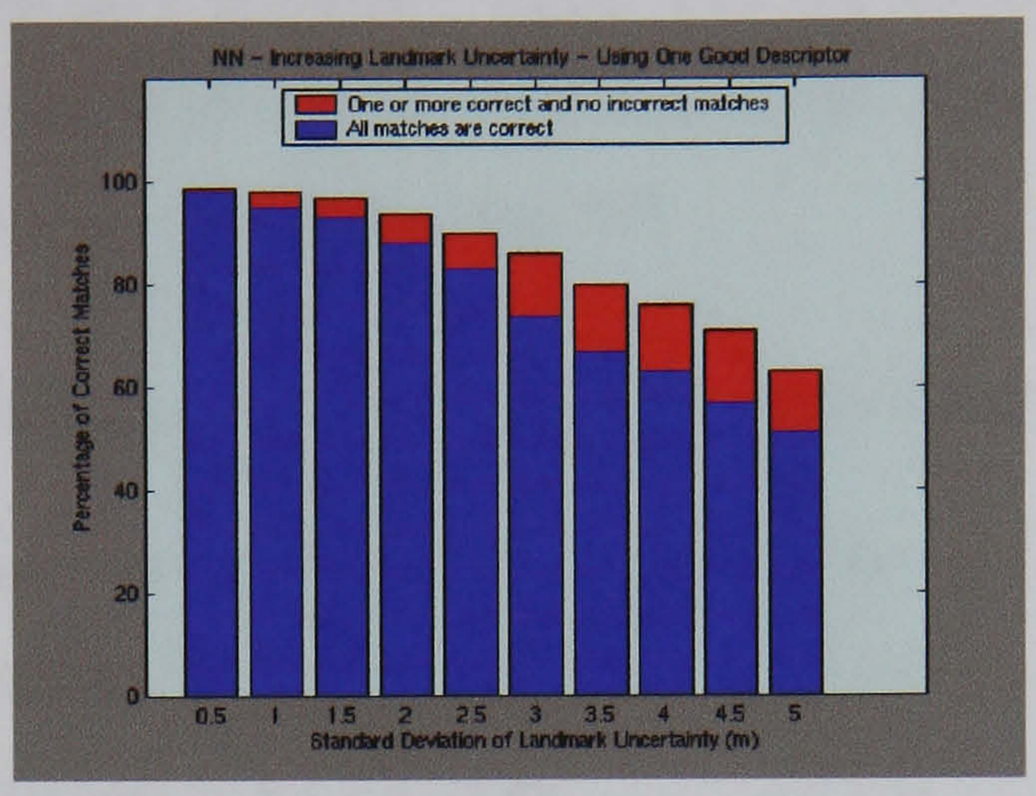

(a)

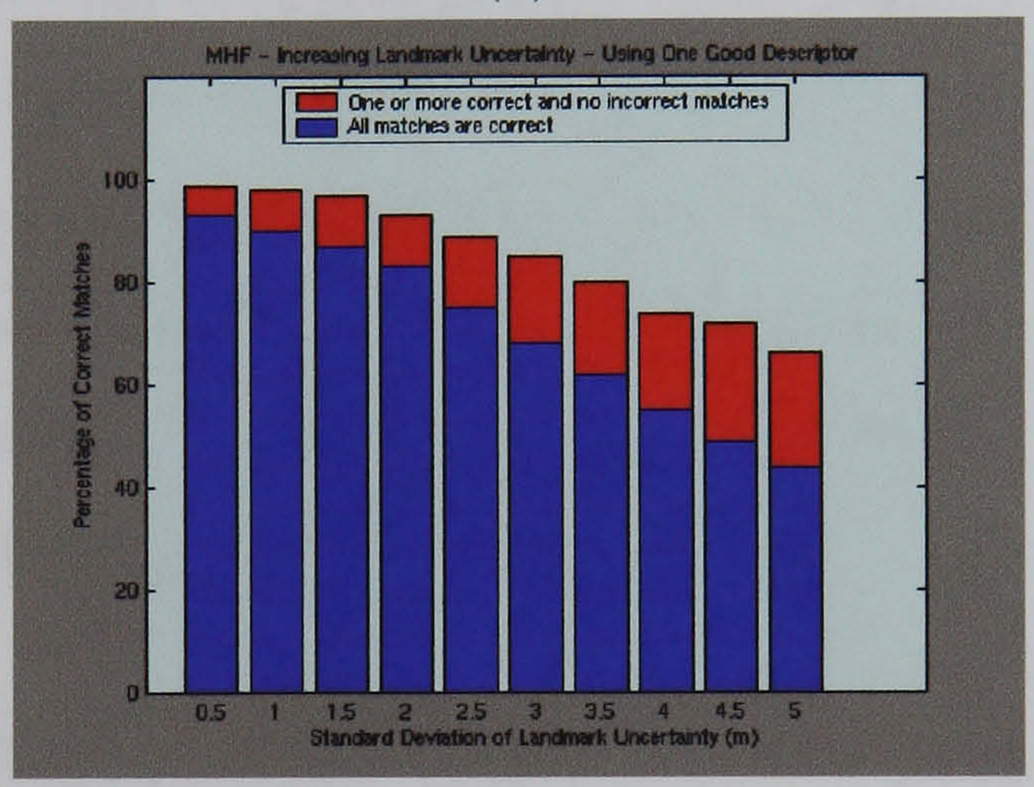

(b)

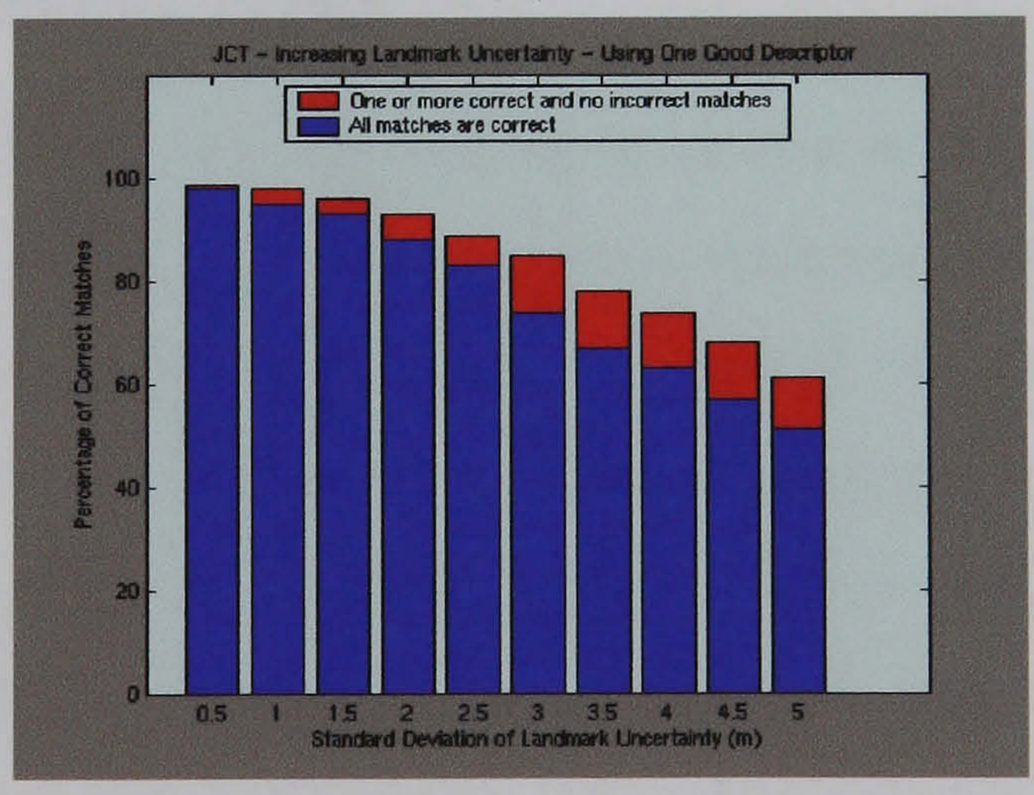

(c)

Figure 4.17: Results obtained aided by one good landmark descriptor, for (a) NN, (b) MHF and (c) JCT. Each column illustrates the correct associations obtained from 100 data association experiments (blue) and the associations where at least one observation was correctly associated and the rest were not associated to any other landmark (red). The increasing values of the columns are the 1σ values of the landmarks' positions.

discrimination of the descriptor. The results also show that the most probable MHF outcome, figure 4.18 (b), produces considerably worse results than the other two approaches. The JCT approach, figure 4.18 (c), demonstrates the advantages of taking into account landmark correlations in the data association process, by producing marginally better results than NN.

Increasing Vehicle's Heading Uncertainty and Error

The systematic behaviour observed in the previous set of results can better be seen in the case of increasing vehicle's heading uncertainty and error, figure 4.19. The sharp drop in performance when the uncertainty changes from 10° to 20° is expected. As the errors in the vehicle's position increase so does the association deteriorate. However, instead of a monotonically decreasing performance pattern, the opposite occurs. Again this phenomenon, as before, can be easily understood. As the uncertainty in the vehicle's position increases, the dominant term in the validation region is that of the descriptor. The descriptor has a much better discriminatory capability and thus the results improve.

4.5.3 Data Association Experiments Aided by Two Landmark Descriptors

The performance of the data association strategies is now observed for cases with two landmark descriptors. The addition of an extra uncorrelated descriptor will give a clear indication as to how the data association will benefit from the inclusion of an extra descriptor. The two descriptors will be simulated and, again, take a uniformly distributed random value between 0 and 10. The map stores these values taking the true values as the mean and with Gaussian random errors of standard deviation 0.1. The results should improve considerably when compared to both sets of experiments described above. Table 4.7 shows the data association results obtained for instances of low uncertainty, as given by the standard deviation values in table 4.4.

Results for Increasing Vehicle's Position Error Aided by One Good Descriptor

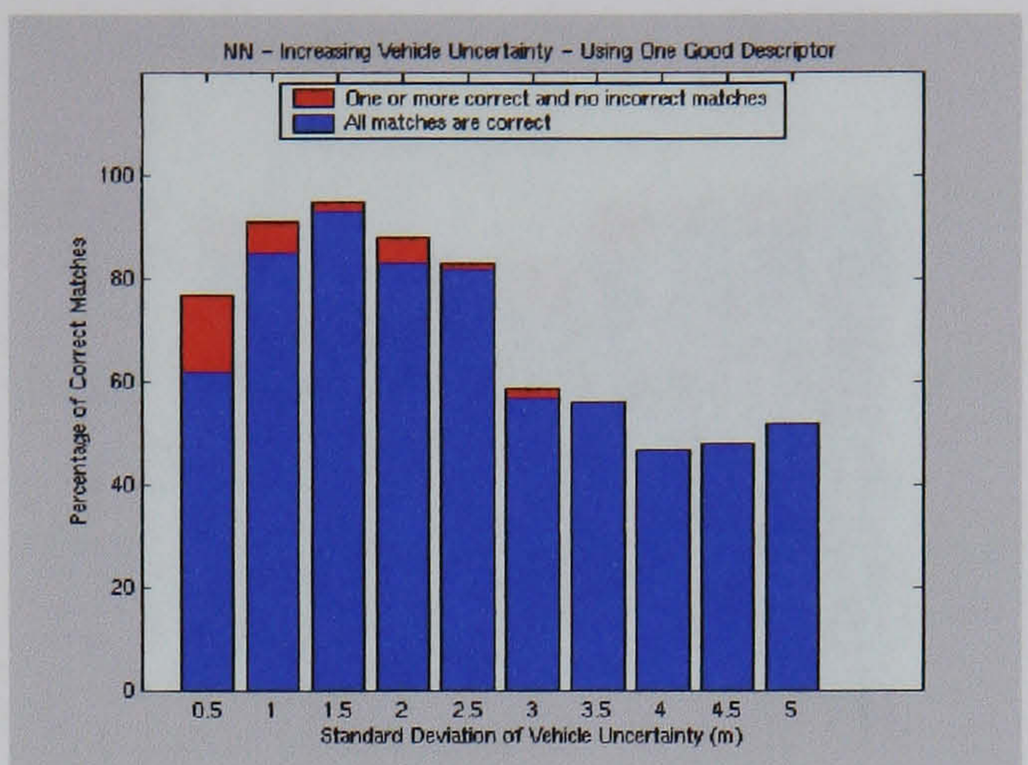

(a)

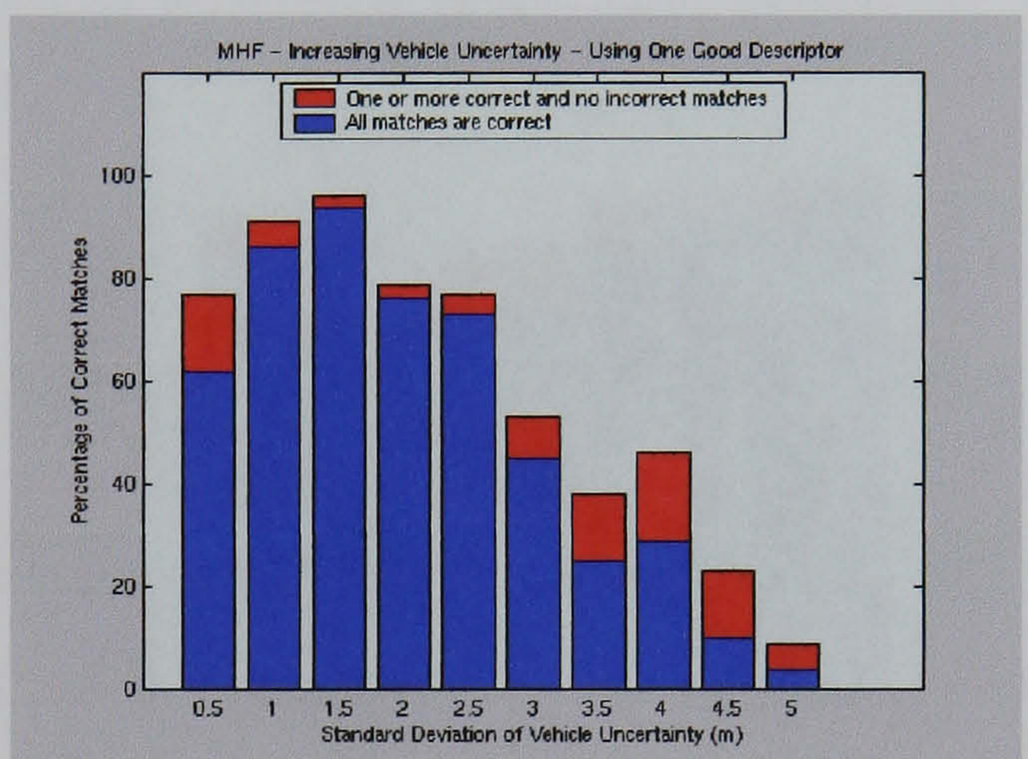

(b)

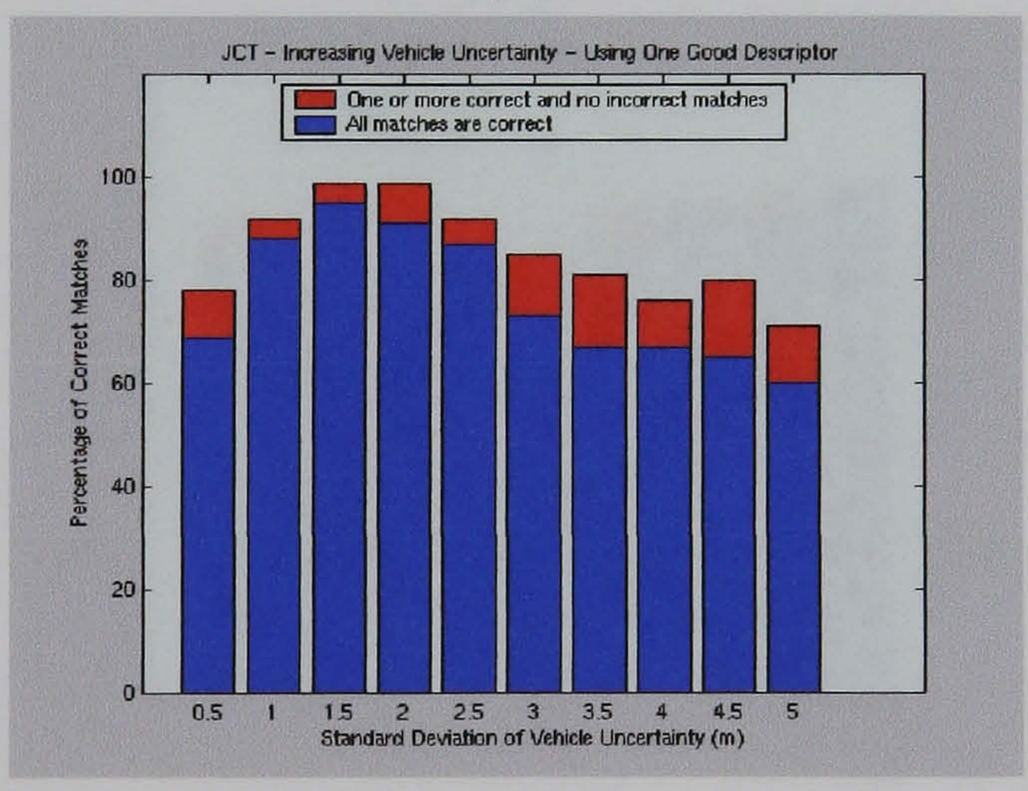

(c)

Figure 4.18: Results obtained aided by one good landmark descriptor, for (a) NN, (b) MHF and (c) JCT. Each column illustrates the correct associations obtained from 100 data association experiments (blue) and the associations where at least one observation was correctly associated and the rest were not associated to any other landmark (red). The increasing values of the columns are the 1σ values of the vehicle's position.

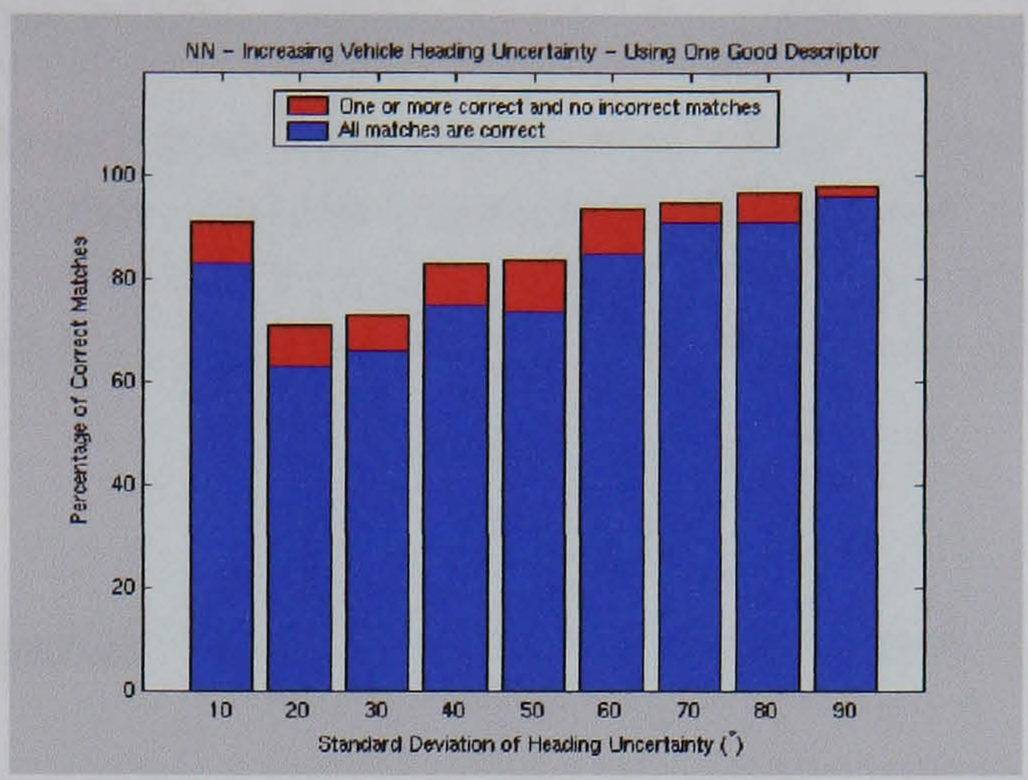

(a)

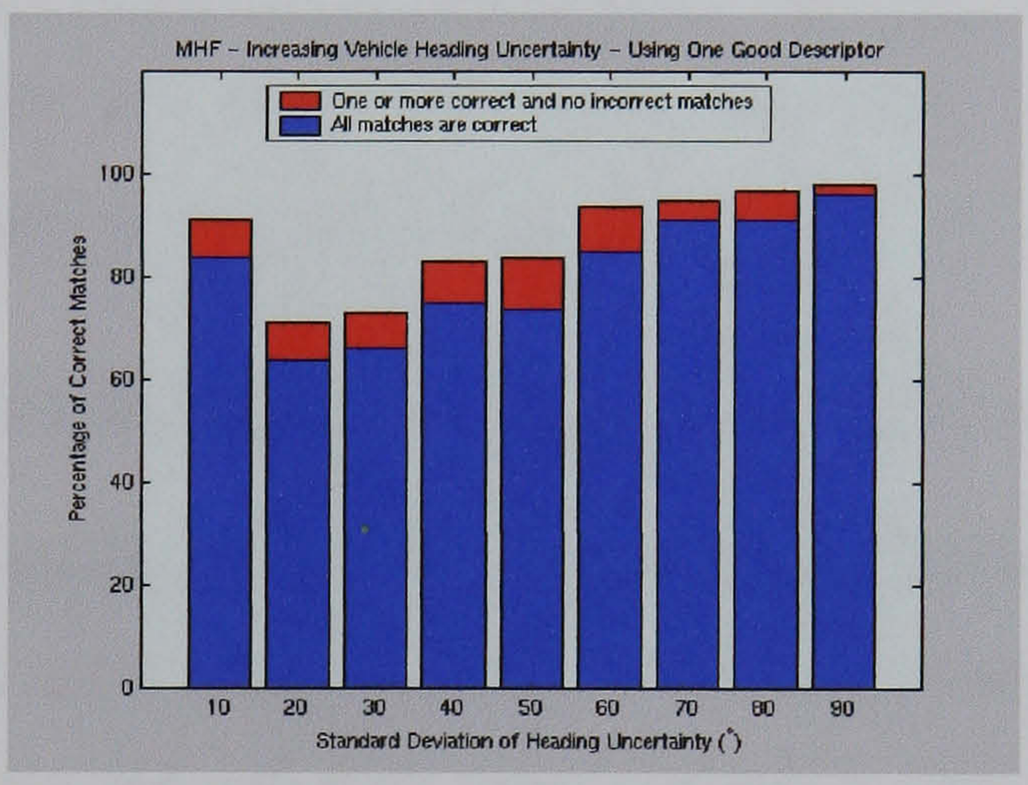

(b)

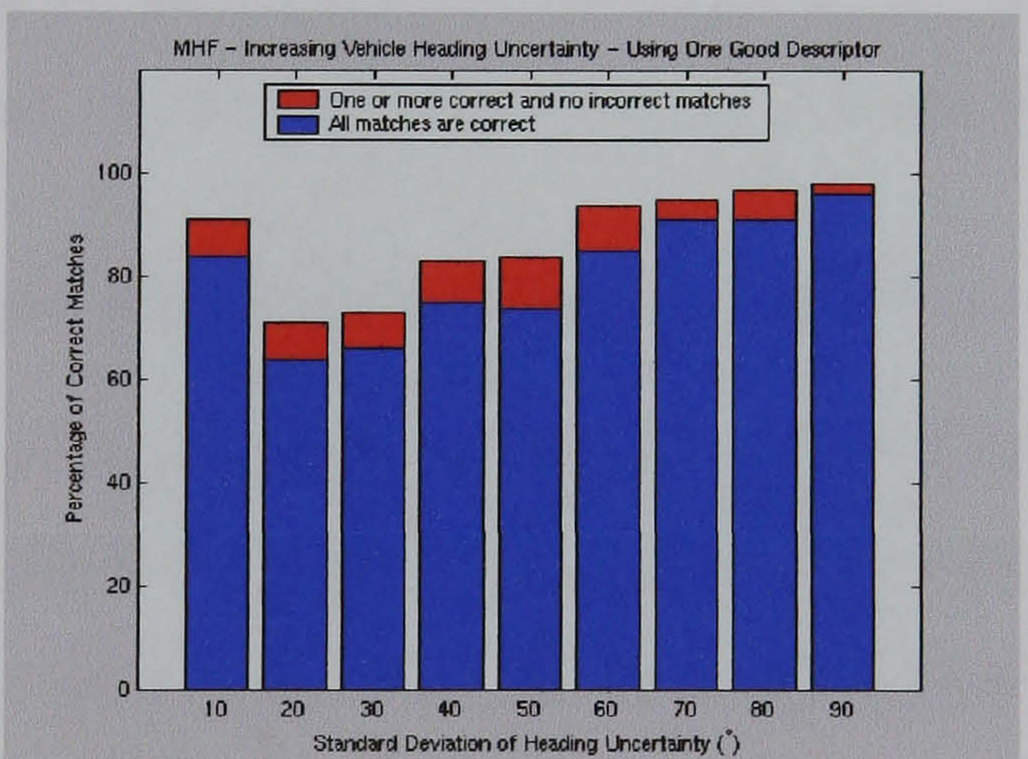

(c)

Figure 4.19: Results obtained aided by one good landmark descriptor, for (a) NN, (b) MHF and (c) JCT. Each column illustrates the correct associations obtained from 100 data association experiments (blue) and the associations where at least one observation was correctly associated and the rest were not associated to any other landmark (red). The increasing values of the columns are the 1σ values of the vehicle's heading.

	NN	MHF	JCT
Correct Associations (%)	92	92	97
Non-incorrect Associations (%)	100	100	100

Table 4.7: Data Association Two Descriptors - Low Uncertainty: When all landmarks are correctly associated the experiment will be classed as *Correct Association.* When at least one observation was correctly associated and the rest were not associated to any other landmark the experiment will be classed as *Non-incorrect Association.*

Increasing Landmarks' Positions Uncertainty and Error

Not surprisingly the results have considerably improved, figure 4.20. Proving that the inclusion of more descriptors should improve the performance of the association strategies: NN, MHF and JCT. The results also show that the three strategies perform approximately as well as each other.

Increasing Vehicle's Position Uncertainty and Error

Improved data association results are also apparent for the case of an increasing vehicle error, figure 4.21. The systematic behaviour observed before can still be noticed. However, for the range of vehicle position errors tested, as the error is increased, the results do not fall below the initial results obtained with a standard deviation of $0.5m$ and, in the case of the NN, lie between 83 % and 94 % success.

Increasing Vehicle's Heading Uncertainty and Error

Figure 4.22 shows the results obtained with the different data association strategies as the uncertainty and error of the vehicle's heading is increased. In this case the inclusion of an extra descriptor does not noticeably improve results with respect to the previous experiment. The behaviour observed in earlier experiments is still noticeable.

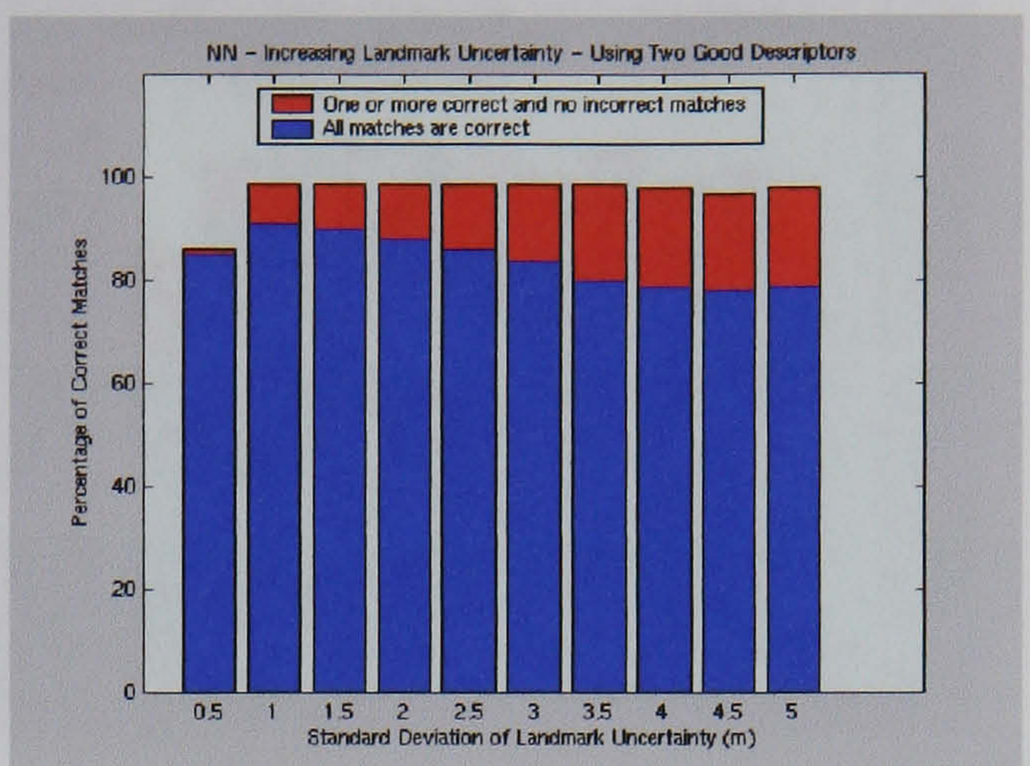

(a)

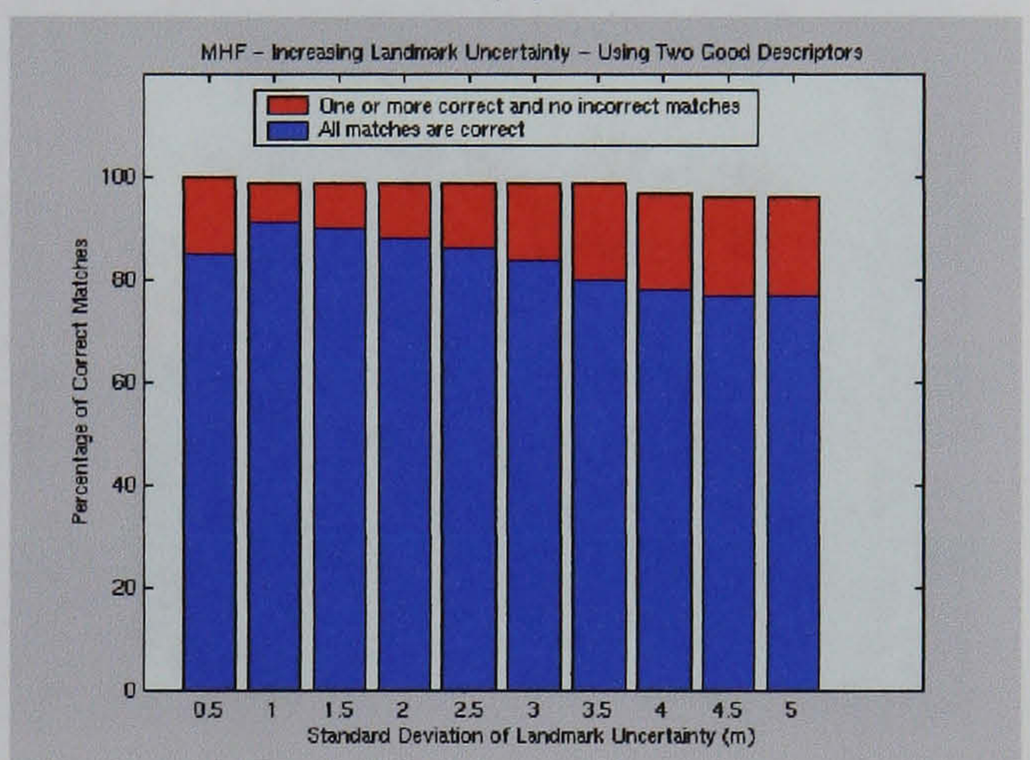

(b)

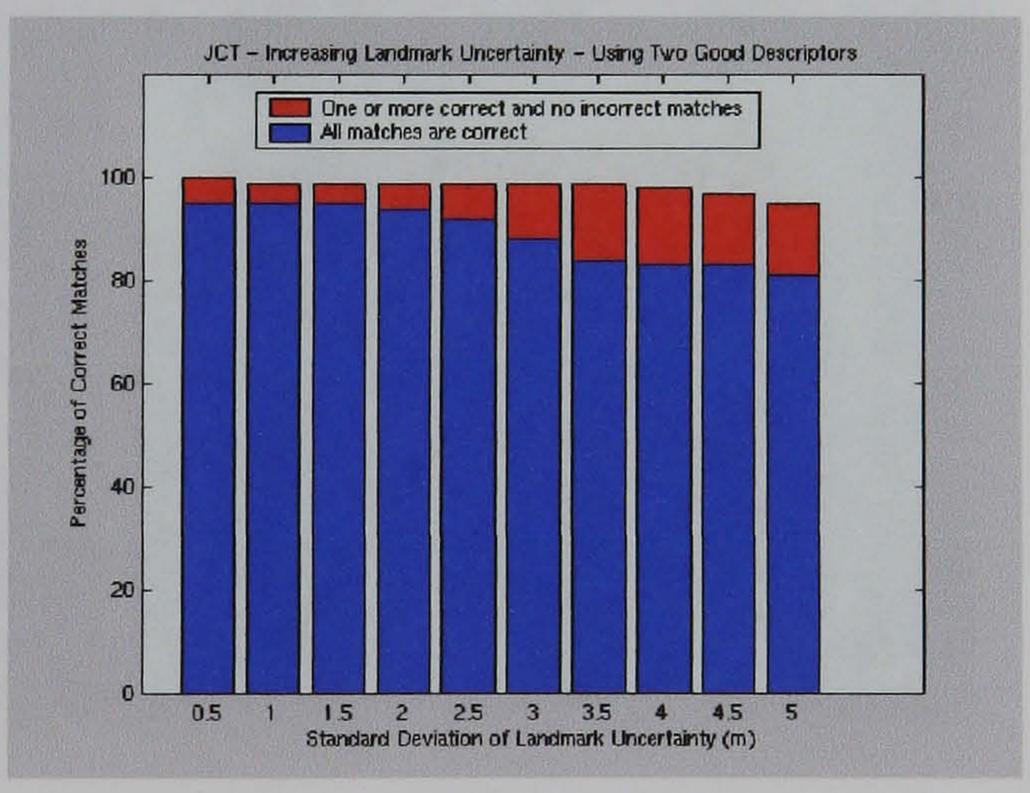

(c)

Figure 4.20: Results obtained aided by two good landmark descriptors, for (a) NN, (b) MHF and (c) JCT. Each column illustrates the correct associations obtained from 100 data association experiments (blue) and the associations where at least one observation was correctly associated and the rest were not associated to any other landmark (red). The increasing values of the columns are the 1σ values of the landmarks' positions.

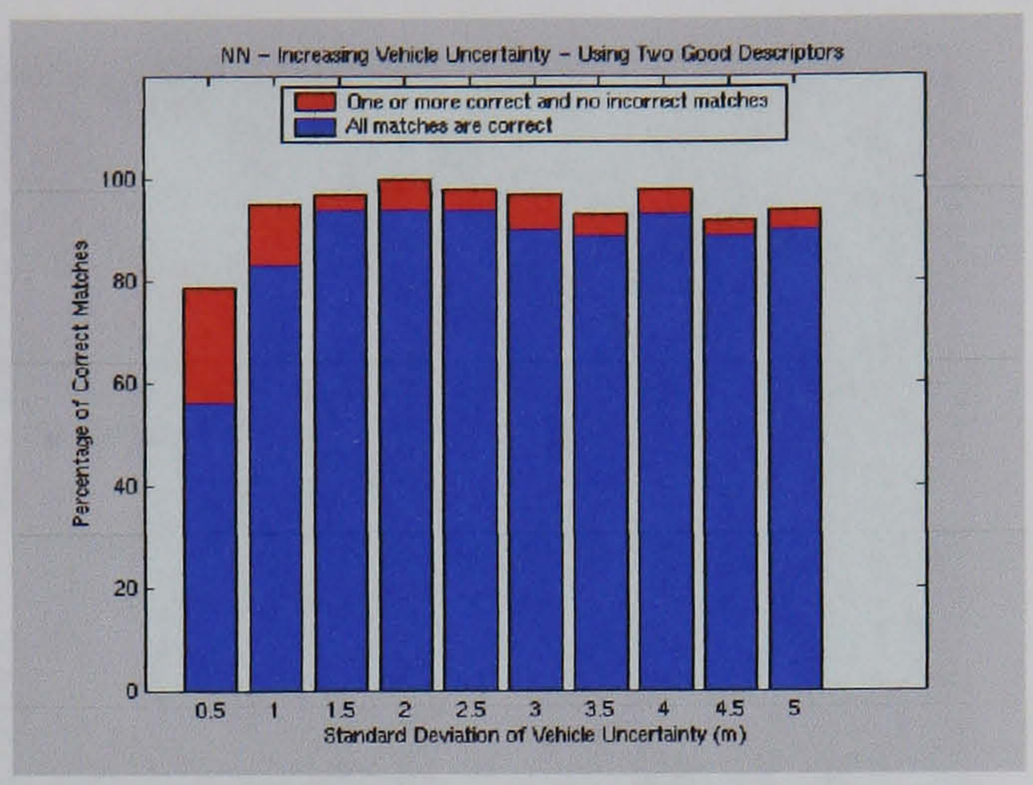

(a)

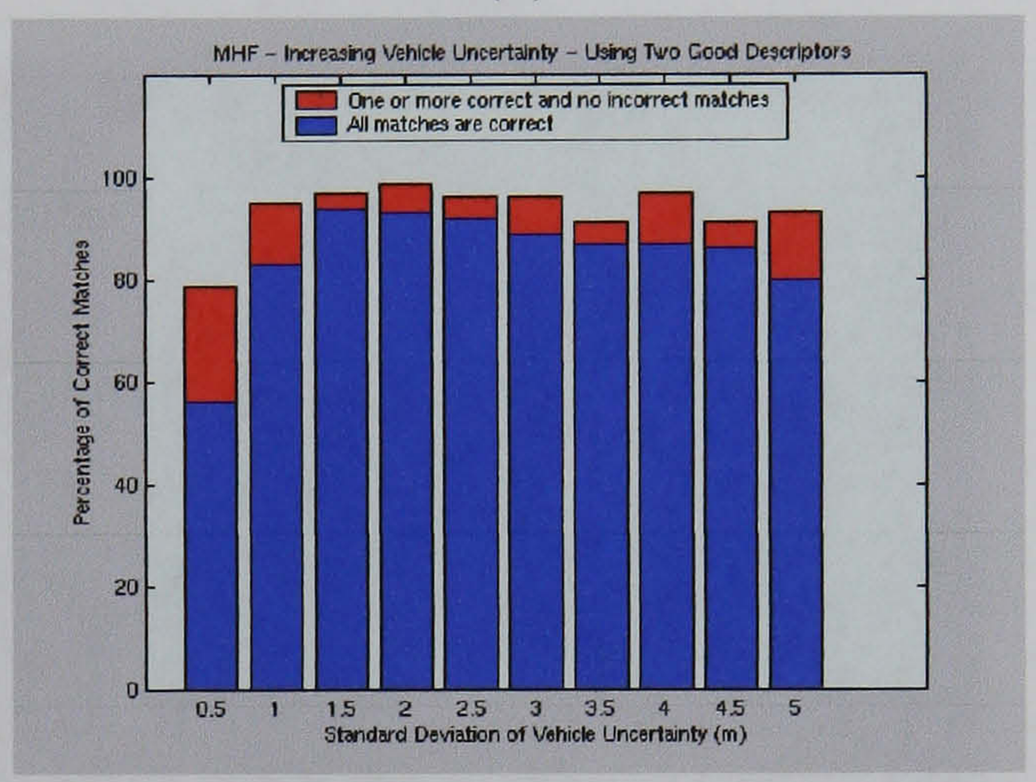

(b)

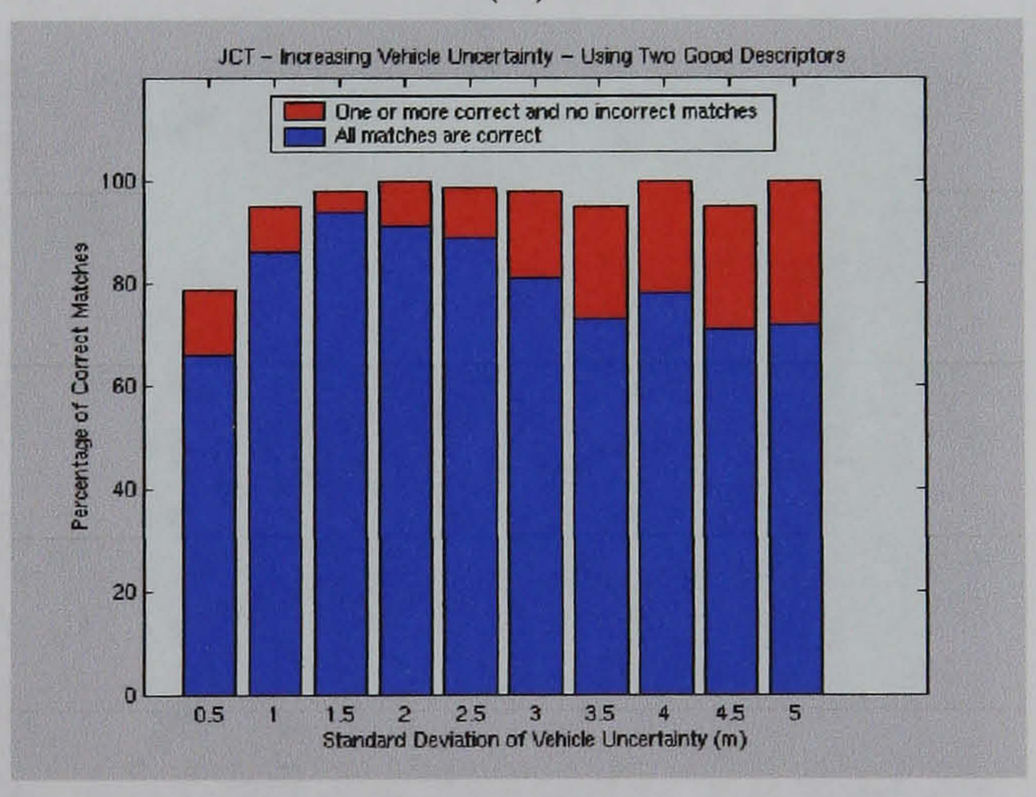

(c)

Figure 4.21: Results obtained aided by two good landmark descriptors, for (a) NN, (b) MHF and (c) JCT. Each column illustrates the correct associations obtained from 100 data association experiments (blue) and the associations where at least one observation was correctly associated and the rest were not associated to any other landmark (red). The increasing values of the columns are the 1σ values of the vehicle's position.

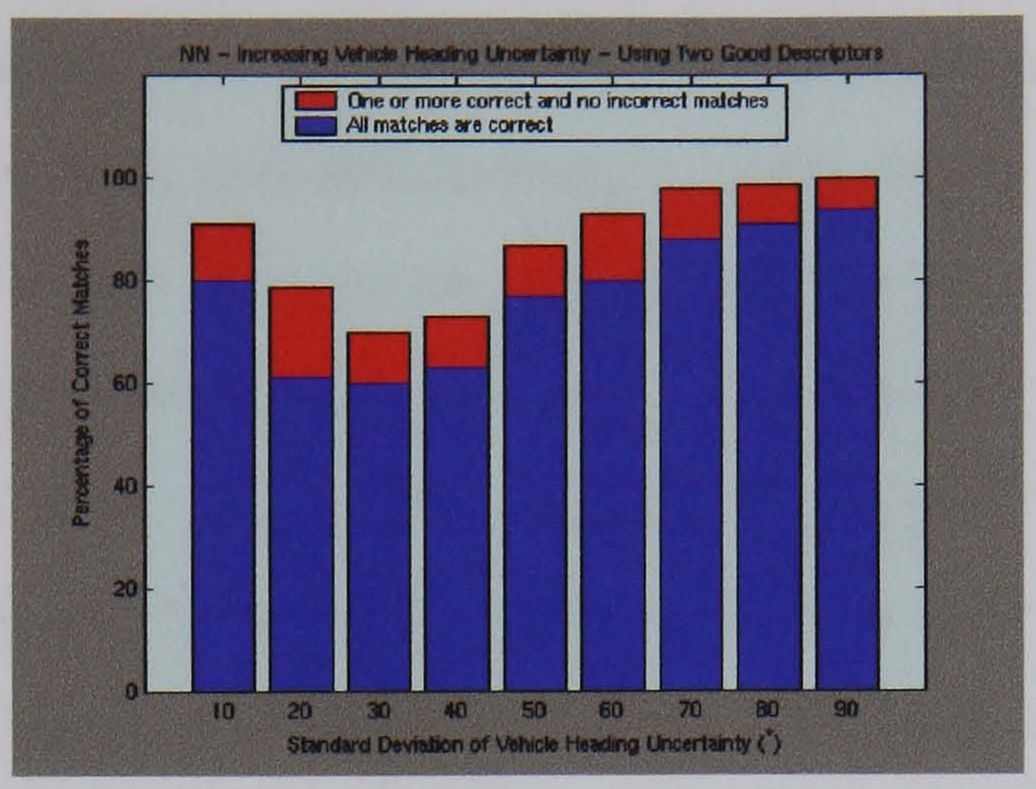

(a)

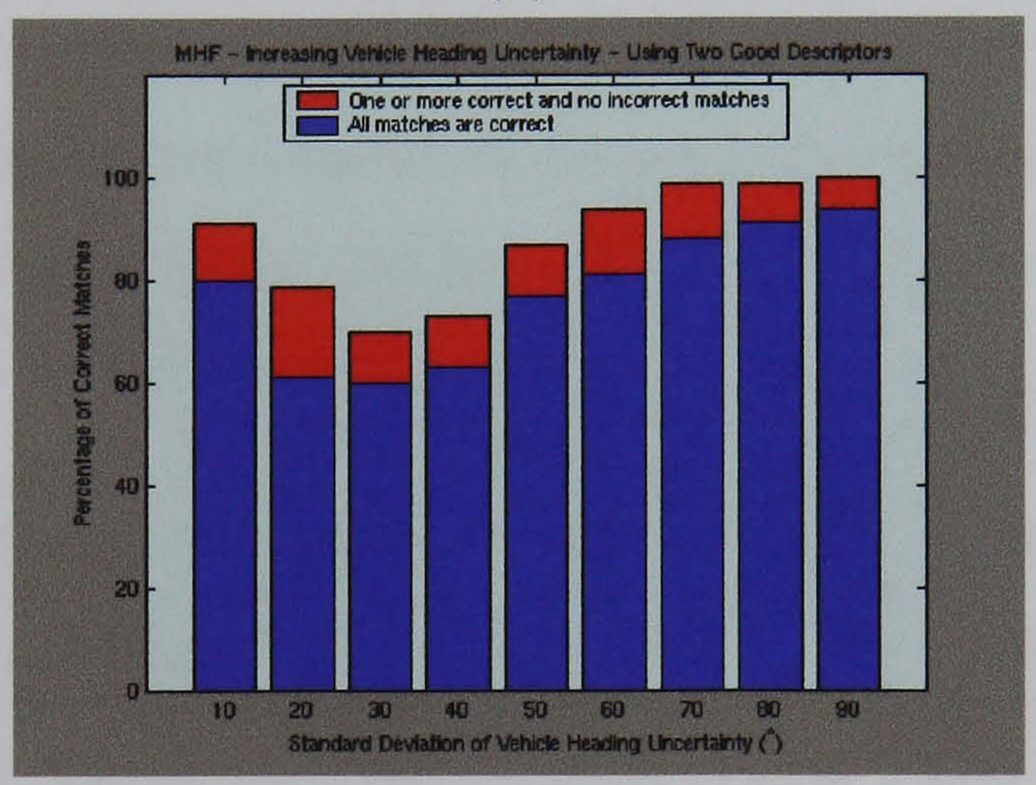

(b)

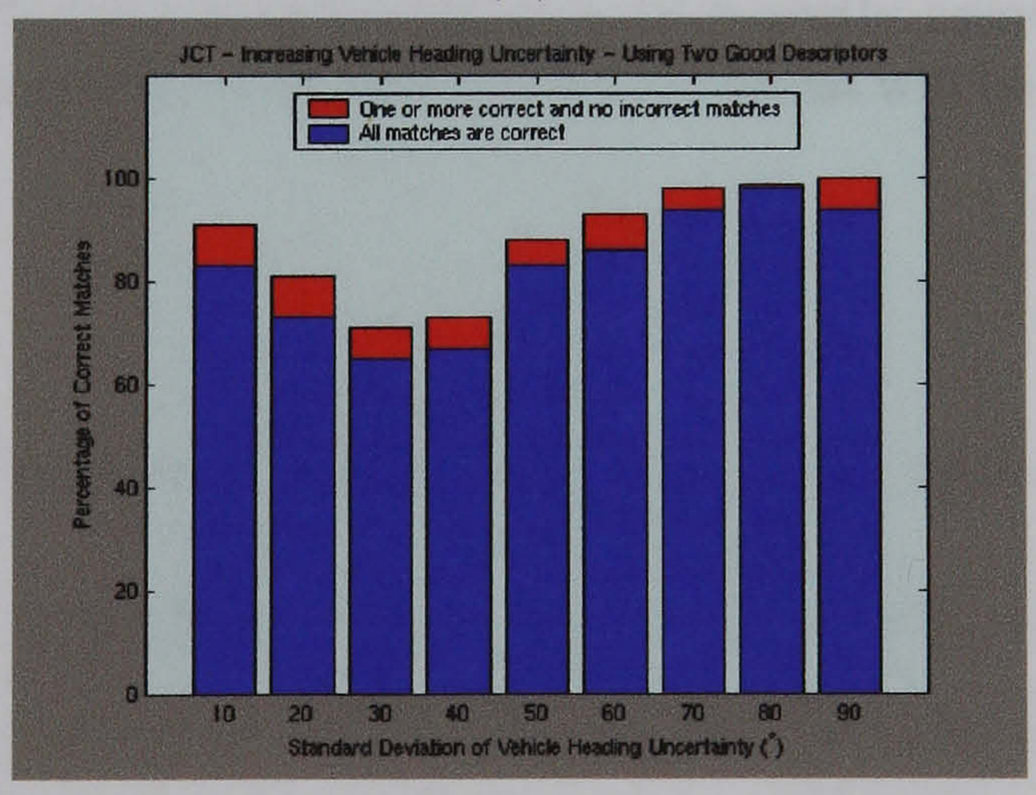

(c)

Figure 4.22: Results obtained aided by two good landmark descriptors, for (a) NN, (b) MHF and (c) JCT. Each column illustrates the correct associations obtained from 100 data association experiments (blue) and the associations where at least one observation was correctly associated and the rest were not associated to any other landmark (red). The increasing values of the columns are the 1σ values of the vehicle's heading.

4.5.4 Data Association Experiments with Poor Landmark Descriptors

This set of experiments has been set up to test the performance of the different data association schemes with non-informative, in other words *poor*, feature descriptors. The state vector for the observation model incorporates one landmark descriptor. This landmark descriptor takes a uniformly distributed random value between 0 and 10. The map stores this value taking the true value as the mean and with a Gaussian random error of standard deviation 10. The three association strategies are examined and the results compared to the previous sets of results. Table 4.8 shows the data association results obtained for instances of low uncertainty, as given by the standard deviation values in table 4.4. The following sections will again explore the effects of increasing the uncertainty and error in the landmarks' positions estimates, the vehicle's position estimate and the vehicle's heading estimate.

	NN	MHF	JCT
Correct Associations (%)	95	91	98
Non-incorrect Associations (%)	99	98	99

Table 4.8: Data Association One Poor Descriptor - Low Uncertainty: When all landmarks are correctly associated the experiment will be classed as *Correct Association.* When at least one observation was correctly associated and the rest were not associated to any other landmark the experiment will be classed as *Non-incorrect Association.*

Increasing Landmarks' Positions Uncertainty and Error

The results, figure 4.23, show similar performance to those obtained when only range and bearing measurements were made, except for the most probable hypothesis output from the MHF, figure 4.23(b), where a significant drop in performance can be observed.

Increasing Vehicle's Position Uncertainty and Error

The results obtained from the most probable output using the MHF, figure 4.24 (b), are considerably worse for the case of increasing vehicle position error using a poor

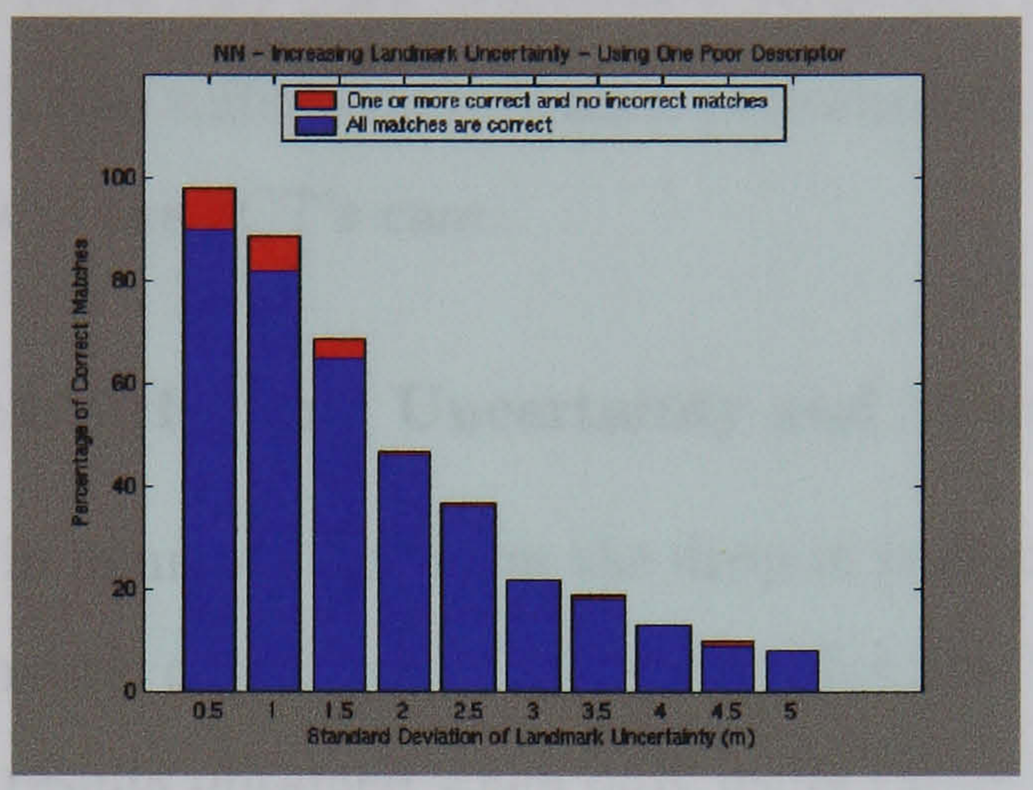

(a)

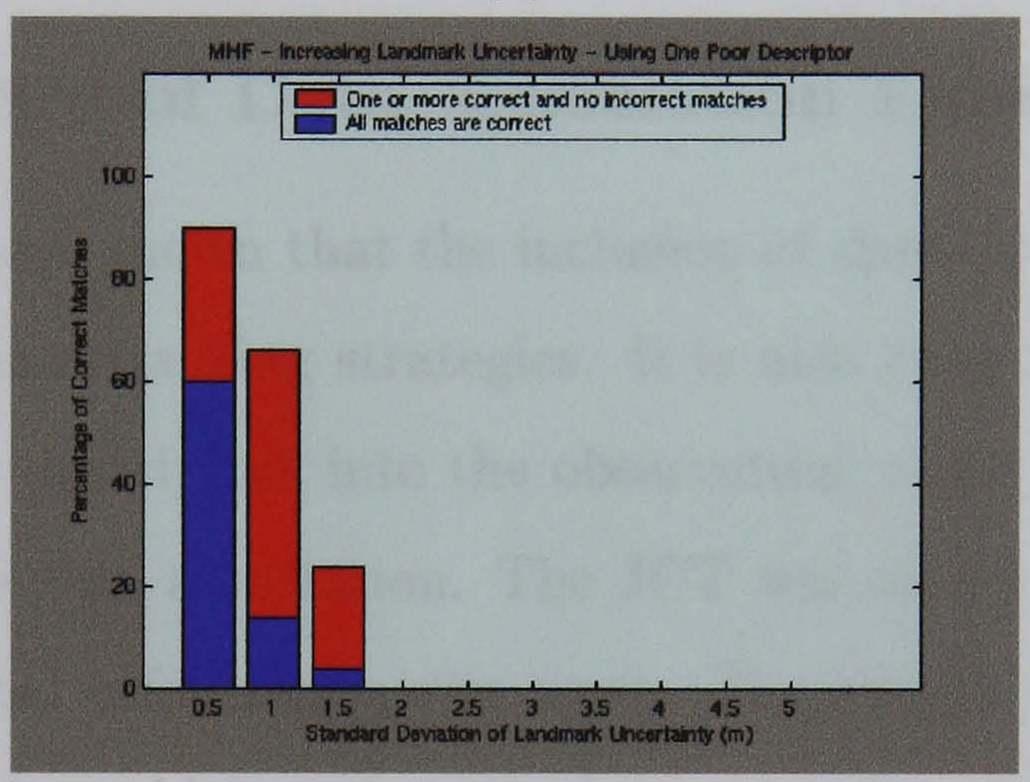

(b)

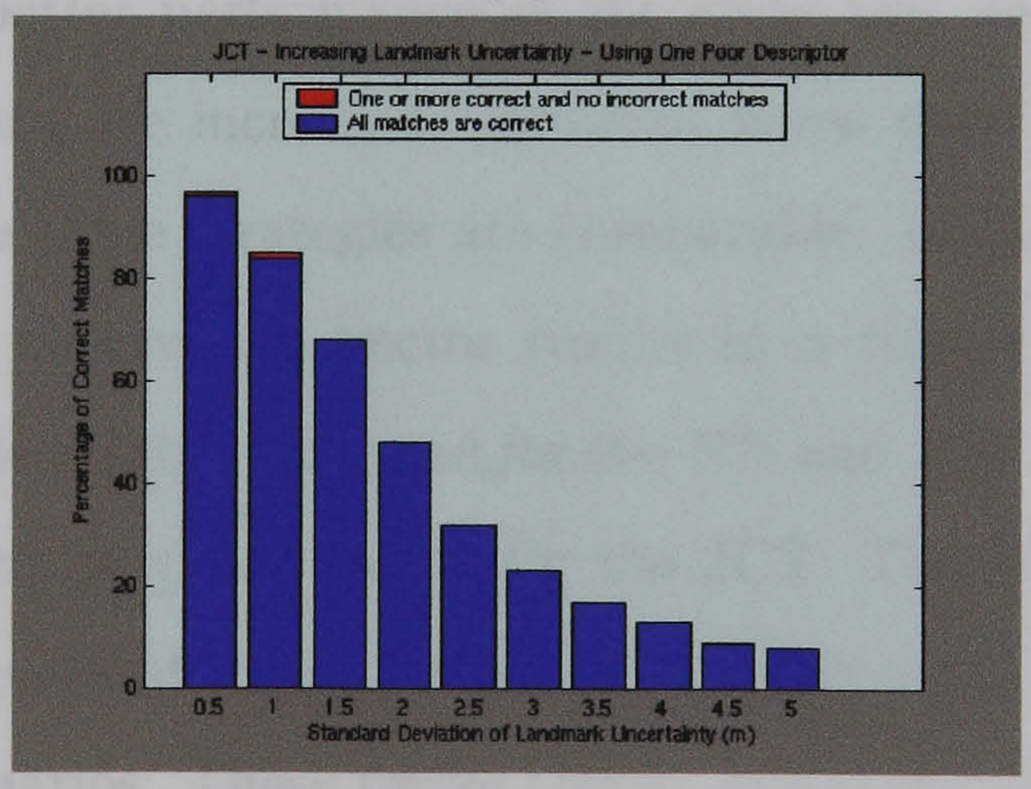

(c)

Figure 4.23: Results obtained aided by one poor landmark descriptor, for (a) NN, (b) MHF and (c) JCT. Each column illustrates the correct associations obtained from 100 data association experiments (blue) and the associations where at least one observation was correctly associated and the rest were not associated to any other landmark (red). The increasing values of the columns are the 1σ values of the landmarks' positions.

descriptor when compared to the results obtained when only positional information was used. As in the previous experiment, the MHF's performance has dropped considerably. The other two data association strategies NN, figure 4.24 (a), and JCT, figure 4.24 (b), also suffer a drop in their performance. This is not so noticeable in the NN's case as in the JCT's case.

Increasing Vehicle's Heading Uncertainty and Error

The results shown in figure 4.19 confirm the drop in performance of the MHF when using a poor landmark descriptor. The results for the other two strategies are comparable to the results obtained when only using range and bearing information.

4.5.5 Summary of Data Association Experiments

The experiments have shown that the inclusion of descriptors will improve the performance of the three tracking strategies. It is also clear from the results that the addition of further descriptors into the observation vector will further improve the performance of the data association. The JCT was shown to be the best approach when only positional information was used. The elegant way in which this strategy accounts for the vehicle-to-landmark and landmark-to-landmark correlations translates into a better performance as the error and uncertainty of the vehicle's position and heading are increased. However, when good descriptors are used, the performance of the three strategies are comparable. Including poor discriminatory descriptors in the observation vector results in a comparable performance to instances where no descriptors are used for the NN and JCT. Though close inspection reveals a slight drop in performance for the JCT. The MHF performance, on the other hand, is seriously affected. Tables 4.9 through to 4.11 illustrate the results for the worst case scenarios. These tables clearly reveal the benefits of the descriptors. The improved performance for all strategies is clearly seen as descriptors are added. The drop in performance for the JCT when a poor descriptor is added can also be observed.

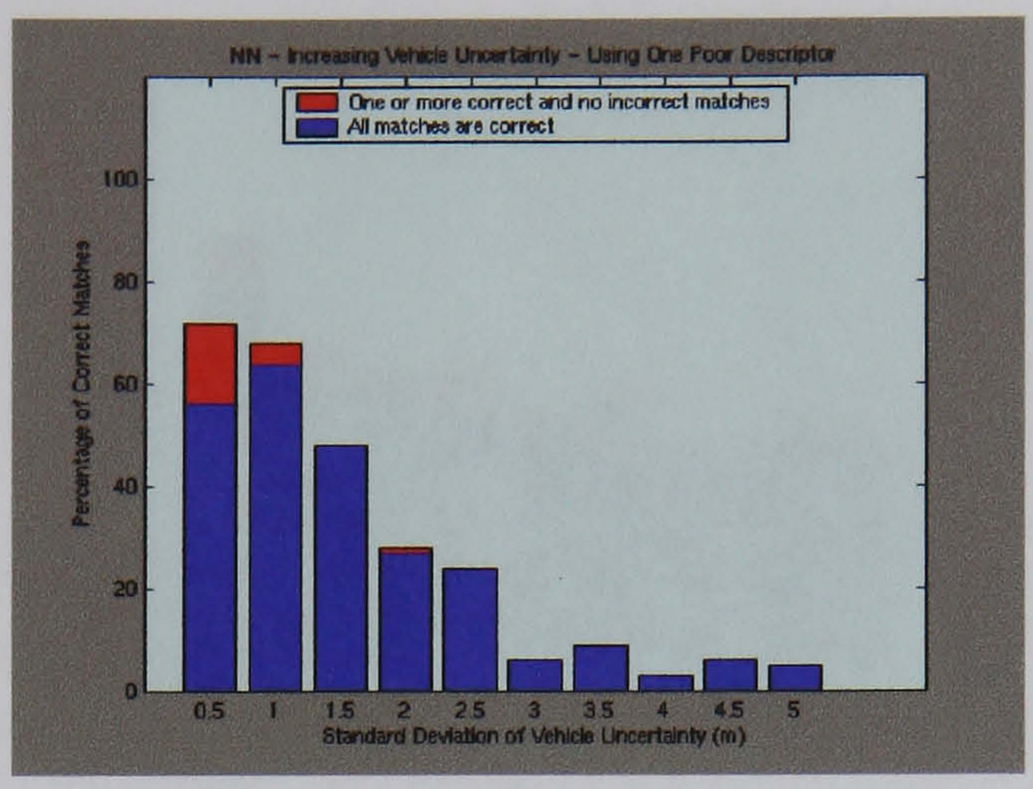

(a)

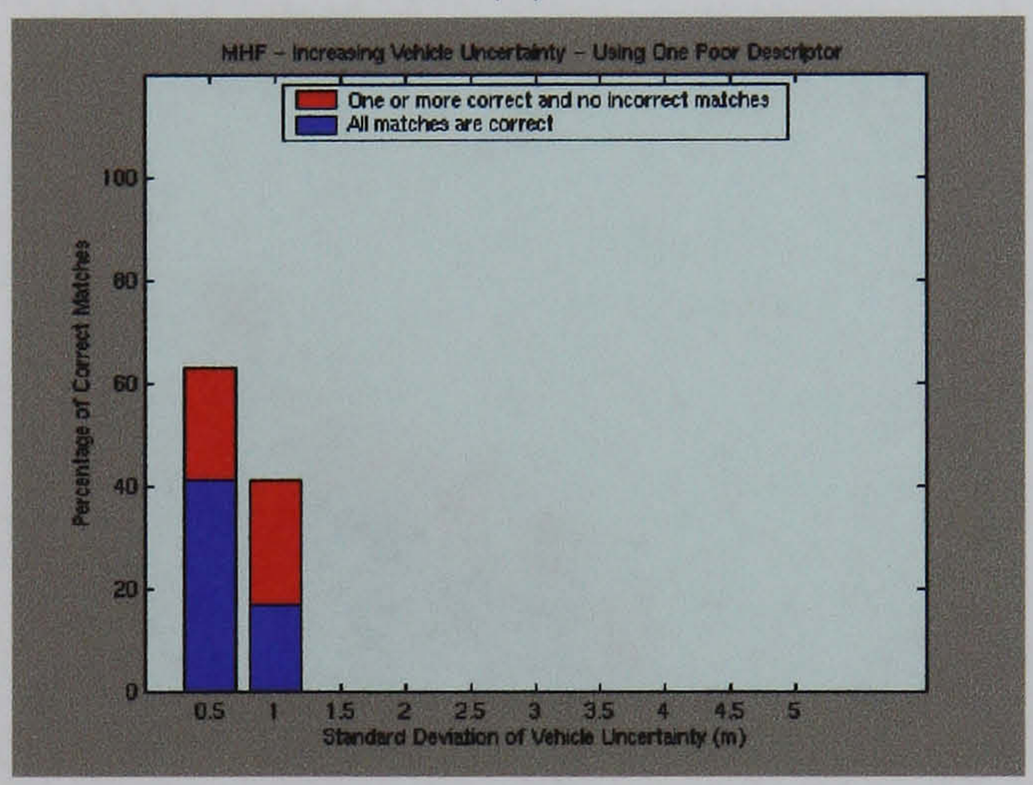

(b)

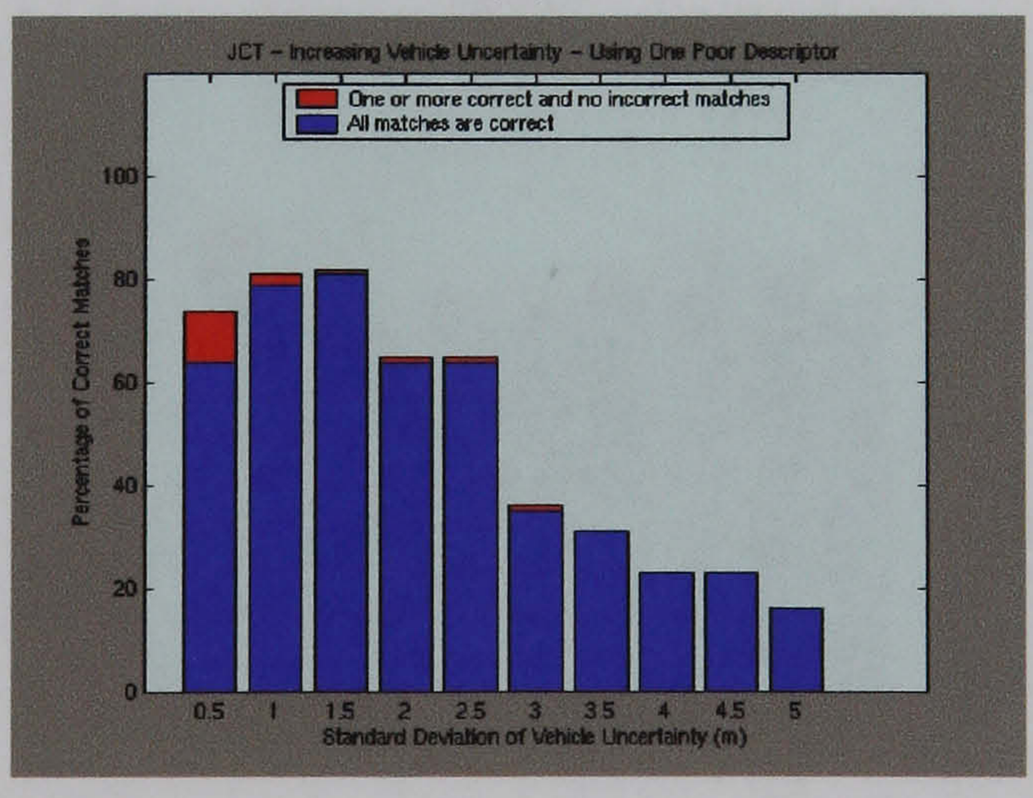

(c)

Figure 4.24: Results obtained aided by one poor landmark descriptor, for (a) NN, (b) MHF and (c) JCT. Each column illustrates the correct associations obtained from 100 data association experiments (blue) and the associations where at least one observation was correctly associated and the rest were not associated to any other landmark (red). The increasing values of the columns are the 1σ values of the vehicle's position.

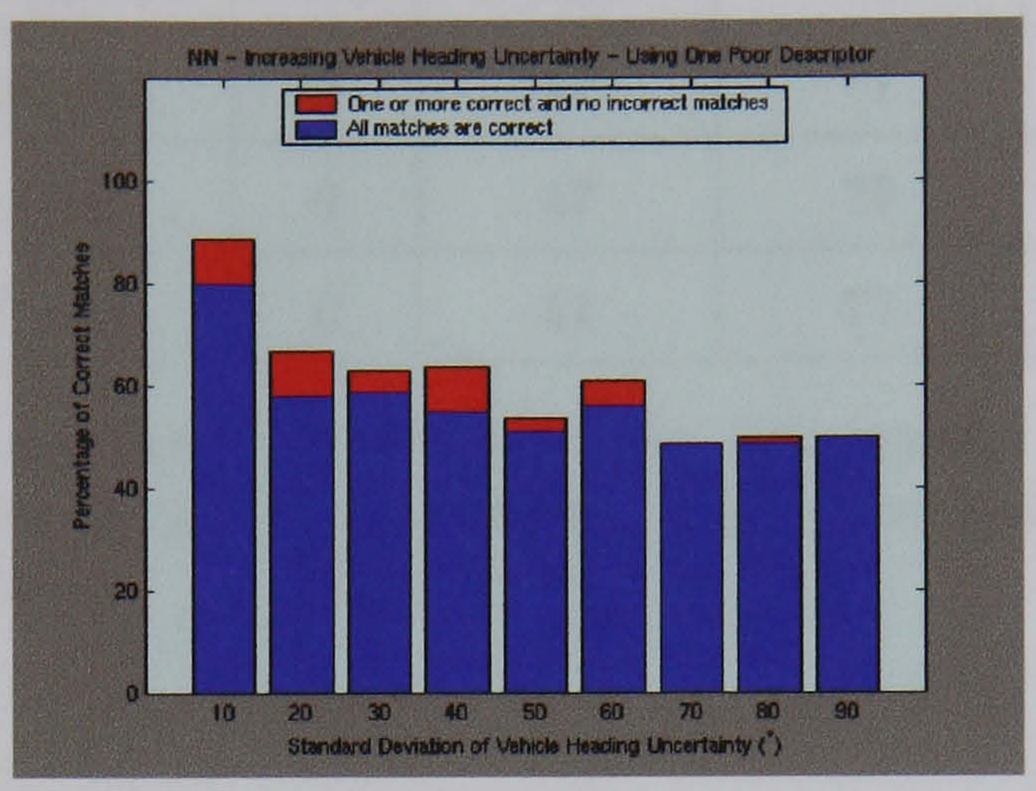

(a)

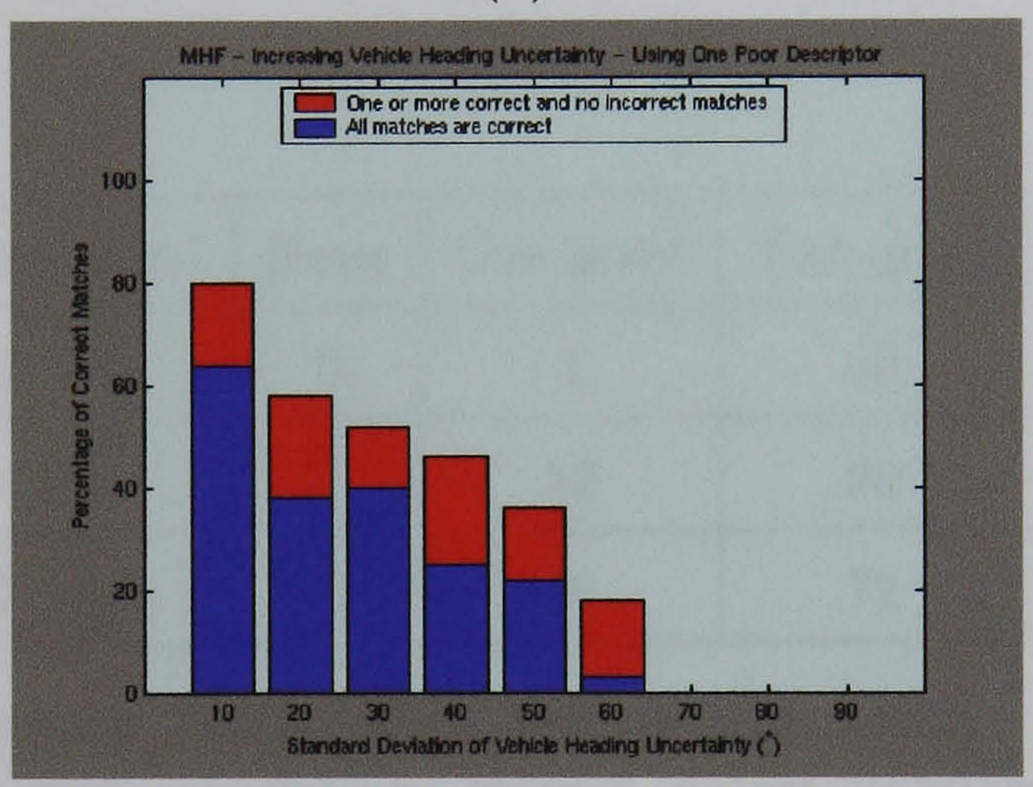

(b)

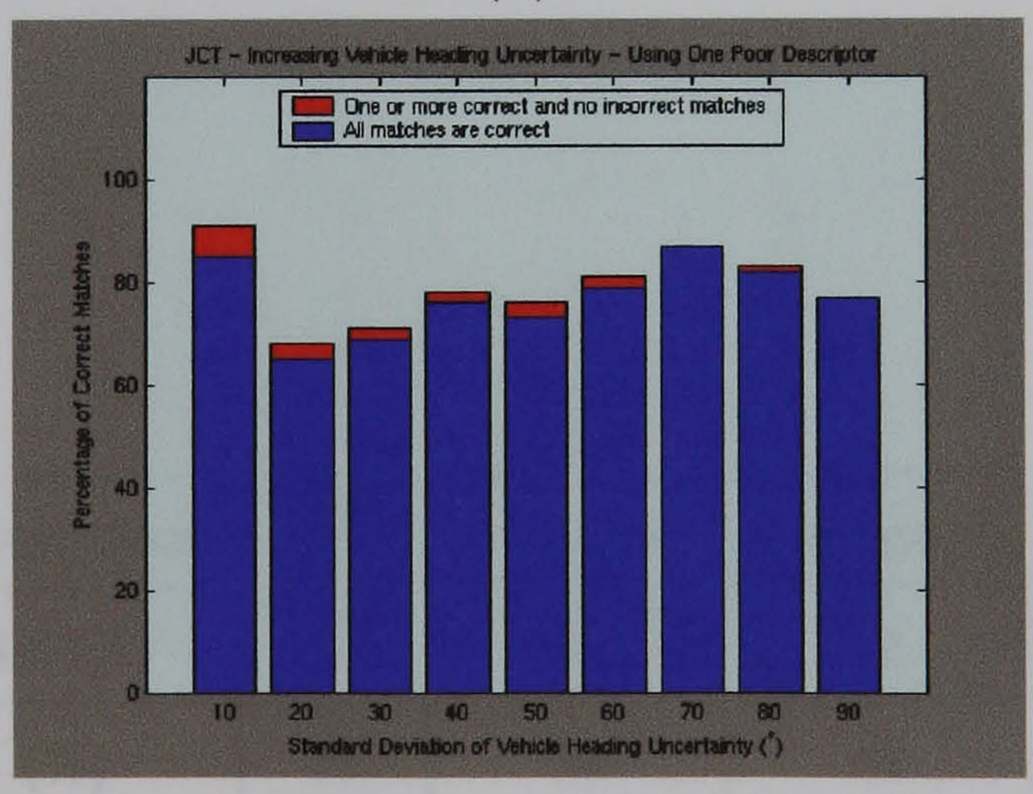

(c)

Figure 4.25: Results obtained aided by one poor landmark descriptor, for (a) NN, (b) MHF and (c) JCT. Each column illustrates the correct associations obtained from 100 data association experiments (blue) and the associations where at least one observation was correctly associated and the rest were not associated to any other landmark (red). The increasing values of the columns are the 1σ values of the vehicle's heading.

Descriptors:	None	One good	Two good	One poor
MHF (%)	0	44	77	0
NN (%)	0	47	79	8
JCT (%)	0	51	77	8

Table 4.9: Summary Table - High Landmarks' Uncertainty: Table summarising the percentages of correct associations given 5 meters standard deviation error in the landmarks' positions.

Descriptors:	None	One good	Two good	One poor
MHF (%)	0	4	80	0
NN (%)	7	52	90	5
JCT (%)	31	60	72	16

Table 4.10: Summary Table - High Vehicle Uncertainty: Table summarising the percentages of correct associations given 5 meters standard deviation error in the vehicle's position.

Descriptors:	None	One good	Two good	One poor
MHF (%)	44	96	94	0
NN (%)	48	96	94	50
JCT (%)	82	93	94	77

Table 4.11: Summary Table - High Heading Uncertainty: Table summarising the percentages of correct associations given 90° standard deviation error in the vehicle's heading.

4.6 Data Association Aided by Landmark Descriptors Using Real Sonar Data

In this section the main positive effect of using landmark descriptors with real sonar data will be explored. Previous work with sonar has shown that some targets change significantly in shape over time and with respect to the viewing angle. Single targets may also split into several, and vice versa, due to shadowing and/or sidelobe pick-up at short ranges [22, 60]. Another common cause of errors when tracking targets with sonar data is that caused by additive noise and, even for cases where the changes in shape are less apparent, the segmentation can significantly change the look of a target. Take for instance figures 4.26 (a) and 4.26 (b). These images show two consecutive returns from a sonar. The update rate is of 9 Hz. Four landmarks are clearly visible. It will be the role of the segmentation algorithm to identify those four landmarks. The range and bearing to the centroids will be used to update a stochastic map. However, the outcome of the segmentation, seen in figures 4.27 (a) and 4.27 (b), have altered the look of the most central and closest landmark. Consequently, the range and bearing will also be shifted. By associating this new look landmark to the old mapped landmark an error will be introduced into the stochastic map calculations. A data association scheme that is aided by landmark descriptors will identify the differences between these two observations of the landmark and the new observation will not be matched with the old observation. Eventually spurious observations of a landmark will be released from the map, see section 2.3.4. Thus, with landmark descriptors, the introduction of errors due to the poor quality of the sonar data should be avoided. These findings will be fully exploited and demonstrated when implementing a stochastic map that works with real sonar data in the next chapter, section 5.4.

4.7 Discussion

In the context of CML, work on data association has been concerned with solving the correspondence problem when equipped with only only range and bearing information about a target.

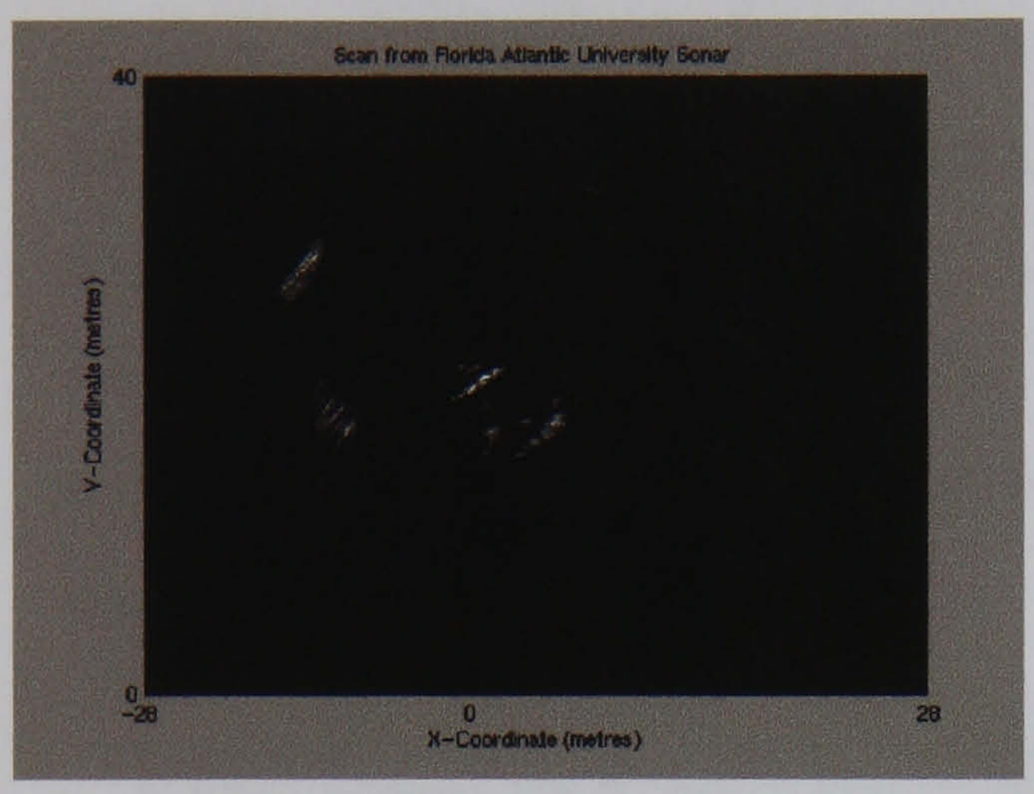

(a)

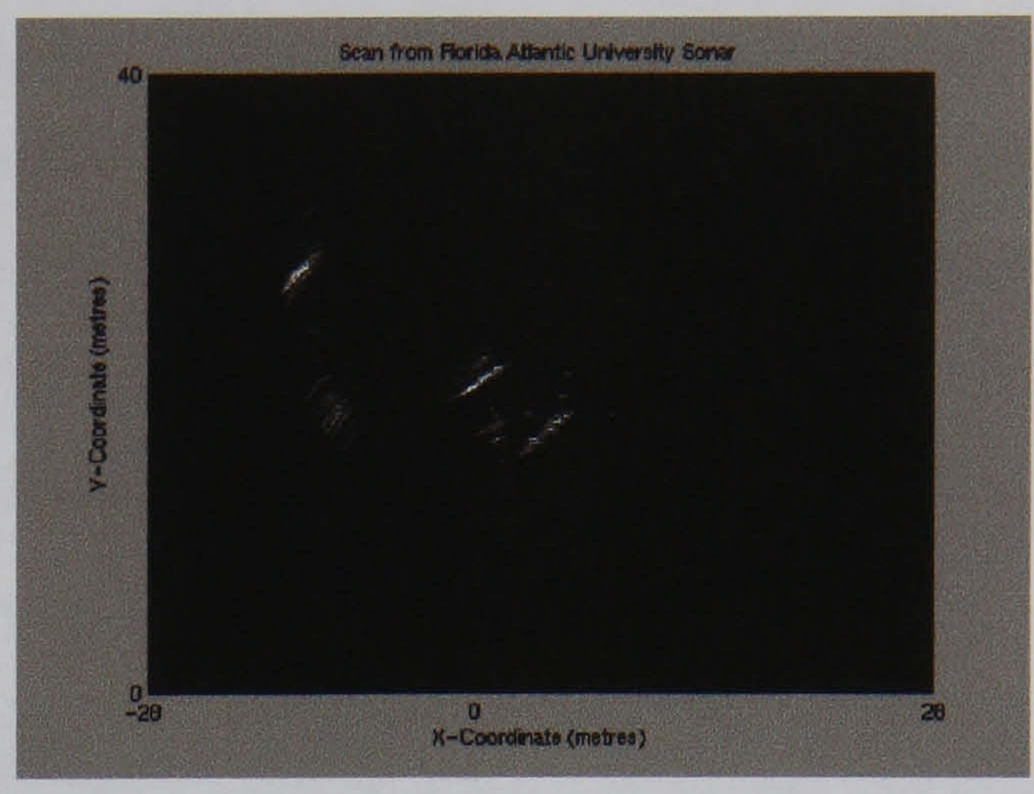

(b)

Figure 4.26: Images (a) and (b) are two consecutive frames obtained with Barney, the Florida Atlantic University concept sonar.

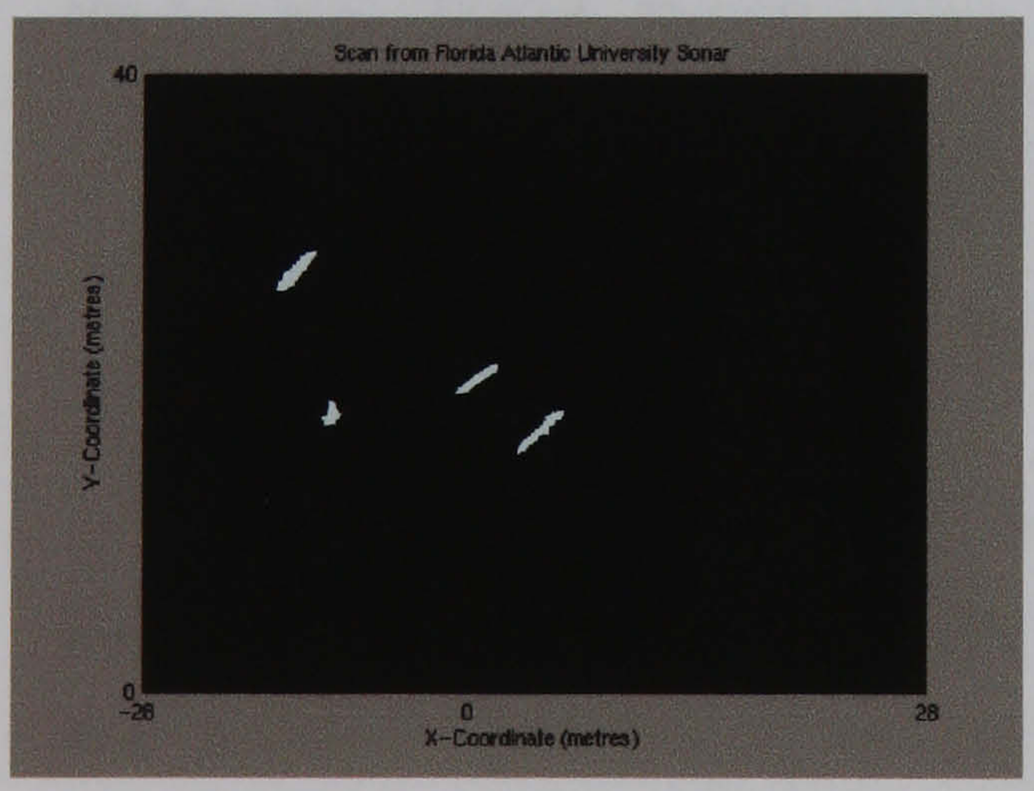

(a)

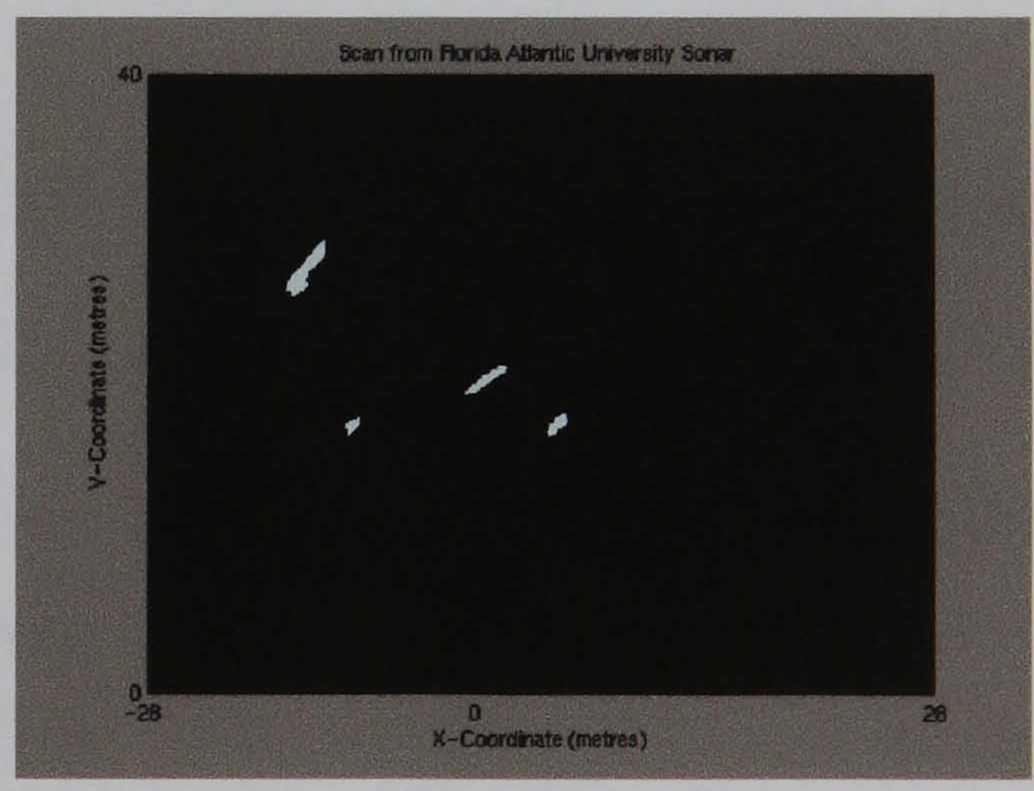

(b)

Figure 4.27: Images (a) and (b) show the result of segmenting figures 4.26(a) and 4.26(b).

This chapter has presented the most relevant data association methods reported in the literature up to date.

Only two approaches, by R. N. Carpenter [17] and the author's own efforts [103], have exploited other available information to aid the data association. The approach proposed in this thesis permits the inclusion of landmark descriptors in most conventional data association strategies. The thesis demonstrated the power of using these descriptors through a simple example. However, a thorough study was also carried out.

The chapter compared three different data association strategies: the NN, the MHF and the JCT. The thesis shows how all of these methods benefit from the inclusion of uncorrelated feature descriptors.

The experiments showed that the results improved for all the strategies as more landmark descriptors were included. Nevertheless, the landmark descriptors are assumed uncorrelated and distinguishable, i.e. the descriptors must be sufficiently different for all landmarks. These assumptions are reasonable in the context of sonar returns, obtained in sufficiently unstructured scenes, given the results obtained in the previous chapter, section 3.4.3.

The experiments also showed comparable results for all the data association methods when aided by descriptors.

This essentially means that the simple NN algorithm can be adopted instead of the more expensive, in terms of processing power, MHF and JCT. It was also found that the MHF's performance was noticeably poorer when either no descriptors were used or the descriptors used were of poor discriminatory capabilities. The author believes the reason for this to lie in the selection of values for $\mu_F(\phi)$, $\mu_N(\nu)$ and P_D^t, the densities of false and new targets and the probability of detecting prior targets respectively. These *a priori* determined values are used in equation 4.23. In fact the effects of altering these values have been studied in the field of multiple target tracking [6] and their influence has been shown to significantly alter the results. A more

significant finding, in terms of the role played by the descriptors, was the systematic behaviour observed as the vehicle's position and heading error and uncertainty were increased. The three data association schemes illustrated an initial worsening of the results as the uncertainty and error grew. Although the results were still better than without the descriptors, followed by an improvement of these as the error and uncertainty kept increasing. This behaviour indicates that the descriptors are a much better association tool than the position, so that when the uncertainty for the position increases and the innovation due to the descriptors becomes predominant, the results improve due to the fact that the position information is ignored. Why not then just use the descriptors? Due to the simple fact that with no vehicle uncertainty, the position is in fact the best descriptor. Two landmarks might have similar descriptor values, but they will never have the same world coordinates. Further, as seen in the experiments, poor descriptors do nothing to improve the performance of the algorithm and, in certain environments, can actually confuse matters. The use of descriptors with real data will be explored in the next chapter. An example of when they become useful will be examined, and it will be shown how errors can in fact be reduced thanks to the property outlined in the last section of this chapter.

4.8 Summary

This chapter has presented the most common data association methods encountered in multiple target tracking literature, section 4.1. Section 4.2 used those algorithms to explore the state of the art in data association algorithms for the purposes of CML. The chapter argued that the inclusion of landmark descriptors in the matching process should improve the results obtained when using the algorithms, section 4.4. A set of experiments was presented where it was shown that descriptors, if sufficiently distinguishable, can improve the performance of the NN, MHF and JCT algorithms. The results also showed that the NN can provide comparable results to the more complex JCT, section 4.5. Section 4.6 showed how errors can actually be filtered out when using descriptors with real sonar data. Finally, the chapter's findings were thoroughly discussed in section 4.7. The next chapter will incorporate the feature descriptors into a stochastic map framework to perform CML with real sonar data.

Chapter 5

Underwater Concurrent Mapping and Localisation

The previous chapter has shown that the inclusion of feature descriptors can both simplify and improve data association. However, if as discussed previously, the landmark descriptors are similar, then the performance does not necessarily improve. This section will show examples of concurrent mapping and localisation carried out with data from three different sonar systems. Section 5.2 will show results from the Ocean Systems Laboratory tank where ground truth results demonstrate the capabilities of the stochastic map. In section 5.3, data obtained from a man-built structure is examined. In this instance the landmark descriptors can actually degrade the data association process due to the similarity of the landmarks. The true benefits of these descriptors can be observed in section 5.4 where noisy data and returns from unspecified targets obtained in a real AUV mission can be used to create a stochastic map under a simple nearest neighbour scheme if landmark descriptors are used. These results when compared to those obtained not using descriptors clearly show an improved performance. Other work using real forward-looking sonar data obtained in underwater environments is limited. A brief overview of this work follows below.

5.1 CML Using Real Forward Looking Sonar - Current Achievements

The volume of work done performing CML using real forward-looking sonar systems can be traced to two efforts, [17, 116]. These two efforts, briefly described in chapter 2, demonstrated that CML is indeed possible. The work in this chapter will corroborate this statement. The first effort was carried out with data obtained

from a sensor suite which was mounted over the side of a converted U.S. Navy yard freighter. These sensors were at approximately 5.5 meters depth. This effort produced a data set which was used in two different CML experiments [17, 63]. The sensors included the Naval Underwater Warfare Center Division Newport's High Resolution Array. This forward-looking receive-only array has a coverage of 90° azimuth and 45° elevation. The received data was processed every 20 seconds. The transmit transducer was a high frequency projector developed by the International Transducer Corporation. The other sensors were an Allied Signal Model RL-34 INS, an Edo Model 3050 DVL and a Trimble Model NT200D Differential Global Positioning System mounted on the surface over the equipment. The data from the INS and the DVL was fused in a Kalman filter and served as a comparison for their CML strategies. The DGPS was used as ground truth. Three legs of approximately one kilometre were carried out during the exercise in an area known as Halfway Rock in Narragansett Bay, Rhode Island. The first CML experiment carried out using this data set consisted of creating a Kalman based landmark map [17]. The method initiates a new Kalman filter for each observed landmark. The filter's state vectors hold the state of the vehicle and the observed landmark. The filters are thus fused ignoring the correlations. The system error was shown. However the uncertainty bounds were not reported and the adequacy of the system remains unverified. The second CML experiment produced a full stochastic map [63] for one of the legs. The approach used the data from the dead-reckoning sensors to model the unrecorded control inputs required by their vehicle model. In this case the uncertainty bounds were shown and the error was shown to be within those bounds, demonstrating for the first time a CML system working with forward-look sonar.

The second effort was performed with data gathered with Oberon, an ROV specifically developed at the University of Sydney to research AUV technologies [82]. The sonar used was a SeaKing by Tritech, see appendix D. The data was gathered off the coast of Sydney. Artificial landmarks were used to simplify the process. No other absolute positioning sensor was used to compare the results. The CML system developed was a full stochastic map. The prediction process took control inputs and the process was aided by a gyro. The results, although encouraging, cannot be verified due to the lack of ground-truth.

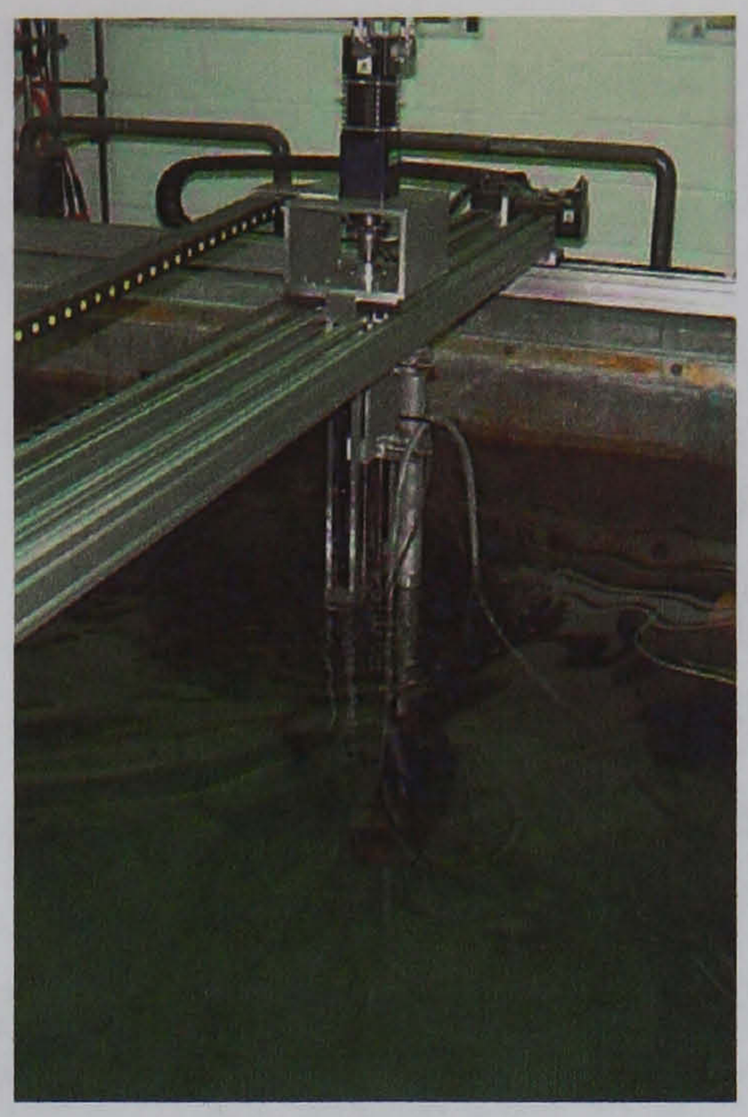

Figure 5.1: Cartesian robot in the OSL tank

5.2 Ocean System Laboratory - Tank Experiment

The first experiment in this chapter was carried out with data obtained in the Ocean Systems Laboratory tank. This experiment was carried out using a Tritech SeaKing Dual Frequency Sonar, see appendix D. This is a mechanically scanned sonar. It has a horizontal beam-width of 2° and a vertical beam-width of 20° when operating at 675 kHz. The sonar was set to scan a sector of 90° size with an operating range of 5m. The sonar offers a 0.05 m range resolution. With these settings the scans are produced at 0.5 Hz. The sonar was mounted on the laboratory's planar Cartesian robot, see figure 5.1, this system allows the sonar to be placed anywhere within the tank. The planar Cartesian robot has optical encoders allowing a position accuracy of 1 mm. The experiment is thus ground truthed allowing the performance of the stochastic map to be accurately tested. In the experiment, two cylinders where placed in the tank and used as targets. A heuristic was added to the algorithm so that it would ignore the tank walls and any multipath measurements appearing outside. The model used for the dynamics of the vehicle is identical to that described in section 4.4.2, equations 4.51 through to 4.55. The data association strategy implemented was the NN. Figures 5.2 through to 5.6 illustrate the sequential flow of the experiment and the growing stochastic map. The sonar data from which the map is created can also be seen in these figures. During the experiments only two

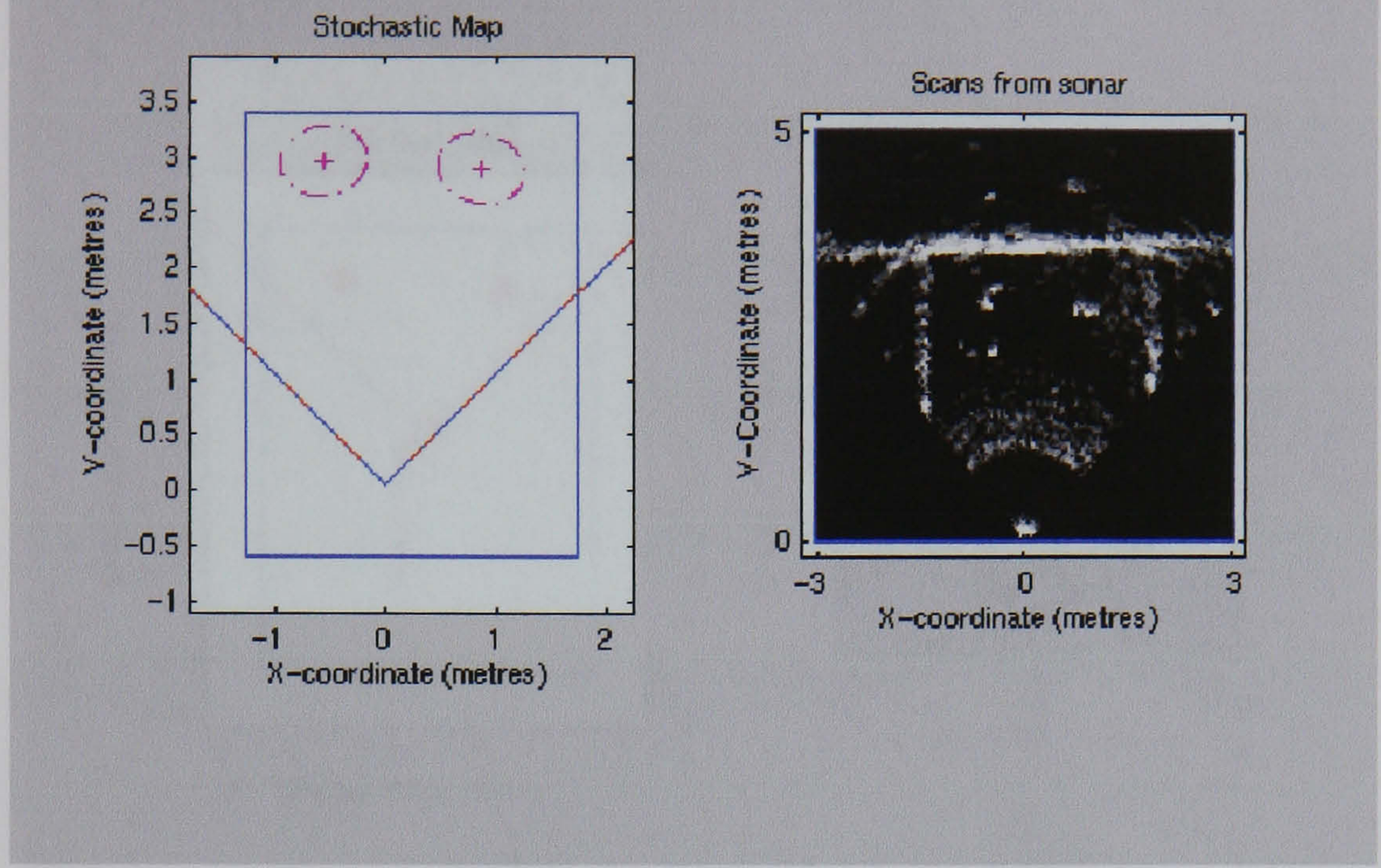

Figure 5.2: Landmark map of OSL tank and sonar scan: Iteration 1

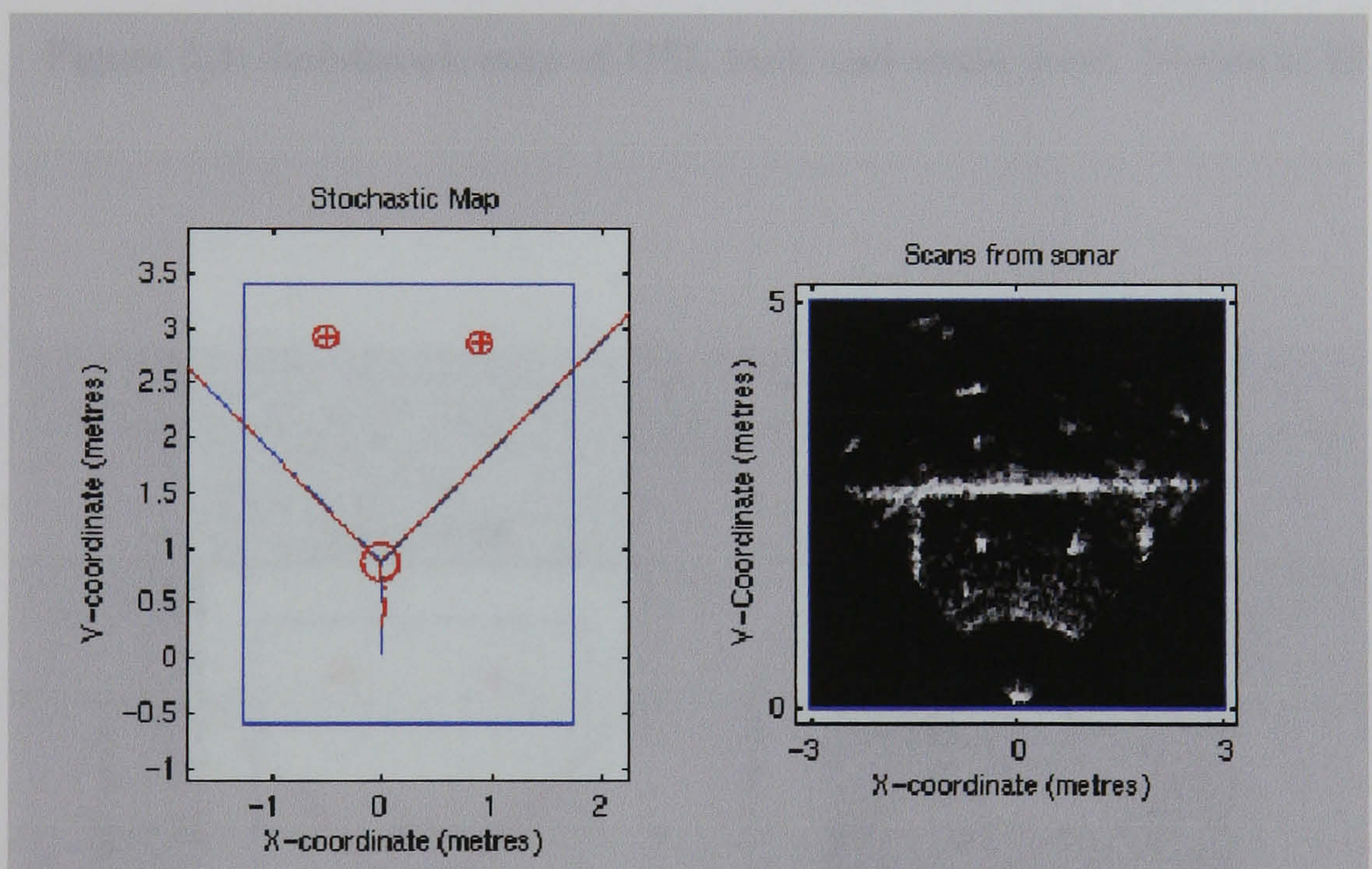

Figure 5.3: Landmark map of OSL tank and sonar scan: Iteration 20

landmarks were mapped and they were not always visible to the algorithm.

The stochastic map performed well, and the results were identical for instances where the landmark descriptors were integrated and when not. The consistency of the map can be corroborated by examining figures 5.7 and 5.8. These show the

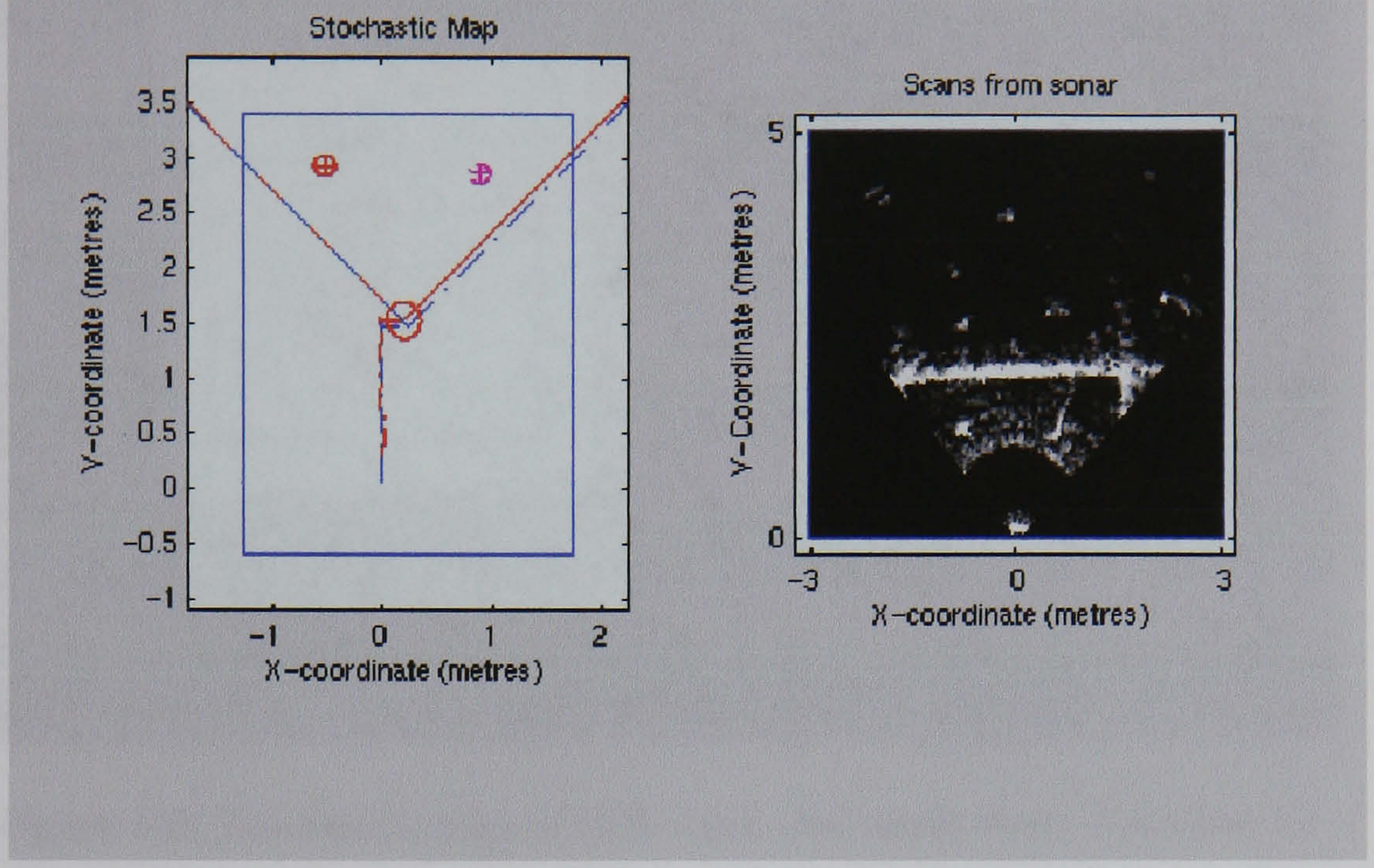

Figure 5.4: Landmark map of OSL tank and sonar scan: Iteration 40

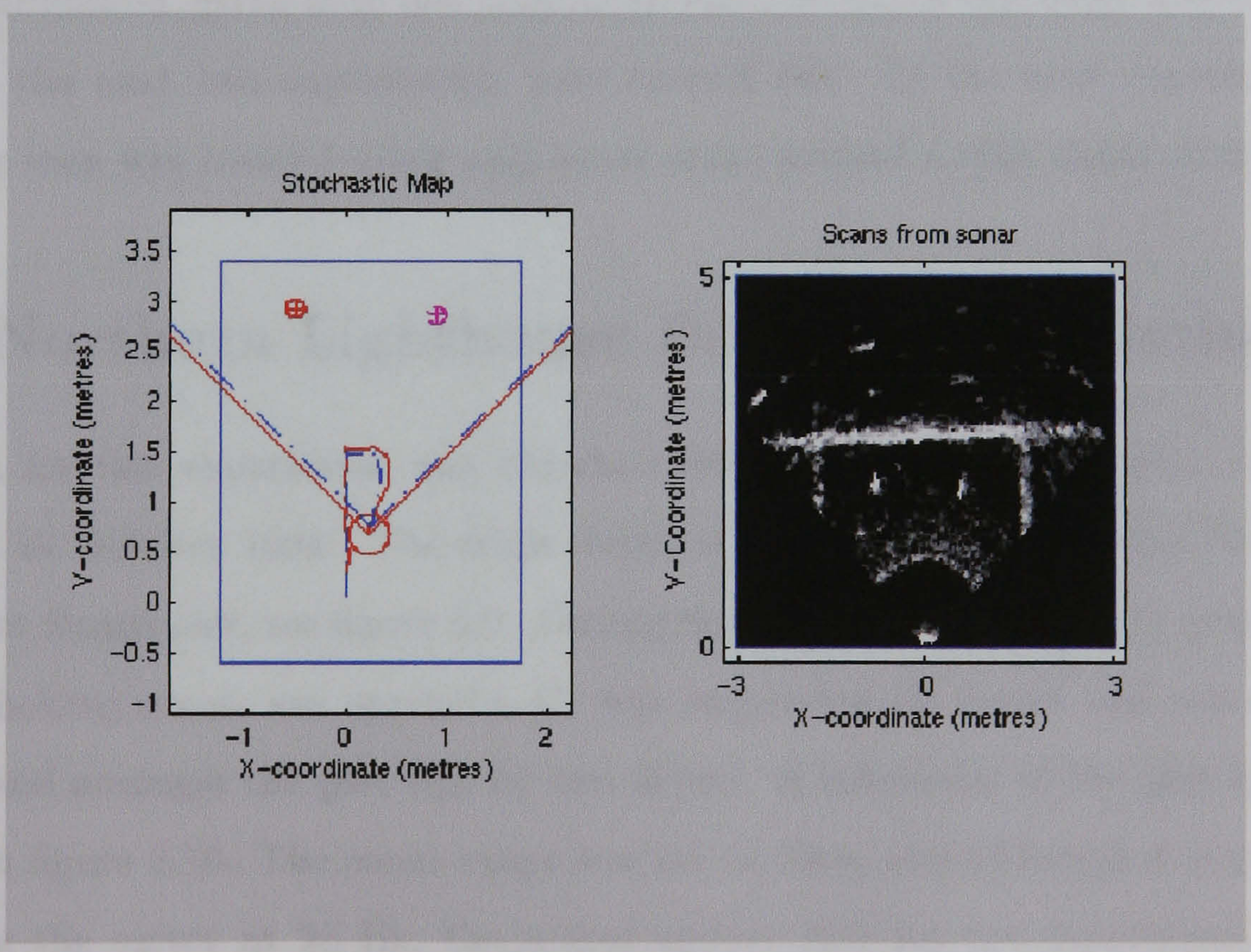

Figure 5.5: Landmark map of OSL tank and sonar scan: Iteration 60

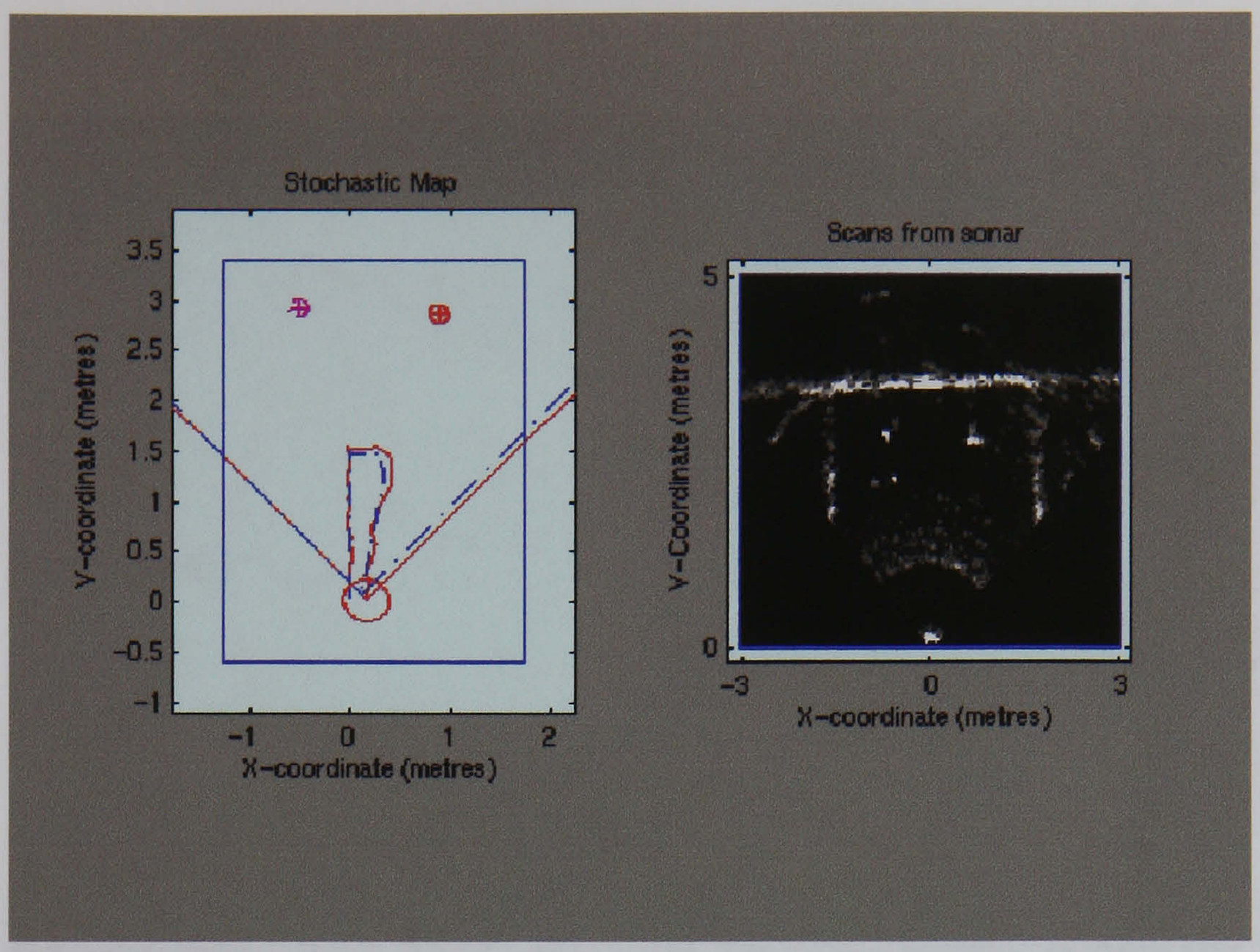

Figure 5.6: Landmark map of OSL tank and sonar scan: Iteration 75

true errors in X and Y coordinates and the three standard deviation uncertainty bounds. These results show that the position of the sonar can be found using a simple linear model, and a stochastic map can be maintained without any other sensor information, given only two landmarks and infrequent sightings. Given these qualities, the next two experiments were carried out. In the next experiment a stochastic map was created using *only* sonar scans around a man-made structure.

5.3 Northern Lighthouse Board Pier Experiment

The data for this experiment was obtained during trials in Oban, west coast of Scotland, in October 1994. The trials were carried out underneath the Northern Lighthouse Board pier, see figure 5.9. During the trials, the Seabat 6012 multibeam forward-looking sonar, see appendix C, was suspended by buoys and was moved towards and amongst the pier legs by two divers. A schematic of the pier legs can be seen in figure 5.10. The sonar range was set to $10m$, and although it is possible to sample the sector at 25 Hz, the actual update rate for the experiment was 5 Hz. The trials were not ground truthed. However, the divers travelled forward into the pier and then attempted to retrace their trajectory backwards. Thus, for the

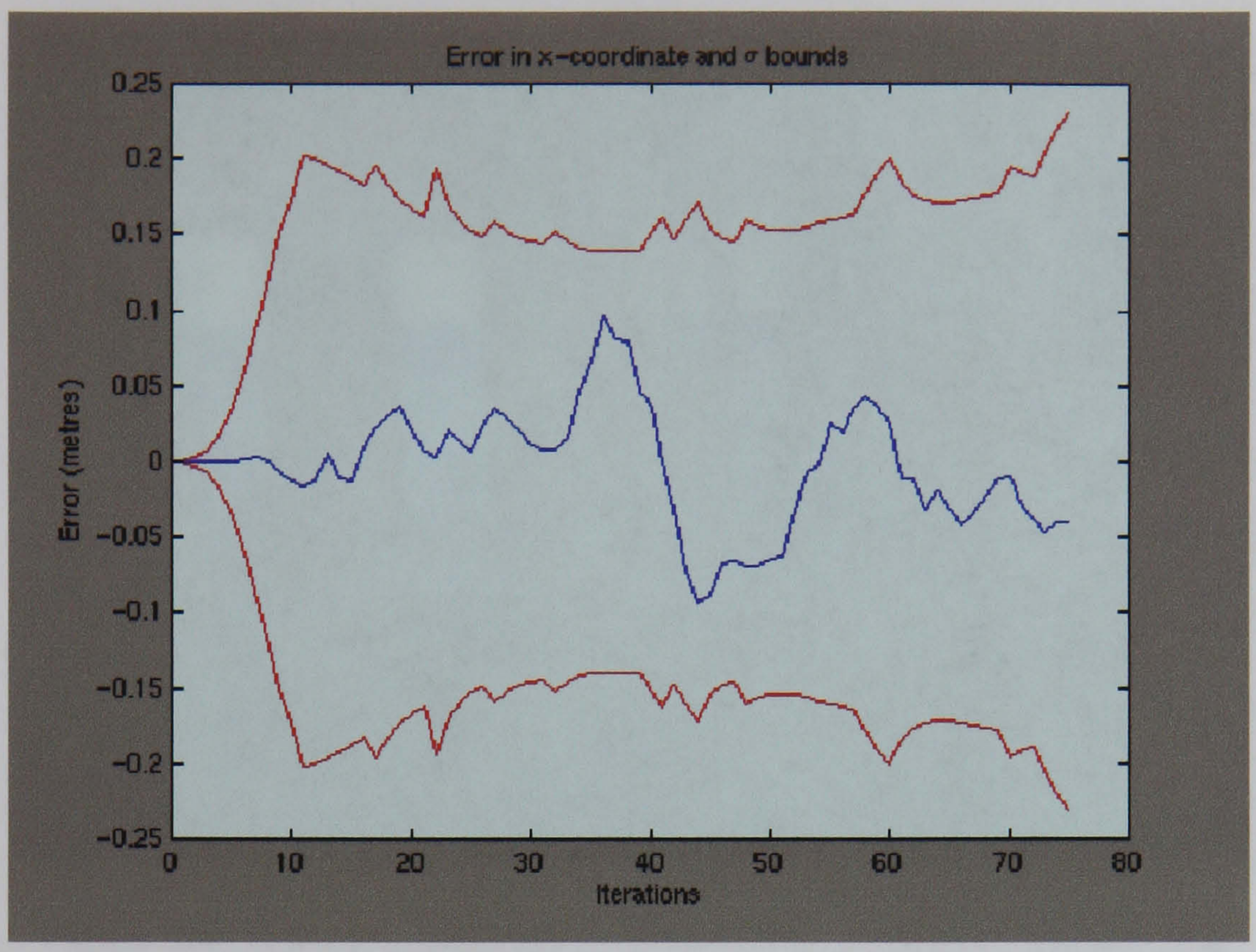

Figure 5.7: Tank experiment: x-coordinate error and 3σ bounds

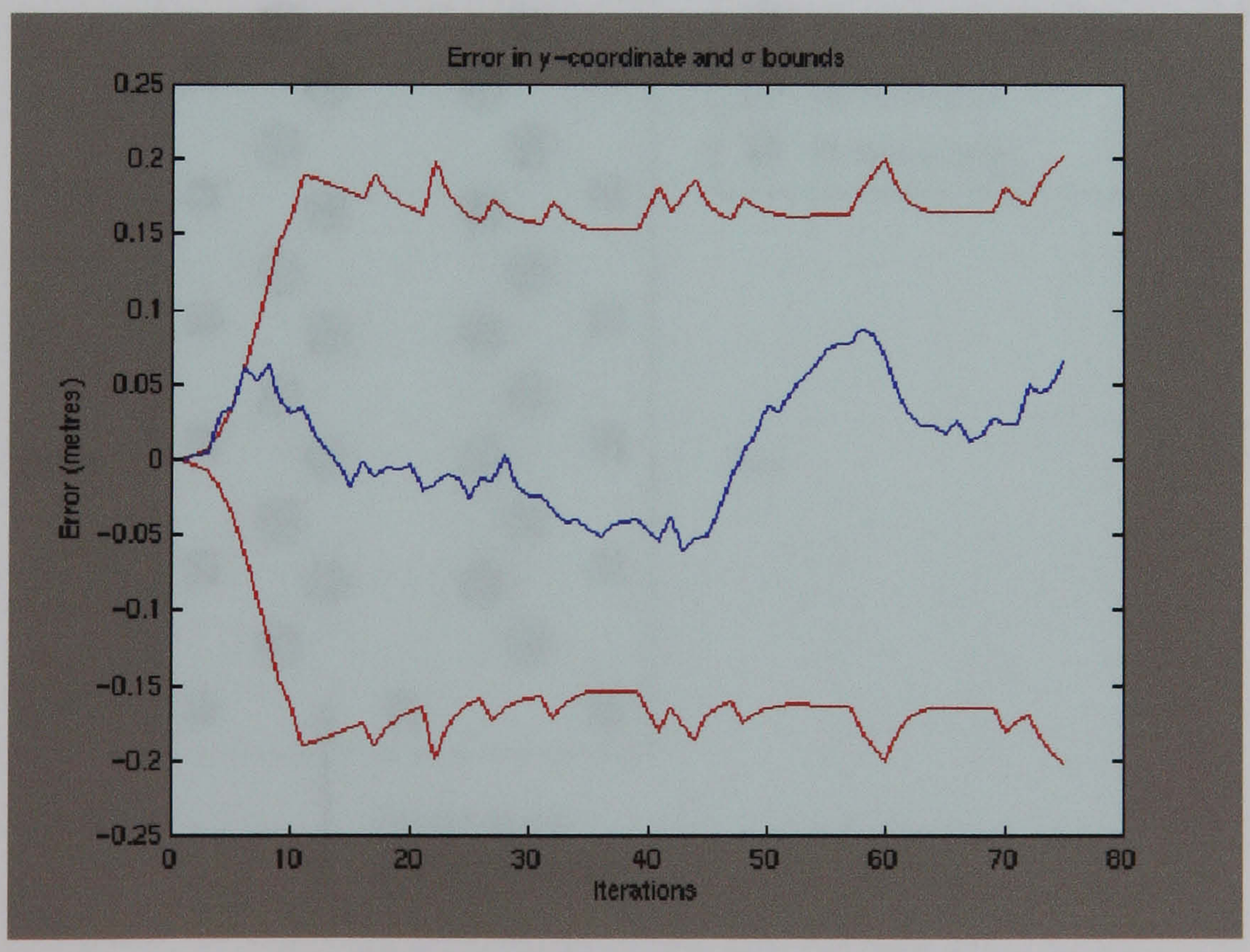

Figure 5.8: Tank experiment: y-coordinate error and 3σ bounds

Figure 5.9: Northern Lighthouse Board Pier: A view of the pier legs

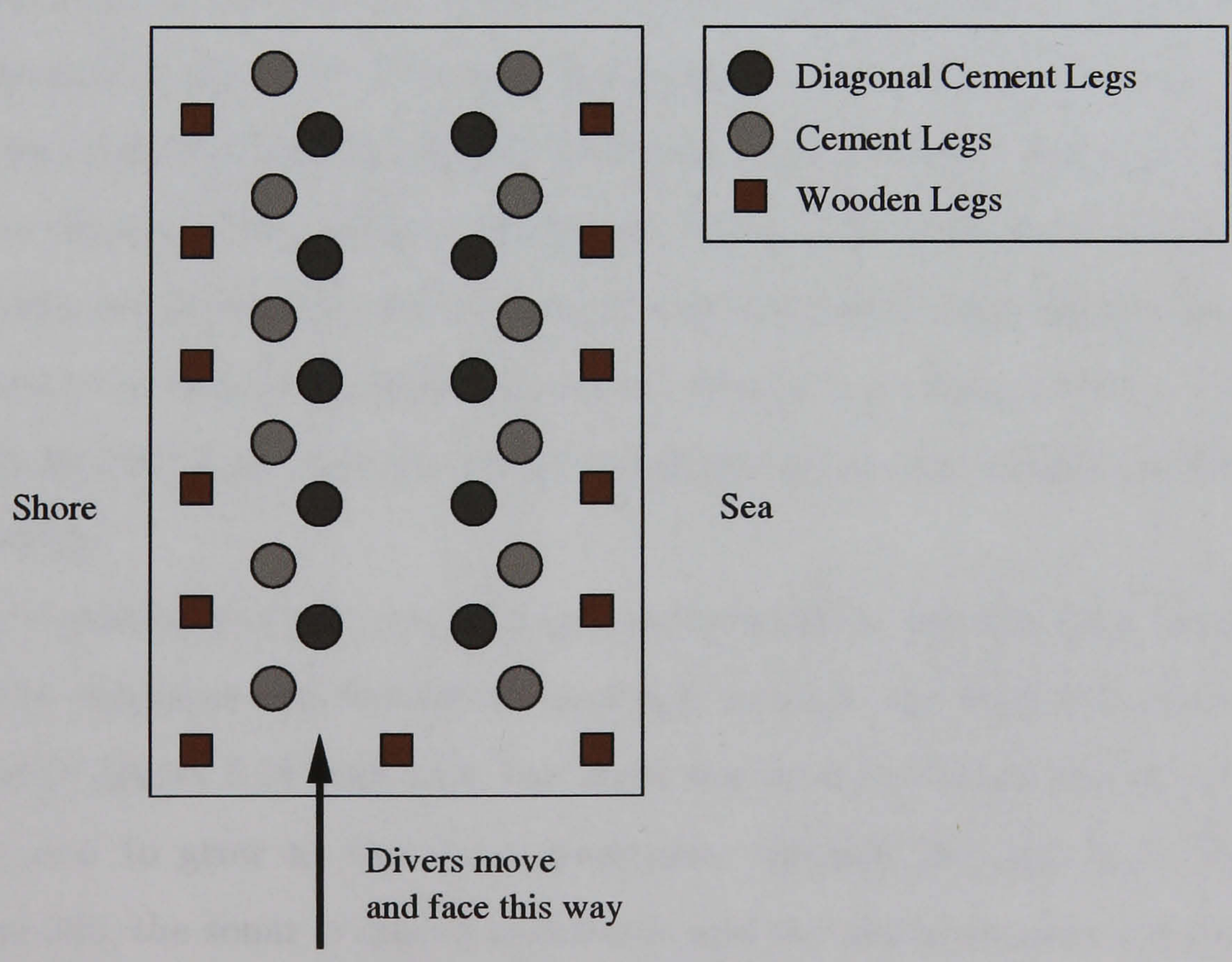

Figure 5.10: Northern Lighthouse Board Pier: A plan view of the pier (not to scale)

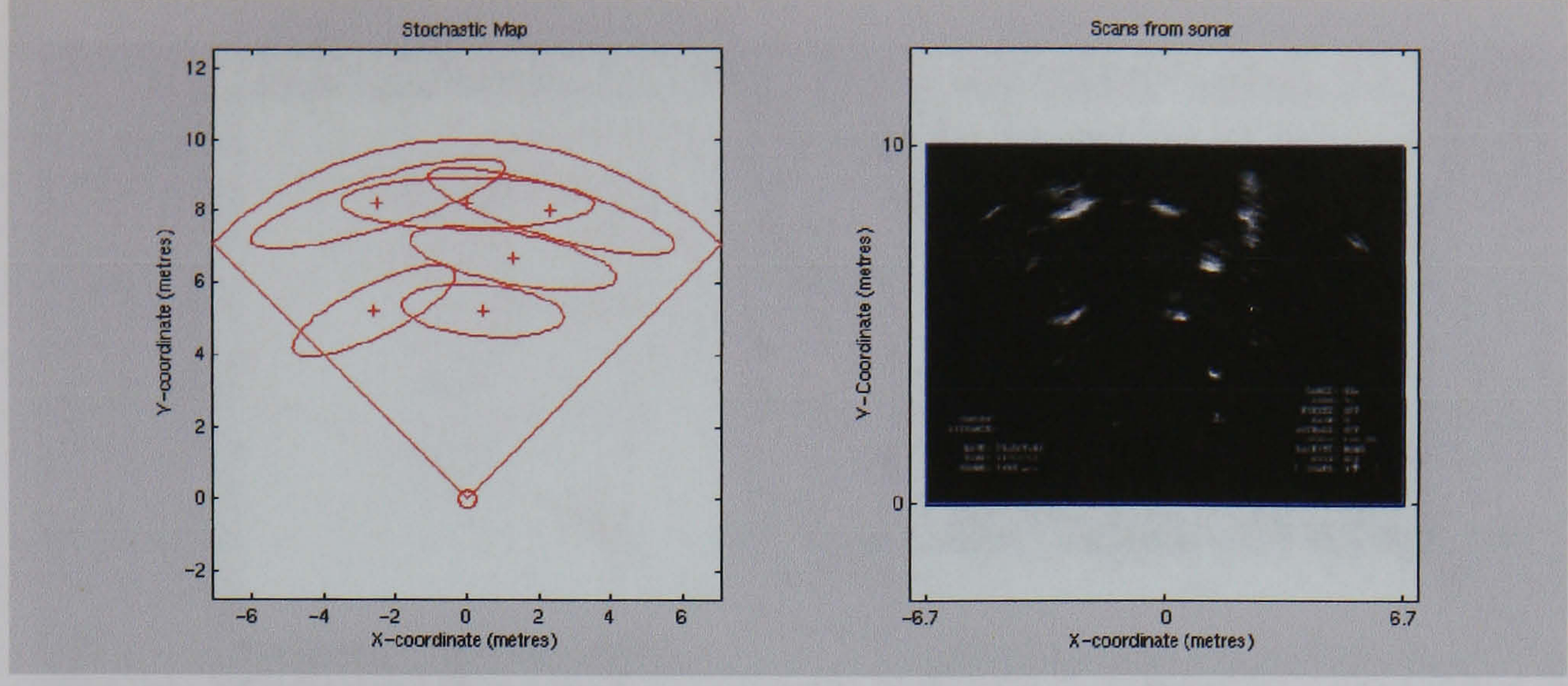

Figure 5.11: Landmark map of Oban Pier: Iteration 1

algorithm to function correctly, the section of the pier which had previously been mapped must be recognised upon reentry. The whole sequence was composed of 1092 sector scans. The model used for the dynamics of the sonar head (moved by the divers) is again identical to that described in section 4.4.2, equations 4.51 through to 4.55. The divers moved relatively slowly and this linear model of the dynamics produced good results given the frequent update rate. The data association strategy implemented was the NN. In this experiment, the landmarks are mostly cylinders and the sonar is, for most of the run, facing in the same general direction. Thus, the landmarks are not seriously affected by the view dependency issues described in the previous chapter. The similarity of the pier legs was found to have an adverse effect when using the landmarks descriptors. It was found that when these were used, the stochastic map clearly diverged. However, figures 5.11 through to 5.17 show how the map is created as the scans are processed by the system using only the centroid information.

The consistency of the map can be corroborated by the fact that the algorithm is able to recognise old landmarks and not commit any data association errors. Examining figures 5.18 and 5.19, the three standard deviation uncertainty bounds can be seen to grow as the sonar progresses through the pier legs. At around iteration 800, the sonar is moved backwards and the old landmarks are re-observed. Consequentially, the uncertainty becomes smaller as the region has already been mapped. These results show that the feature descriptors must be used with care. Clearly, in a workspace where all prospective landmarks *appear* the same, adding

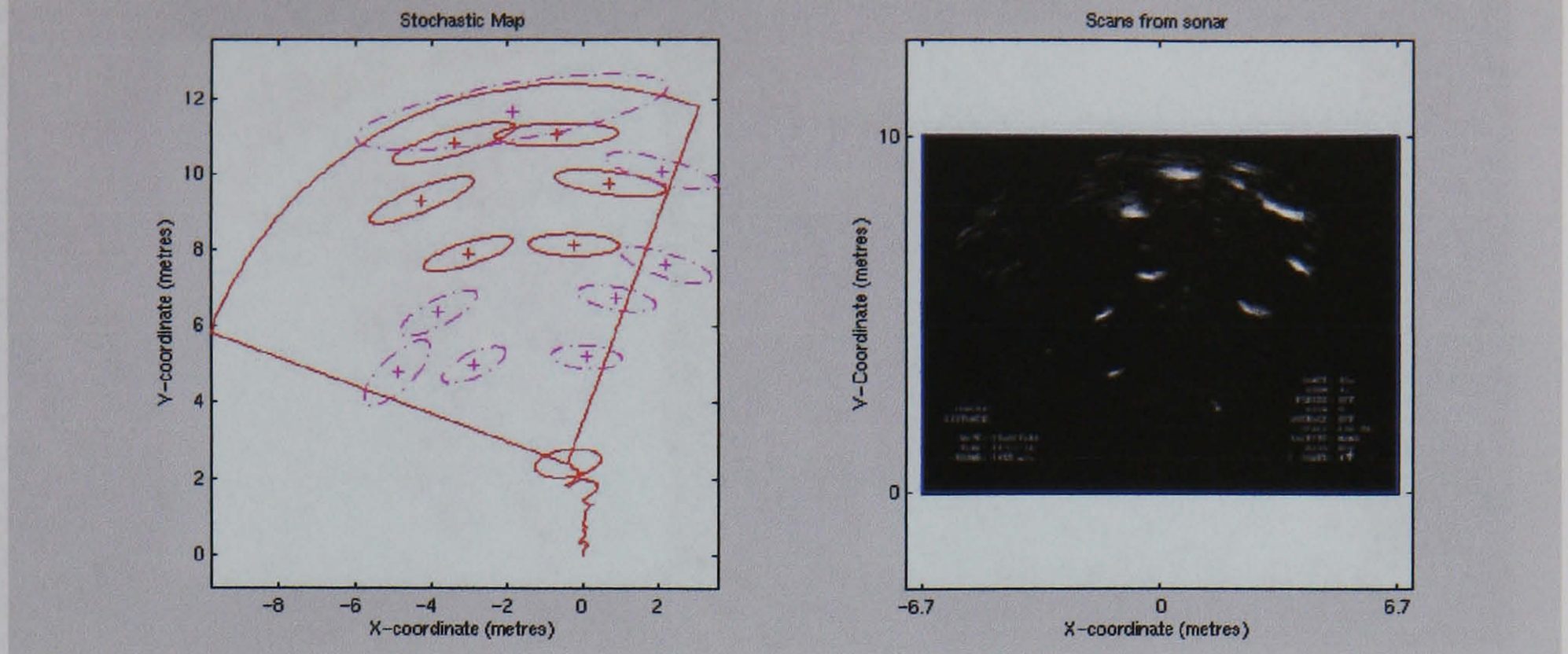

Figure 5.12: Landmark map of Oban Pier: Iteration 100

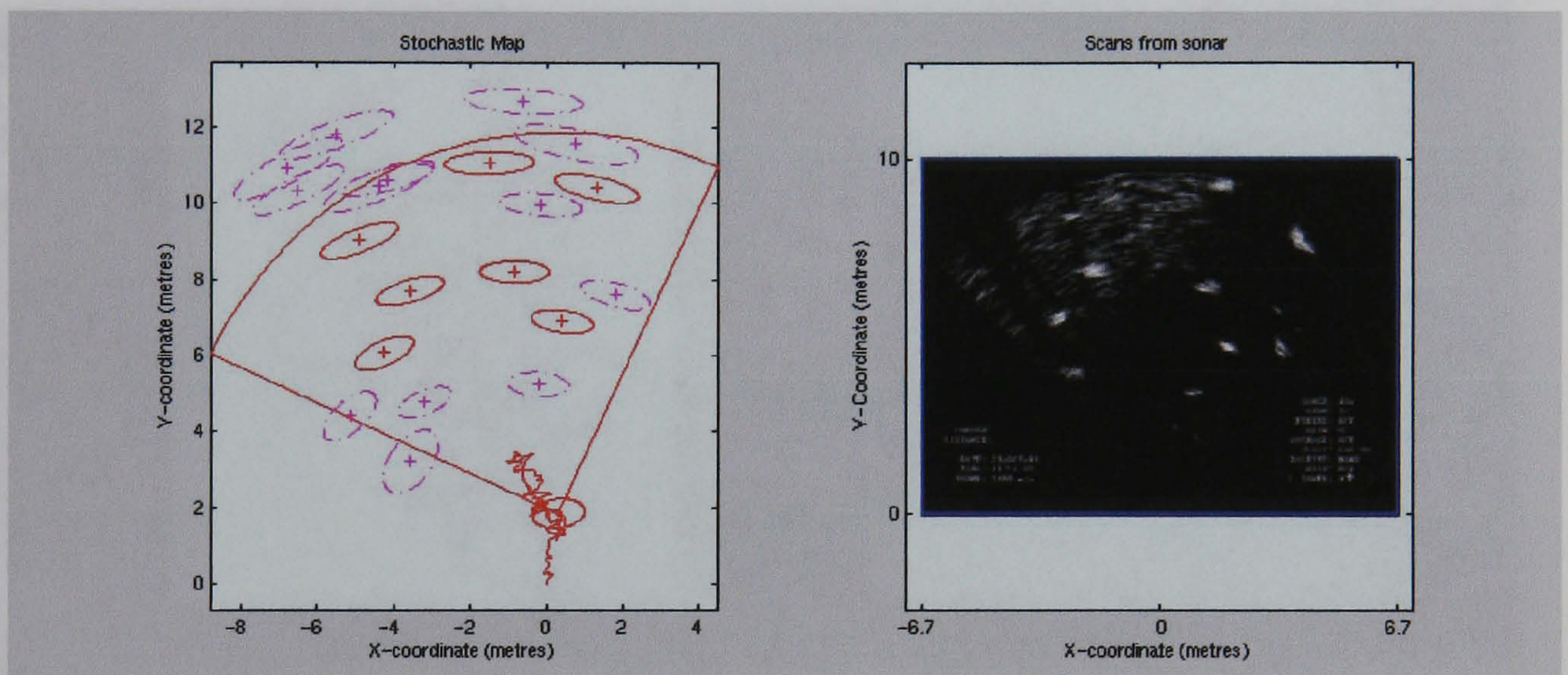

Figure 5.13: Landmark map of Oban Pier: Iteration 300

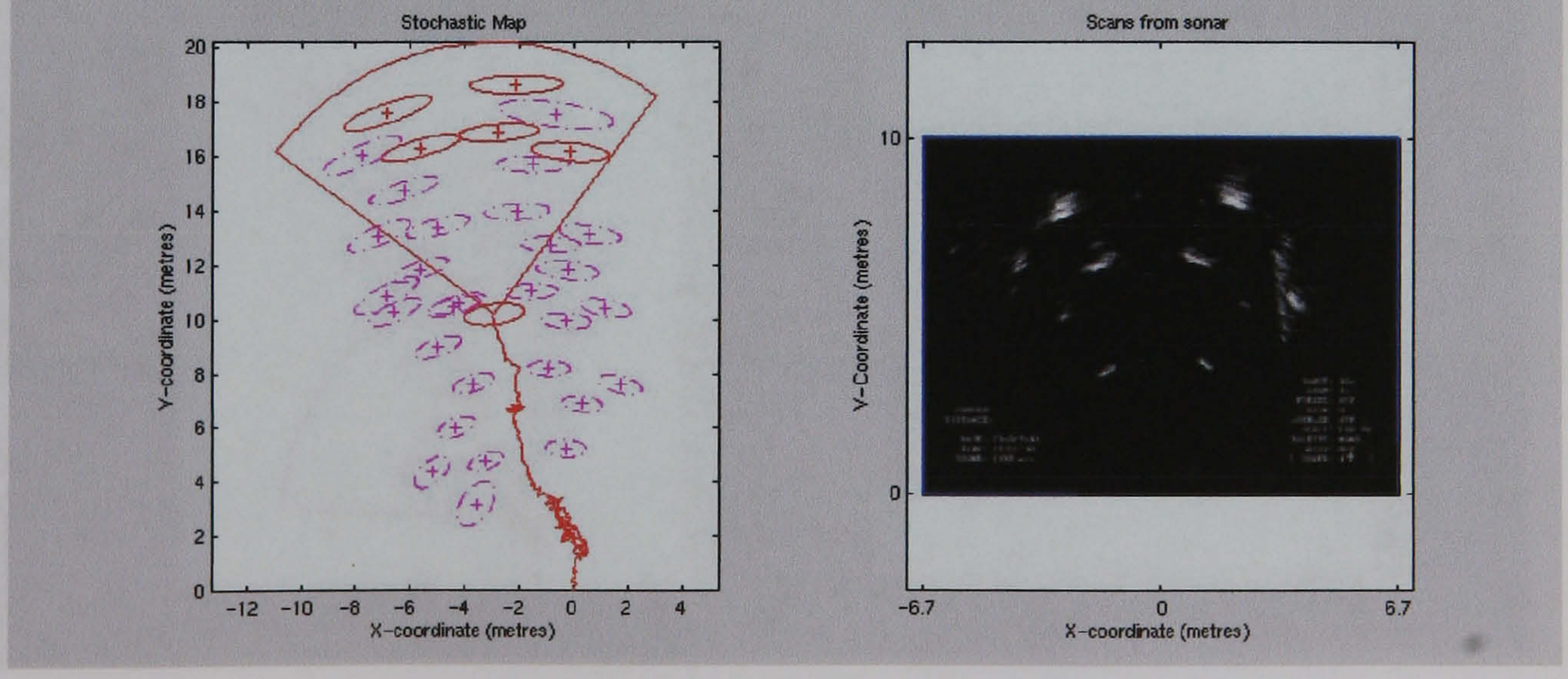

Figure 5.14: Landmark map of Oban Pier: Iteration 700

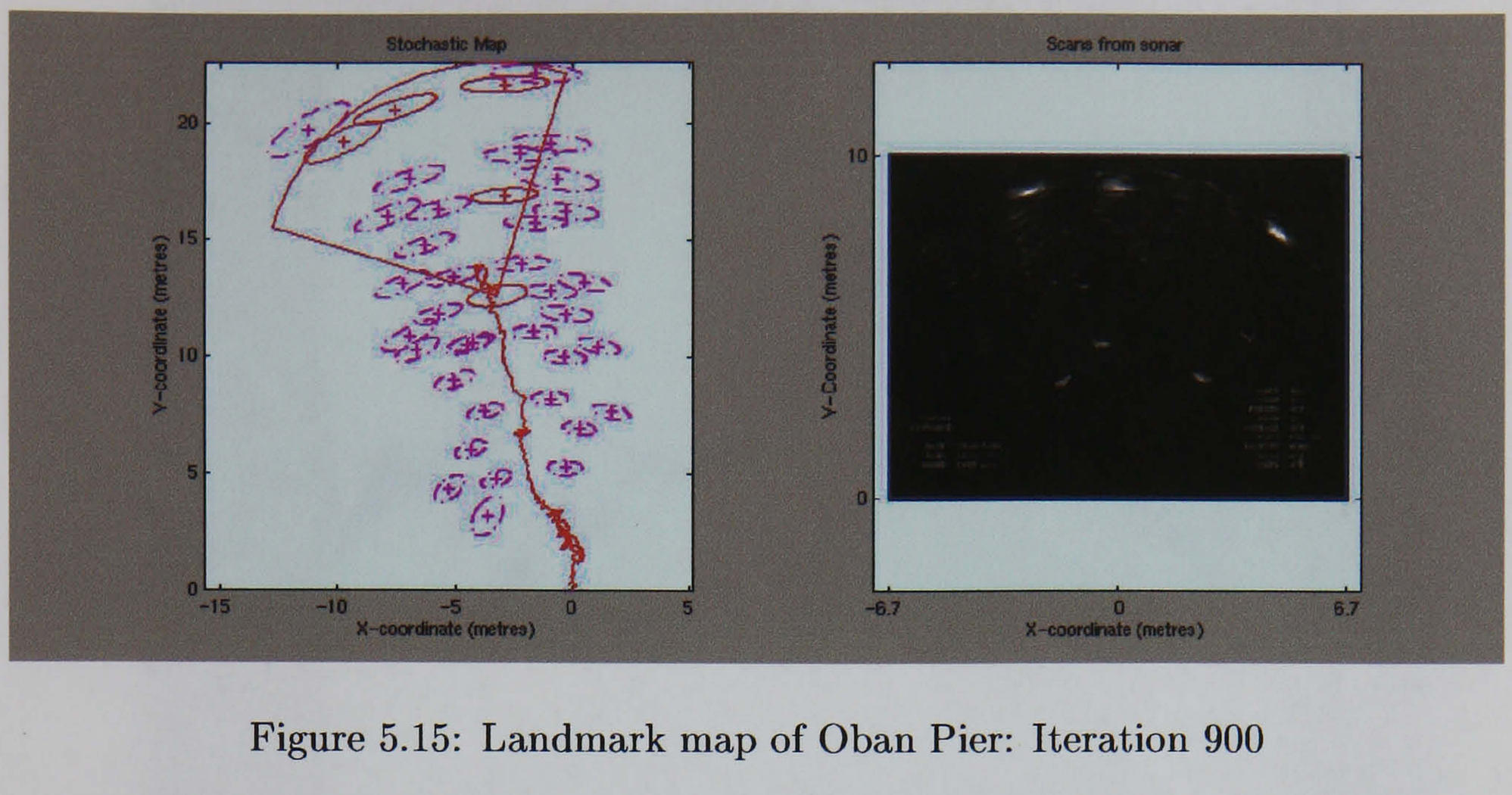

Figure 5.15: Landmark map of Oban Pier: Iteration 900

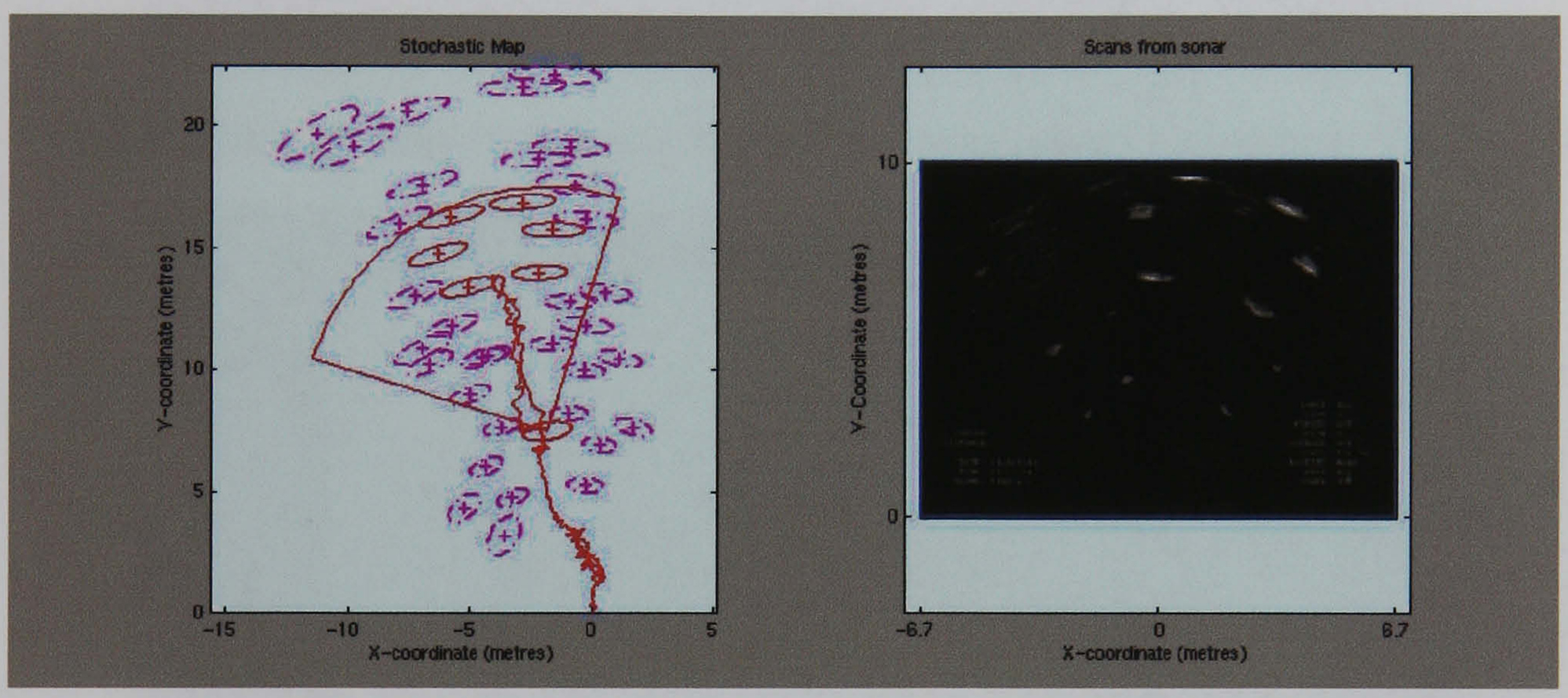

Figure 5.16: Landmark map of Oban Pier: Iteration 1100

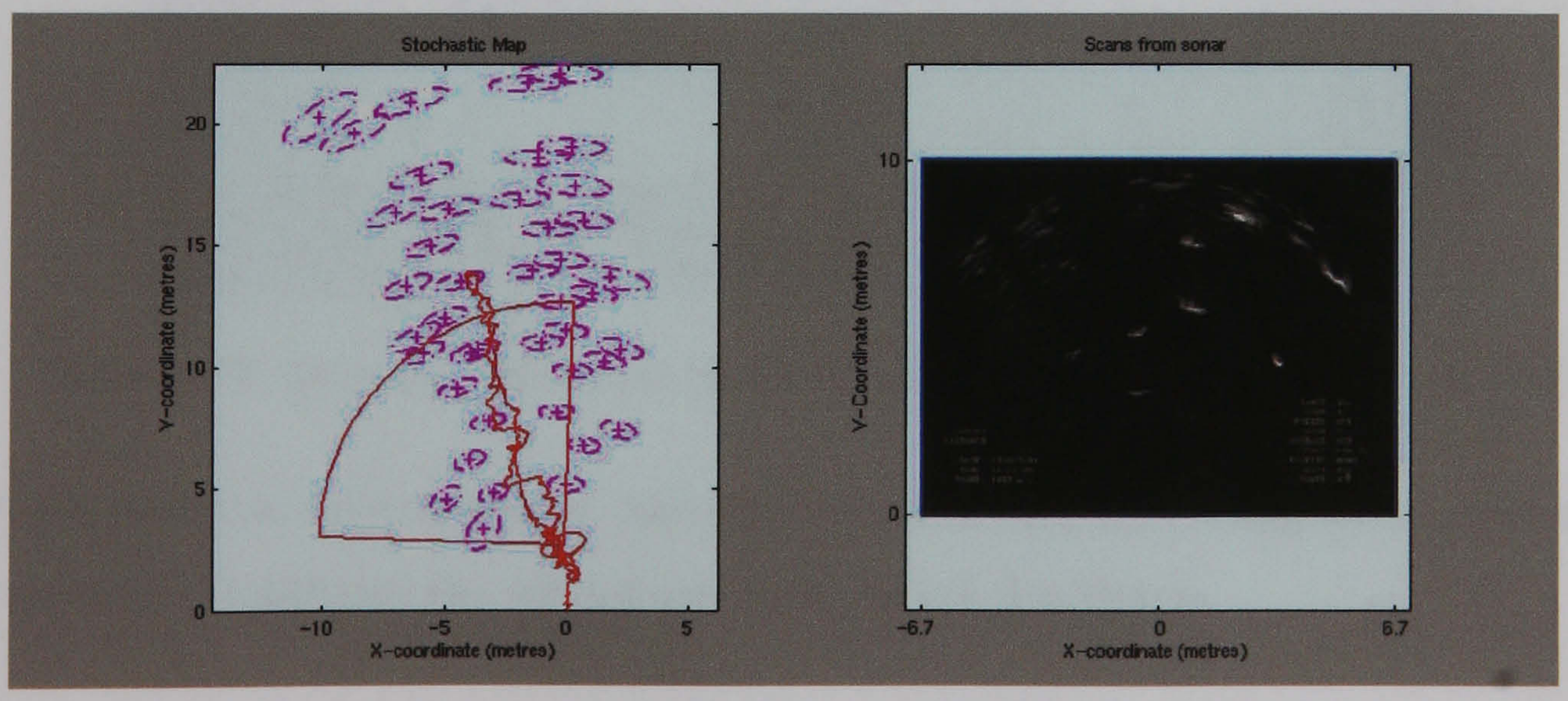

Figure 5.17: Landmark map of Oban Pier: Iteration 1292

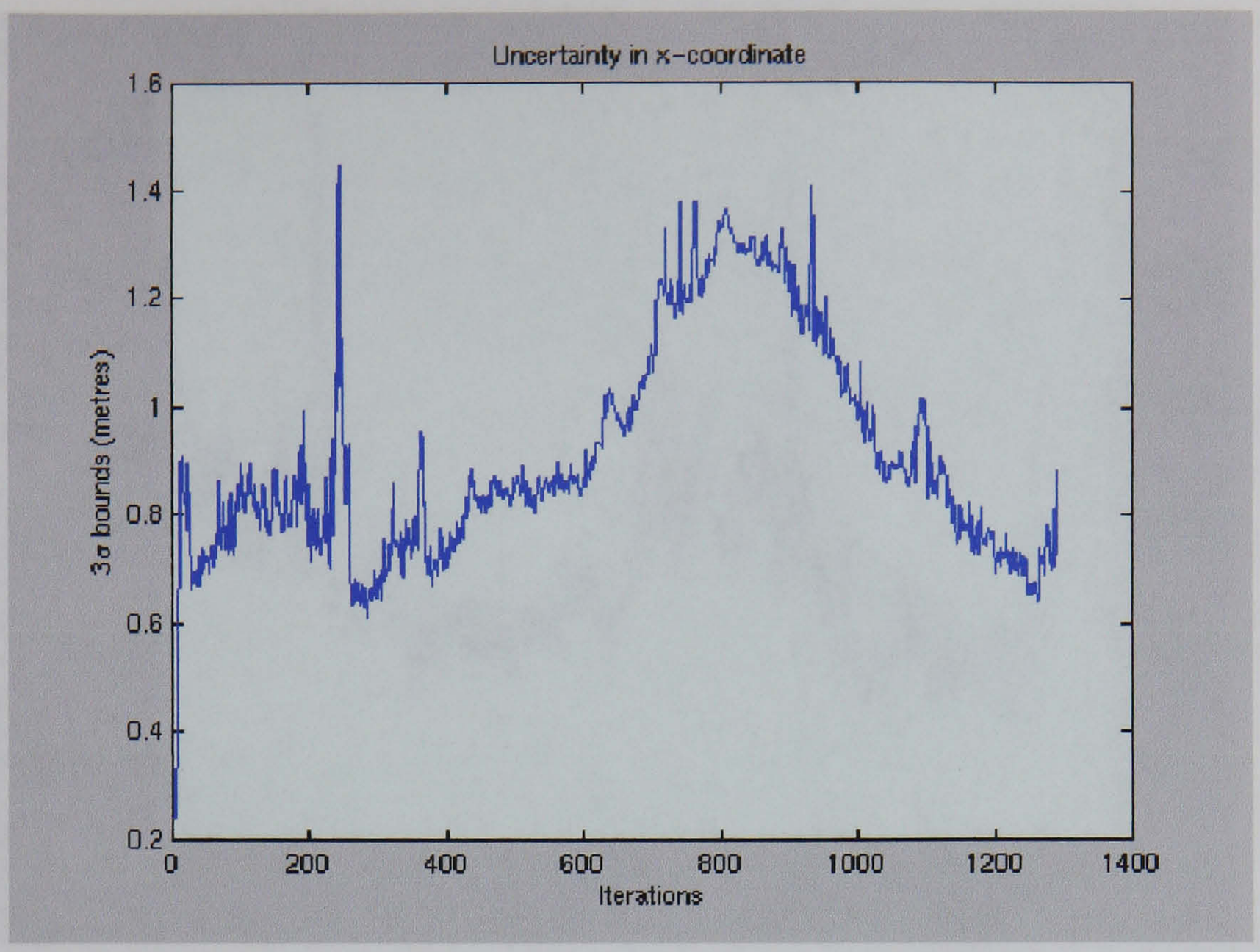

Figure 5.18: Northern Lighthouse Board Pier experiment: x-coordinate 3σ bounds

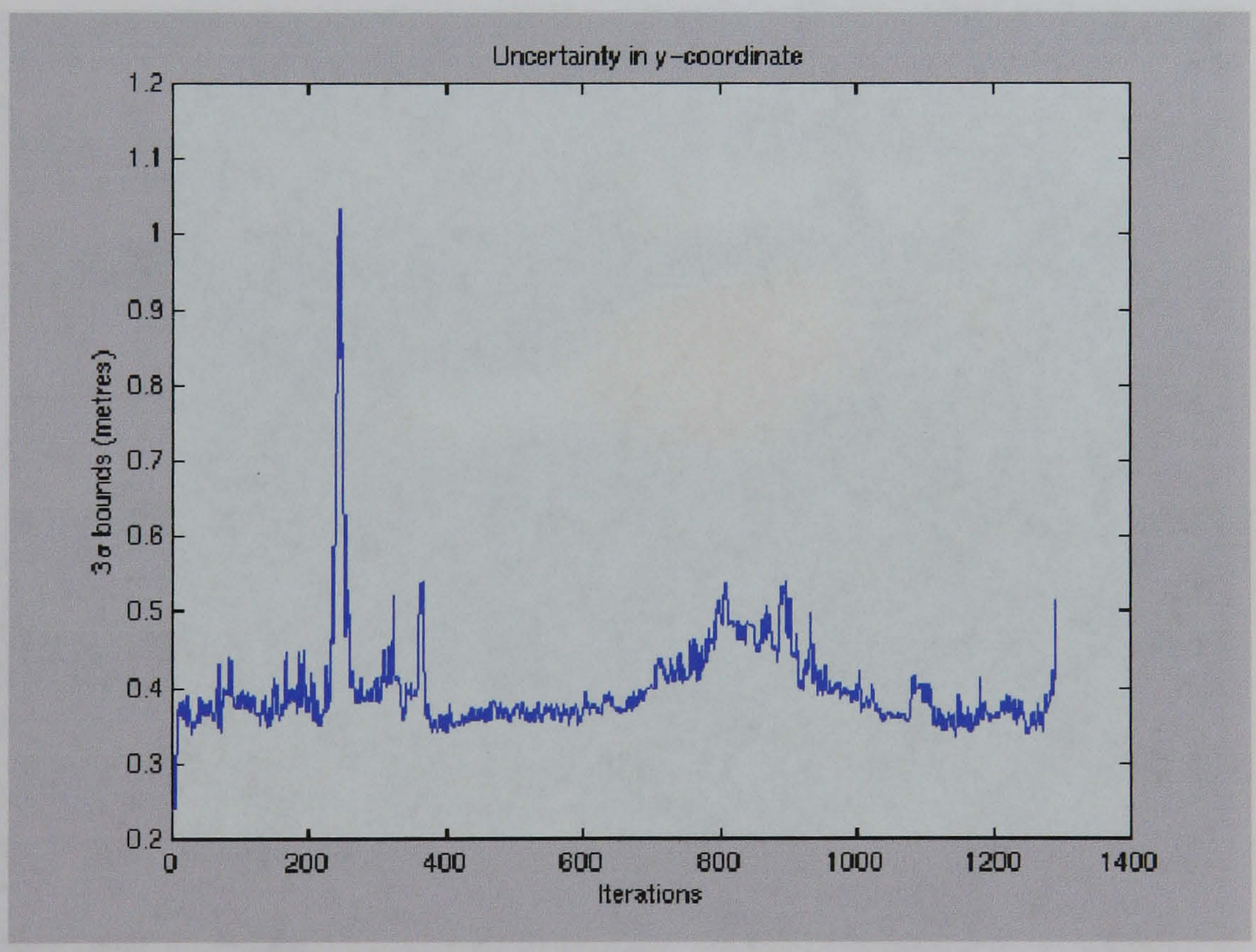

Figure 5.19: Northern Lighthouse Board Pier experiment: y-coordinate 3σ bounds

states based on the landmarks' *appearances* is not the clever thing to do. The next experiment highlights the advantages of landmark descriptors.

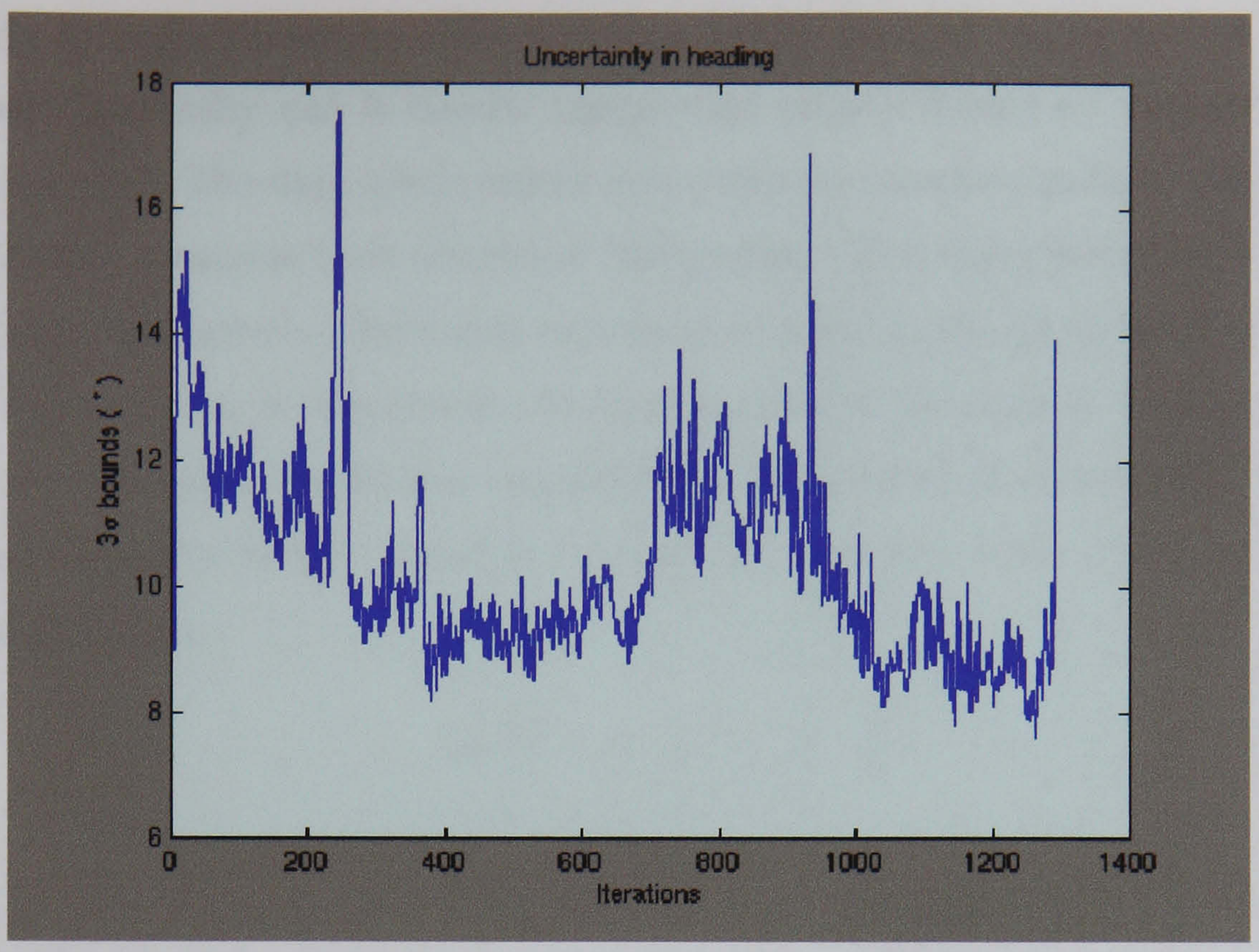

Figure 5.20: Northern Lighthouse Board Pier experiment: heading 3σ bounds

Figure 5.21: Florida Atlantic University's Ocean Explorer

5.4 Ocean Explorer Experiment

This experiment was performed with data from Barney, a concept electronically scanned sonar developed by Florida Atlantic University, see appendix E. Barney was mounted on the Ocean Explorer, see figure 5.21, an AUV also developed by

Florida Atlantic University. The data was kindly donated to the author by Florida Atlantic University and it depicts unspecified targets during an unspecified Ocean Explorer trial. The data incorporates asynchronous compass updates obtained using a TCM2-50 compass from Precision Navigation. The experiment was carried out using only a sequence of 300 sonar returns as an input to the algorithm. The compass data was used only to corroborate the performance of the system. In this experiment a different dynamic model was implemented. The Ocean Explorer AUV is designed so that it travels in the direction it is facing. The new state vector and dynamic model was thus,

$$\mathbf{x_v}(k) = \begin{bmatrix} x & y & v & \phi & \dot{\phi} \end{bmatrix}' \tag{5.1}$$

$$\mathbf{f_v}[\hat{\mathbf{x}}_\mathbf{v}(k-1), \mathbf{u}(k), \mathbf{0}, k] = \hat{\mathbf{x}}_\mathbf{v}(k-1) + \begin{bmatrix} \cos(\phi(k-1))\, v\, dt \\ \sin(\phi(k-1))\, v\, dt \\ 0 \\ \dot{\phi}\, dt \\ 0 \end{bmatrix} \tag{5.2}$$

And process noise,

$$\mathbf{Q_v}(k) = \begin{bmatrix} 0 & 0 & 0 & 0 & 0 \\ 0 & 0 & 0 & 0 & 0 \\ 0 & 0 & \sigma_v^2 & 0 & 0 \\ 0 & 0 & 0 & 0 & 0 \\ 0 & 0 & 0 & 0 & \sigma_{\dot{\phi}}^2 \end{bmatrix} \tag{5.3}$$

The data association strategy implemented was the NN. Figures 5.22 through to 5.27 show how the map is created as the scans are processed by the system. The algorithm uses the landmark descriptors in the observation model as described in section 4.4.2.

During the experiment, the average estimated speed for the AUV was 0.7865 m/s^2. Throughout the run, the algorithm initialised a total of 115 landmarks. Only 41 of these landmarks were maintained by the filter. These were observed as little as 6 times (2/3 sec) and up to 99 times (11 sec). The rest were released as they were not reobserved sufficient times. Figure 5.28 shows the estimates of the descriptor states for one of the landmarks from its initialisation until the end

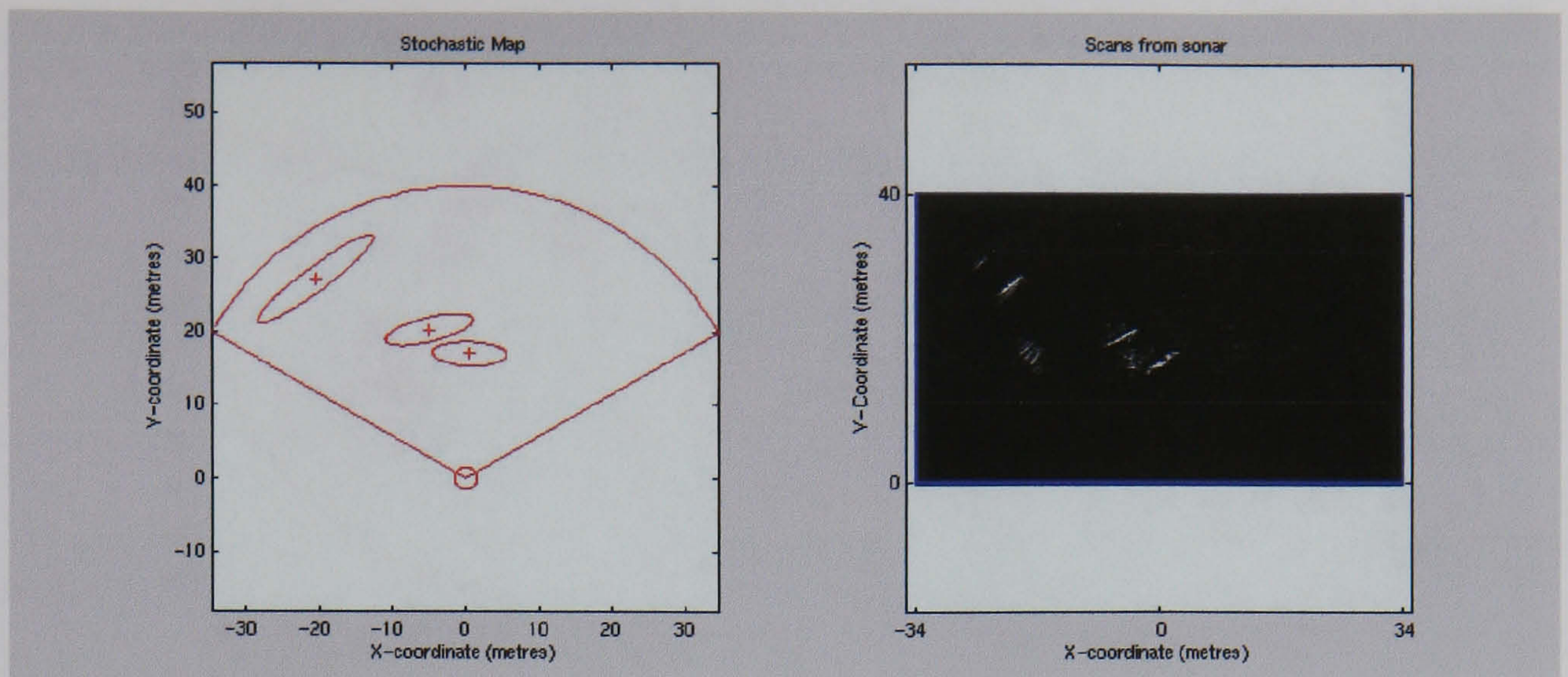

Figure 5.22: Landmark map of Barney's data: Iteration 1

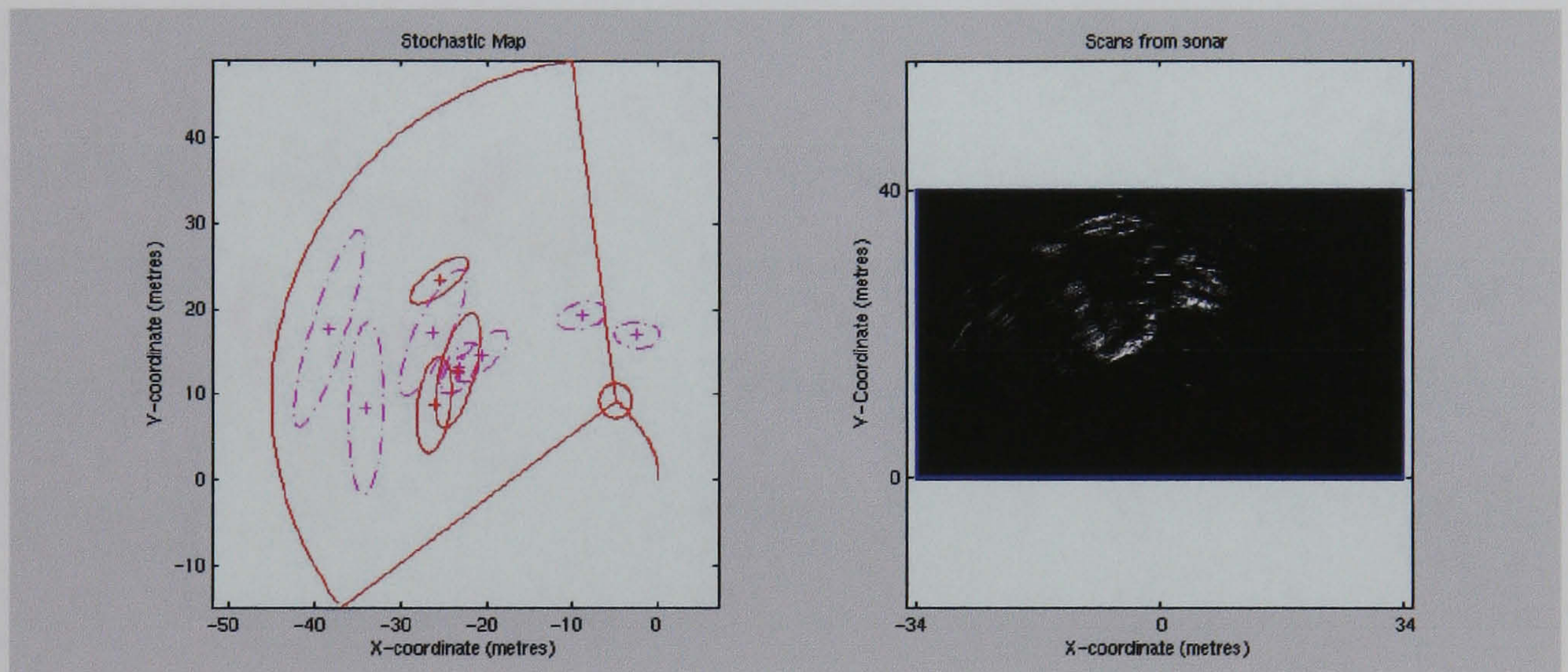

Figure 5.23: Landmark map of Barney's data: Iteration 100

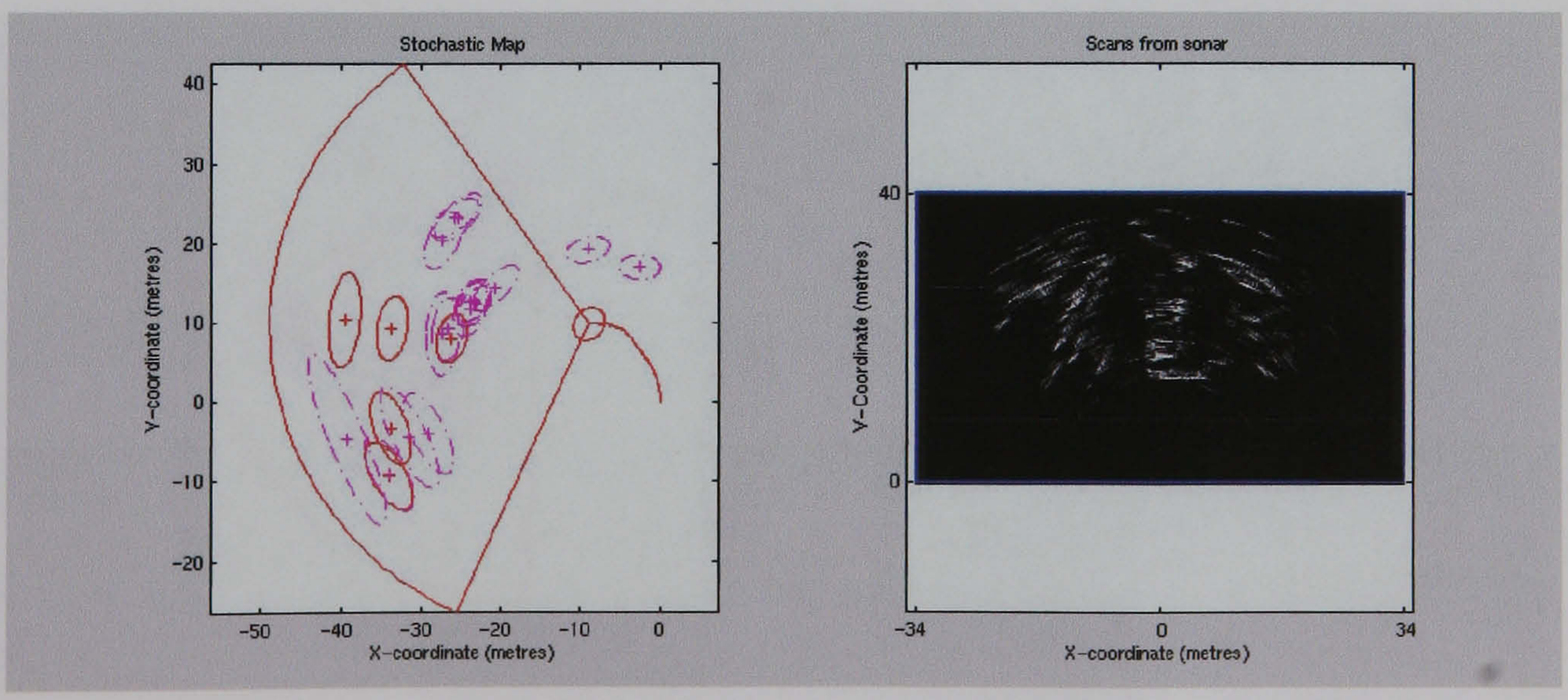

Figure 5.24: Landmark map of Barney's data: Iteration 150

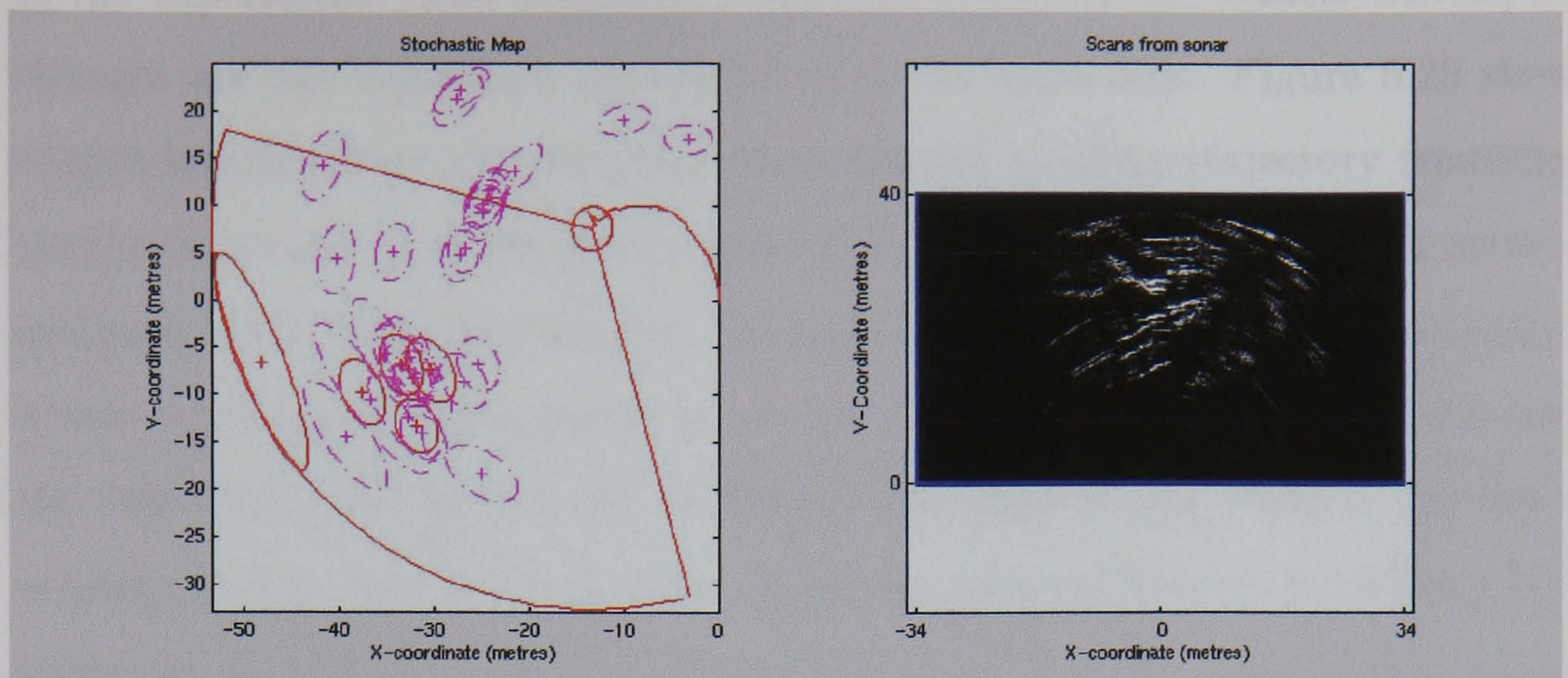

Figure 5.25: Landmark map of Barney's data: Iteration 200

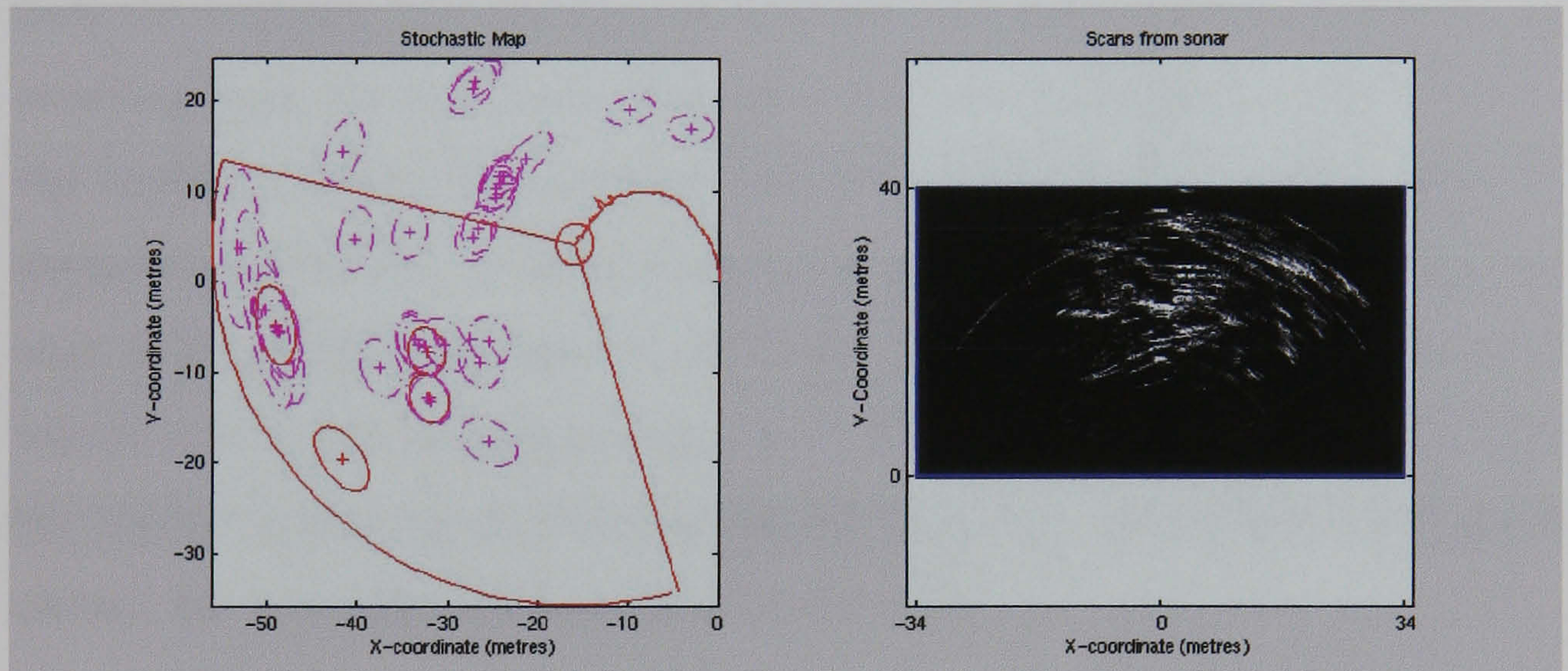

Figure 5.26: Landmark map of Barney's data: Iteration 250

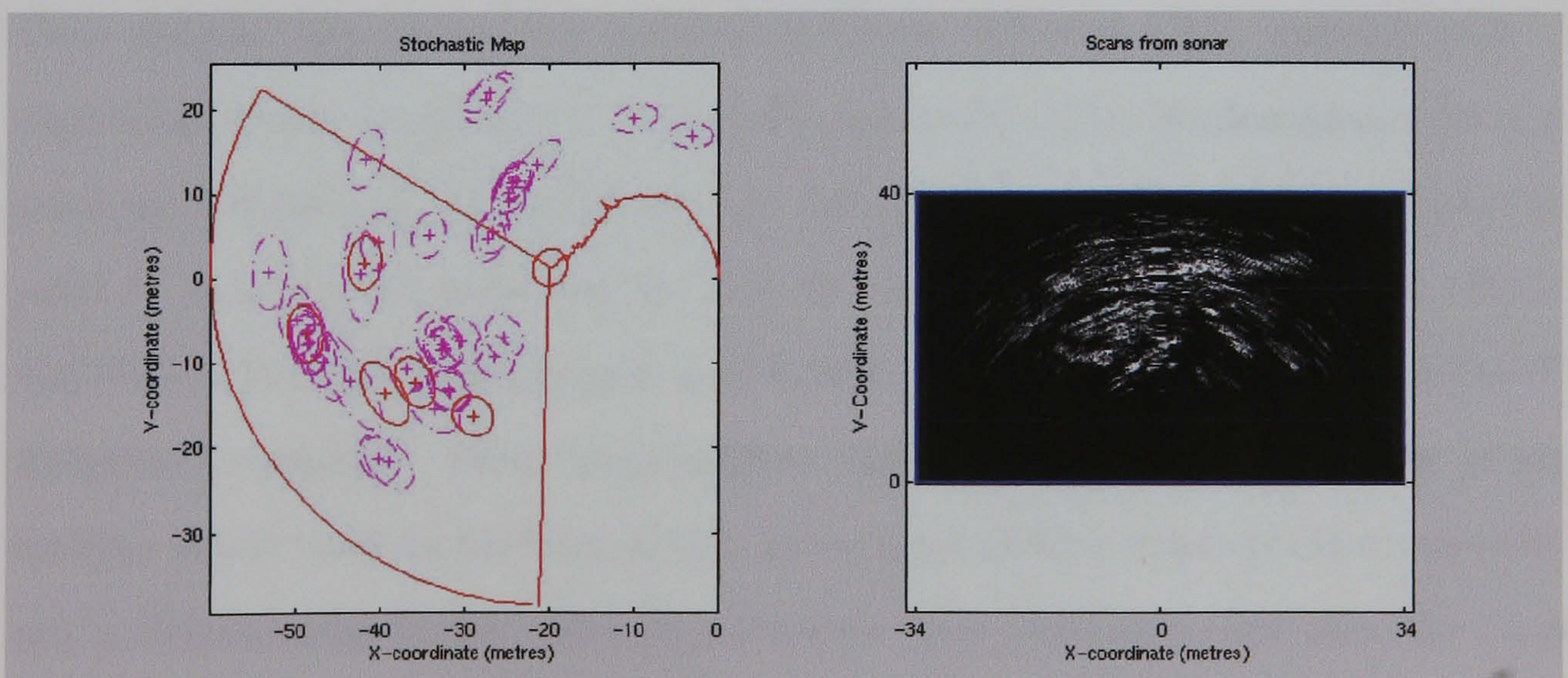

Figure 5.27: Landmark map of Barney's data: Iteration 300

of the experiment. The descriptor states do change as the vehicle travels, but the changes are not significant enough to drop the landmark. Figure 5.29 shows the output heading from the compass, the estimated heading trajectory resulting from the stochastic map and the three standard deviation uncertainty bounds around that estimate. Note that the compass has only been updated 36 times throughout the whole sequence and intermediate values have been interpolated. Clearly the estimate sits well within the 3σ bounds. Obviously it is hard to tell which of the two states is closer to the true heading state. The compass calibration procedure for these trials was unavailable. Figures 5.30 and 5.31 show that the sonar's uncertainty of its position estimate, whilst initially growing, reaches a saturation level when observing previously mapped landmarks. Finally, figure 5.32 again shows the output heading from the compass, but this time it is shown with the estimated heading trajectory resulting from the stochastic map when only the landmarks centroids are used in the landmark state. The compass output clearly falls outside the three standard deviation uncertainty bounds around the estimate. Therefore, in this case, the error is higher than the expected 99% error bounds (the three sigma bounds). The vehicle's estimated heading has diverged. This result demonstrates the usefulness of the landmark descriptors with real non-artificial data. It is also the first experiment carried out with data gathered from a real AUV.

5.5 Discussion

This chapter has shown the results for three different CML experiments. These experiments can be added to the list of successful CML implementations using the stochastic map and a forward-looking sonar. The number of sonars used for this purpose can now be increased to include the Seabat 6012, a standard off-the-shelf multibeam forward-looking unit, and Barney, a concept sonar developed by Florida Atlantic University. These experiments clearly indicate that the type of forward-looking sonar used to perform CML, given appropriate segmentation procedures, is not a determining factor. The experiments have demonstrated that the stochastic map is capable of performing CML using only an appropriate vehicle model and forward-looking sonar inputs. With no control inputs or dead-reckoning sensor in-

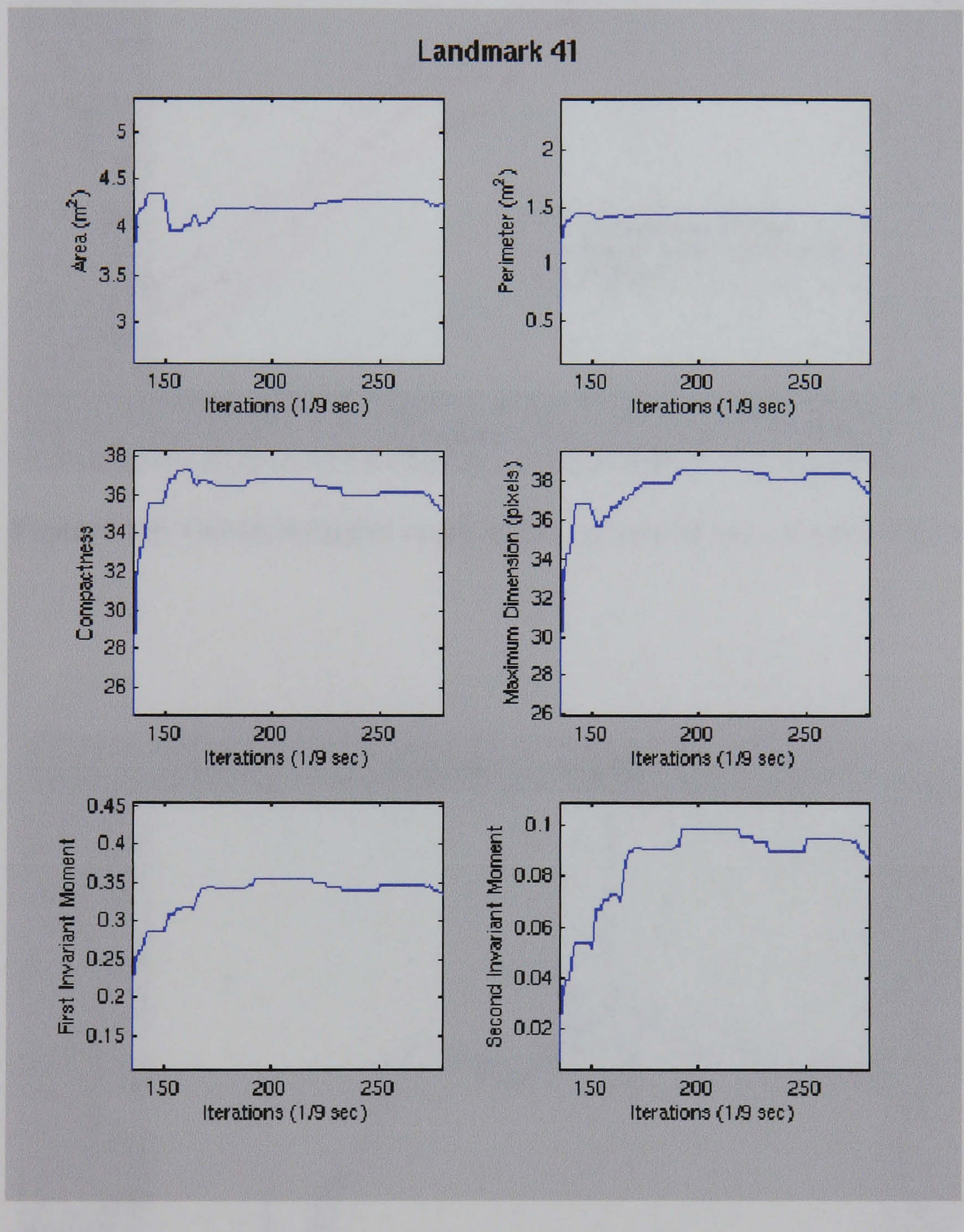

Figure 5.28: Ocean Explorer experiment: descriptor states for a sample landmark

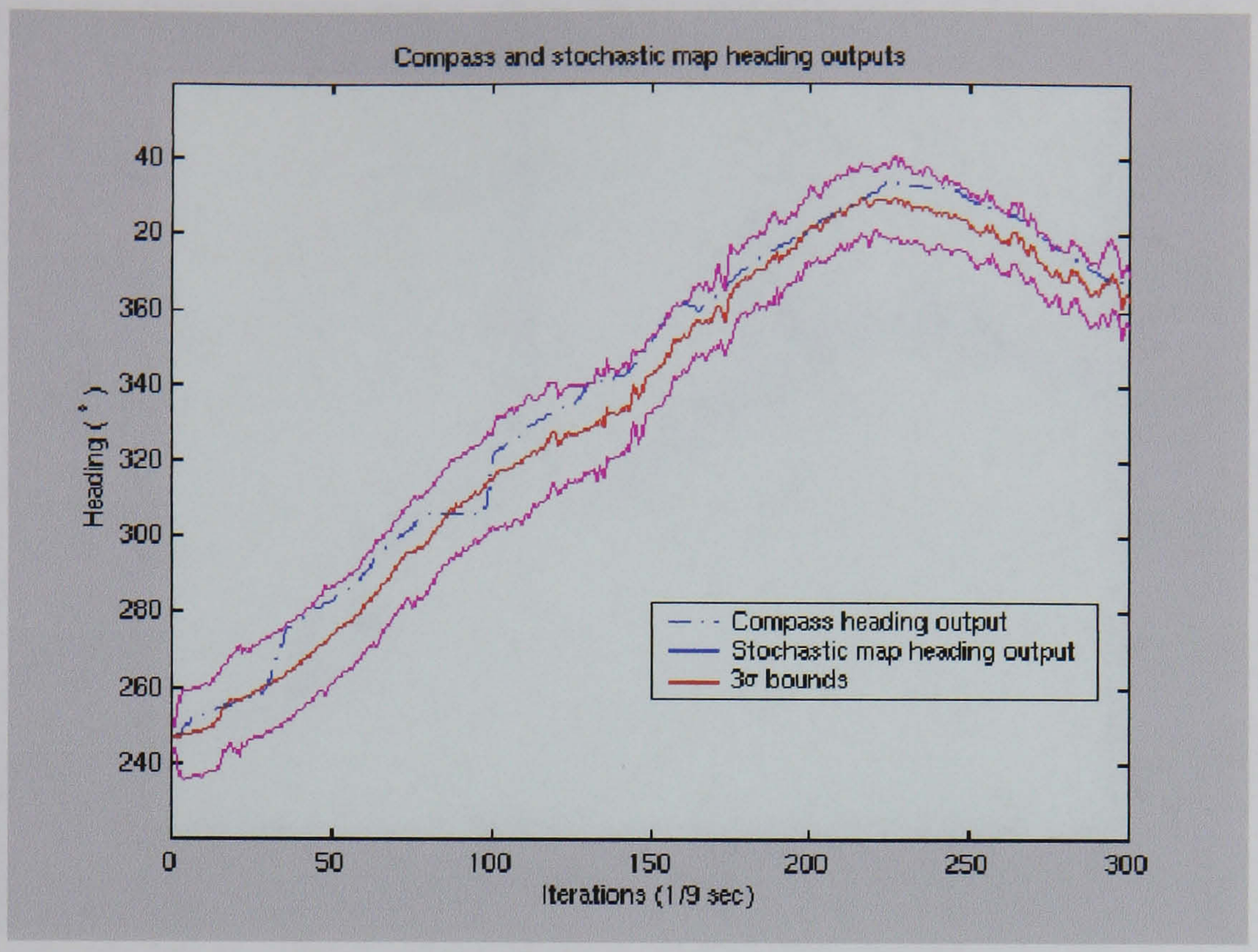

Figure 5.29: Ocean Explorer experiment: estimated vs. compass heading

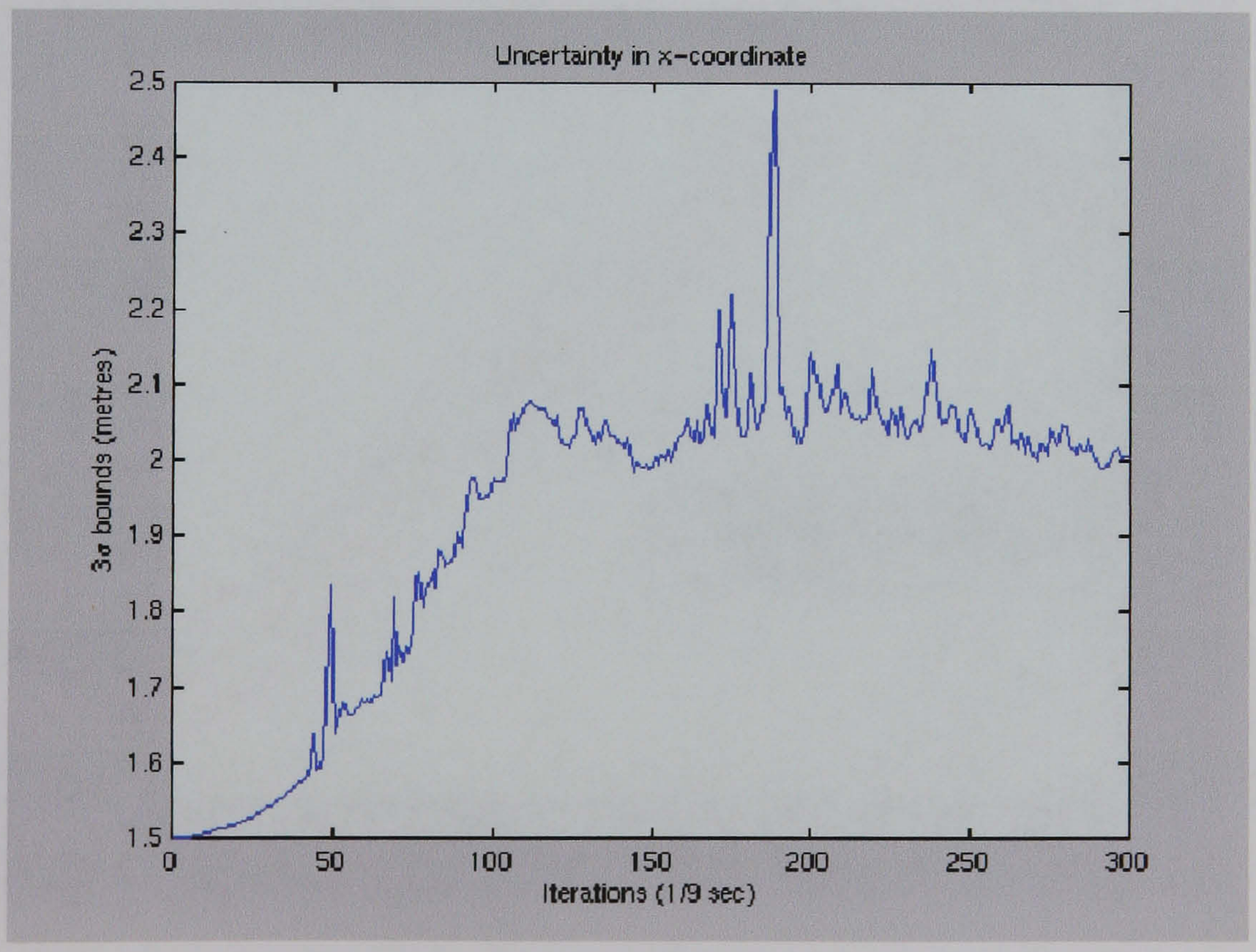

Figure 5.30: Ocean Explorer experiment: x-coordinate 3σ bounds

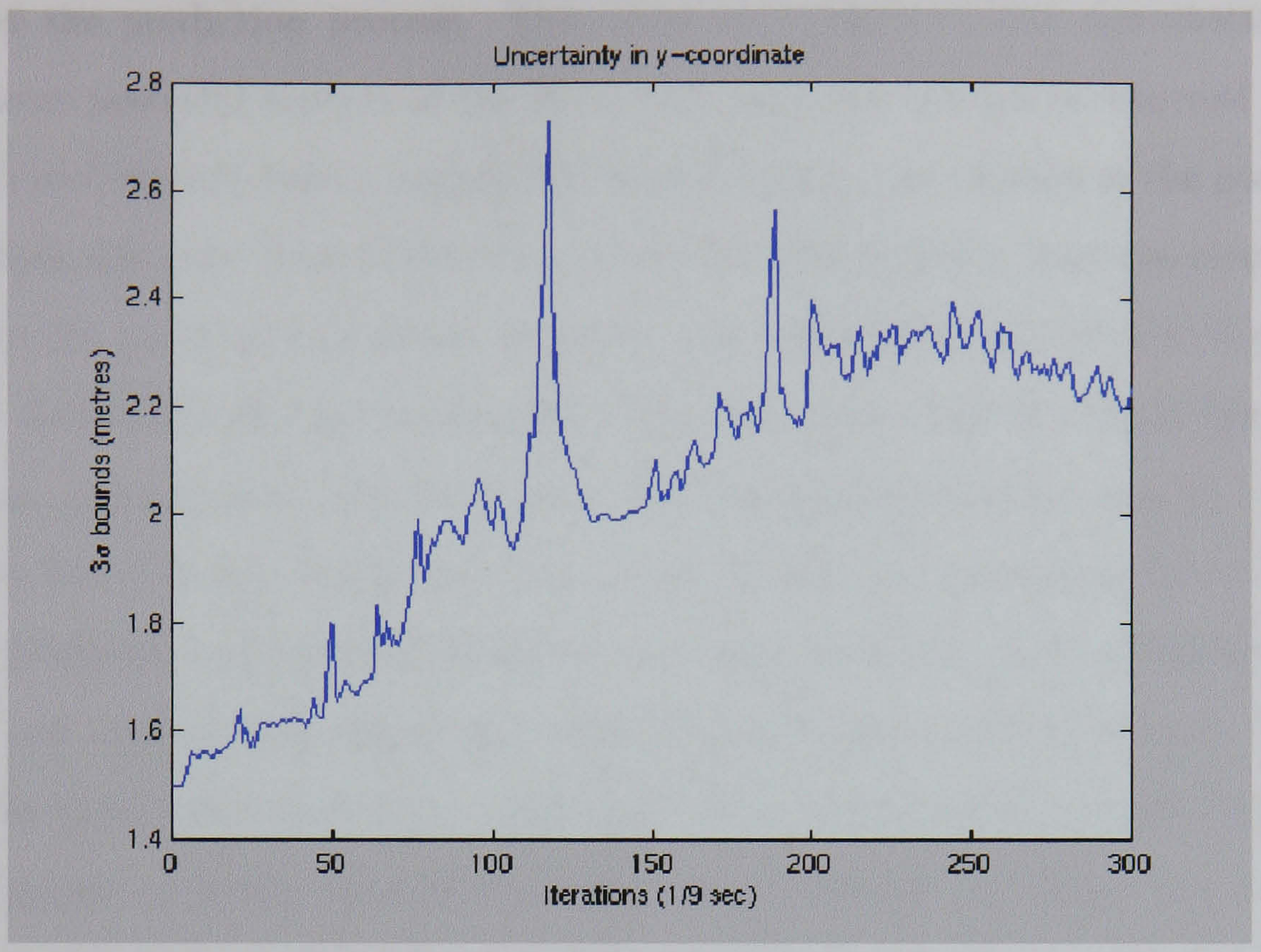

Figure 5.31: Ocean Explorer experiment: y-coordinate 3σ bounds

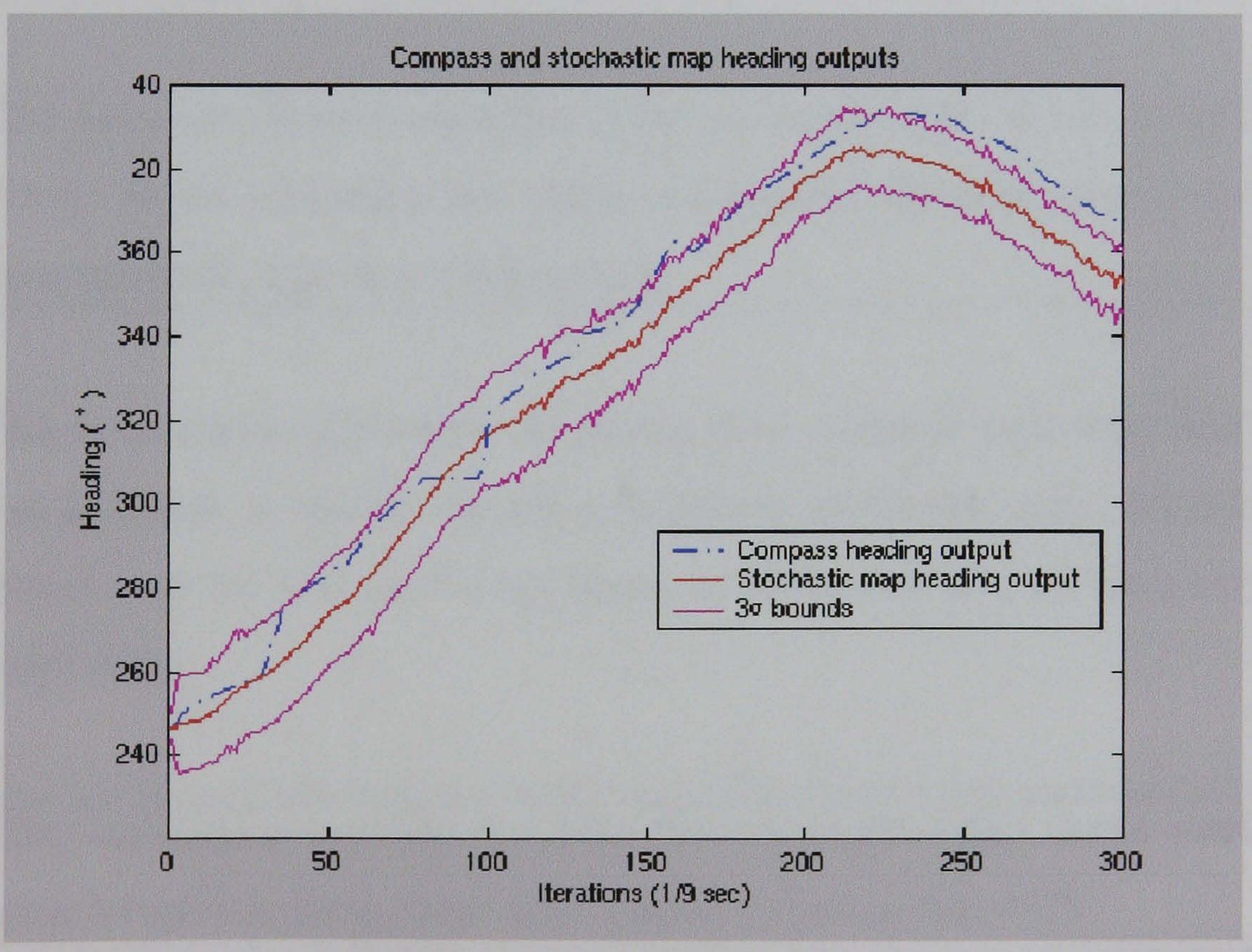

Figure 5.32: Ocean Explorer experiment: estimated vs. compass heading using no descriptors

formation. The previous attempts, section 5.1, have used dead-reckoning sensors to aid the prediction process. The Oban experiment clearly demonstrates one of the most powerful aspects of the stochastic map. As the divers returned to a region which had already been mapped, the filter became more certain of the position. The fact that the data association was successful demonstrates that the error remained within the uncertainty bounds. However, this experiment also showed that the landmark descriptors are not necessarily an improvement, and in certain cases they can become a hindrance, especially when the landmarks all share similar values. The results from the last experiment provide an insight into when these become essential. The proposed architecture initialises new landmarks for each unmatched observation and releases those landmarks which haven't been updated enough times. This architecture, when used with a landmark state vector which includes the landmark descriptors, is better exploited in noisy environments. In these, the returns from the targets vary considerably in apperance between frames. A new landmark will be initialised each time a target changes its apperance considerably. This will filter out the errors that might be caused by a centroid changing coordiantes. This was experimentally proven with the Ocean Explorer experiment.

The last experiment showed that, given an appropriate environment, consistency can be achieved if the vector of landmark descriptors is incorporated into the stochastic map's framework.

This is an important result. It proves that a simple data association strategy, such as NN, can be used to create a consistent stochastic map. Although the two experiments in [17, 63] used descriptors to perform CML, no comparative results were provided.

This experiment has demonstrated that enhanced CML works consistently with forward-looking sonar data gathered from a real AUV.

5.6 Summary

This chapter has shown comparative results obtained using real sonar data. Building on earlier limited experimentation, section 5.1, the experiments in this chapter have demonstrated successful enhanced CML implementations. The first experiment, section 5.2, showed that the stochastic map could work without any dead-reckoning sensor data, or control inputs, with irregular landmark updates. The results also showed that, for certain applications, the landmark descriptors do not benefit or harm the resulting stochastic map. Section 5.3 showed the resulting map obtained during trials in Oban. In this experiments the targets were pier legs. These targets had similar descriptors and the stochastic map suffered as a result. However, the system worked when only using positional information. The landmark descriptors showed their true potential on the last experiment, section 5.4. The first experiment to be carried out with data from an AUV. This experiment showed that given a sonar sequence of noisy returns with landmark variability, not only does the enhanced stochastic map work, but it is essential to achieve consistency. The chapter was closed with a thorough discussion of the results, section 5.5.

Chapter 6

Conclusion and Future Work

This chapter summarises the contributions made by this thesis and proposes future areas of research. Section 6.1 identifies the contributions made by this thesis individually and offers a brief discussion on each of these. In section 6.2 the author identifies those aspects of the work which still need development by the research community if real-time CML is to become a reality.

6.1 Summary of Contributions

This thesis aimed to develop an enhanced CML framework using forward-looking sonar for consitent AUV navigation. The chosen tool to perform CML was the stochastic map. This tool provides a number of advantages over other tools, outlined in section 2.1.5, and its properties, defined in section 2.4, make it the ideal choice. However, these properties are only assured given perfect data association. Thus the thesis task was to provide a framework for improving the current state of the art in data association algorithms for CML. A new enhanced CML strategy was proposed.

In enhancing the CML process the following objectives were met:

- A new landmark state vector was developed for landmarks extracted with a forward looking sonar. This new vector held, in addition to the landmark's coordinates, the landmark descriptors.
- The new landmark state vector was succesfully used to improve the data association process.
- The enhanced CML capabilities were demonstrated using data obtained from a sonar mounted on a real AUV.

6.1.1 Landmark Extraction and Interpretation

An important aspect that must be considered when building a stochastic map is the accuracy of the range and bearing measurements, which will dictate the accuracy of the map itself. The accuracy will be affected by the choice of sensor and landmark extraction algorithm. Not much effort by the research community has been directed towards segmenting forward-looking sonar returns. The approach proposed in this thesis uses ROIs which allow for a refined segmentation and, also, a considerable decrease in processing time. This approach uses the knowledge of the landmarks' estimated positions, which are stored on the map, to segment the returns. The segmentation extracts compact high-intensity regions from the returns. These regions will constitute the landmarks. Landmarks extracted in this manner can be assigned geometric descriptors. These descriptors will help define the landmarks. The suitability of the descriptors was tested by performing a t-test on real data obtained with the Florida Atlantic University concept sonar, Barney. This is a standard tool used in the context of classification to asses class separability. The results showed that the six descriptors taken into consideration performed considerably well, see table 3.3. Further tests were carried out to define which of the descriptors should be used, based on the inter-correlation between them. These tests were the Divergence, Brattacharyya and scatter matrices criteria $J1$, $J2$ and $J3$. Four of these tests proposed that all the descriptors should be used, see table 3.4. Thus the descriptors can be assumed to be uncorrelated, for the purposes of data association.

6.1.2 Data Association

This thesis has reviewed the state of the art in data association algorithms designed for CML. Of all these methods only two approaches [17, 103] have used information other than range and bearing measurements to improve the data association results. A method for incorporating descriptors into conventional data association algorithms was developed. The descriptors were then used to carry out a thorough study of three different data association strategies. The chosen algorithms were the NN, the MHF and the JCT. The study demonstrated that,

- descriptors of sufficient discriminatory capabilities can improve the perfor-

mance of all these data association strategies;

- the addition of more descriptors, if uncorrelated to each other, further improves the results;
- the three data association techniques display a comparable performance when aided by descriptors; and
- if the descriptors do not posses sufficient discriminatory capabilities the data association does not improve in performance.

The descriptors can also help to reduce the introduction of errors into the estimation process when working with real sonar data. The introduction of these errors is caused by noisy signals. Regions of compact high-intensity, when affected by noise, can considerably change in appearance, to the point of splitting and forming various regions or merging with other regions. When this occurs the centroids are shifted. Conventional data association techniques will assign the new centroids to stored landmarks, and thus introduce errors into the calculations. However, if descriptors are used, the new formed regions, if considerably different, will fall outside the validation regions used by the data association schemes. This will stop the errors from creeping into the system.

6.1.3 CML with Real Forward-looking Sonar Data

The thesis has extended the list of successful CML implementations using the stochastic map and a forward-looking sonar. It has also increased the list of forward-looking sonars used in these implementations with the addition of the Seabat 6012, a standard off-the-shelf multibeam forward-looking unit, and Barney, a concept sonar developed by Florida Atlantic University. Most importantly, the experiments demonstrate that CML is feasible using the stochastic map and forward-looking sonar returns as the only input, given observable landmarks. The experiments also showed that the descriptors are not a useful addition when mapping regions where the landmarks all look the same, in particular pier legs. However, given a certain amount of variability, the descriptors not only provide better data association,

but CML remains consistent when using them. Finally the aim of this thesis was achieved:

- This thesis has demonstrated, experimentally, that enhanced CML works consistently with forward-looking sonar data gathered from a real AUV.

6.2 Future Work

This thesis has enhanced the CML process by introducing featured descriptors in the landmark vectors. The robustness of these vectors, as the angle of view and range change, must still be determined. Work with side-scan sonars and multibeam echo sounders enchanced with feature descriptors can also be envisaged. Several aspects of the stochastic map still need to be addressed before the final challenge of a real-time CML implementation is possible. Of these, *map management* is possibly the most important aspect that still requires to be resolved. Finally, a 3D stochastic map implementation must also be developed in order to implement the system in highly dynamic environments.

6.2.1 View Dependency of Sonar

The new landmark vector has shown experimentally to aid the data association process. In the right environment it has also been shown to allow consistent CML. However, the values of the descriptors in the landmark vector depend on both the geometry and reflective properties of the target, and the range and angle of view between the target and the sonar. This thesis has not provided a theoretical or experimental interpretation of this dependency. Future work should consider this issue. This will be especially of benefit for CML systems designed to operate around man made structures, i.e. Piers, harbours or oil rigs. In these types of environments, where the structures have been made of known materials and following standard design methods, the modeling of the sonar process and the introduction of specular and diffuse models for the target returns, should prove helpful in the development of view independent descriptors.

6.2.2 Side-scan sonars and Multibeam Echo Sounders

These types of sensors are downward looking and are not useful for missions where only one pass of the sea floor is performed. For multi-pass missions, such as narrow lawnmower, these sensors might prove a useful ally. The work proposed in this thesis would lend itself readily to images acquired with side-scan sonars. Other descriptors can be produced for the three dimensional profiles acquired with the multibeam echo sounders. These sensors are an essential part of a survey AUV's payload and should be seriously considered.

6.2.3 Map Management

The current approach [32] to keep the size of the stochastic map manageable and the processing time constant relies on dropping landmarks from the stochastic map's state vector. The standard process for deleting a landmark consists of quantifying information lost in deleting the landmark and then deleting those landmarks which hold the least information. Future work should consider the spatial distribution of the landmarks and the predefined mission plan as an input to the function. Storing landmarks which will never be seen again in the state vector will be ill advised, once they have served their purpose. Other efforts have seen the decoupling of the stochastic map. These efforts approximate the map by ignoring some or all of the vehicle-to-landmark and landmark-to-landmark correlations. These methods could all be enhanced with the work performed in this thesis. Performance comparisons between these approaches and a constant size stochastic map should also be taken on board by the community.

6.2.4 3D Stochastic Map

To the author's knowledge the current published work, in CML for underwater applications, has assumed that the vehicle has only three degrees of freedom, and thus work under the constraint that pitch, roll and heave effects can be assumed negligible. This assumption might hold with most AUV designs. It will, in any case, be desirable to extend the scope of the map to a three-dimensional workspace. Theoretically this work should not pose a significant problem. The structure of the

stochastic map is such that extra states can be easily modelled and included in the state vector. However, using a forward-looking sonar to triangulate uncertain range and bearing measurements to then estimate the position of three-dimensional point landmarks is an important challenge in itself. Perhaps, the solution lies in the use of 3D acoustic cameras, although current AUV budgets would certainly not allow the incorporation of such systems.

Appendix A

The Kalman Filter

A.1 The Kalman Filter

This section will provide the reader with an overview of the optimal linear estimator, the Kalman filter [6, 71]. Conceptually, any type of filter tries to minimise the error in an estimate of a desired quantity from noisy data. As explained in [71]: *"If we adopt a Bayesian viewpoint, then we want the filter to propagate the conditional probability density of the desired quantities, conditioned on knowledge of the actual data coming from the measuring devices... Once such a conditional probability density function is propagated, the 'optimal' estimate can be defined. Possible choices would include... the mean... the mode... the median..."*.

A Kalman filter is simply an *optimal recursive data processing algorithm.* It processes all available measurements, no matter how precise these are, to make an estimate of the variables of interest to it. It propagates the conditional probability density for problems in which the system can be described using a *linear* model with *white* and *Gaussian* system and measurement noises. Under these conditions the mean, mode and median all coincide.

The Kalman filter uses

- a model of the system and of the dynamics of the measurement devices,
- the statistical description of the system noises, measurement errors, and uncertainties in the dynamics model
- and any other information about the initial conditions of the variables of interest to generate an overall best estimate of the variables it is attempting to estimate.

In the general case we have,

$$\mathbf{x}(k) = \mathbf{F}(k)\mathbf{x}(k-1) + \mathbf{B}(k)\mathbf{u}(k) + \mathbf{G}(k)\mathbf{w}(k) \tag{A.1}$$

where $\mathbf{x}(.,.)$ is an n-vector state process, $\mathbf{u}(.)$ is an r-vector of piecewise continuous deterministic control input functions, and $\mathbf{w}(.)$ is a white Gaussian noise s-vector, $\mathbf{F}(.)$ is an n-by-n system dynamic matrix, $\mathbf{B}(.)$ is an n-by-r deterministic input matrix, and $\mathbf{G}(.)$ is an n-by-s noise input matrix.

The observation model takes the form,

$$\mathbf{z}(k) = \mathbf{H}(k)\mathbf{x}(k) + \mathbf{v}(k) \tag{A.2}$$

where $\mathbf{z}(.)$ is an m-vector measurement process, $\mathbf{x}(.)$ is the state vector process, $\mathbf{v}(.)$ is a white Gaussian noise m-vector, and $\mathbf{H}(.)$ is an m-by-n measurement matrix.

The Kalman filter works by finding expectations over equation A.1 (for a thorough derivation refer to [71]). The propagated state estimate is thus

$$\hat{\mathbf{x}}(k) = \mathbf{F}(k)\hat{\mathbf{x}}(k-1) + \mathbf{B}(k)\mathbf{u}(k) \tag{A.3}$$

and its associated covariance

$$\mathbf{P}(k) = \mathbf{F}(k)\mathbf{P}(k-1)\mathbf{F}'(k) + \mathbf{Q}(k) \tag{A.4}$$

where $\mathbf{Q}(k)$ is the n-by-n process noise covariance matrix and $'$ signifies the transpose of a matrix.

Then the Kalman filter gain $\mathbf{K}(k)$ is defined and employed in both the mean and the covariance relations,

$$\mathbf{K}(k) = \mathbf{P}(k)\mathbf{H}'(k)[\mathbf{H}(k)\mathbf{P}(k)\mathbf{H}'(k) + \mathbf{R}(k)]^{-1} \tag{A.5}$$

$$\hat{\mathbf{x}}(k+1) = \hat{\mathbf{x}}(k) + \mathbf{K}(k)[\mathbf{z}(k) - \mathbf{H}(k)\hat{\mathbf{x}}(k)] \tag{A.6}$$

$$\mathbf{P}(k+1) = \mathbf{P}(k) - \mathbf{K}(k)\mathbf{H}(k)\mathbf{P}(k) \tag{A.7}$$

where $\hat{\mathbf{x}}(.)$ and $\mathbf{P}(.)$ are the expectation and its covariance for the state vector $\mathbf{x}(.)$ respectively and $\mathbf{R}(.)$ is the error covariance matrix.

A.2 Tracking Nonlinear Systems

The Kalman filter uses linear models for the plant and observation dynamics. It is not always the case that the system can be adequately linearly modelled. In cases where the nonlinearities are not negligible, the Kalman filter is susceptible to failure. In these cases the filter can "learn the wrong state too well [54]". To account for this problem several methods have been put forward (the interested reader should refer to [72], Chapter 9, for a more detailed description). The most popular is the extended Kalman filter (EKF). Some of these methods are summarised below including the EKF, sections A.2.1 to A.2.5.

A.2.1 Addition of Pseudonoise

Increasing the values inside $\mathbf{Q}(k)$. This method effectively shifts the weight of the Kalman filter gain towards the measurements. Similarly, the values of $\mathbf{P}(k)$ could be artificially increased before the actual time propagation of the state occurs.

A.2.2 Limiting the Effective Filter Memory

In some systems, a linear model will be adequate for a set length of time, but previous data could be considered meaningless. In this case, limiting the memory of the filter is a valid solution. Various implementations exist to limit the filter memory. In a common implementation, the measurement noise strengths $\mathbf{R}(k)$ are put into a sequence where $\mathbf{R}(1) > \mathbf{R}(last)$.

A.2.3 Finite Memory Filtering

This implementation was developed for systems where models are only considered valid for the latest N sample periods, but inadequate for longer periods. Another more descriptive name for this method is the "sliding window [72]" filter.

A.2.4 Linearised Kalman Filtering

The system state is now modelled by the nonlinear stochastic differential equation

$$\mathbf{dx}(k) = \mathbf{f}[\mathbf{x}(k), \mathbf{u}(k), k]dk + \mathbf{Gd}\boldsymbol{\beta}(k) \tag{A.8}$$

where $\mathbf{f}[\cdot, \cdot, \cdot]$ is a known n-vector of functions of three arguments, $\mathbf{u}(\cdot)$ is an r-vector of deterministic control input functions, and $\boldsymbol{\beta}(\cdot, \cdot)$ is a Brownian motion with diffusion $\mathbf{Q}(k)$ for all $k \in T$. This can be seen as a modest generalisation of the model considered in the Kalman filter, where $\mathbf{f}[\mathbf{x}(k), \mathbf{u}(k), k]$ replaces $[\mathbf{Fx}(k) + \mathbf{B}(k)\mathbf{u}(k)]$. Let the discrete-time measurements be modelled in general as a nonlinear function of the state plus linearly additive noise for all $k_i \in T$, as

$$\mathbf{z}(k_i) = \mathbf{h}[\mathbf{x}(k_i), k_i] + \mathbf{v}(k_i) \tag{A.9}$$

Again this is a modest increase in complexity where $\mathbf{h}[\mathbf{x}(k_i), k_i]$ replaces $[\mathbf{H}(k_i)\mathbf{x}(k_i)]$. In many applications either $\mathbf{f}$ or $\mathbf{h}$ are linear functions. Using a nominal (reference) trajectory

$$\dot{\mathbf{x}}_\mathbf{n}(k) = \mathbf{f}[\mathbf{x}_\mathbf{n}(k_i), \mathbf{u}(k), k] \tag{A.10}$$

with the following sequence of nominal measurements

$$\mathbf{z}_\mathbf{n}(k_i) = \mathbf{h}[\mathbf{x}_\mathbf{n}(k_i), k_i] \tag{A.11}$$

we consider the perturbation of the state from the assumed nominal trajectory: $[\mathbf{x}(k) - \mathbf{x}_\mathbf{n}(k)]$ for all $k \in T$. This is a stochastic process that satisfies

$$[\dot{\mathbf{x}}(k) - \dot{\mathbf{x}}_\mathbf{n}(k)] = \mathbf{f}[\mathbf{x}(k), \mathbf{u}(k), k] - \mathbf{f}[\mathbf{x}_\mathbf{n}(k), \mathbf{u}(k), k] + \mathbf{G}(k)\mathbf{w}(k) \tag{A.12}$$

a nonlinear stochastic differential equation with $\mathbf{x}_\mathbf{n}(k)$ given for all $k \in T$, expressed as a series by expanding about $\mathbf{x}_\mathbf{n}(k)$:

$$[\dot{\mathbf{x}}(k) - \dot{\mathbf{x}}_\mathbf{n}(k)] = \left.\frac{\partial \mathbf{f}[\mathbf{x}, \mathbf{u}(k), k]}{\partial \mathbf{x}}\right|_{\mathbf{x}=\mathbf{x}_\mathbf{n}(k)} [\mathbf{x}(k) - \mathbf{x}_\mathbf{n}(k)] + \text{h.o.t.} + \mathbf{G}(k)\mathbf{w}(k) \tag{A.13}$$

where the zero-order term in the Taylor series has been cancelled by the second order term and where "h.o.t." are higher order terms. A first order approximation known as the "perturbation equation [72]" can be made

$$\dot{\boldsymbol{\delta}\mathbf{x}}(k) = \mathbf{F}_{\mathbf{x}_\mathbf{n}}(k)\boldsymbol{\delta}\mathbf{x}(k) + \mathbf{G}(k)\mathbf{w}(k) \tag{A.14}$$

where $\boldsymbol{\delta}\mathbf{x}(\cdot)$ is a first order approximation to the process $[\mathbf{x}(\cdot) - \mathbf{x_n}(\cdot)]$, and $\mathbf{F_{x_n}}(k)$ is the n-by-n matrix of partial derivatives of $\mathbf{f}$ with respect to its first argument, evaluated along the nominal trajectory,

$$\mathbf{F_{x_n}}(k) \triangleq \left.\frac{\partial \mathbf{f}[\mathbf{x}, \mathbf{u}(k), k]}{\partial \mathbf{x}}\right|_{\mathbf{x}=\mathbf{x_n}(k)} \tag{A.15}$$

The perturbation equation A.14 can be considered a viable solution as long as the variation with respect to the nominal trajectory are small enough for higher order terms to be negligible. The perturbation measurement model can be similarly derived to obtain

$$\dot{\boldsymbol{\delta}}\mathbf{z}(k_i) = \mathbf{H_{x_n}}(k_i)\boldsymbol{\delta}\mathbf{x}(k_i) + \mathbf{v}(k_i) \tag{A.16}$$

where $\boldsymbol{\delta}\mathbf{z}(\cdot)$ is a first order approximation to the process $[\mathbf{z}(\cdot) - \mathbf{z_n}(\cdot)]$, and $\mathbf{H_{x_n}}(k_i)$ is the m-by-n matrix of partial derivatives of $\mathbf{h}$ with respect to its first argument, evaluated along the nominal trajectory,

$$\mathbf{H_{x_n}}(k_i) \triangleq \left.\frac{\partial \mathbf{h}[\mathbf{x}, k_i]}{\partial \mathbf{x}}\right|_{\mathbf{x}=\mathbf{x_n}(k_i)} \tag{A.17}$$

Linear filtering theory can now be applied to equations A.14 and A.16, providing that the derivatives involved in constructing $\mathbf{F_{x_n}}(k)$ and $\mathbf{H_{x_n}}(k_i)$ exist. The input measurement for the filter at time k_i will be the difference value $[\mathbf{z}(k_i, \omega_j) - \mathbf{z_n}(k_i)]$. The output of such filter will be the optimal estimate of $\boldsymbol{\delta}\mathbf{x}(k)$ for all $k \in T$, $\widehat{\boldsymbol{\delta}\mathbf{x}}(k)$. And the total estimate of the state can be simply found by adding this value to the nominal value $\mathbf{x_n}(k)$:

$$\hat{\mathbf{x}}(t) \triangleq \mathbf{x_n}(k) + \widehat{\boldsymbol{\delta}\mathbf{x}}(k) \tag{A.18}$$

The linearised Kalman filter provides a good compromise between the quality of the estimates and the processing time required to obtain these. For applications where the differences between the nominal and true trajectory don't differ significantly it can be a much better choice than an optimal nonlinear filter.

A.2.5 The Extended Kalman Filter

The EKF, similar to the linearised Kalman filter, assumes a nonlinear dynamic model.

$$\mathbf{x}(k) = \mathbf{f}[\mathbf{x}(k-1), k] + \mathbf{w}(k) \tag{A.19}$$

For simplicity it is assumed that there is no control input, $\mathbf{u}(k)$, and that the process noise is additive, zero-mean, and white. The nonlinear measurement model is as equation A.9 with additive, zero-mean, and white noise. This filter relinearises about each new estimate to create a new and better reference state trajectory. Measurement $\mathbf{z}(k)$ is used to obtain $\hat{\mathbf{x}}(k)$ and the filter relinearises from that value instead of $\mathbf{x_n}(k)$, the state of the nominal trajectory. To obtain the predicted state $\hat{\mathbf{x}}(k)$ the nonlinear function, equation A.19, is expanded in Taylor series around $\hat{\mathbf{x}}(k-1)$, the expansion not including second or higher order terms is

$$\mathbf{x}(k) = \mathbf{f}[\hat{\mathbf{x}}(k-1), k] + \mathbf{F}_{\hat{\mathbf{x}}}(k-1)[\mathbf{x}(k-1) - \hat{\mathbf{x}}(k-1)] + \text{h.o.t} + \mathbf{w}(k) \tag{A.20}$$

where $\mathbf{F}_{\hat{\mathbf{x}}}(k-1)$ is the n-by-n matrix of partial derivatives of $\mathbf{f}$, the Jacobian, with respect to its first argument, evaluated at the latest estimate of the state. The new prediction of the state is thus,

$$\hat{\mathbf{x}}(k) = \mathbf{f}[\hat{\mathbf{x}}(k-1)] \tag{A.21}$$

The first order term is approximately zero-mean and does not appear in equation A.21. Its associated covariance, strictly speaking the approximated mean-square error as $\hat{\mathbf{x}}(k-1)$ is not the exact conditional mean, is obtained as follows

$$\mathbf{P}(k) = \mathbf{F}_{\hat{\mathbf{x}}}(k-1)\mathbf{P}(k)\mathbf{F}'_{\hat{\mathbf{x}}}(k-1) + \mathbf{Q}(k) \tag{A.22}$$

Similarly, the first-order measurement prediction is

$$\hat{\mathbf{z}}(k) = \mathbf{h}[\hat{\mathbf{x}}(k), k] \tag{A.23}$$

The innovation becomes

$$\upsilon(k) = \mathbf{z}(k) - \hat{\mathbf{z}}(k) \tag{A.24}$$

and the innovation covariance (approximate mean-square error) is

$$\mathbf{S}(k) = \mathbf{H}_{\hat{\mathbf{x}}}(k)\mathbf{P}(k)\mathbf{H}'_{\hat{\mathbf{x}}}(k) + \mathbf{R}(k) \tag{A.25}$$

where $\mathbf{H}_{\hat{\mathbf{x}}}(k)$ is the m-by-n matrix of partial derivatives of $\mathbf{h}$, the Jacobian, with respect to its first argument, evaluated at the latest estimate of the state. The filter gain becomes,

$$\mathbf{K}(k) = \mathbf{P}(k)\mathbf{H}'_{\hat{\mathbf{x}}}(k)\mathbf{S}^{-1}(k) \tag{A.26}$$

The update for the filter state estimate at time $k+1$

$$\hat{\mathbf{x}}(k+1) = \hat{\mathbf{x}}(k) + \mathbf{K}(k)\upsilon(k) \tag{A.27}$$

with covariance

$$\mathbf{P}(k+1) = \mathbf{P}(k) - \mathbf{K}(k)\mathbf{H}_{\hat{\mathbf{x}}}(k)\mathbf{P}(k) \tag{A.28}$$

Appendix B

ANGUS 002 Dynamic Model

ANGUS 002, seen in figure B.1, is a work-class ROV previously built and characterised in-house. Although no longer used for experiments, a non-linear dynamic model has been experimentally identified in a test tank with a planar motion mechanism [10]. This vehicle possesses two independent back thrusters (port and starboard) for forward motion and heading motion (using differential thrusters' values to rotate). ANGUS also has four vertical thrusters for heave motion, and two side thrusters for sway. The vertical thrusters cannot be controlled independently, therefore roll and pitch motions are not controllable. Figure B.2 illustrates the thrusters' configuration. In the following paragraphs, we describe the mathematical expression of the dynamic model. Numerical values are given in section B.1.

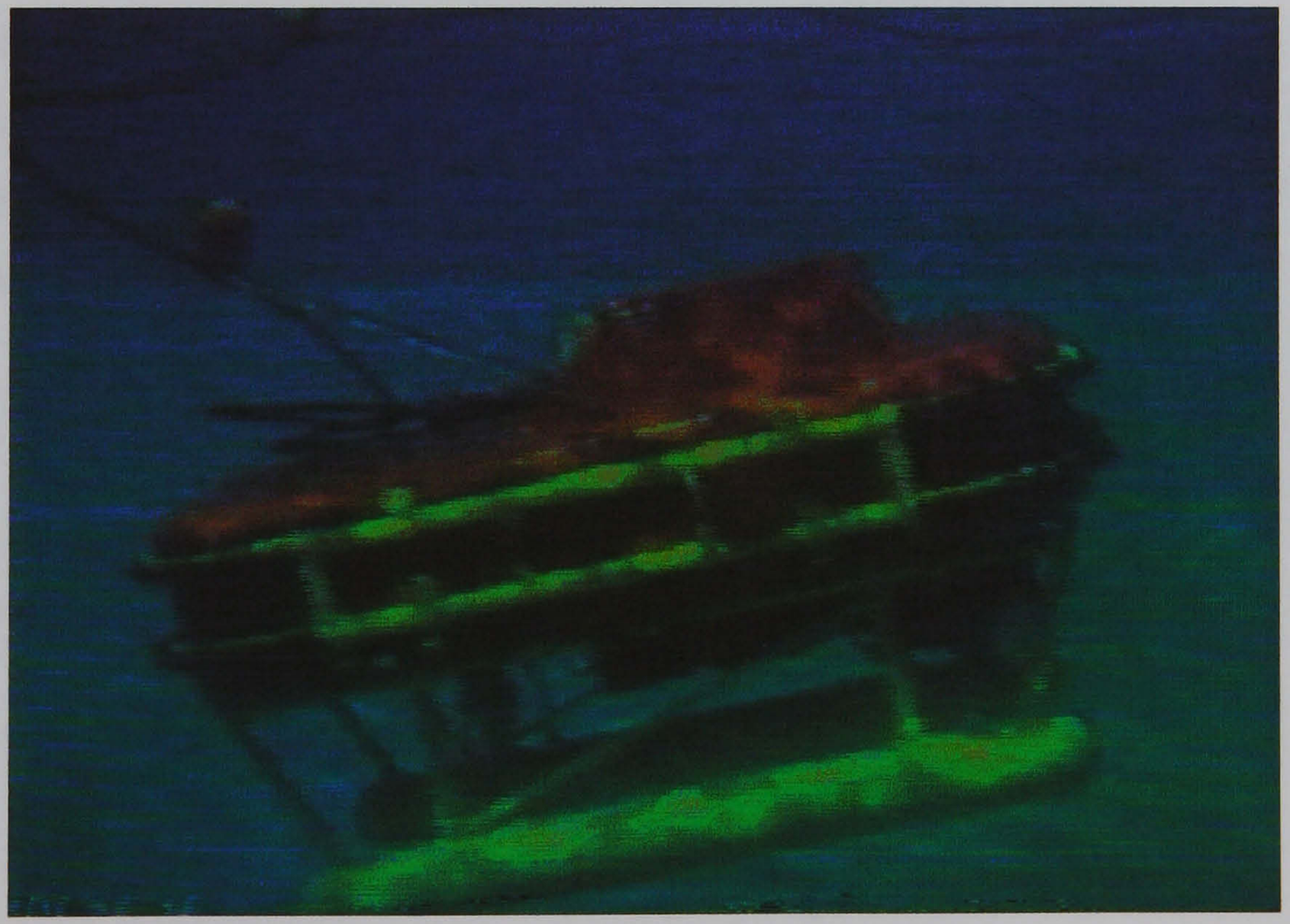

Figure B.1: ROV ANGUS 002

Two main reference frames are necessary to describe the vehicle's motion: an

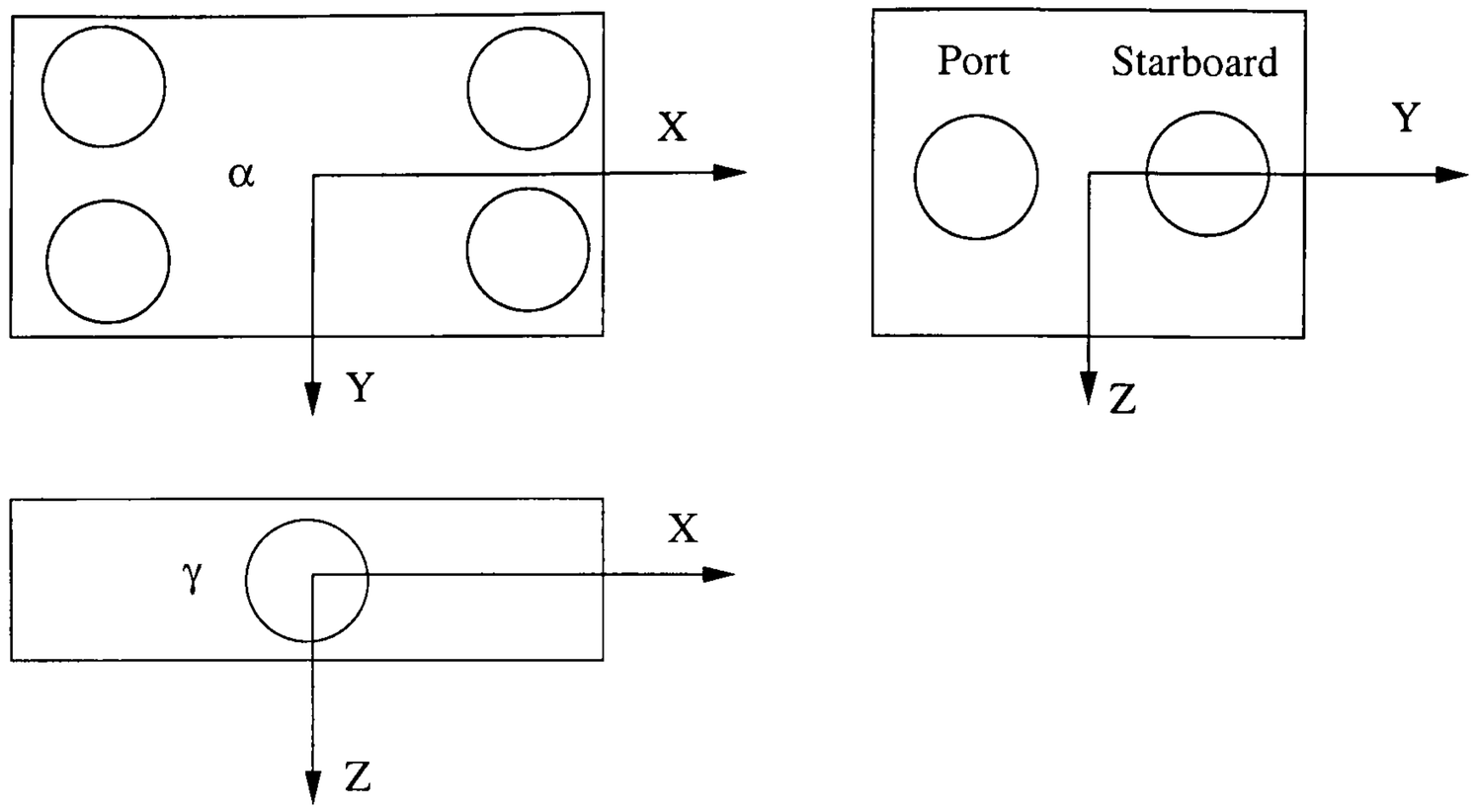

Figure B.2: ANGUS 002 thrusters' configuration

earth-fixed frame which is assumed to be inertial, and a body-fixed frame, attached to the vehicle. The axes (X, Y, Z) of the body-fixed frame coincide with the principal axes of inertia of the vehicle, and the origin is generally taken at the centre of gravity (figure B.3 summarises the notation). The vehicle position, $\boldsymbol{\eta}_p = [x, y, z]^T$, and orientation, $\boldsymbol{\eta}_o = [\phi, \theta, \psi]^T$, (roll, pitch and yaw angles) are then described with respect to the inertial reference frame, while the linear velocity vector $\boldsymbol{\nu}_p = [u, v, w]^T$ (surge, sway, and heave) and the angular velocity vector $\boldsymbol{\nu}_o = [p, q, r]^T$ (roll rate, pitch rate and yaw rate) are expressed with respect to the body-fixed frame. Let us note $\boldsymbol{\nu} = [\boldsymbol{\nu}_p^T, \boldsymbol{\nu}_o^T]^T$ and $\boldsymbol{\eta} = [\boldsymbol{\eta}_p^T, \boldsymbol{\eta}_o^T]^T$; the vehicle flight path relative to the earth-fixed coordinate system is given by the velocity transformation:

$$\dot{\boldsymbol{\eta}} = \mathbf{J}(\boldsymbol{\eta}_o)\,\boldsymbol{\nu} \tag{B.1}$$

where

$$\mathbf{J} = \begin{bmatrix} \mathbf{J}_1 & \mathbf{0}_3 \\ \mathbf{0}_3 & \mathbf{J}_2 \end{bmatrix} \tag{B.2}$$

and

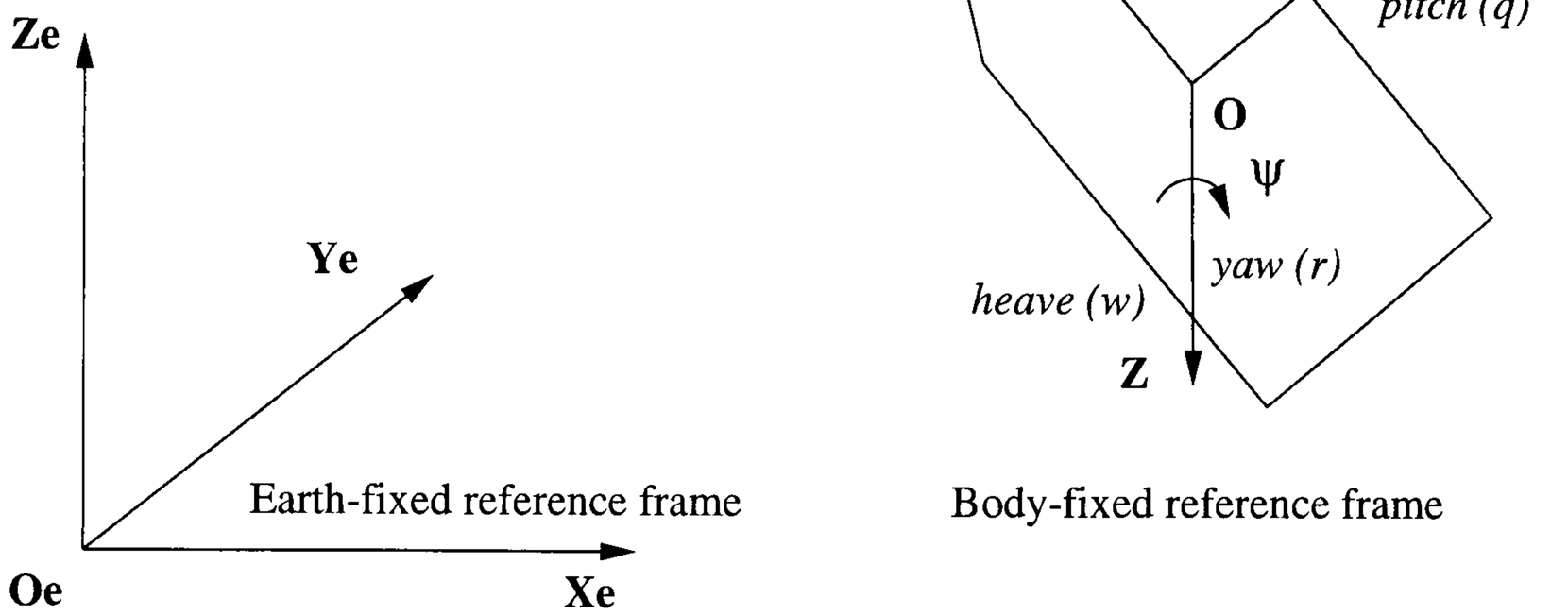

Figure B.3: UUV coordinate frames and motion variables

$$\mathbf{J}_1(\boldsymbol{\eta}_o) = \begin{bmatrix} c\psi c\theta & -s\psi c\phi + c\psi s\theta s\phi & s\psi s\phi + c\psi c\phi s\theta \\ s\psi c\theta & c\psi c\phi + s\phi s\theta s\psi & -c\psi s\phi + s\theta s\psi c\phi \\ -s\theta & c\theta s\phi & c\theta c\phi \end{bmatrix} \tag{B.3}$$

$$\mathbf{J}_2(\boldsymbol{\eta}_o) = \begin{bmatrix} 1 & s\phi c\theta & c\phi s\theta \\ 0 & c\phi & -s\phi \\ 0 & s\phi/c\theta & c\phi/c\theta \end{bmatrix} \tag{B.4}$$

where $s\cdot$ and $c\cdot$ stand for the sin() and cos() functions, e.g. $s\psi = \sin(\psi)$.

The external hydrodynamic forces and moments acting upon the vehicle are identified for underwater vehicles moving at low speeds,

- added mass and inertia,
- drag forces,
- hydrostatic (or restoring) forces,
- propulsion forces and

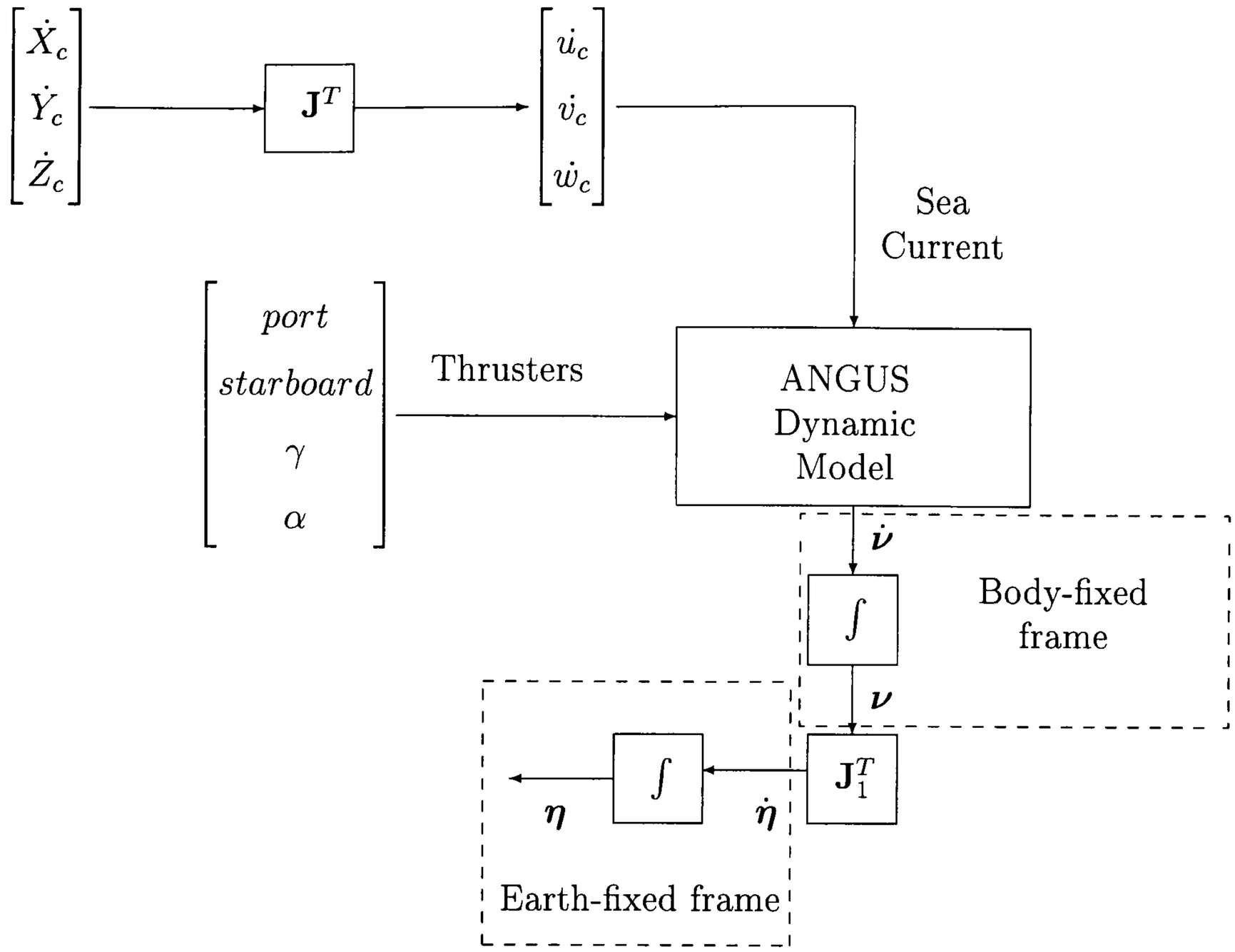

Figure B.4: Block diagram of the dynamic model of ANGUS 002

- environmental disturbances (sea currents, tether).

The dynamic model of the vehicle, figure B.4, can then be expressed as:

$$\mathbf{M}\,\dot{\boldsymbol{\nu}} = \mathbf{B}\begin{bmatrix} \tilde{u}(|\tilde{u}| + D_u) \\ \tilde{v}(|\tilde{v}| + D_v) \\ \tilde{w}(|\tilde{w}| + D_w) \\ p(|p| + D_p) \\ q(|q| + D_q) \\ r(|r| + D_r) \end{bmatrix} + \mathbf{C}(\boldsymbol{\nu}) + \mathbf{g}(\boldsymbol{\eta}) + \mathbf{E}(\boldsymbol{\nu})\,\mathbf{U}_\tau + \mathbf{F}(\boldsymbol{\nu})\,|\mathbf{U}_\tau| \tag{B.5}$$

where $\mathbf{M}$ is a 6×6 mass matrix which includes the added mass and inertial terms, $\mathbf{B}$ is a 6×6 drag matrix and $\mathbf{D} = [D_u, D_v, D_w, D_p, D_q, D_r]^T$ is a 6×1 laminar flow drag vector. The hydrostatic wrench $\mathbf{g}$ in ANGUS' case has been shown to be:

$$\mathbf{g}(\boldsymbol{\eta}) = \begin{bmatrix} (B-W)s\theta \\ (W-B)c\theta s\phi \\ (W-B)c\theta c\phi \\ -HBc\theta s\phi \\ -HBs\theta \\ 0 \end{bmatrix} \tag{B.6}$$

where H is the *metacentric height*, i.e. the height of the centre of buoyancy above the centre of gravity.

The *environmental forces*, $\boldsymbol{\tau}_E$, are caused by sea currents acting on the vehicle body, and disturbances created by the tether (in the case of an ROV). In this model only the sea currents' disturbances are considered. The hydrodynamic forces and moments depend directly on the velocity of the vehicle with respect to the water surrounding it. Consequently, the sea current velocity must be involved in the equations of motion. It is convenient to express the sea current velocity in the world coordinate system.

Let X_c, Y_c and Z_c be the components of the sea current velocity in the world (inertial) reference frame, and u_c, v_c and w_c its components in the body-fixed frame. The transformation between the inertial frame and the body-fixed frame is given by

$$\begin{bmatrix} u_c \\ v_c \\ w_c \end{bmatrix} = \mathbf{J}_1^{-1} \begin{bmatrix} \dot{X}_c \\ \dot{Y}_c \\ \dot{Z}_c \end{bmatrix} = \mathbf{J}_1^{T} \begin{bmatrix} \dot{X}_c \\ \dot{Y}_c \\ \dot{Z}_c \end{bmatrix} \tag{B.7}$$

Note $\tilde{\boldsymbol{\nu}} = [\tilde{u}, \tilde{v}, \tilde{w}, p, q, r]^T$ (where $\tilde{u} = u - u_c$, etc.) to be the velocity vector of the submersible's centre of gravity with respect to the water.

Since the propellers are less efficient when turning in reverse, the action of the thrusters has been encoded in the two 6×4 thrust matrices $\mathbf{E}$ and $\mathbf{F}$. The thrust forces and moments vector, $\boldsymbol{\tau}$, is then expressed as:

$$\boldsymbol{\tau} = \mathbf{E}(\boldsymbol{\nu})\,\mathbf{U}_\tau + \mathbf{F}(\boldsymbol{\nu})\,|\mathbf{U}_\tau| = \mathbf{E}(\boldsymbol{\nu}) \begin{bmatrix} port \\ starboard \\ \gamma \\ \alpha \end{bmatrix} + \mathbf{F}(\boldsymbol{\nu}) \begin{bmatrix} |port| \\ |starboard| \\ |\gamma| \\ |\alpha| \end{bmatrix} \tag{B.8}$$

where $\mathbf{U}_\tau$ is a normalised control vector whose components' values range between -100 % and $+100$ %. The control parameter of the two lateral thrusters is γ, while α is the control parameter of the four vertical thrusters. As their names suggest, *port* and *starboard* are the control parameters of the port and starboard backward thrusters respectively.

The vector of centrifugal forces $\mathbf{C}(\boldsymbol{\nu})$ has been greatly simplified, because of the lack of knowledge concerning the values of most of its elements. The basic centrifugal forces, applied by the virtual inertias of the vehicle, have been taken into account by means of the following vector:

$$\mathbf{C}(\boldsymbol{\nu}) = \begin{bmatrix} \mathbf{M}_{11}(vr - wq) \\ \mathbf{M}_{22}(wq - ur) \\ \mathbf{M}_{33}(uq - vp) \\ (\mathbf{M}_{55} - \mathbf{M}_{66})qr - \mathbf{M}_{46}pq \\ (\mathbf{M}_{66} - \mathbf{M}_{44})pr + \mathbf{M}_{46}(p^2 - r^2) \\ (\mathbf{M}_{44} - \mathbf{M}_{55})pq + \mathbf{M}_{64}qr \end{bmatrix} \tag{B.9}$$

This model, although simplified, is highly nonlinear in many aspects. The thrusters efficiency is different depending on the propellers direction of rotation, and of the vehicle's speed. Cross-coupling terms between axes are another element of nonlinearity. Finally, one of the elements of the drag matrix $\mathbf{B}$ depends on the sign of the surge speed u. For a more detailed description of this model the reader is referred to [66].

B.1 ANGUS 002 3D Dynamic Model Numerical Values

The numerical values of the dynamic parameters of ANGUS 002 used in this thesis are listed below.

$$\mathbf{M} = \begin{bmatrix} 1800 & 0 & 0 & 0 & 50 & 0 \\ 0 & 2200 & 0 & -35 & 0 & 110 \\ 80 & 0 & 3200 & 0 & -50 & 0 \\ 0 & -30 & 0 & 600 & 0 & 15 \\ 50 & 0 & -50 & 0 & 850 & 0 \\ 0 & 110 & 0 & 15 & 0 & 750 \end{bmatrix}$$

$$\mathbf{B}(\boldsymbol{\nu}) = \begin{bmatrix} -350 & 0 & 0 & 0 & 35 & 0 \\ 0 & -680 & 0 & -60 & 0 & 160 \\ 30\,\frac{u}{|u|} & 0 & -1300 & 0 & -33 & 0 \\ 0 & -60 & 0 & -300 & 0 & 20 \\ 35 & 0 & -33 & 0 & -550 & 0 \\ 0 & 140 & 0 & 5 & 0 & -450 \end{bmatrix}$$

$$\mathbf{E}(\boldsymbol{\nu}) = \begin{bmatrix} 250 & 250 & 0 & 70\,u \\ 0 & 0 & 250 & 50\,v \\ 0 & 0 & 0 & 400 \\ 0 & 0 & -15 & 0 \\ 25 & 25 & 0 & 15 \\ 100 & -100 & 0 & 20\,r \end{bmatrix}$$

$$\mathbf{F}(\boldsymbol{\nu}) = \begin{bmatrix} 100 & 100 & 0 & -340\,u \\ 0 & 0 & 0 & -250\,v \\ 0 & 0 & 0 & 50 \\ 0 & 0 & 0 & 0 \\ 5 & 5 & 0 & 0 \\ 40 & -40 & 0 & -100\,r \end{bmatrix}$$

$$\mathbf{D}^T = \begin{bmatrix} 0.6 & 0.6 & 0.4 & 1.2 & 1.1 & 0.6 \end{bmatrix}$$

The buoyancy force $W = 6031\,N$, dry mass is $m = 615\,kg$ or a weight of $W = 6027\,N$. The metacentric height is $H = 0.165\,m$.

B.2 ANGUS 002 2D Dynamic Model

This model is simpler then the one examined earlier. The key changes will now be specified. The axes (X, Y) of the body-fixed frame now only have two degrees of freedom. The vehicle position, $\boldsymbol{\eta}_p = [x, y]^T$, and orientation, ψ, (yaw angle) are still described with respect to the inertial reference frame, while the linear velocity vector $\boldsymbol{\nu}_p = [u, v]^T$ (surge, sway) and the angular velocity r (yaw rate) are expressed with respect to the body-fixed frame. Let us note $\boldsymbol{\nu} = [\boldsymbol{\nu}_p^T, r]^T$ and $\boldsymbol{\eta} = [\boldsymbol{\eta}_p^T, r]^T$; the vehicle flight path relative to the earth-fixed coordinate system is now given by the velocity transformation:

$$\dot{\boldsymbol{\eta}} = \mathbf{J}(\boldsymbol{\eta}_o)\,\boldsymbol{\nu} \tag{B.10}$$

where

$$\mathbf{J} = \begin{bmatrix} \mathbf{J}_1 & \mathbf{0}_{1\times 2} \\ \mathbf{0}_{2\times 1} & 1 \end{bmatrix} \tag{B.11}$$

and

$$\mathbf{J}_1(\boldsymbol{\eta}_o) = \begin{bmatrix} c\psi & -s\psi \\ s\psi & c\psi \end{bmatrix} \tag{B.12}$$

where $s\cdot$ and $c\cdot$ stand for the sin() and cos() functions, e.g. $s\psi = \sin(\psi)$.

The dynamic model of the vehicle is now,

$$\mathbf{M}\,\dot{\boldsymbol{\nu}} = \mathbf{B} \begin{bmatrix} \tilde{u}(|\tilde{u}| + D_u) \\ \tilde{v}(|\tilde{v}| + D_v) \\ r(|r| + D_r) \end{bmatrix} + \mathbf{C}(\boldsymbol{\nu}) + \mathbf{g}(\boldsymbol{\eta}) + \mathbf{E}(\boldsymbol{\nu})\,\mathbf{U}_\tau + \mathbf{F}(\boldsymbol{\nu})\,|\mathbf{U}_\tau| \tag{B.13}$$

where $\mathbf{M}$ is a 3×3 mass matrix which includes the added mass and inertial terms, $\mathbf{B}$ is a 3×3 drag matrix and $\mathbf{D} = [D_u, D_v, D_r]^T$ is a 3×1 laminar flow drag vector. The hydrostatic wrench $\mathbf{g}$ will now be discarded,

$$\mathbf{g}(\boldsymbol{\eta}) = \begin{bmatrix} 0 \\ 0 \\ 0 \end{bmatrix} \tag{B.14}$$

$\dot{X}_c$ and $\dot{Y}_c$ are the components of the sea current velocity in the world (inertial) reference frame, and u_c and v_c its components in the body-fixed frame. The transformation between the inertial frame and the body-fixed frame is given by

$$\begin{bmatrix} u_c \\ v_c \end{bmatrix} = \mathbf{J}_1^{-1} \begin{bmatrix} \dot{X}_c \\ \dot{Y}_c \end{bmatrix} = \mathbf{J}_1^T \begin{bmatrix} \dot{X}_c \\ \dot{Y}_c \end{bmatrix} \tag{B.15}$$

The velocity vector of the submersible centre of gravity with respect to the water is now $\tilde{\boldsymbol{\nu}} = [\tilde{u}, \tilde{v}, r]^T$ (where still $\tilde{u} = u - u_c$, etc.).

The thrust forces and moments vector, $\boldsymbol{\tau}$, are:

$$\boldsymbol{\tau} = \mathbf{E}(\boldsymbol{\nu})\, \mathbf{U}_\tau + \mathbf{F}(\boldsymbol{\nu})\, |\mathbf{U}_\tau| = \mathbf{E}(\boldsymbol{\nu}) \begin{bmatrix} port \\ starboard \\ \gamma \end{bmatrix} + \mathbf{F}(\boldsymbol{\nu}) \begin{bmatrix} |port| \\ |starboard| \\ |\gamma| \end{bmatrix} \tag{B.16}$$

The vector of centrifugal forces $\mathbf{C}(\boldsymbol{\nu})$ have been further simplified:

$$\mathbf{C}(\boldsymbol{\nu}) = \begin{bmatrix} \mathbf{M}_{11}(vr) \\ \mathbf{M}_{22}(-ur) \\ 0 \end{bmatrix} \tag{B.17}$$

The numerical values are given in the next section.

B.3 ANGUS 002 2D Dynamic Model Numerical Values

The numerical values of the dynamic parameters of the ANGUS 002 2D model used in this thesis are listed below.

$$\mathbf{M} = \begin{bmatrix} 1800 & 0 & 0 \\ 0 & 2200 & 110 \\ 0 & 110 & 750 \end{bmatrix}$$

$$\mathbf{B}(\boldsymbol{\nu}) = \begin{bmatrix} -350 & 0 & 0 \\ 0 & -680 & 160 \\ 0 & 140 & -450 \end{bmatrix}$$

$$\mathbf{E}(\boldsymbol{\nu}) = \begin{bmatrix} 250 & 250 & 0 \\ 0 & 0 & 250 \\ 100 & -100 & 0 \end{bmatrix}$$

$$\mathbf{F}(\boldsymbol{\nu}) = \begin{bmatrix} 100 & 100 & 0 \\ 0 & 0 & 0 \\ 40 & -40 & 0 \end{bmatrix}$$

$$\mathbf{D}^T = \begin{bmatrix} 0.6 & 0.6 & 0.6 \end{bmatrix}$$

Appendix C

The Seabat 6012

The Seabat 6012, see figure C.1, is a multi-beam forward looking sonar system. The sonar head is a pressure sealed solid state sonar that transmits, receives and conducts preliminary processing of sonar data prior to transmitting to the surface processor via a cable link. The processor unit controls the processing, display and output of data.

Figure C.1: Seabat 6012

The Seabat 6012 has a 90° (horizontal) by 15° (vertical) field of view, and a maximum range of up to 200 metres. It operates at 455 kHz by means of a ceramic array which transmits one fan shaped beam with a coverage of 165° (horizontal) by 15° . The returned signal is received by the same curved array and is formed into sixty independent beams each having a 1.5° (horizontal) by 15° (vertical) angular beamwidth. The transmit pulse width is $77\mu s$ (35 cycles) equivalent to a range

resolution of 5 cm. The average range accuracy is ± 5 cm and can only be exactly determined by taking into account, as well as the internal electronic range accuracy of 0.1 %, environmental factors such as the correct speed of sound in water, the incident angle at which the signal is reflected from the target, the reflectivity of the target and the actual distance to the target. The technical specifications for the system are summarised in table C.1.

Range(m):	2.5	5	10	25	50	100	200
Update Rate (Hz):	30	30	30	27	14	7	3.5
Operating Frequency(kHz):	455						
Range Resolution (cm):	5						
Angular Resolution (°):	1.5						
Transmit Beamwidth (°):	Horizontal: 165 Vertical: 15						
Receive Beamwidth (°):	Horizontal: 1.5 (-3 dB points) Vertical: 15						
Number of Beams:	60						

Table C.1: Seabat 6012 Technical Specifications

Appendix D

The Tritech SeaKing DFS

The Tritech SeaKing Dual Frequency Sonar (DFS), see figure D.1, is a mechanically scanned forward looking sonar. The sonar head is a pressure sealed solid state sonar that transmits, receives and conducts preliminary processing of sonar data prior to transmitting to the surface processor via a cable link. The processor unit controls the processing, display and output of data.

Figure D.1: The Tritech SeaKing DFS

The Tritech SeaKing DFS offers two operational frequencies. The lower frequency (325 kHz) allows the user to scan sectors of up to 300 metres in range. The higher frequency (675 kHz) has a more limited range, but offers greater range and angular resolution. The sonar operates by insonifying the environment with the transducer, waiting the return echos and then stepping on to the next pre-planned scanning direction until the whole sector has been covered. The limits on the update rate of the data are set by the mechanical constraints of the step-motor on the lower ranges and the speed of sound in water on the higher ranges. The technical specifications for the system are summarised in table D.1.

Operating Frequency(kHz):		325	675
Range(m):		0.4-300	0.4-100
Range Resolution (cm):		10	5
Angular Resolution (°):		3	2
Transmit Beamwidth (°):	Horizontal:	3	2
	Vertical:	20	20
Receive Beamwidth (°):	Horizontal:	3	2
	Vertical:	20	20
Scanning Motor Step size (°):		0.05625	

Table D.1: The Tritech SeaKing Dual Frequency Sonar Technical Specifications

Appendix E

The Florida Atlantic University Sonar

Barney, the Florida Atlantic University forward-looking sonar, was designed to be fitted in the Ocean Explorer AUV. The sonar consists of a projector and a receiver hydrophone. The sonar has been developed as a part of Florida Atlantic University research efforts into subsea technology. A detailed description can be found in [62].

Figure E.1: Barney - The Florida Atlantic University Sonar

The projector is a semi-circular transducer that insonifies a region of 120° (horizontal) by 40° (vertical). The emitted signal is a chirp with a 40 kHz bandwidth centred at 220 kHz. The receiver is a 64 element array, each forming 1.875° (horizontal) by 40° (vertical) independent beams. The technical specifications for the system are summarised in table E.1.

Operating Frequency(kHz):		220
Range(m):		40
Update Rate (Hz):		9
Range Resolution (cm):		3
Angular Resolution (°):		1.875
Transmit Beamwidth (°):	Horizontal:	120
	Vertical:	40
Receive Beamwidth (°):	Horizontal:	1.875
	Vertical:	40
Number of Beams:		64

Table E.1: Barney's Technical Specifications

References

[1] G. C. Anousaki and K. J. Kyriakopoulos. Simultaneous localization and map building for mobile robot navigation. *IEEE Robotics & Automation Magazine*, 6(3):42–53, September 1999.

[2] E. G. Araujo and R. A. Grupen. Feature extraction for autonomous navigation using an active sonar head. In *IEEE International Conference in Robotics and Automation*, volume 4, pages 3823–3828, San Francisco, California, USA, April 2000.

[3] O. Aycard, P. Laroche, and F. Charpillet. Mobile robot localization in dynamic environments using places recognition. In *IEEE International Conference on Robotics and Automation*, volume 4, pages 3135–3140, Leuven, Belgium, May 1998.

[4] T. Bailey, E. M. Nebot, J. K. Rosenblatt, and H. F. Durrant-Whyte. Data association for mobile robot navigation: a graph theoretic approach. In *IEEE International Conference on Robotics and Automation*, volume 3, pages 2512–2517, 2000.

[5] S. Banks. *Signal processing, image processing and pattern recognition.* Prentice Hall, 1990.

[6] Y. Bar-Shalom and T. E. Fortmann. *Tracking and data association*, volume 179 of *Mathematics in Science and Engineering.* Academic Press, 1988.

[7] R. Beckman, A. Martinez, and B. Bourgeois. AUV positioning using bathymetry matching. In *OCEANS'00 IEEE*, volume 3, pages 2123–2127, Providence, Rhode Island, USA, September 2000.

[8] J. M. Bell. *A model for the simulation of sidescan sonar.* PhD thesis, Heriot-Watt University, Edinburgh, Scotland, September 1995.

[9] J. M. Bell. Synthesising sonar images and resulting textures using physical based models. In *Eurel meeting on radar and sonar signal processing*, pages 20/1–20/2, Peebles, England, July 1998.

[10] P. Bellec. Simulation of the Six-Degrees-of-Freedom motion of a remotely controlled unmanned submersible. Master's thesis, Department of Electrical and Electronic Engineering, Heriot-Watt University, Edinburgh, UK, 1983.

[11] O. Bergem. *Bathymetric navigation of autonomous underwater vehicles using a multibeam sonar and a Kalman filter with relative measurement covariance matrices.* PhD thesis, Univeristy of Trondheim, Norway, December 1993.

[12] J. Borenstein, H. R. Everett, and L. Feng. "Where am I?" Sensors and methods for mobile robot positioning. Technical report, The University of Michigan, USA, April 1996.

[13] Ö. Bozma and R. Kuz. Novel sonar map-building based on physical principles of reflection. In *IEEE International Conference on Systems, Man, and Cybernetics. Decision Aiding for Complex Systems*, volume 1, pages 75–80, 1991.

[14] A. Branca, E. Stella, and A. Distante. Autonomous navigation of underwater vehicles. In *OCEANS'98 IEEE*, pages 61–65, Nice, France, September 1998.

[15] W. Burgard, A. Derr, D. Fox, and A. B. Cremers. Integrating global position-ing estimation and position tracking for mobile robots: the dynamic Markov localization approach. In *IEEE/RSJ Proceedings of the International Conference on Intelligent Robots and Systems*, pages 730–735, Victoria, B. C., Canada, October 1998.

[16] W. Burgard, D. Fox, D. Henning, and T. Schmidt. Estimating the absolute position of a mobile robot using position probability grids. In *Proceedings of the National Conference on Artificial Intelligence*, pages 896–901, 1996.

[17] R. N. Carpenter. Concurrent mapping and localization with FLS. In *1998 Workshop on Autonomous Underwater Vehicles*, pages 133–148, Cambridge, Massachusetts, USA, August 1998.

[18] A. R. Cassandra, L. P. Kaelbling, and J. A. Kurien. Acting under uncertainty: discrete Bayesian models for mobile-robot navigation. In *IEEE/RSJ Proceedings of the International Conference on Intelligent Robots and Systems*, pages 963–972, 1996.

[19] J. A. Castellanos, J. M. Martínez, J. Neira, and J. D. Tardós. Simultane-

ous map building and localization for mobile robots: a multisensor fusion approach. In *IEEE International Conference on Robotics and Automation*, volume 2, pages 1244–1249, Leuven, Belgium, May 1998.

[20] J. A. Castellanos, J. D. Tardos, and G. Schmidt. Building a global map of the environment of a mobile robot: the importance of correlations. In *IEEE International Conference on Robotics and Automation*, pages 1053–1059, Albuquerque, New Mexico, USA, April 1997.

[21] M. J. Chantler, J. Clark, and M. Umasuthan. Calibration and operation of an underwater laser triangulation sensor: the varying baseline problem. *Optical Engineering*, 36(9):2604–2611, September 1997.

[22] M. J. Chantler, D. M. Lane, D. Dai, and N. Williams. Detection and tracking of returns in sector-scan sonar image sequences. *IEE Proceedings Radar and Sonar Navigation*, 143(3):157–162, 1996.

[23] M. J. Chantler and J. P. Stoner. Automatic interpretation of sonar image sequences using temporal feature measures. *IEEE Journal of Oceanic Engineering*, 22(1):47–56, January 1997.

[24] C. K. Chen and D. Y. Y. Yun. Unifying graph matching problems with a practical solution. In *International Conference on Systems, Signals, Control, Computers*, September 1998.

[25] K. S. Chong and L. Kleeman. Mobile robot map building for an advanced sonar array and accurate odometry. *International Journal Robotics Research*, 18(1):20–36, January 1999.

[26] I. J. Cox and J. J. Leonard. Modeling a dynamic environment using a Bayesian multiple hypothesis approach. *Artificial Intelligence*, 66:311–344, 1994.

[27] J. Cuschieri and S. Negahdaripour. Use of forward scan sonar images for positioning and navigation by an AUV. In *OCEANS'98 IEEE*, pages 752–756, Nice, France, September 1998.

[28] S. Daniel, F. Le Leannec, C. Roux, B. Solaiman, and E. P. Maillard. Side-scan sonar image matching. *IEEE Journal of Oceanic Engineering*, 23(3):245–259, July 1998.

[29] A. J. Davison. *Mobile robot navigation using active vision.* PhD thesis, Uni-

versity of Oxford, Oxford, England, October 1999.

[30] F. Dellaert, D. Fox, W. Burgard, and S. Thrun. Monte Carlo localization for mobile robots. In *IEEE International Conference in Robotics and Automation*, pages 1322–1328, Detroit, Michigan, USA, May 1999.

[31] D. E. Di Massa. *Terrain-relative navigation for autonomous Underwater Vehicles.* PhD thesis, Massachusetts Institute of Technology and Woods Hole Oceanographic Institution, Massachusetts, USA, 1997.

[32] M. W. M. G. Dissanayake, H. Durrant-Whyte, and T. Bailey. A computationally efficient solution to the simultaneous localisation and map building (SLAM) problem. In *IEEE International Conference in Robotics and Automation*, pages 1009–1014, San Francisco, California, USA, April 2000.

[33] M. W. M. G. Dissanayake, P. Newman, H. F. Durrant-Whyte, S. Clark, and M. Csorba. A solution to the simultaneous localisation and map building (SLAM) problem. Technical Report ACFR-TR-01-99, Australian Center for Field Robotics, University of Sydney, Australia, January 1999.

[34] T. Duckett and U. Nehmzow. Knowing your place in real world environments. In *Third European Workshop on Advanced Mobile Robots (EUROBOT '96)*, pages 135–142, 1996.

[35] T. Duckett and U. Nehmzow. Exploration of unknown environments using a compass, topological map and neural network. In *IEEE International Symposium on Computational Intelligence in Robotics and Automation*, pages 312–317, 1999.

[36] H. J. S. Feder. *Simultaneous stochastic mapping and localization.* PhD thesis, Massachusetts Institute of Technology, Cambridge, Massachusetts, USA, June 1999.

[37] G. L. Foresti, S. Gentili, and M. Zampato. A vision-based system for autonomous underwater vehicle navigation. In *OCEANS'98 IEEE*, pages 195–199, Nice, France, September 1998.

[38] T. E. Fortmann, Y. Bar-Shalom, and M. Scheffe. Sonar tracking of multiple targets using joint probabilistic data association. *IEEE Journal of Oceanic Engineering*, 8(3):173–184, July 1983.

[39] P. Gilkerson and P. Probert. A diffuse reflection model for time of flight sonar. In *IEEE International Conference in Robotics and Automation*, pages 624–629, Detroit, Michigan, USA, May 1999.

[40] R. C. Gonzalez and R. E. Woods. *Digital Image Processing.* Addison-Wesley, Reading, Massachusetts, USA, 3 edition, 1992.

[41] N. Gracias and J. Santos-Victor. Automatic mosaic creation of the ocean floor. In *OCEANS'98 IEEE*, pages 257–262, Nice, France, September 1998.

[42] S. Guillaudeux, S. Daniel, and E. Maillard. Optimization of a sonar image processing chain: a fuzzy rules based expert system approach. In *OCEANS'96 MTS/IEEE*, volume 3, pages 1319–1323, Fort Lauderdale, Florida, USA, 1996.

[43] J. C. T. Hallam. *Intelligent automatic interpretation of active marine sonar.* PhD thesis, University of Edinburgh, Edinburgh, Scotland, 1984.

[44] R. K. Hansen and P. A. Andersen. The application of real 3D acoustical imaging. In *OCEANS'98 IEEE*, pages 738–741, Nice, France, September 1998.

[45] A. J. Harris and N. A. Thacker. Map building and path planning using computer vision. In R. B. Fisher and G. M. Hayes, editors, *Proceedings of the 6th International Symposium on Intelligent Robotic Systems*, pages 205–212, Edinburgh, Scotland, July 1998.

[46] D. A. Harville. *Matrix algebra from a statistician's perspective.* Springer-Verlag, New York, USA, 1997.

[47] L. Henriksen. An integrated environment for fast development and performance assessment of sonar image processing algorithms - SSIE. In *Symposium on Autonomous Underwater Vehicle Technology*, pages 330–340, 1996.

[48] L. Henriksen. Real-time underwater object detection based on an electrically scanned high-resolution sonar. In *Symposium on Autonomous Underwater Vehicle Technology*, Cambridge, Massachusetts, USA, 1996.

[49] J. Hertzberg and F. Kirchner. Landmark-based autonomous navigation in sewerage pipes. In *First Euromicro Workshop on Advanced Mobile Robots (EUROBOT '96)*, pages 68–73. IEEE Press, 1996.

[50] U. Hoelscher-Hoebing and D. Kraus. Unsupervised image segmentation and image fusion for multi-beam/multi-aspect sidescan sonar images. In

OCEANS'98 IEEE, volume 1, pages 571–576, Nice, France, September 1998.

[51] M. Hu. Visual recognition by moment invariants. *IRE Transaction on Information Theory*, 8:179–187, 1962.

[52] A. Huster, S. D. Fleischer, and S. M. Rock. Demonstration of a vision-based dead-reckoning system for navigation of an underwater vehicle. In *OCEANS'98 IEEE*, pages 326–330, Nice, France, September 1998.

[53] B. Jalving and K. Gade. Positioning accuracy for the HUGIN detailed seabed mapping UUV. In *OCEANS'98 IEEE*, pages 108–112, Nice, France, September 1998.

[54] A. H. Jazwinski. *Stochastic processes and filtering theory.* Academic Press, New York, USA, 1970.

[55] P. Jensfelt, D. J. Austin, O. Wijk, and M. Andersson. Feature based condensation for mobile robot localization. In *IEEE International Conference in Robotics and Automation*, pages 2531–2537, San Francisco, California, USA, April 2000.

[56] D. Johnson and S. Eppig. Aided inertial navigation systems for underwater vehicles. In *Fith International Symposium on Unmmanned Untethered Submersible Technology*, volume 1, pages 265–282, University of New Hampshire, New Hampshire, USA, June 1987.

[57] D. Kortenkamp and D. Weymouth. Topological mapping for mobile robots using a combination of sonar and vision sensing. In *12th National Conference on Artificial Intelligence*, volume 2, pages 979–984, Seattle, Washington, USA, July 1994.

[58] B. J. Kuipers and Y.-T. Byun. A robot exploration and mapping strategy based on a semantic hierarchy of spatial representations. *Journal of Robotics and Autonomous Systems*, 8:47–63, 1991.

[59] D. M. Lane, M. Chantler, D. Y. Dai, and I. Tena Ruiz. Tracking and classification of multiple objects in multi-beam sector scan sonar image sequences. In *International Symposium on Underwater Technology*, pages 269–273, Tokyo, Japan, April 1998.

[60] D. M. Lane, M. J. Chantler, and D. Dai. Robust tracking of multiple objects in

sector-scan sonar image sequences using optical flow motion estimation. *IEEE Journal of Oceanic Engineering*, 23(1):31–46, January 1998.

[61] D. M. Lane and J. P. Stoner. Automatic interpretation of sonar imagery using qualitative feature matching. *IEEE Journal of Oceanic Engineering*, 19(3):391–405, July 1994.

[62] L. LeBalanc, J. M. Cuschieri, P. Beaujean, and M. Singer. Electronically steered and focused forward-looking scan sonar. In *AUV 96*, Monterey, California, USA, June 1996.

[63] J. J. Leonard, R. N. Carpenter, and H. J. S. Feder. Stochastic mapping using forward look sonar. In *Proceedings of International Conference on Field and Service Robotics*, pages 69–74, Pittsburgh, Pennsylvania, USA, August 1999.

[64] J. J. Leonard and H. F. Durrant-Whyte. *Directed sonar sensing for mobile robot navigation.* Kluwer Academic Publishers, 1992.

[65] D. Lerro and Y. Bar-Shalom. Automated tracking with target amplitude information. In *Proc. of the 1990 American Control Conference*, pages 2875–2880, San Diego, California, USA, May 1990.

[66] J.-F. Lots. *Application of visual servoing to the dynamic positioning of an underwater vehicle.* PhD thesis, Heriot-Watt University, 2001. In preparation.

[67] L. Lucido, J. Opderbecke, V. Rigaud, R. Deriche, and Z. Zhang. An integrated multiscale approach for terrain referenced underwater navigation. In *International Conference on Image Processing*, volume 2, pages 633–636, Laussane, Switzerland, September 1996.

[68] L. Lucido, B. Popescu, J. Opderbecke, V. Rigaud, R. Deriche, Z. Zhang, P. Costa, and P. Larzabal. Segmentation of bathymetric profiles and terrain matching for underwater vehicle navigation. In *6th IARP Workshop on Underwater Robotics*, Toulon, France, March 1996.

[69] A. Mallet and S. Lacroix. Toward real-time localization in outdoor environments. In *IEEE International Conference on Robotics and Automation*, volume 4, pages 2827–2832, Leuven, Belgium, May 1998.

[70] M. J. Mataric. A distributed model for mobile robot environment learning and navigation. Master's thesis, MIT, Cambridge, Massachusetts, USA, January

1990.

[71] P. S. Maybeck. *Stochastic models, estimation, and control. Volume 1*, volume 141 of *Mathematics in Science and Engineering*. Academic Press, 1979.

[72] P. S. Maybeck. *Stochaistic models, estimation, and control. Volume 2*, volume 141 of *Mathematics in Science and Engineering*. Academic Press, 1982.

[73] M. Mignotte, C. Collet, P. Pérez, and P. Bouthemy. Three-class markovian segmentation of high-resolution sonar images. *Computer Vision and Image Understanding*, 76(3):191–204, December 1999.

[74] M. Mignotte, C. Collet, P. Pérez, and P. Bouthemy. Markov random field and fuzzy logic modeling in sonar imagery: application to the classification of underwater floor. *Computer Vision and Image Understanding*, 79:4–24, 2000.

[75] M. Mignotte, C. Collet, P. Pérez, and P. Bouthemy. Sonar image segmentation using an unsupervised hierarchical MRF model. *IEEE Transactions on Image Processing*, 9(7):1216–1231, July 2000.

[76] B. A. Moran. *Underwater shape reconstruction in two dimensions*. PhD thesis, Massachusetts Institute of Technology, Cambridge, Massachusetts, USA, May 1994.

[77] C. L. Morefield. Application of 0-1 integer programming to multitarget tracking problems. *IEEE Transactions on Automatic Control*, 22(3):302–312, June 1977.

[78] P. Moutalierand and R. Chatila. Stochastic multisensor data fusion for mobile robot location and environmental modelling. In *International Symposium on Robotics Research*, pages 85–94, Tokyo, Japan, 1989.

[79] A. J. Muñoz and J. Gonzalez. Two-dimensional landmark-based position estimation from a single image. In *IEEE International Conference on Robotics and Automation*, volume 4, pages 3709–3714, Leuven, Belgium, May 1998.

[80] S. Negahdaripour, X. Xu, and A. Khamene. Applications of direct 3D motion estimation for underwater machine vision systems. In *OCEANS'98 IEEE*, pages 51–55, Nice, France, September 1998.

[81] J. Neira and J. D. Tardós. Robust and feasible data association for simultaneous localization and map building. In *IEEE International Conference in*

Robotics and Automation, volume Workshop W4, Mobile Robot Navigation and Mapping, San Francisco, California, USA, April 2000.

[82] P. Newman. *On the structure and solution of the simultaneous localisation and map building problem.* PhD thesis, The University of Sydney, Sydney, Australia, 1999.

[83] I. Nourbakhsh, R. Powers, and S. Birchfield. DERVISH an office-navigating robot. *AI Magazine*, 16(2):53–60, 1995.

[84] R. C. Patel and A. R. Greig. Segmentation of 3D acoustic images for object recognition purposes. In *OCEANS'98 IEEE*, volume 1, pages 577–581, Nice, France, September 1998.

[85] Y. Petillot, I. Tena Ruiz, D. M. Lane, Y. Wang, E. Trucco, and N. Pican. Underwater vehicle path planning using a multi-beam forward looking sonar. In *OCEANS'98 IEEE*, volume 2, pages 1194–1199, Nice, France, September 1998.

[86] N. Pican, E. Trucco, M. Ross, D. M. Lane, Y. Petillot, and I. Tena Ruiz. Texture analysis for seabed classification: co-occurrence matrices vs. self-organizing maps. In *OCEANS'98 IEEE*, volume 1, pages 424–427, Nice, France, September 1998.

[87] K. Plakas, E. Trucco, and A. Fusiello. Uncalibrated vision for 3-D underwater applications. In *OCEANS'98 IEEE*, pages 272–276, Nice, France, September 1998.

[88] Z. Politis and P. Probert. Perception of an indoor robot workspace by using CTFM sonar imaging. In *IEEE International Conference on Robotics and Automation*, volume 4, pages 2801–2806, Leuven, Belgium, May 1998.

[89] D. B. Reid. An algorithm for tracking multiple targets. *IEEE Transactions on Automatic Control*, 24(6), December 1979.

[90] F. Schöncherr, J. Hertzberg, and W. Burgard. Probabilistic mapping of unexpected objects by a mobile robot. In *IEEE International Conference on Intelligent Robot Systems*, pages 474–481, 1999.

[91] A. Schultz and W. Adams. Continuous localization using evidence grids. In *IEEE International Conference on Robotics and Automation*, volume 4, pages

2833–2839, Leuven, Belgium, May 1998.

[92] A. Shoukry and M. Aboutabl. Neural network approach for solving the maximal common subgraph problem. *IEEE Transactions on Systems, Man, and Cybernetics*, 26(5):785–790, 1996.

[93] R. Simmons and S. Koenig. Probabilistic navigation in partially observable environments. In *Joint Conference on Artificial Intelligence*, Montreal, Canada, August 1995.

[94] H. Singh, J. Howland, D. Yoerger, and L. Whitcomb. Quantitative photomosaicking of underwater imagery. In *OCEANS'98 IEEE*, pages 263–266, Nice, France, September 1998.

[95] M. Sistiaga, J. Opderbecke, and M. Aldon. Depth image matching for underwater vehicle navigation. In *International Conference on Image Analysis and Processing*, pages 624 –629, 1999.

[96] M. Sistiaga, J. Opderbecke, M. J. Aldon, and V. Rigaud. Map based underwater navigation using a multibeam echosounder. In *OCEANS'98 IEEE*, volume 2, pages 747–751, Nice, France, September 1998.

[97] C. M. Smith. *Integrating mapping and navigation.* PhD thesis, Massachusetts Institute of Technology, Cambridge, Massachusetts, USA, June 1998.

[98] R. Smith. *Terrain-aided navigation of an underwater vehicle.* PhD thesis, University of Oxford, Oxford, England, 1997.

[99] R. Smith, M. Self, and P. Cheeseman. Estimating uncertain spatial relationships in robotics. In I.Cox and G. Wilfong, editors, *Autonomous Robot Vehicles.* Springer-Verlag, 1990.

[100] M. Sonka, V. Hlavac, and R. Boyle. *Image processing analysis and machine vision.* International Thomson Computer Press, 1993.

[101] I. Tena Ruiz, D. M. Lane, and M. J. Chantler. A comparison of inter-frame feature measures for robust classification in sector scan sonar image sequences. *IEEE Journal of Oceanic Engineering*, 24(4):458–469, 1999.

[102] I. Tena Ruiz, Y. Petillot, D. M. Lane, and J. M. Bell. Tracking objects in underwater multibeam sonar images. In *IEE Colloquium on Motion Analysis and Tracking*, pages 11/1–11/7, London, England, 1999.

[103] I. Tena Ruiz, Y. Petillot, D. M. Lane, and C. Salson. Feature extraction and data association for AUV concurrent mapping and localisation. In *IEEE International Conference in Robotics and Automation*, pages 2785–2790, Seoul, Korea, 2001.

[104] S. Theodiridis and K. Koutroumbas. *Pattern recognition.* Academic Press, London, UK, 1999.

[105] S. Thrun. Bayesian landmark learning for mobile robot navigation. *Machine learning*, 33(1), 1998.

[106] S. Thrun. Finding landmarks for mobile robot navigation. In *IEEE International Conference on Robotics and Automation*, volume 2, pages 958–963, Leuven, Belgium, May 1998.

[107] S. Thrun, W. Burgard, and D. Fox. A probabilistic approach to concurrent mapping and localization for mobile robots. *Machine Learning and Autonomous Robots (joint issue)*, 31(5), 1998.

[108] S. Thrun, D. Fox, W. Burgard, and F. Dellaert. Robust Monte Carlo localization for mobile robots. *Artificial Intelligence Journal*, To appear 2001.

[109] T. Tommasini, A. Fusiello, V. Roberto, and E. Trucco. Robust feature tracking in underwater video sequences. In *OCEANS'98 IEEE*, pages 46–50, Nice, France, September 1998.

[110] D. Troop. Summary of battery chemistry technologies. Technical Report 0007-01, The Autonomous Undersea Systems Institutes, New Hampshire, USA, July 2000.

[111] E. Trucco, Y. Petillot, I. Tena Ruiz, C. Plakas, and D. M. Lane. Feature tracking in video and sonar subsea sequences with applications. *Computer Vision and Image Understanding*, 79:92–122, 2000.

[112] J. Uhlmann. *Dynamic map building and localization: new theoretical foundations.* PhD thesis, University of Oxford, Oxford,England, 1995.

[113] L. Whitcomb, D. Yoerger, and H. Singh. Advances in Doppler-based navigation of underwater robotic vehicles. In *IEEE International Conference in Robotics and Automation*, pages 399–406, Detroit, Michigan, USA, May 1999.

[114] O. Wijk and H. I. Christensen. Triangulation-based fusion of sonar data with

application in robot pose tracking. *IEEE Transactions on Robotics and Automation*, 16(6):740–752, December 2000.

[115] N. Williams. *Recognising objects in sector-scan sonar image sequences.* PhD thesis, Heriot-Watt University, Edinburgh, Scotland, June 1998.

[116] S. B. Williams, P. Newman, M. W. M. G. Dissanayake, and H. Durrant-Whyte. Autonomous underwater simultaneous localisation and map building. In *IEEE International Conference on Robotics and Automation*, volume 2, pages 1793–1798, 2000.

[117] S. Woolven and M. Field. POS/SV - an aided inertial navigation system for submersible vehicles. In *OCEANS'98 IEEE*, pages 103–107, Nice, France, September 1998.

[118] X. Xu. *Vision-based ROV system.* PhD thesis, University of Miami, Coral Gables, Florida, USA, May 2000.

[119] T. Yamamoto, S. Maeyama, A. Ohya, and S. Yuta. An implementation of landmark-based position estimation function as an autonomous and distributed system for a mobile robot. In *IEEE/RSJ International Conference on Intelligent Robots and Systems*, pages 1141–1148, 1999.

[120] B. Yamauchi, A. Schultz, and W. Adams. Mobile robot exploration and map-building with continuous localization. In *IEEE International Conference on Robotics and Automation*, volume 4, pages 3715–3720, Leuven, Belgium, May 1998.

[121] S. M. Zanoli and P. Zingaretti. Underwater imaging system to support ROV guidance. In *OCEANS'98 IEEE*, pages 56–60, Nice, France, September 1998.

[122] B. Zerr and B. Stage. Three-dimensional reconstruction of underwater objects from a sequence of sonar images. In *International Conference on Image Processing*, volume 3, pages 927–930, 1996.